UiT The Arctic University of Norway

Faculty of Engineering Science and Technology

Beam based Finite element modelling of Herøysund bridge

Project report

Patrick Norheim Berg

Master's thesis in Engineering design END-3900-1 23V May 2023

Master thesis on Beam based FEM Herøysund bridge

University of Tromsø – The Arctic University of Norway

IVT, Faculty of Engineering Science and Technology

Engineering Design

Title:

Beam based Finite element modelling of Herøysund bridge

Date:

15.5.2023

Number of report pages:

54

Attachment pages:

99

Total number of pages:

153

Subject code:

END-3900-1 23V

Subject name:

Master thesis

Author:

Patrick Norheim Berg

Department:

Department of Computer Science and Computational Engineering (IDBI)

Field of study:

Master Engineering Design

Supervisors:

Researcher Harpal Singh, UiT Narvik

Professor Vanni Nicoletti, Marche Polytechnic University

Partners:

Nordland Fylkeskommune, Statens Vegvesen, NTNU, SINTEF.

Keywords:

FEM, Post tensioned bridge, Herøysund bridge, Tendons, concrete, Structural analysis, Modal analysis Structural health monitoring (SHM).

Table of Contents

List of Tables

List of Figures

Abstract

In this thesis the candidate aims to model two finite elements models of the post tensioned concrete Herøysund bridge. First a solid element model is modelled using the documentation from the bridge construction, then a beam element model is modelled using the solid model as a foundation. These models are subjected to a structural analysis that applies boundary conditions, joints, mass, gravity, asphalt, railings, and the post tensioning system. Then the structural analysis is used as a pre-stress condition for a modal analysis on each model. The modal analysis is used to find the eigenfrequencies and corresponding mode shapes of the bridge models. Interesting results from both models' analyses is compared to reveal how similar the models are and which model gives the most reliable results. The modes are compared using the modal assurance criterion. The modes are then evaluated, and significant modes are suggested for comparison with operational modes that will be extracted from the bridge in the future.

Acknowledgements

Front page picture: Herøysund bridge © Nordland fylkeskommune.

This thesis is produced by the candidate alone, but the candidate wants to thank the students working on similar theses simultaneously, Zeeshan Azad and Macdonald Elochukwu Nwamma for the good teamwork through the thesis work.

The candidate wishes to appreciate the project's supervisors, Harpal Singh and Vanni Nicoletti, for their assistance and guidance. In addition, the candidate has received a great deal of guidance and assistance from IDBI employees Andreas Seger, Guy Beeri Mauseth, and Per Johan Nicklasson; thank you for your guidance and assistance.

The candidate would also like to thank the supervisors and partners for an engaging, educational, and challenging assignment.

Furter the candidate would like to thank Roy Eivind Antonsen (project leader Statens Vegvesen) Per Ove Ravatsås for providing the project basis files, documentations and pictures required to do finite element modelling.

Finally, the candidate would like to thank his family, particularly his wife, for their support throughout his studies.

Foreword

This problem was assigned in the course END-3900-1 23V master thesis, which is the final course in the engineering design master's programme at UiT Narvik. The subject comprises of a project on a candidate-selected topic, assigned by the institute and formulated by the supervisors. The endeavour will be documented with a report of approximately 50 pages, plus appendices and other pertinent files. The objective of the master's thesis project is to provide candidates with an opportunity to implement the knowledge gained in previous courses and to equip candidates with the skills necessary to complete an individual project on a topic pertinent to the master's programme. Additionally, it provides an opportunity to evaluate the candidate's academic learning outcomes. The undertaking will include both theoretical and practical components. The candidate will acquire a broad understanding of the topic through literature studies of the previous work in the field and related disciplines, and a thorough understanding through problem solving.

Software used

- Figures in the discretization appendix is modelled in Autodesk Inventor [1].
- The sketch in the discretization appendix is drawn in Autodesk Autocad [2].
- This report is written in Microsoft word [3].
- Some calculations and tables are made in Microsoft excel [4].
- Modelling of the finite element models is performed in Ansys SpaceClaim [5].
- Structural and modal analyses is performed in Ansys Workbench [6] and Ansys Mechanical [7].

1 Introduction

1.1 Background

The "Beam-based Finite Element Modelling of Herøysund Bridge" project task is based on initiatives surrounding the Herøysund bridge in Herøy municipality, Nordland Fylkeskommune. The initiative is managed by Nordland fylkeskommune and Statens Vegvesen in partnership with UiT Narvik, NTNU, and SINTEF. The work on this paper was supported by the project Herøy FoU [100397]. In 2017, the Herøysund bridge was evaluated, and detrimental chlorides were discovered in the concrete structure. Attempts were made to restore the bridge, but additional damage was discovered during the restorations; consequently, the bridge was closed to heavy traffic. In several locations, it was discovered that the conduits for the post tensioning tendons lacked up to 50%of injection grout and that there was corrosion in the post tensioning tendons. It was determined that the damage was too extensive to restore, so a new bridge would be built nearby. The old bridge will remain accessible until the new bridge is completed in 2024, but with weight restrictions (max 50 tonnes). Further Nordland Fylkeskommune and Statens Vegvesen decided to put this bridge as an example for scientific study where the researchers can work and collaborate on various technologies that are classified into four work packages:

WP1: Structural health monitoring.
WP2: Corrosion inspection, assessment, and repair.
WP3: Structural assessment with damaged post-tension.
WP4: Reliability and uncertainty quantification.

The work on this thesis is part of WP1, where the main task is to make two finite element models of Herøysund bridge, one solid element model and one beam element model, then analyze them to find their natural frequencies and mode shapes, then compare results. Further the main goal of the Herøy FoU is to determine why defects manifested in the bridge's construction, how to prevent these issues in the future to make bridges safer and to develop structural health monitoring techniques in order to have better operations and maintenance routines. By doing so we can decrease the down time of the bridge which has a great impact on the economy of the region. According to the senior scientist in SINTEF, Tor Arne Martius-Hammer, the results from Herøy FoU will contribute to savings of at least 100 billion NOK, and the decrease of estimated carbon emissions of at least 10000 tonnes the next 10 years [8]. UiT assigned some of the project's duties as master's theses, and this is where this master thesis begins.

1.2 Problem description

The modelling of structures is nowadays a fundamental step in the design and assessment processes of structures because engineers need to understand the behaviour of a structure subjected to different load conditions. Usually, the modelling is performed using commercial software based on the Finite Element Modelling (FEM) principle. During the modelling procedure, some critical issues must be considered: the element to be used for modelling the structural members (mono-, bi-, tri-dimensional elements), their schematization, the material mechanical properties, the applied loads and masses, and the boundary restraints. The choice of these parameters is not trivial since it affects (sometimes sensibly) the response of the model and its reliability in representing the actual structural behaviour.

The main task of this master thesis is to model a beam-based finite element model of a bridge case study, the Herøysund bridge, using the commercial software Ansys [9]. The bridge case study is located in Nordland, and it will be in-situ tested in the near future. Hence, the developed model must represent as accurately as possible the actual behaviour of the bridge to be used for the design and then the interpretation of the experimental test outcomes.

Further while the candidate was working on the thesis, the candidate found several interesting aspects that could be added to further develop the finite element model in light of this master thesis. This includes the following aspects:

- Structural analysis.
- Modal analysis.
- Modal assurance criterion (MAC).
- Participation factor analysis.

These aspects are included in the work of this master thesis.

1.3 Delimitation of task

Modelling and analysing an entire bridge using the finite element method is a large undertaking, and given the project's available resources, it is necessary to limit the scope of the modelling and analysis to the most essential and pertinent aspects. The candidate has chosen to restrict the scope of the assignment so that the project will produce two finished and functional finite element models, first a solid element model and then a beam element model derived from the solid model.

Consequently, the task is limited at various stages in certain activities. The candidate desires more time for preliminary research and case studies in order to delve deeper into the subject matter, as well as more time with seasoned experts in the field. But primarily, the candidate wishes they had more time to delve deeper into the results of the analyses and examine additional load cases, but there is not enough time in the thesis to do so. Additional load cases are recommended for future work.

Since the primary objective of this thesis is to model a solid and a beam model and determine their natural frequencies and modal shapes in order to compare them with operational mode analyses in the future, therefore various load cases (i.e. wind loads, traffic loads etc.) are disregarded. The structural analyses primarily serve as pre-stress conditions for the modal analyses, but they are also used to validate the mesh and make general observations regarding the structural health of the bridge construction subjected to loads from its own mass and gravity.

1.4 Thesis framework

All work from beginning to end will be documented through the thesis report in accordance with the project description's guidelines. At the conclusion of the endeavour on 5/15/23, all documentation will be delivered to supervisors and sensors for evaluation.

The thesis was executed in accordance with the NS-EN standards and Statens Vegvesens directives, which are elucidated upon in the report. The execution of the project requires proficiency with finite element modelling (Ansys SpaceClaim 2023 R1 [5]), analytical calculations, numerical methods, elasticity theory, numerical structural and modal analyses (ANSYS Workbench 2023 R1 [6] and Ansys Mechanical 2023 R1 [7]), and scientific report writing. The candidate has acquired advanced skills of these topics through a master's degree in engineering design from UiT, as well as through personal experiences during FEM projects and 2.5 years of professional engineering experience.

On this endeavour, the candidate will devote 645 hours. There is no compensation or billing during the endeavour. UiT Narvik and/or the candidate are responsible for practical work materials. The results and methodologies used in this thesis to obtain the goals of the project will be documented in a report with appendices. The finite element model and analysis files developed during the thesis work will be included in the project folder.

1.5 Objectives

The objective of this thesis is to develop two finite element models, one solid model and one beam model. Then, both models will be structurally analysed numerically by applying relevant loads and boundary conditions. This structural analysis will serve as a pre-stress condition for the thesis's primary objective, which is to acquire the natural frequencies and modal shapes of the bridge through numerical modal analysis.

Further, Macdonald Nwamma will use the models developed in this master's thesis to develop an algorithm for the optimal sensor placement of accelerometers in Herøysund bridge. In the future, the accelerometers will be mounted on the bridge to collect vibration data to obtain operational frequencies and modes from the old Herøysund bridge. The results and findings of this master thesis will be used in the future to compare with the operational modal frequencies and mode shapes.

When all results are analysed and combined, they will be used to better comprehend why the Herøysund bridge has poor structural health and to develop strategies and methods for automated structural health monitoring of bridges, that might improve and streamline operations and maintenance activities in order to make bridges structurally safer.

The candidate aims to acquire knowledge and skills regarding large finite element modelling projects, Ansys software [9], element selection and usage, structural health monitoring, relevant load cases for bridges, natural frequencies and modal shape analyses, as well as general knowledge and experience regarding bridge constructions.

1.6 Societal impact-oriented goals

The broader community objective of this thesis is to contribute to the development of improved bridge-building and maintenance techniques for the future. During the lifespan of a bridge, a substantial amount of time and money is spent in assessing and maintaining structural health. Improving the construction methods of bridges and developing methods to autonomously monitor their health can reduce the need for costly maintenance that will further reduce the down time of the structure. This can help bridge owners (government, Fylkeskommune and Statens Vegvesen) to save a substantial amount of money and time and improve the safety of bridges as described in the background section of this thesis.

Bridges in Norway are not sufficiently inspected and maintained today due to different issues like economy and lack of resources and manpower. Most of the maintenance activities must be done in the summer, so the time window is small. Norway has approximately 17000 bridges, and Statens Vegvesen has violated inspection regulations for approximately half of them, which could be due to the above-mentioned reasons. Norway has a difficult topology, stretching from 57° 57′ 31″ north latitude to 71° 8′ 2″ north latitude with mountainous terrain, which makes it difficult for supply chain of operation and maintenance equipment between different regions. Therefor the development of automated SHM routines can help to overcome some of these problems. In addition, according to current standards, a little over a thousand bridge structures in Norway have sustained severe damage. More than 650 of approximately 1150 bridges in northern Norway (counties Nordland, Troms, and Finnmark) are not inspected. Along the coast, this is a problem for both human safety and the industry that is continuously expanding, imparting increased loads and wear on an out-of-date infrastructure.

[10] [11]

The Herøysund bridge leads to the outer island Herøysund sør, where there is a fish reception facility. Each week, hefty trailers transport fish deliveries to the market across the bridge. Now that the bridge is closed to large vehicles, more vehicles with lighter cargoes must be used to transport fish to the markets. If the bridge is closed, the factory would be unable to transport fish to the market, which would be disastrous for the business and the small island community, as many of its residents work in the factory. This demonstrates the importance of bridges to a vulnerable infrastructure such as this along the coast of Norway, as well as the importance of inspecting and maintaining this infrastructure.

1.7 Impact oriented goals

Existing solutions for monitoring the structural health of bridges automatically throughout their lifecycle are lacking. The technology for SHM is currently in development in various research groups in Europe. Herøysund bridge has very limited documentation for structural health and lifecycle maintenance surveillance. From the year 2020 forward, there is only one 2D structural analysis performed on the bridge, and there is no 3D finite element model for the bridge available at this time. In this thesis, a 3D finite element model which will form the basis for further development of SHM based solutions in Norway. Findings from the Herøy FoU can be used, for instance, to assess the structural health of the new bridge over time, thereby improving safety, streamlining operations and maintenance, and preserving the intended functionality of vital and vulnerable infrastructure. This can also enhance the current engineering practise of assessing the structural integrity of existing structures.

1.8 Cost/ benefit

As there is no existing beam-based finite element model for the Herøysund bridge, the results of this endeavour will be unique. In the future, the results may make monitoring the structural integrity of bridges and other similar structures simpler, less time-consuming, and less expensive. Instead of companies investing a great deal of time assessing the health of a structure, the structure's health may be monitored automatically; this will result in earlier detection of structural damage or problems and more precise localization of the structural damage problem within the structure. Thus, service personnel can address the issue directly and resolve it more efficiently, cheaply, and quickly.

1.9 Herøysund bridge history

1.9.1 Construction

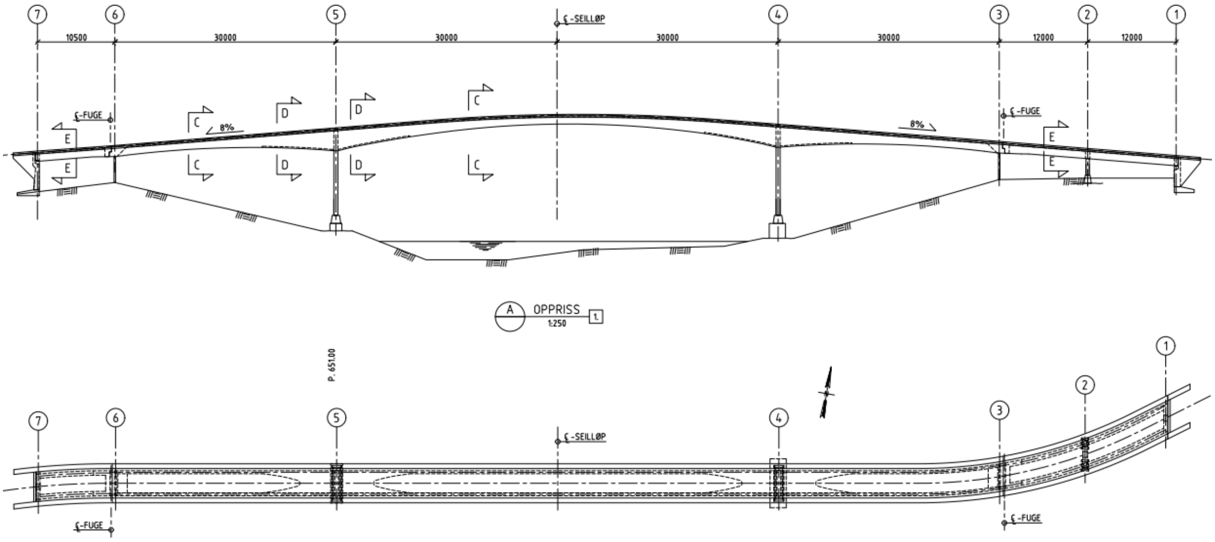

Figure 1: Overview of the bridge including axes and some dimensions. [12]

The Herøysund bridge is a cast-in-place concrete post-tensioned bridge with seven axes consisting of five pillars and two land vessels, a bridge plate, and two concrete load-bearing beams. The post tensioning system is installed on four axes, including the middle axes and the corresponding axes (axes 3 to 6). The bridge connects the two islands of Nord Herøy and Sør-Herøy to country road 828 along the coast of Helgeland in northern Norway. It has a length of 154.5 metres and a width of 5.3 metres. The bridge was completed and opened to traffic in 1966. The main span (axes 4 to 5) measures 60 metres in length and was constructed according to weight regulations 2/1958. There are two pressure plates positioned at the main pillars (axis 4 and 5). The primary portion of the bridge, from axis 3 to axis 6, is braced. The viaducts are girder structures with lax reinforcement. There is no excess reinforcement along the length of the beams. Since the bridge was constructed in the 1960s, we do not have access to the original construction calculations. It is presumed that the cross-section has been dimensioned so that tensile stresses do not occur in the cross section of the bridge.

1.9.2 Rehabilitation

In 2017, it was discovered that the bridge's construction was flawed due to excessive chlorides in the concrete that could corrode the rebars and tendons. In addition, there were cracks on the beams distributed over approximately 15 metres in the middle of the main span, with the largest fracture measuring between 0.5 millimetres and 0.9 millimetres at the foot of the beams. The bridge is also subject to increased traffic volumes, which may have resulted in increased tensile forces in the bridge since it was constructed and because of its intended use. [13]

Due to this, it was decided to restore the bridge with cathodic protection and mechanical repairs. During the rehabilitation of the bridge in 2020, additional damages and construction flaws were discovered, despite the bridge's strengthening. It was discovered that the channels for the post-tensioned tendons were inadequately injection grouted, with only about 50%injection grout in some areas. In addition, some of the tendons in the post-tensioning system were corroded, and some of the wires' threads were fractured. [14]

The capacity of the post tensioning system may be nullified by a lack of injection and subpar grouting. This results in an excessive utilization of the moment capacity in sections of the primary span. [15]

1.9.3 Current state

The bridge will remain accessible until 2024, when the replacement bridge is scheduled to open. There are restrictions on heavier traffic, so the utmost weight is limited to 50 tonnes. The bridge is slated for demolition after the new bridge is fully functional and opened, and the scientific work is finished.

1.10 Literature studies

During the initial phase of this thesis, a comprehensive literature review was conducted. The candidate has received an abundance of documentation regarding the bridge from the project managers and collaborators. Important portions of this documentation have been thoroughly read, noted, and incorporated into the report, see [8], [10], [11], [12], [13], [14], [15], [16], [23], [24], [25], [27], [28] in the works cited section.

1.11 Case studies

The supervisor Vanni Nicoletti has given the candidate an extensive completed finite-element model of the cable bridge “Filomena Delli Castelli”. The candidate has examined this case extensively and learned and understood its intricate details. In addition, a Chalmers University of Technology project report titled "Concrete Bridge Design with FEM" has been thoroughly examined. [16]

The candidate has conducted case studies in the software Ansys Spaceclaim [5] to brush up on necessary modelling skills and to determine whether the bridge can be modelled in this software; it has been determined that this is possible.

The candidate has also conducted several Ansys [9] simulations pertaining to the implementation of the actual model's post-tensioning tendons. A simple beam with four tendons was modelled for this purpose, and axial forces were experimentally applied to the tendons. This effort yielded no positive results that could be applied to the actual finite element model. If the candidate had more time to research and experiment with the implementation of the post-tensioning system, a solution may have been discovered. To maintain the project's schedule, however, the experimental work had to be curtailed. This may be something to investigate further. At present, the post tensioning system is simulated by horizontal forces that compress the primary span.

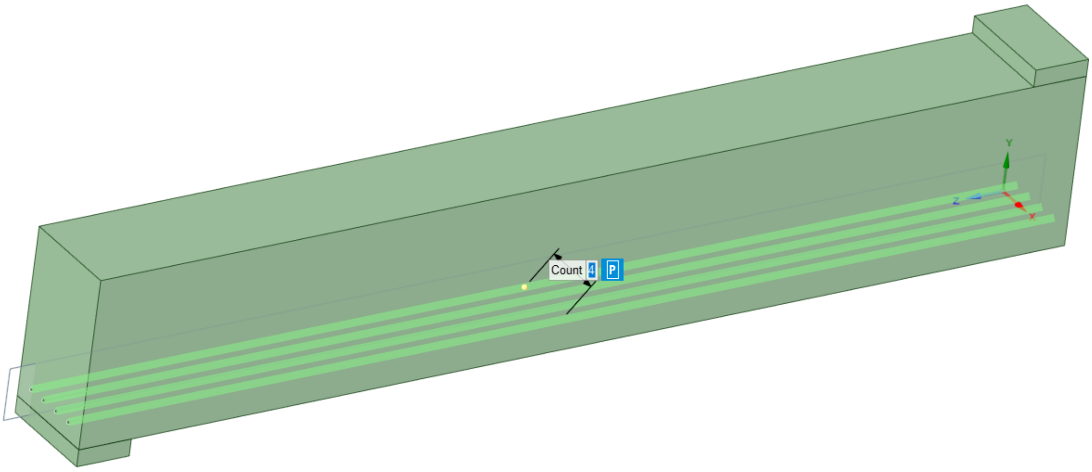

Figure 2: Case study, simple beam with tendons.

2 Governing equations

In the following sections, the governing equations for the computations of the solid model and beam model of the bridge are presented.

2.1 Solid element governing equations

Solid model numerical computations are based on the theory of elasticity. The SOLID187 and SOLID186 element is provided by Ansys [9] for this purpose. SOLID187 is a high-order 3D tetrahedral structural solid element with 10 nodes based on the theory of elasticity. The element is defined by ten nodes, each of which has three degrees of freedom (translations in the x, y, and z dimensions). SOLID187 is used for all pertinent model components, whereas SOLID186 is used for pressure cushions on land vessels and the tilting pillar and is irrelevant to the analysis of results. [17] [18]

The governing equation for elasticity theory is as below:

$$\int_V \sigma_{ij} \delta e_{ij} dV = \int_V f_i^B \delta u_i dV + \int_S f_i^S \delta u_i ds, \qquad 2.1$$

where:

σ_{ij} is the Cauchy stress component,

e_{ij} is the deformation tensor $= \frac{1}{2}\left(\frac{\partial u_i}{\partial x_j} + \frac{\partial u_j}{\partial x_i}\right)$,

u_i is the displacement,

x_i is the current coordinate,

f_i^B is the component of body force,

f_i^S is the component surface traction,

V is the volume of deformed body,

S is the surface of deformed body on which tractions are prescribed,

Further details can be found in the web page for Ansys help [19].

The internal virtual work can be indicated by:

$$\delta W = \int_V \sigma_{ij} \delta e_{ij} dV, \tag{2.2}$$

where:

W is the internal virtual work,

Jaumann rate of Cauchy stress (objective stress):

$$\dot{\sigma}_{ij}^J = \dot{\sigma}_{ij} - \sigma_{ik}\dot{\omega}_{jk} - \sigma_{jk}\dot{\omega}_{ik}, \tag{2.3}$$

where:

$\dot{\sigma}_{ij}^J$ is the Jaumann rate of Cauchy stress,

$\dot{\omega}_{jj}$is the spin tensor = $\frac{1}{2}\left(\frac{\partial v_i}{\partial x_j} + \frac{\partial v_j}{\partial x_i}\right)$,

$\dot{\sigma}_{ij}$ is the time rate of Cauchy stress,

Cauchy stress rate:

$$\dot{\sigma}_{ij} = \dot{\sigma}_{ij}^J + \sigma_{ik}\dot{\omega}_{jk} + \sigma_{jk}\dot{\omega}_{ik}, \tag{2.4}$$

Stress changes due to straining:

$$\dot{\sigma}_{ij}^J = c_{ijkl} d_{kl}, \tag{2.5}$$

where:

$C_{ijkl}d_{kl}$ is the material constitutive tensor,

d_{ij} is the rate of deformation tensor = $\frac{1}{2}\left(\frac{\partial v_i}{\partial x_j} + \frac{\partial v_j}{\partial x_i}\right)$,

v_i is the velocity,

The Cauchy stress rate can be written as:

$$\dot{\sigma}_{ij} = c_{ijkl} d_{kl} + \sigma_{ik}\dot{\omega}_{jk} + \sigma_{jk}\dot{\omega}_{ik,} \tag{2.6}$$

Further details can be found in the web page for Ansys help [19].

2.2 Beam element governing equations

Timoshenko beam theory is used to conduct numerical computations on the beam model. Ansys [9] offers the BEAM188 element for this function. BEAM188 is a linear, quadratic, or cubic 3D 2-node beam element that incorporates shear-deformation effects and is based on Timoshenko beam theory. Each node has six or seven degrees of freedom, including translation along the x, y, and z axes and rotation about the x, y, and z axes. The seventh degree of freedom, which incorporates magnitude warping, is irrelevant to this study [20] .Due to axial loads from the post tensioning system and axial loads on the pillars, the governing equation accounts for axial effects. This formulation also calculates frequencies. The equation is solved using numerical integration. Ansys [9] does not provide detailed information on what form of Timoshenko beam governing equation it is using. Therefore, the general Timoshenko beam governing equation is presented:

$$\begin{aligned} EI\left(\frac{\partial^4\omega}{\partial x^4}\right)+N\left(\frac{\partial^2\omega}{\partial x^2}\right)+\mathrm{m}\left(\frac{\partial^2\omega}{\partial t^2}\right)-\left(\mathrm{J}+\frac{mEI}{\kappa AG}\right)\frac{\partial^4\omega}{\partial x^2\partial t^2}+\frac{\mathrm{mJ}}{\kappa AG}\frac{\partial^4\omega}{\partial t^4} \\ =q+\frac{\mathrm{J}}{\kappa AG}\frac{\partial^2 q}{\partial t^2}-\frac{EI}{\kappa AG}\frac{\partial^2 q}{\partial x^2}, \end{aligned} \tag{2.7}$$

where:

m is mass (ρA)

N is an externally applied axial force,

J is ρI

ρ is density

A is the cross-section area,

E is the elastic modulus,

G is the shear modulus,

I is the second moment of area,

κ is the Timoshenko shear coefficient,

q is a distributed load.

The Timoshenko equation gives a critical frequency:

$$\omega_c=2\pi f_c=\sqrt{\frac{\kappa GA}{\rho\mathrm{I}}}, \tag{2.8}$$

Further details can be found in the HandWiki web page [21].

2.3 Modal analysis governing equation

The modal analysis in Ansys Mechanical [7] is an eigenvalue problem solved by using the following equation of motion:

$$[M]\{\ddot{u}\} + [C]\{\dot{u}\} + [K]\{u\} = \{f(t)\} \qquad 2.9$$

where:

[M] is the mass matrix,
{ü} is acceleration (second derivative of displacement),
[C] is the damping matrix,
{u̇} is the velocity (derivative of displacement)
[K] is the stiffness matrix,
{u} is the displacement
{f(t)} is the force vector.

The system is undamped for this modal analysis, hence damping = 0, thus the equation used is of the following form:

$$[M]\{\ddot{u}\} + [K]\{u\} = \{0\} \qquad 2.10$$

Solved as a frequency domain problem:

$$x = Asin(\omega t + \theta) \qquad 2.11$$

where:

A = amplitude,
ω = angular frequency,
θ = phase angle.

[22]

3 Method

In this thesis, one solid element model and one beam element model were created in the commercial parametric 3D CAD modelling software Ansys SpaceClaim direct editor [5].

When modelling a bridge as a solid 3D model with complex geometry, in a parametric 3D CAD modelling software, simplifications are typically required. When the solid model is converted into a beam model, additional simplifications are required. In order to achieve the end objective, that is to construct a beam model, additional simplifications were added to the solid model to accommodate the conversion. All the simplification procedures are described in the section below.

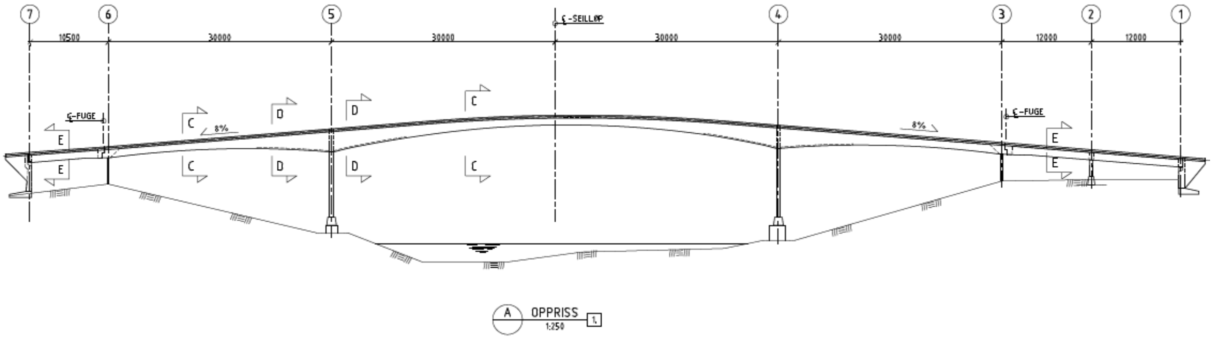

Figure 3: Vertical plane geometry of Herøysund bridge, axis 1-3 is called Sildval landspan, axis 3-6 is the main span, axis 6-7 is called Herøyholmen landspan. [12]

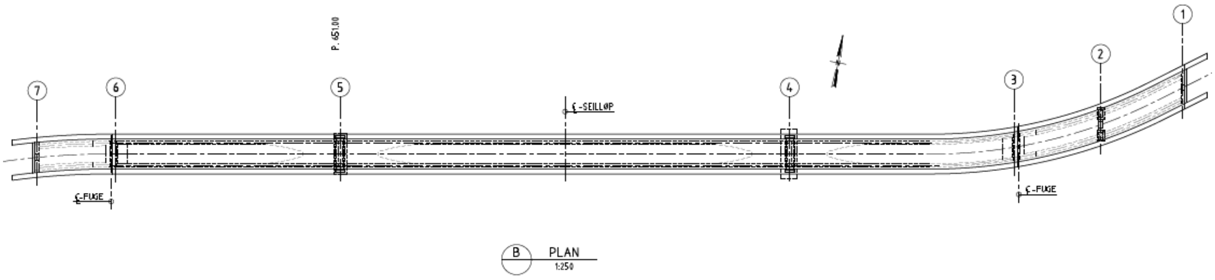

Figure 4: Horizontal plane geometry of Herøysund bridge, here the pressure plates at axis 4 and 5 is shown. [12]

3.1 Solid model method

3.1.1 Simplifications method

Following simplifications were made to the solid model:

• Horizontal plane curvature is disregarded, so the bridge is depicted as if it were perfectly straight.

• The transverse inclination of the bridge deck is disregarded, and it is assumed to be perfectly horizontal.

• Pressure plates beneath the primary pillars (axes 4 and 5) are discretized at the locations where circular/oval cuts are made in the outer extremities. These pressure plates are of 5 metre length along the longitudinal axis of the bridge and can be found in four locations: on both sides of both primary pillars, under the bridge span where the pillars meet the bridge span. Instead of modelling the oval edge of the pressure plates, the 5m sections were divided into 5 pieces, each 1m in length, and the volume of material within each component was calculated and substituted with a solid plate of the same volume. This is described with figures and calculations in the appendix B. This modification was made to the solid model to facilitate its conversion to a beam model. These simplifications are shown in the figures 5 and 6 below.

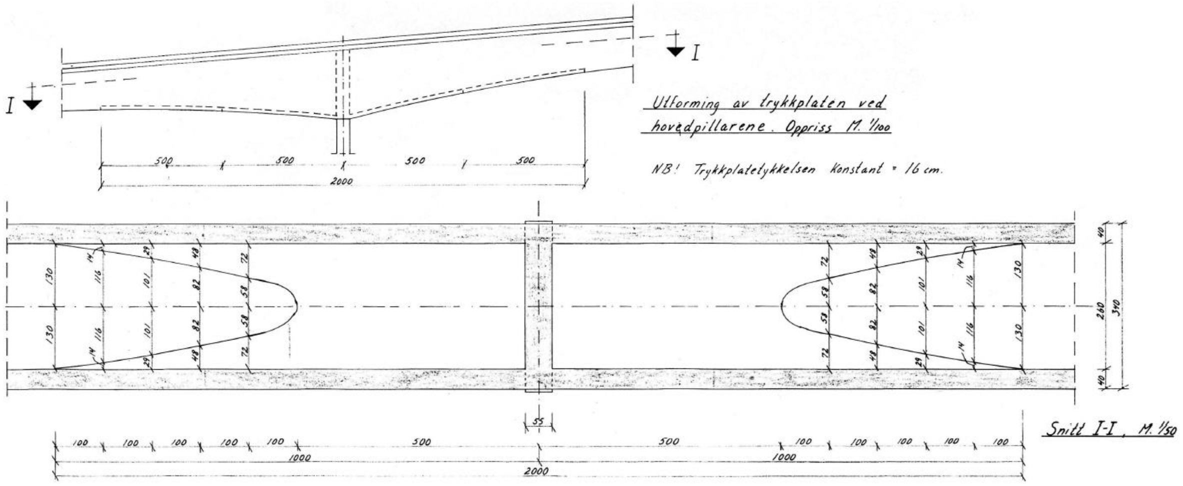

Figure 5: Geometry of the main pillar pressure plates [23]

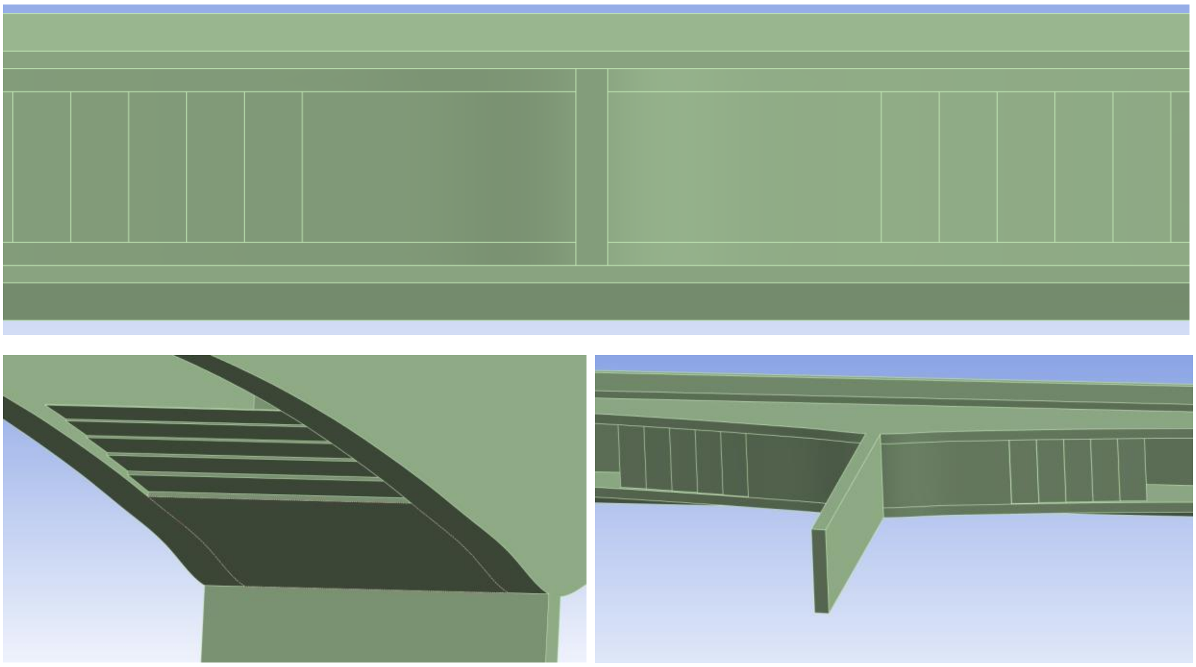

Figure 6: Discretization of the main pillar pressure plates

- The pillars are modelled as constructed, with the exception of their bases, which are not modelled because they contribute nothing structurally to the analysis.

- Rebars in the bridge's concrete are not modelled, so the reinforcement's effects are disregarded. Implementing the rebars (lax reinforcement) can be incorporated as further work.

- The post tensioning system is not modelled, but rather simplified by horizontal forces compressing the main span to simulate the post tension force. These post tensioning simulating forces are positioned just outside axis 3 and 6, where the main span begins and ends.

- According to Statens Vegvesen's "handbok V412, Bæreevneklassifisering av bruer, laster" [24], the 60 mm layer of asphalt and railing is not modelled, but rather simulated by a pressure of 7 kN/m along the longitudinal span of the bridge.

- The tilting pillar under the land span on the Sildval side (axis 2) is connected to the bridge by a joint allowing only rotation around the z axis and no translation of movement. This prevents the bridge deck from detaching from the pillar, which is unrealistic given that it can move up (+y direction) to detach from the pillar, but it is necessary to ensure the deck does not bend through the pillar downwards (-y direction). Attempting to accommodate the realistic behaviour would result in nonlinear analysis, which is undesirable for this master thesis.

- The primary pillars protrude 50 mm from the beams transversally; however, this is not modelled to prevent stress singularities in the minor faces and edges that this would cause.

3.1.2 Modelling method

The upper and lower margins of the bridge deck, as well as the lower edge of the beams, were determined using the coordinates contained in the document titled "Oversikt. Utforming av brubanen" [25] located in the project basis folder. This document pertains to the construction of the bridge, so it should be a reliable source since the objective is to model the bridge as it was initially constructed and without defects.

These spline curves were created by transferring these coordinates into a .txt file using the import type "point curve text" curve insert method. [26]

The .txt files generated for this matter will be submitted in the folder containing the compressed project files.

After importing the spline curves into SpaceClaim [5], it was only necessary to move the spline curves in order to generate surfaces that could be extruded into solids. First, a 200 mm thick bridge deck was extruded from a plane formed by the upper and lower deck curves that were 200 mm apart vertically.

Using the spline curves for the lower edge of the deck and the lower edge of the beams, a surface was then created for the beam. This surface was then extruded into a beam and joined to the bridge deck to form a single unit.

The railing surface and walking deck were created by drawing its shape on a transverse plane at one end of the bridge, then extruding this surface along the path of the bridge deck all the way to the other end of the bridge longitudinally and joining it as one solid (one coherent piece of mass) piece with the bridge deck and beam.

Taking advantage of mirroring, initially only half of the bridge was modelled transversely; it was then mirrored through a longitudinally spanning plane positioned in the bridge's transverse centre.

It was necessary to divide the bridge into its three sections, the two land spans and the central span, once the bridge's basic form had been established. This was accomplished by inserting planes through the solid and utilising them to cut through the solid. Using the coordinate sheet used to generate the spline curves, the separation and positioning of the pillars were simultaneously determined and positioned.

The solid was cut into three sections and five pillars were extruded, with four main pillars joining the main span solid and one tilting pillar constructed as a separate solid. The geometry of the pillars can be found in the document titled "Herøysund bru" [12] that can be found in the project basis folder.

The geometry of the two land vessels at each end of the bridge was derived from the documents "Landkar Herøyholmen. Forskaling og armering" [27] and "Landkar Sildval. Forskaling og armering." [28] The top portion of the land vessels was extruded from the shape of the beginning of the land spans, and the bottom portion was drawn, extruded, and united so that the land vessels became distinct solids.

The beams on the land spans are 200 mm thicker than the beams on the main span; this was achieved by transversely extruding the beams towards the midsection of the bridge span.

Then, the details between the beams were modelled, including transverse beams and reinforcements where the pillars and land vessels interact with the bridge span. These features were drawn directly onto the existing solids and then extruded and joined.

The four pressure plates at the main pillars were modelled to make subsequent construction of the beam model simpler and more accurate. These pressure plates extend 10 metres on each side from the intersection of the pillars and longitudinal beams. The first five metres have a thickness of 160 mm, while the last five metres feature an oval-shaped cut out. This ovoid cut out was discretized by volume into one-meter-long sections of flat rectangular slabs with equivalent volume. The geometry of these pressure plates can be found in the document titled "Hovedpilarer m-fundamenter. Trykkplate. Formtegning" [23] which can be found in the project basis folder. Calculations and graphics pertaining to the discretization of the pressure plates are available in the appendix B.

All the minor pressure plates were constructed as discrete solids so they could be excluded from the analysis results in the future. These pressure plates are highlighted in green in the picture below:

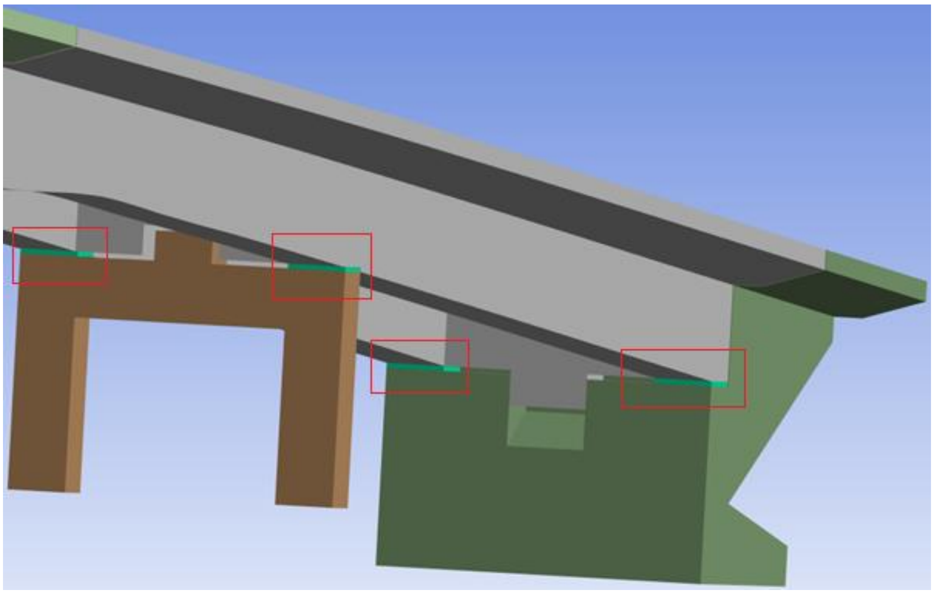

Figure 7: Pressure plates on Sildval side, axis 1-2.

3.2 Beam model method

3.2.1 Simplification method

These simplifications were made to the beam model:

- All simplifications made to the solid model have been transferred to the beam model.
- Land vessels were excluded from the beam model as there was no way to discretize them in any meaningful way to a constant cross section beam.
- Each beam section was made into approximately 1-metre-long sections, using the cross section at the middle of each section of solid. This implies that the beam model will not be a 100% representation of the real bridge, but a good estimate.
- The tilting pillar under the Sildval land span is discretized to a constant cross section. This is done by calculating the volume of the transverse beam in the top of the pillar to spread that volume over the entire height of the pillar as described in appendix B.

3.2.2 Modelling method

Using the solid model as a basis, the beam model was created. First, one-meter-long straight lines were traced along the top edge of the solid model bridge's deck. The reason for the lines being approximately one metre in length is to adjust the model to the distance between each pillar using equal lengths that are as close to one metre as possible. At the sites where the pillars meet the bridge superstructure, 0.5-meter-long lines were drawn in both directions from the connection points to accommodate pillar connections and capture the larger cross sections at these points. The actual length of the lines that do not accommodate pillars is approximately 1 metre, but adjustments have been made to ensure a satisfactory fit. After drawing all the lines along the top of the deck, new lines perpendicular to the top deck lines were positioned at the midpoints of the top deck lines. Planes were positioned along these normal lines. Each of these planes transversely slices the solid to facilitate the drafting of cross sections.

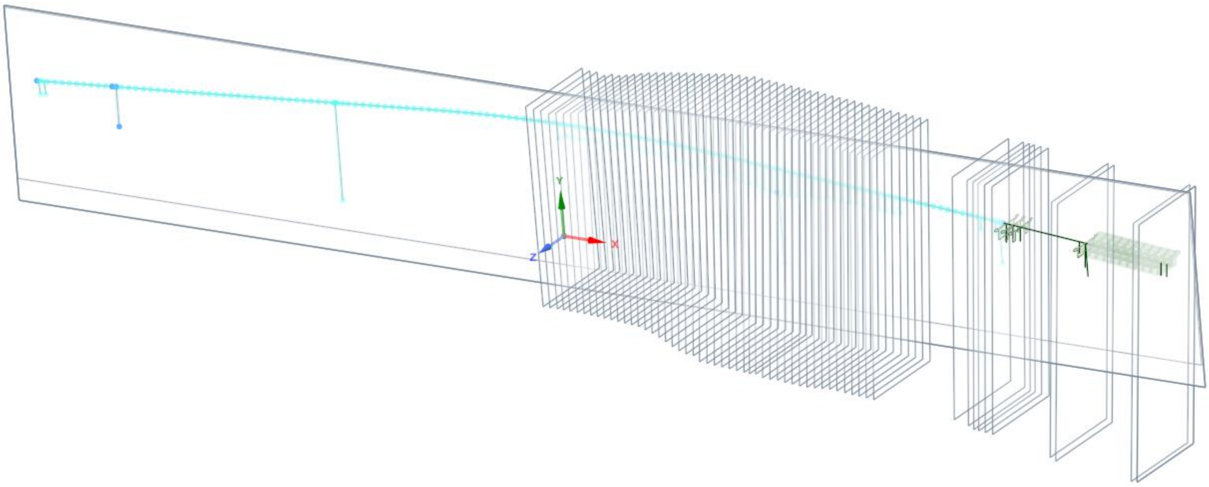

Figure 8: Planes along the bridge to capture cross sections.

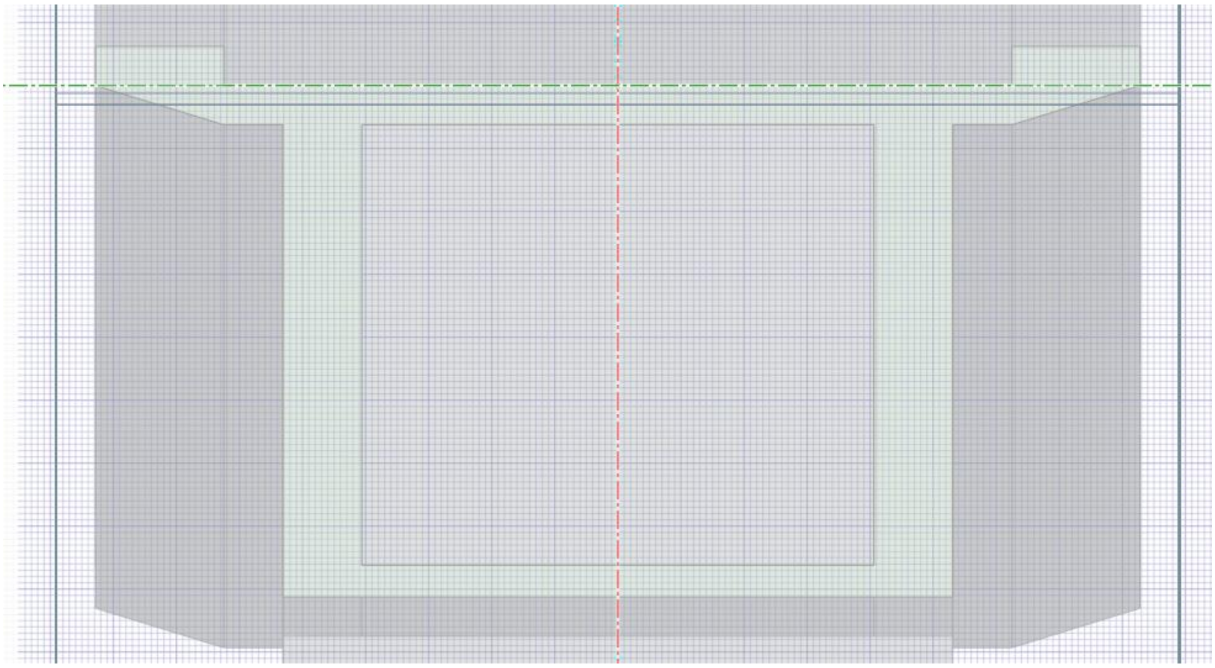

Figure 9: View of one plane capturing one cross section, close to a main pillar, including pressure plate, making it a box section.

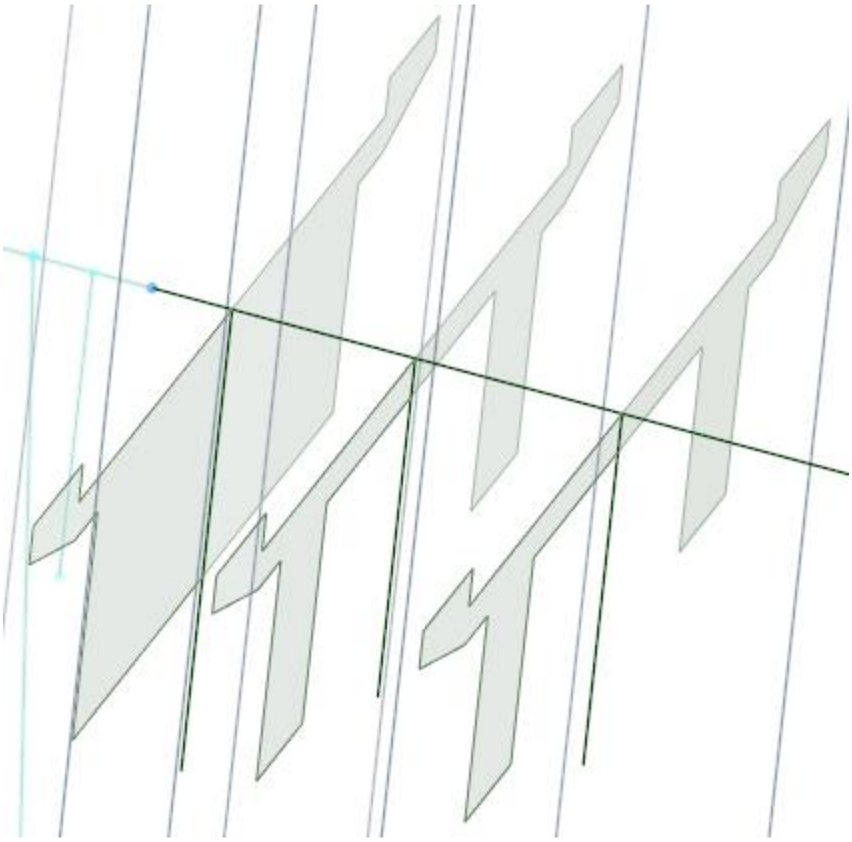

Figure 10: Three different cross sections drawn onto planes.

All cross sections were traced onto the planes, extruded to discrete solids, and then converted to beams using the Ansys SpaceClaim [5] function for solid-to-beam transformation.

The solid and planes were then removed, and cross sections were added to the top deck lines. The pillars were converted to beams by:

- Creating lines from pillar-accommodating vertices of the same length as the pillars' height.
- Placing a plane in the cross section of the pillar.
- Drawing the cross section onto the plane.
- Extruding the cross section into a solid, converting it to a beam.
- Finally applying the beam cross section to the pillar line.

The correct orientation of each beam section and the equal orientation of the section triads were given special care. When a beam section was assigned to all upper deck lines and pillars, all solids corresponding to the section were removed.

The lines were then grouped into separate components based on what bridge sections they represent (land span Herøyholmen, main span, land span Sildval, and tilting pillar under Sildval land span). Then, each component's topology was set to be shared; this bonded the beams and caused them to share vertices. Grouping into separate components using shared topology proved to be an effective method for making the beam model function as intended. Beams that share topology are bonded in one vertex, whereas beams that are not bonded by shared topology are not bonded and both vertices still exist so that they can be used for applying joints in the analysis.

As the scale of the drawings and models increased, some software issues surfaced during the solid and beam modelling process. Particularly affected was the sketching mode, where the software lagged so badly that every operation (such as drawing a line) took approximately 30 seconds. This slowed down the work considerably. It is plausible that SpaceClaim [5] is better adapted for drawing small components than large structures such as bridges. This will not be investigated further as part of this thesis. Unfortunately, this caused the modelling portion of the project to take much longer than it should have, leaving less time for model and analysis refinement.

4 Important results from the analysis

Here important results from the structural and modal analysis will be presented, including comparisons of the results between the two models.

4.1 Comparing solid and beam element model analyses

4.1.1 Deflection

Table 1: Comparison of deflections between non post tensioned and post tensioned solid and beam model.

	Without post tensioning [mm]	With post tensioning [mm]	Difference [%]
Solid	102,2	36,08	64
Beam	111,41	70,753	36,5
Difference [%]	9	96	

Table 1 shows a comparison of the effects on deflection the post tensioning is inducing on the solid and beam model. The table also compares deflections on the solid and beam model. From these results we can see the post tensioning system has more effect on the solid model than on the beam model. It is also apparent that there is a smaller difference between the deflections of the models when the post tensioning system is removed. To get a clue on which model to put confidence in, these results can be compared to other structural analyses and real-world tests conducted in the report from AAS-Jacobsen titled “18-1069 Herøysund bru. Bæreevneberegninger” [15].

In the AAS-Jacobsen report there have been conducted a structural analysis and real-world test placing 50 tonnes evenly distributed over the middle of the main span.

The AAS-Jacobsen analysis gave a deflection of the middle of the main span of 45 mm, and in the real-world test they measured 31 mm to 33 mm deflection in the middle of the main span. Since they in the AAS-Jacobsen report compare these results, it is unclear if the deflection results from their analysis is presented excluding the deflection from mass of the bridge and gravity as the measured deflection cannot include deflection from mass of the bridge and gravity.

The same case of 50 tonnes evenly distributed on 16 metres in the middle of the main span was added to both the beam and solid model in this analysis, which gave these results:

Deflection solid = 41,338 mm, deflection beam = 40,037 mm.

Holding this together with the high deflection of the beam model (70,753 mm) and relatively low deflection of the solid model (36,08 mm) found in this thesis, the results from the solid model is considered to be the most reliable. The solid element technology (Elasticity theory) should be more precise than the beam element technology (Timoshenko), even though the solid element has weaknesses like being prone to stress singularities and locking. The beam element is a simplified theory where cross section information is given to the centre line of the beam as stiffness information. It is possible the way of simulating the post tensioning system used in this thesis malfunctions with the beam element technology.

4.1.2 Volume and mass

Table 2 below shows a difference in volume and mass between the solid and beam model of 0,24%, which is an acceptable difference and well within the accuracy one would expect from a conversion between solid and beam element models.

Table 2: comparison of volume and mass of the solid and beam model.

	Volume [m^3]	Mass [Kg]
Solid	445,15	1062300
Beam	444,1	1064800
Difference [%]	0,24	0,24

4.1.3 CPU time

Table 3: Specifications of the computer used for the analyses.

Processor	Intel® Core™ i9-10980XE CPU @ 3.00 GHz
RAM	128 GB

Table 4: CPU time comparison for static structural analysis.

Parameter	Solid element model	Beam element model
Total CPU time for all threads	50,9 seconds	1,9 seconds
Sum of memory used on all processes	10115 MB	546 MB
Total amount of I/O written to disk	3.3 GB	0,0 GB
Total amount of I/O read from disk	1,7 GB	0,0 GB

Table 5: CPU time comparison for modal analysis.

Parameter	Solid element model	Beam element model
Total CPU time for all threads	166,6 seconds	3,8 seconds
Sum of memory used on all processes	20406 MB	205 MB
Total amount of I/O written to disk	6.6 GB	0,1 GB
Total amount of I/O read from disk	84 GB	0,4 GB

Table 4 and 5 shows CPU time for Structural and odal analyses respectively. Comparing the CPU time of solid and beam analyses, it is apparent that the beam model requires a lot less resources to compute than the solid model, which can be useful for quick analyses when low on computing power or if the analyses is made more complex in the future. Although the engineering hours required to convert the solid model to a beam model (approximately 75 hours) is most likely not worth it compared to buying more computing power.

4.1.4 Frequencies and modal shapes

For the modal analysis both models have been analysed using the same static structural precondition as pre-stress. The results from both models were then compared to each other using the modal assurance criterion index.

4.1.4.1 Modal assurance criterion theory

The modal assurance criterion between two real solutions is computed using the equation:

$$mac\left(\o_i^{(1)}, \o_j^{(2)}\right) = \frac{(\o_i^{(1)^t} \cdot m^{(k)} \cdot \o_j^{(2)})^2}{(\o_i^{(1)^t} \cdot m^{(k)} \cdot \o_i^{(1)})(\o_j^{(2)^t} \cdot m^{(k)} \cdot \o_j^{(2)})} \qquad 4.1$$

Where:

$\o_i^{(1)}$ is the i’th solution vector of solution 1. (From file 1)

$\o_j^{(2)}$ is the j’th solution vector of solution 2. (From the .rst file)

[29]

4.1.4.2 Modal assurance criterion

The modal assurance criterion is used to compare the modes extracted from the solid model to the modes extracted from the beam model. It gives answers to how similar each mode in the two models is in a table and presents them as values ranging from 0 to 1 in each cell, where 0 means the modes are totally different, and 1 means the modes are exactly the same. These numbers can of course be multiplied by 100 to give a percentage of match.

First a general comparison between all the modes was extracted. Nodes in both models was automatically matched to the nearest nodes, and their eigenvectors was compared. A node matching tolerance of 10 mm was used.

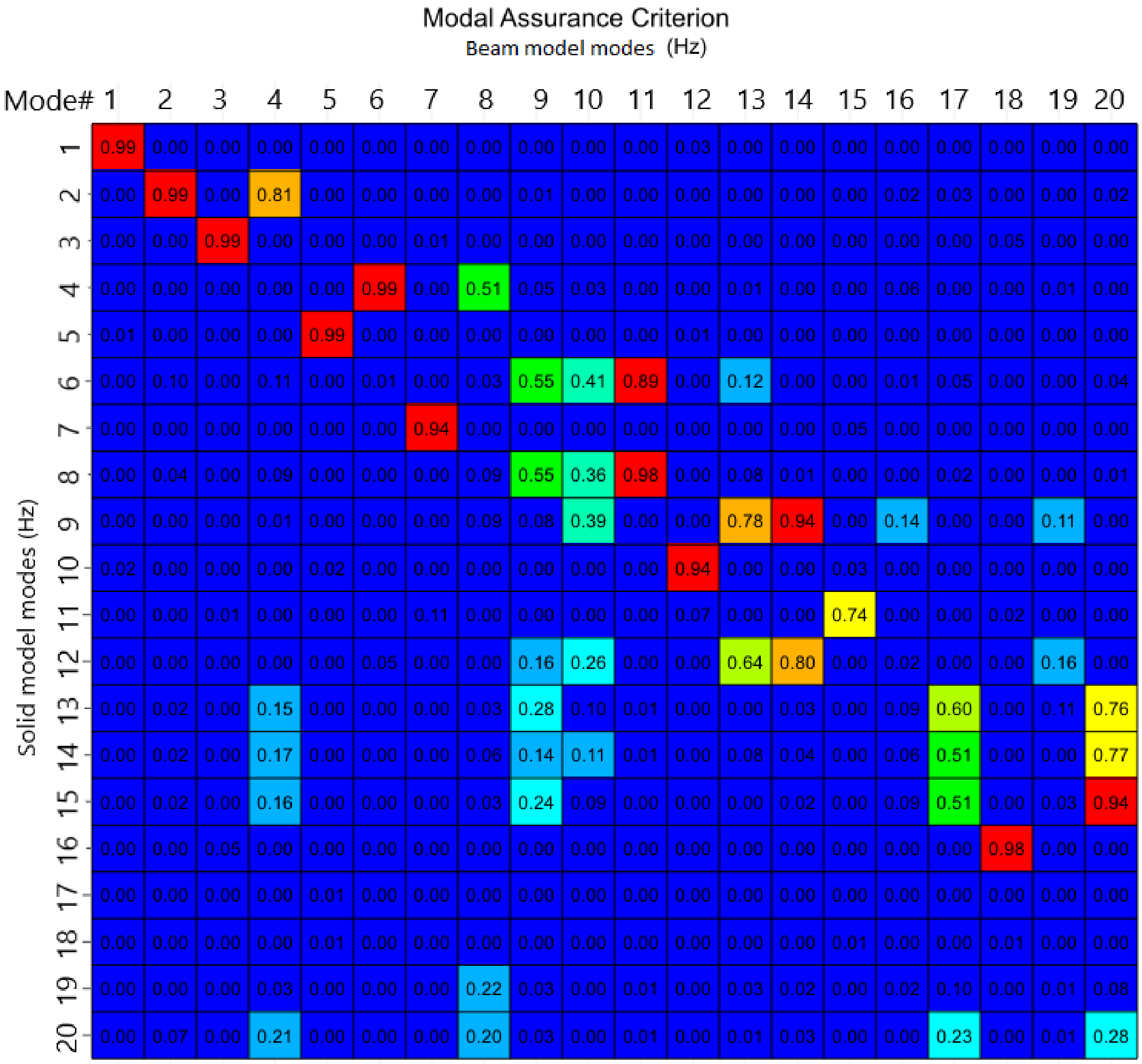

Mode#	1	2	3	4	5	6	7	8	9	10	11	12	13	14	15	16	17	18	19	20
1	0.99	0.00	0.00	0.00	0.00	0.00	0.00	0.00	0.00	0.00	0.00	0.03	0.00	0.00	0.00	0.00	0.00	0.00	0.00	0.00
2	0.00	0.99	0.00	0.81	0.00	0.00	0.00	0.00	0.01	0.00	0.00	0.00	0.00	0.00	0.00	0.02	0.03	0.00	0.00	0.02
3	0.00	0.00	0.99	0.00	0.00	0.00	0.01	0.00	0.00	0.00	0.00	0.00	0.00	0.00	0.00	0.00	0.00	0.05	0.00	0.00
4	0.00	0.00	0.00	0.00	0.00	0.99	0.00	0.51	0.05	0.03	0.00	0.00	0.01	0.00	0.00	0.06	0.00	0.00	0.01	0.00
5	0.01	0.00	0.00	0.00	0.99	0.00	0.00	0.00	0.00	0.00	0.00	0.01	0.00	0.00	0.00	0.00	0.00	0.00	0.00	0.00
6	0.00	0.10	0.00	0.11	0.00	0.01	0.00	0.03	0.55	0.41	0.89	0.00	0.12	0.00	0.00	0.01	0.05	0.00	0.00	0.04
7	0.00	0.00	0.00	0.00	0.00	0.00	0.94	0.00	0.00	0.00	0.00	0.00	0.00	0.00	0.05	0.00	0.00	0.00	0.00	0.00
8	0.00	0.04	0.00	0.09	0.00	0.00	0.00	0.09	0.55	0.36	0.98	0.00	0.08	0.01	0.00	0.00	0.02	0.00	0.00	0.01
9	0.00	0.00	0.00	0.01	0.00	0.00	0.00	0.09	0.08	0.39	0.00	0.00	0.78	0.94	0.00	0.14	0.00	0.00	0.11	0.00
10	0.02	0.00	0.00	0.00	0.02	0.00	0.00	0.00	0.00	0.00	0.00	0.94	0.00	0.00	0.03	0.00	0.00	0.00	0.00	0.00
11	0.00	0.00	0.01	0.00	0.00	0.00	0.11	0.00	0.00	0.00	0.00	0.07	0.00	0.00	0.74	0.00	0.00	0.02	0.00	0.00
12	0.00	0.00	0.00	0.00	0.00	0.05	0.00	0.00	0.16	0.26	0.00	0.00	0.64	0.80	0.00	0.02	0.00	0.00	0.16	0.00
13	0.00	0.02	0.00	0.15	0.00	0.00	0.00	0.03	0.28	0.10	0.01	0.00	0.00	0.03	0.00	0.09	0.60	0.00	0.11	0.76
14	0.00	0.02	0.00	0.17	0.00	0.00	0.00	0.06	0.14	0.11	0.01	0.00	0.08	0.04	0.00	0.06	0.51	0.00	0.00	0.77
15	0.00	0.02	0.00	0.16	0.00	0.00	0.00	0.03	0.24	0.09	0.00	0.00	0.00	0.02	0.00	0.09	0.51	0.00	0.03	0.94
16	0.00	0.00	0.05	0.00	0.00	0.00	0.00	0.00	0.00	0.00	0.00	0.00	0.00	0.00	0.00	0.00	0.00	0.98	0.00	0.00
17	0.00	0.00	0.00	0.00	0.01	0.00	0.00	0.00	0.00	0.00	0.00	0.00	0.00	0.00	0.00	0.00	0.00	0.00	0.00	0.00
18	0.00	0.00	0.00	0.00	0.01	0.00	0.00	0.00	0.00	0.00	0.00	0.00	0.00	0.00	0.01	0.00	0.00	0.01	0.00	0.00
19	0.00	0.00	0.00	0.03	0.00	0.00	0.00	0.22	0.03	0.00	0.01	0.00	0.03	0.02	0.00	0.02	0.10	0.00	0.01	0.08
20	0.00	0.07	0.00	0.21	0.00	0.00	0.00	0.20	0.03	0.00	0.01	0.00	0.01	0.03	0.00	0.00	0.23	0.00	0.01	0.28

Figure 11: Modal assurance criterion using unpaired modes, comparing modes 1-20 in both models.

In figure 11 it is shown what modes match and how good the match is, comparing all 20 first modes of the solid model to all the 20 first modes of the beam model. But there is a way to show this in a compressed table, containing only the important information using “mode pairing”.

Modes were paired using the “pair modes” function in the MAC calculator, this function sets several criteria for the mac table, and with the correct settings it only shows the modes with a good match between the two models in the MAC table. These criteria take into account how good match there is between the frequencies of each mode in addition to the regular MAC criterions. More information about mode pairing can be found in the Ansys help web page [30].

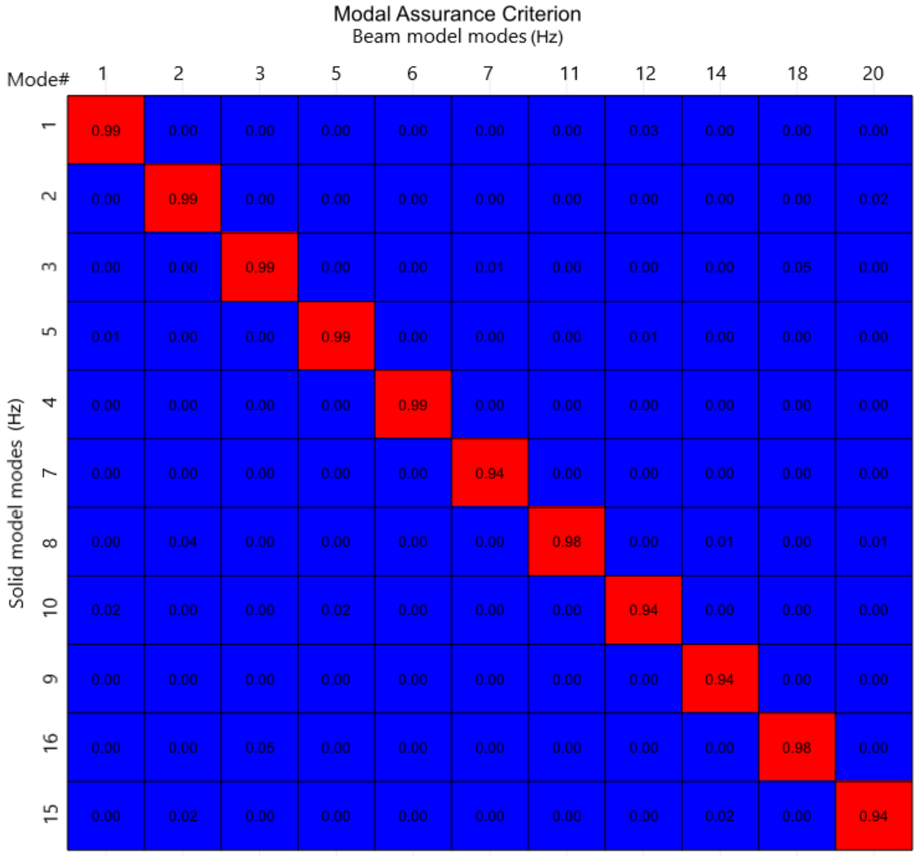

Mode#	1	2	3	5	6	7	11	12	14	18	20
1	0.99	0.00	0.00	0.00	0.00	0.00	0.00	0.03	0.00	0.00	0.00
2	0.00	0.99	0.00	0.00	0.00	0.00	0.00	0.00	0.00	0.00	0.02
3	0.00	0.00	0.99	0.00	0.00	0.01	0.00	0.00	0.00	0.05	0.00
5	0.01	0.00	0.00	0.99	0.00	0.00	0.00	0.01	0.00	0.00	0.00
4	0.00	0.00	0.00	0.00	0.99	0.00	0.00	0.00	0.00	0.00	0.00
7	0.00	0.00	0.00	0.00	0.00	0.94	0.00	0.00	0.00	0.00	0.00
8	0.00	0.04	0.00	0.00	0.00	0.00	0.98	0.00	0.01	0.00	0.01
10	0.02	0.00	0.00	0.02	0.00	0.00	0.00	0.94	0.00	0.00	0.00
9	0.00	0.00	0.00	0.00	0.00	0.00	0.00	0.00	0.94	0.00	0.00
16	0.00	0.00	0.05	0.00	0.00	0.00	0.00	0.00	0.00	0.98	0.00
15	0.00	0.02	0.00	0.00	0.00	0.00	0.00	0.00	0.02	0.00	0.94

Figure 12: Modal assurance criterion using paired modes.

In figure 12 it is shown what modes correspond well (over 90%). The factor of correlation is shown in each cell, where 0 is completely different and 1 is completely similar.

Table 6: Frequency comparison between paired modes on solid and beam model including their respective MAC values.

Solid mode#	Beam mode#	Frequency error	MAC
Mode 1	Mode 1	-0,1 Hz (-4,3%)	0,995
Mode 2	Mode 2	-0,4% (-18,9%)	0,988
Mode 3	Mode 3	0,0 Hz (0%)	0,994
Mode 5	Mode 5	0,2 Hz (5,5%)	0,993
Mode 4	Mode 6	-0,7 Hz (-17,4%)	0,991
Mode 7	Mode 7	-0,3 Hz (-6,4%)	0,940
Mode 8	Mode 11	-0,7 Hz (-12,5%)	0,977
Mode 10	Mode 12	-0,2 Hz (-2,6%)	0,943
Mode 9	Mode 14	-0,8 Hz (-10,5%)	0,935
Mode 16	Mode 18	-0,4 Hz (3,9%)	0,978
Mode 15	Mode20	-1,6 Hz (14,5%)	0,936

In table 6 the modes with a good match is shown including a frequency comparison between paired modes on the solid and beam model and their MAC values. Frequency errors range from 0% to 18,9%, while MAC values range from 93,5% to 99,5%.

4.1.4.3 Matched modes

Here the 11 modes that gave a correspondence above 90% is shown side by side for a visual comparison of the mode shapes.

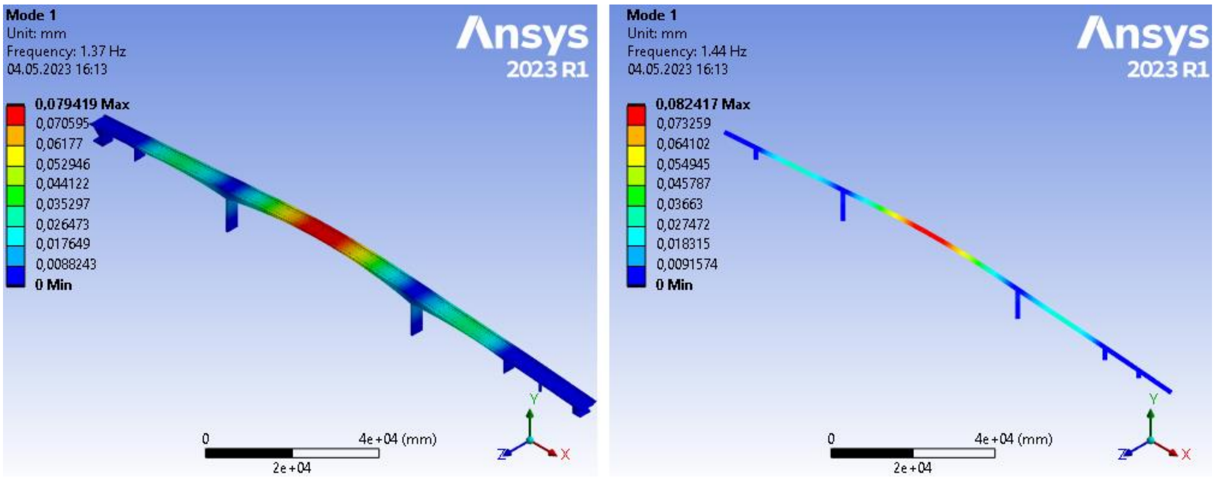

Figure 13: Mode 1 on the solid model matched by 99,5% with mode 1 on the beam model. Frequency error: -4,3%.

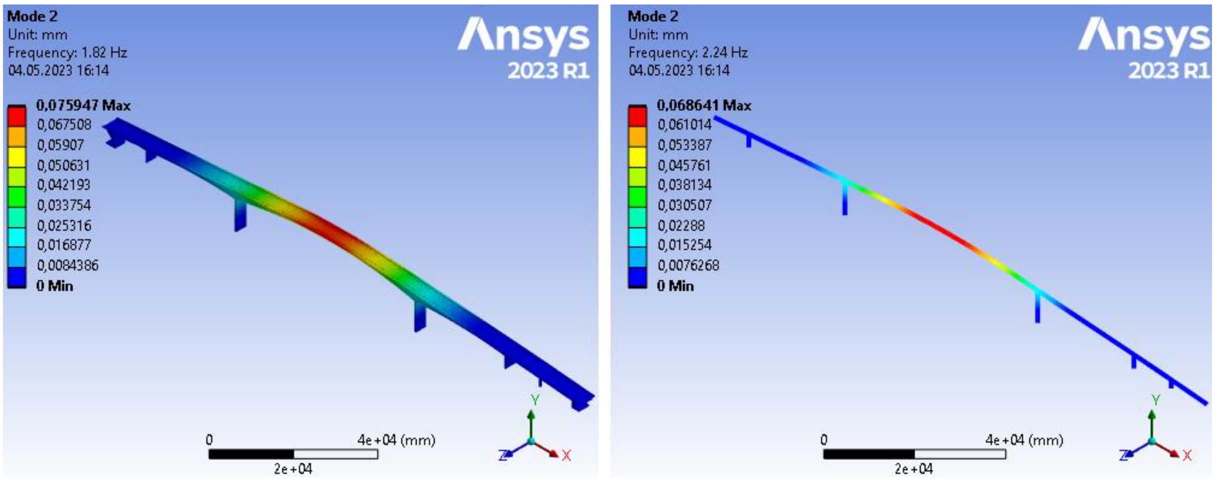

Figure 14: Mode 2 on the solid model matched by 98,8% with mode 2 on the beam model. Frequency error: -18,9%.

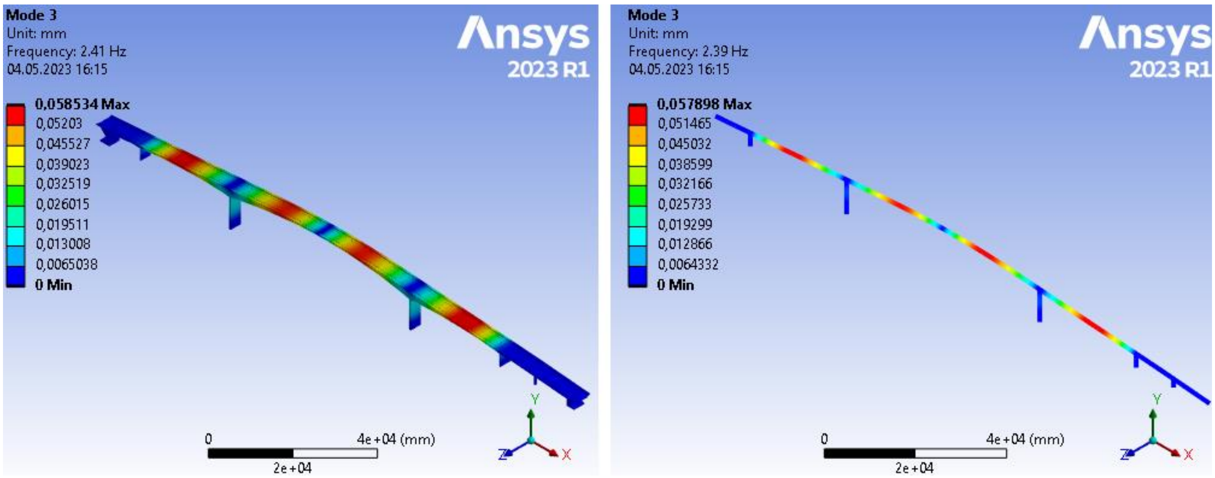

Figure 15: Mode 3 on the solid model matched by 99,4% with mode 3 on the beam model. Frequency error: 1%.

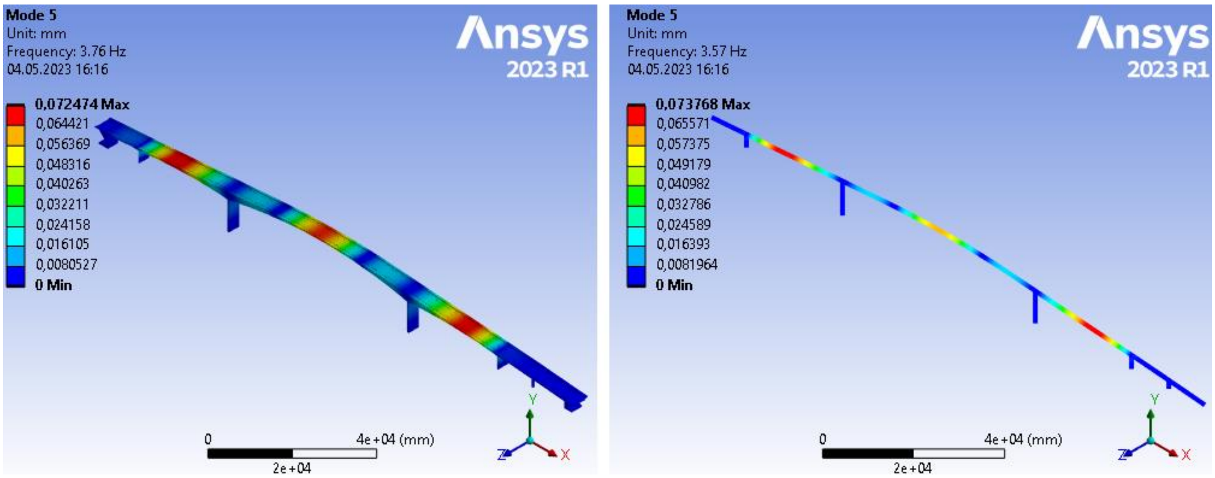

Figure 16: Mode 5 on the solid model matched by 99,3% with mode 5 on the beam model. Frequency error: 5,5%.

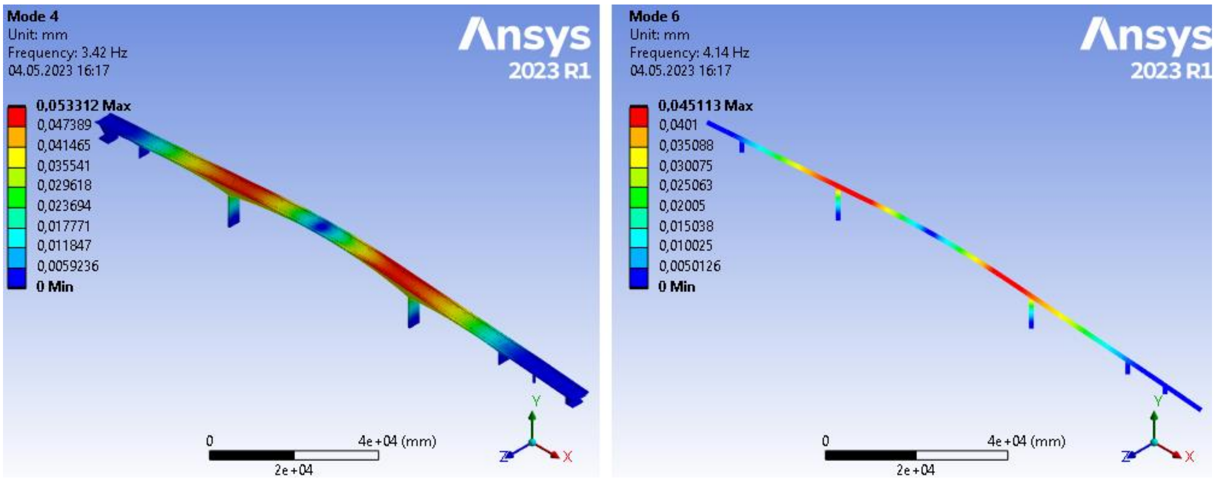

Figure 17: Mode 4 on the solid model matched by 99,1% with mode 6 on the beam model. Frequency error: -17,4%.

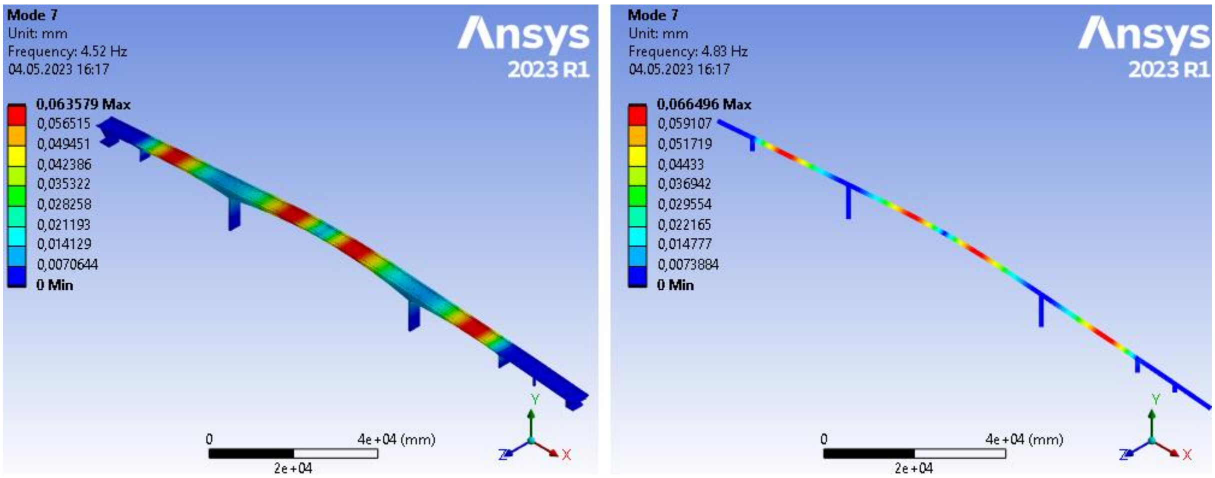

Figure 18: Mode 7 on the solid model matched by 94% with mode 7 on the beam model. Frequency error: -6,4%.

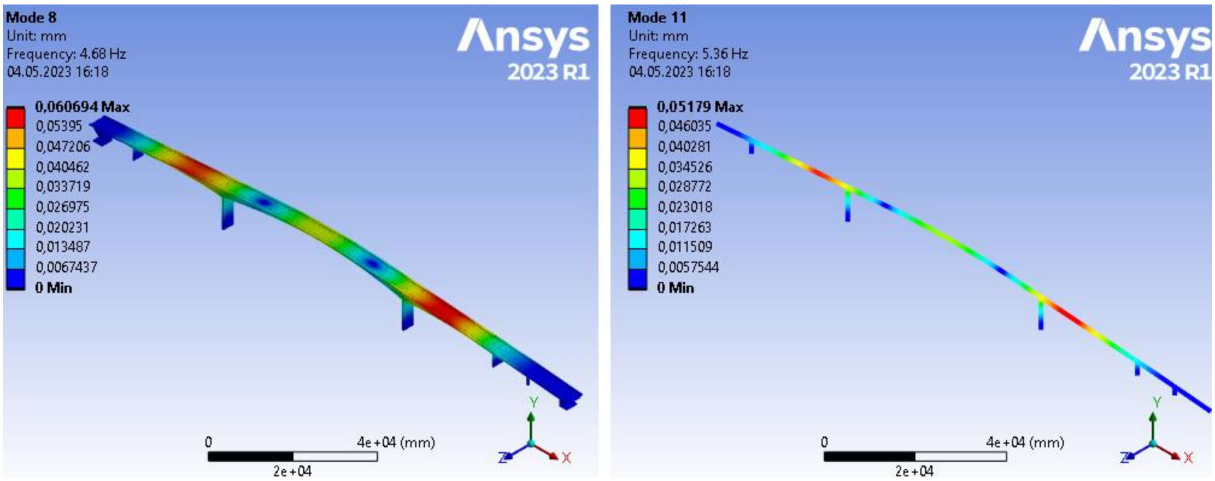

Figure 19: Mode 1 on the solid model matched by 97,7% with mode 1 on the beam model. Frequency error: -12,5%.

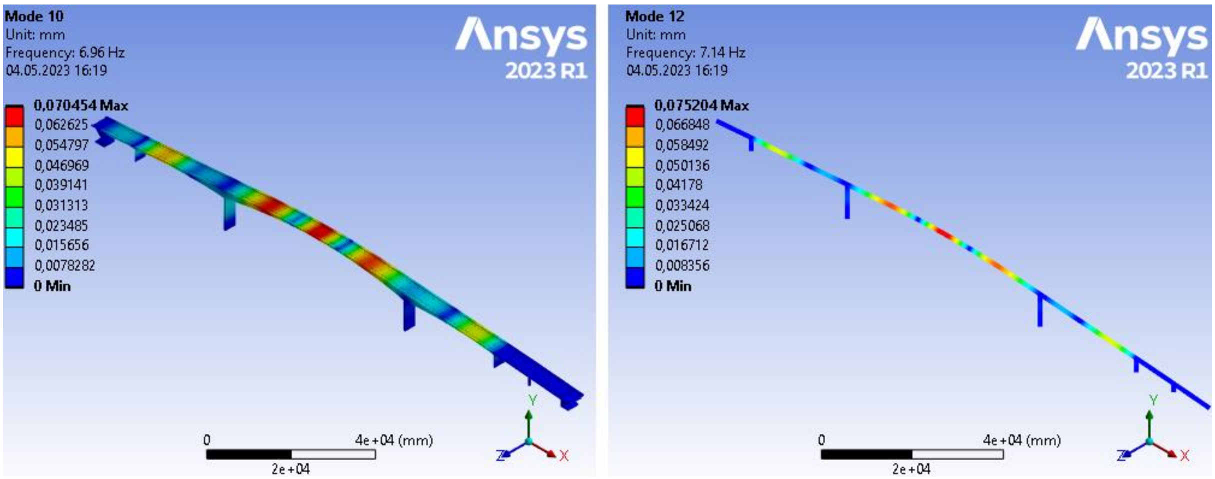

Figure 20: Mode 10 on the solid model matched by 94,3% with mode 12 on the beam model. Frequency error: -2,6%.

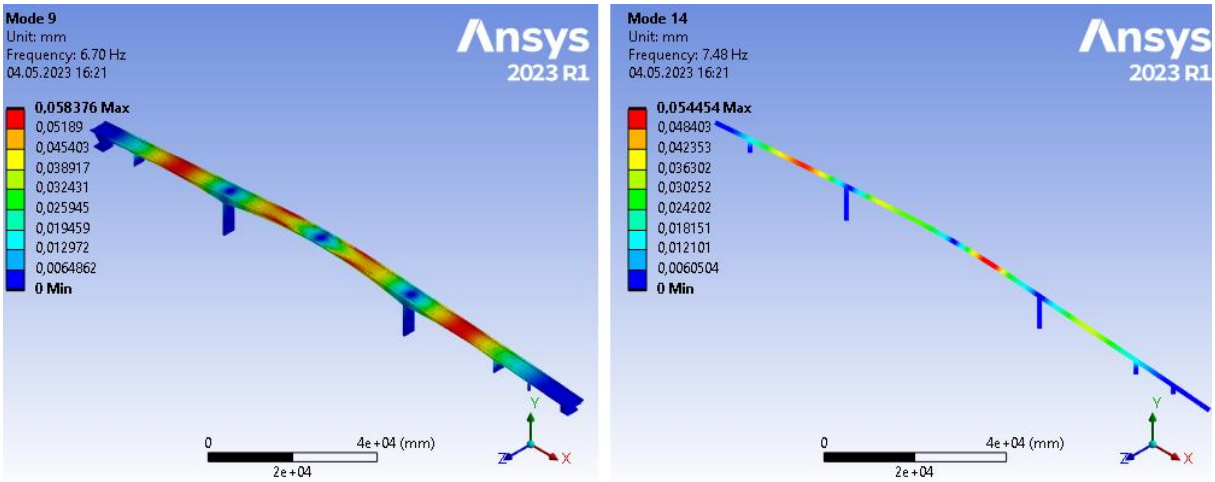

Figure 21: Mode 9 on the solid model matched by 93,5% with mode 14 on the beam model. Frequency error: -10,5%.

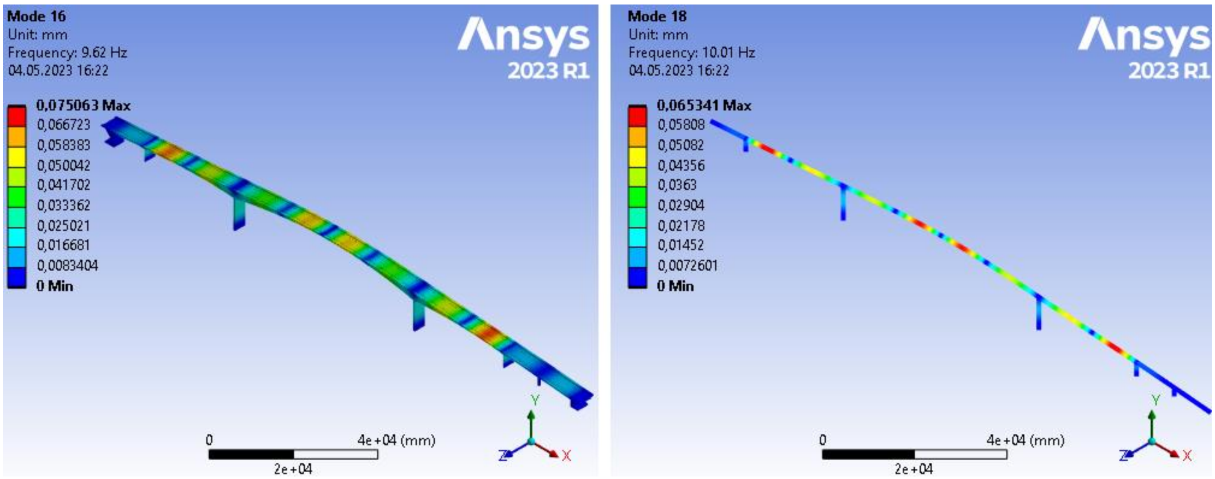

Figure 22: Mode 16 on the solid model matched by 97,8% with mode 18 on the beam model. Frequency error: 3,9%.

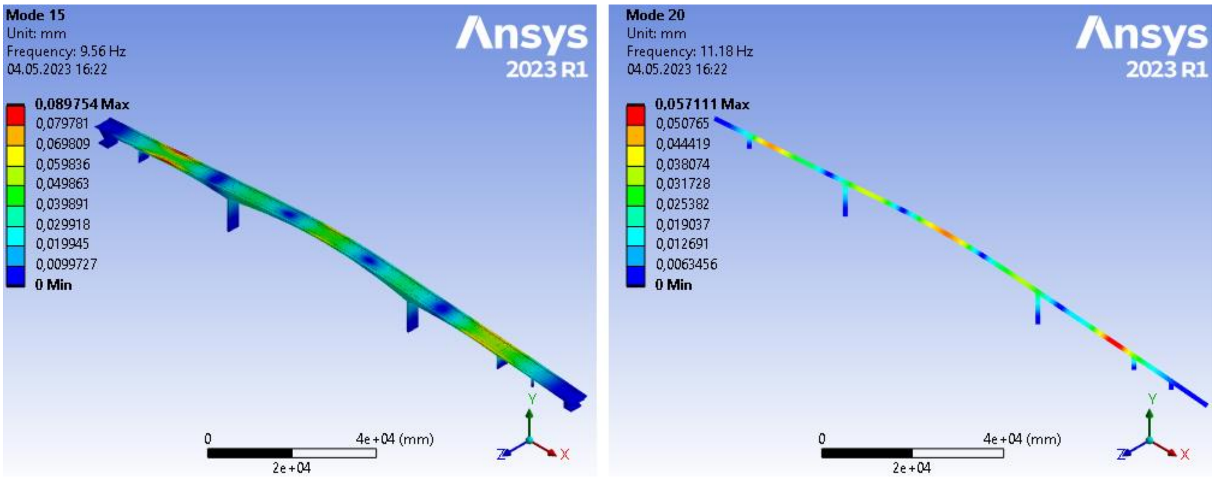

Figure 23: Mode 15 on the solid model matched by 93,6% with mode 20 on the beam model. Frequency error: -14,5%.

4.2 Modes selected for comparison with OMA

4.2.1 Solid model modes

Here the 16 modes from the solid model that is recommended for OMA comparison is shown:

Mode 1:

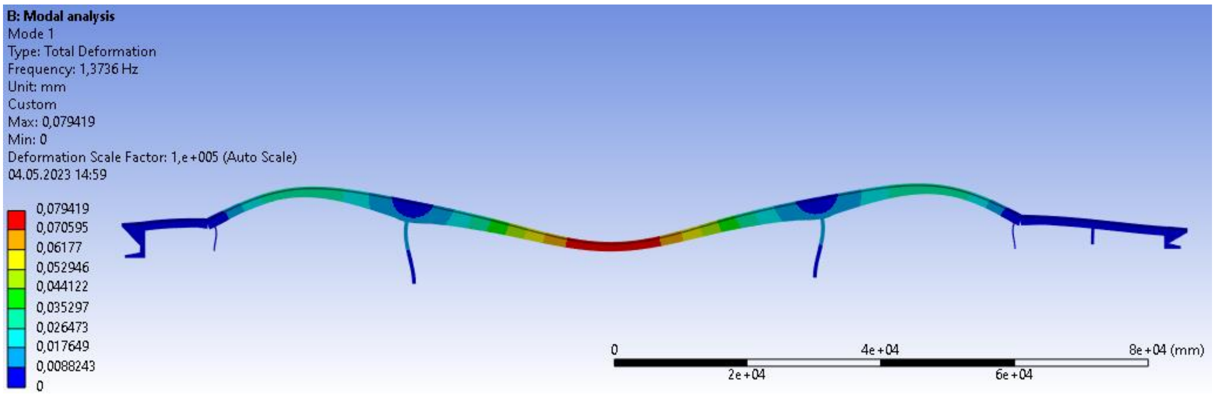

B: Modal analysis
Mode 1
Type: Total Deformation
Frequency: 1,3736 Hz
Unit: mm
Custom
Max: 0,079419
Min: 0
Deformation Scale Factor: 1,e+005 (Auto Scale)
04.05.2023 14:59

Figure 24: Mode 1 shape for the solid model viewed from the side (Z direction).

Mode 1 on the solid model is a longitudinal mode shape, mainly with translation of movement in Y direction and rotation around the Z axis. Mode 1 on the solid model corresponds well (99,5%) with mode 1 on the beam model. Mode 1 is recommended for comparison with operational mode analysis results.

Mode 2:

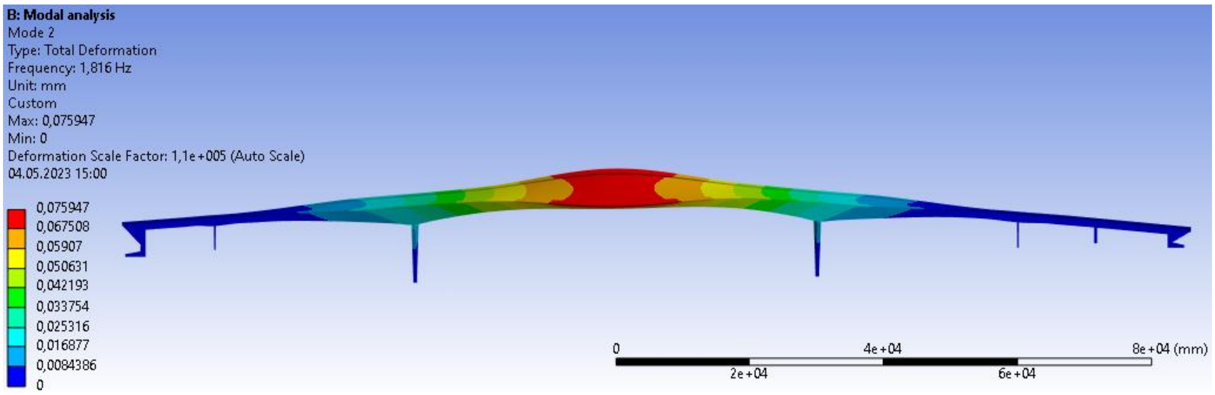

B: Modal analysis
Mode 2
Type: Total Deformation
Frequency: 1,816 Hz
Unit: mm
Custom
Max: 0,075947
Min: 0
Deformation Scale Factor: 1,1e+005 (Auto Scale)
04.05.2023 15:00

Figure 25: Mode 2 shape for the solid model viewed from the side (Z direction).

Mode 2 on the solid model is a transverse mode shape, mainly with translation of movement in Z direction and rotation around the X and Y axes. Mode 2 on the solid model corresponds well (98,8%) with mode 2 on the beam model. Mode 2 is recommended for comparison with operational mode analysis results.

Mode 3:

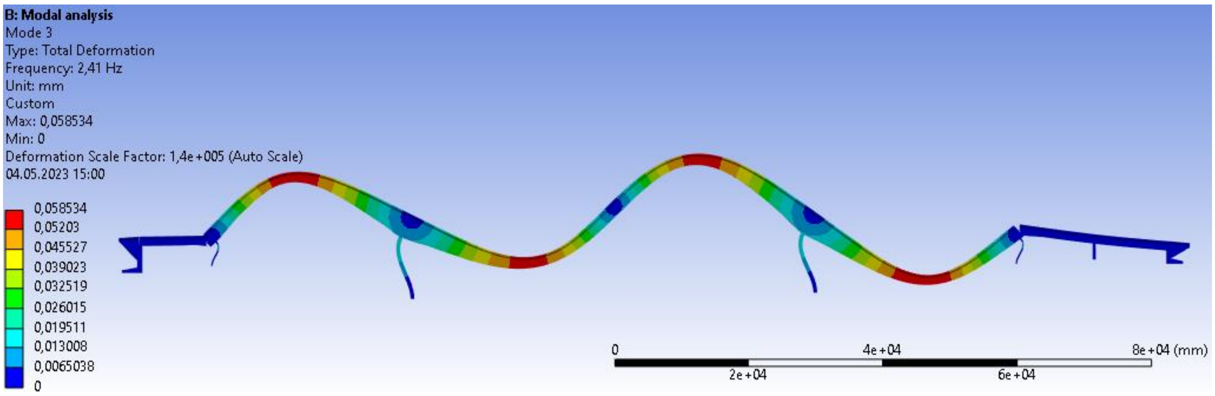

Figure 26: Mode 3 shape for the solid model viewed from the side (Z direction).

Mode 3 on the solid model is a longitudinal mode shape, mainly with rotation around the Z axis. Mode 3 on the solid model corresponds well (99,4%) with mode 3 on the beam model. Mode 3 is recommended for comparison with operational mode analysis results.

Mode 4:

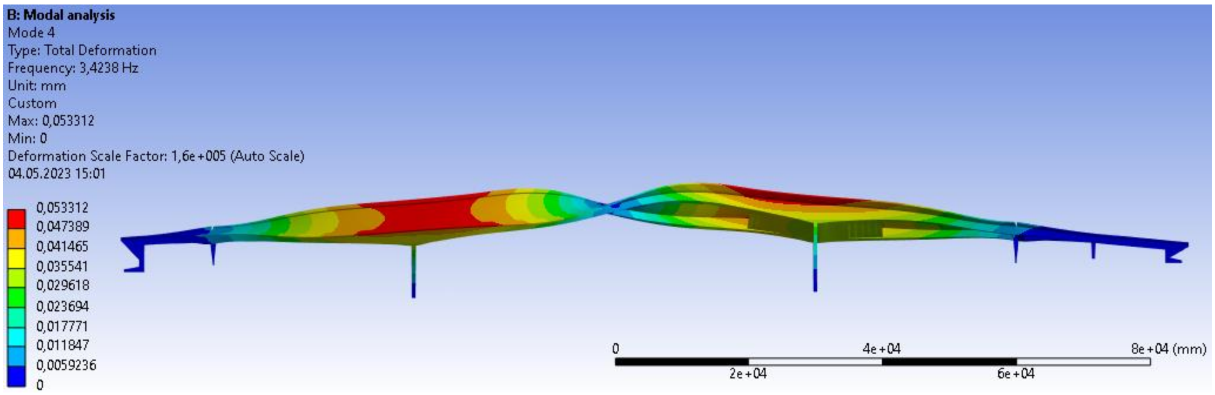

Figure 27: Mode 4 shape for the solid model viewed from the side (Z direction).

Mode 4 on the solid model is a transverse mode shape, mainly with rotation around the X and Y axes. Mode 4 on the solid model corresponds well (99,1%) with mode 6 on the beam model. Mode 4 is recommended for comparison with operational mode analysis results.

Mode 5:

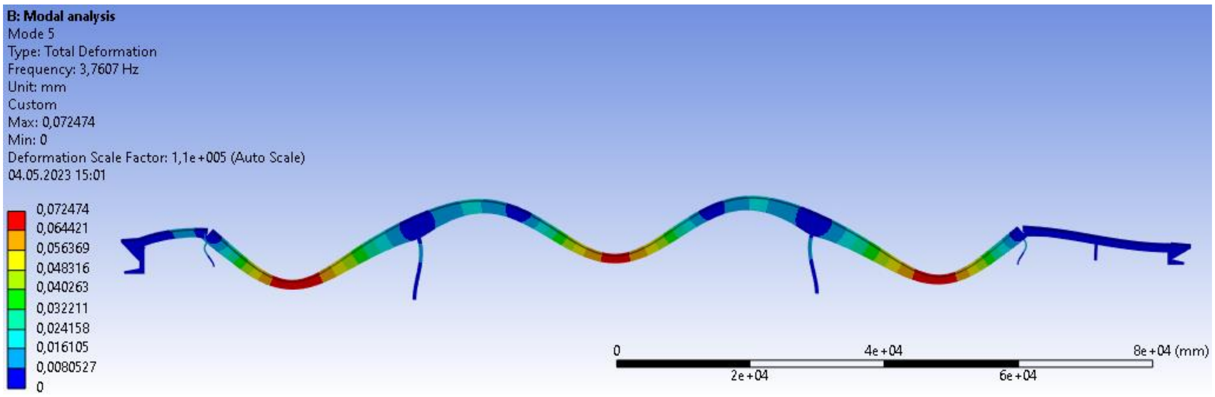

B: Modal analysis
Mode 5
Type: Total Deformation
Frequency: 3,7607 Hz
Unit: mm
Custom
Max: 0,072474
Min: 0
Deformation Scale Factor: 1,1e+005 (Auto Scale)
04.05.2023 15:01

Figure 28: Mode 5 shape for the solid model viewed from the side (Z direction).

Mode 5 on the solid model is a longitudinal mode shape, mainly with translation of movement in Y direction and rotation around the Z axis. Mode 5 on the solid model corresponds well (99,3%) with mode 5 on the beam model. Mode 5 is recommended for comparison with operational mode analysis results.

Mode 6:

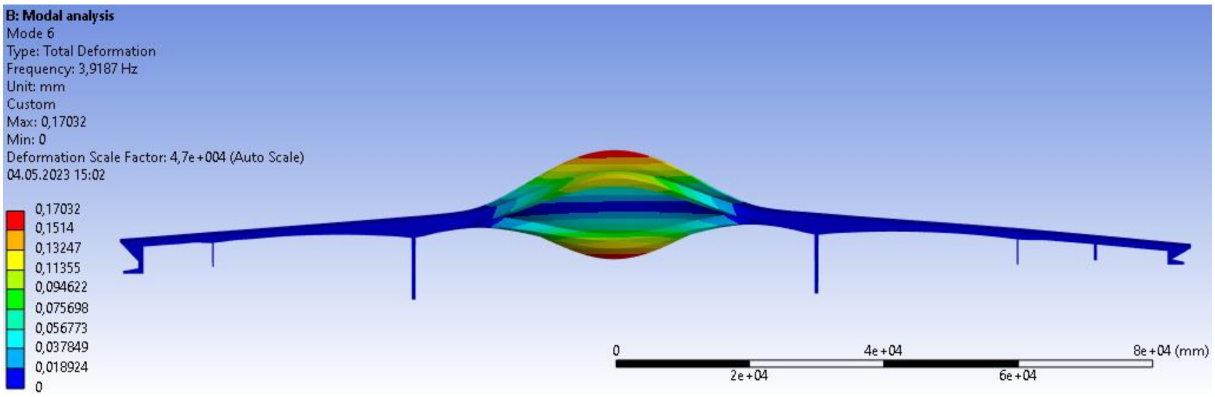

B: Modal analysis
Mode 6
Type: Total Deformation
Frequency: 3,9187 Hz
Unit: mm
Custom
Max: 0,17032
Min: 0
Deformation Scale Factor: 4,7e+004 (Auto Scale)
04.05.2023 15:02

Figure 29: Mode 6 shape for the solid model viewed from the side (Z direction).

Mode 6 on the solid model is a transverse mode shape, mainly with rotation around the X and Y axes. Mode 6 has a relatively high participation factor and low frequency. Mode 6 is recommended for comparison with operational mode analysis results.

Mode 7:

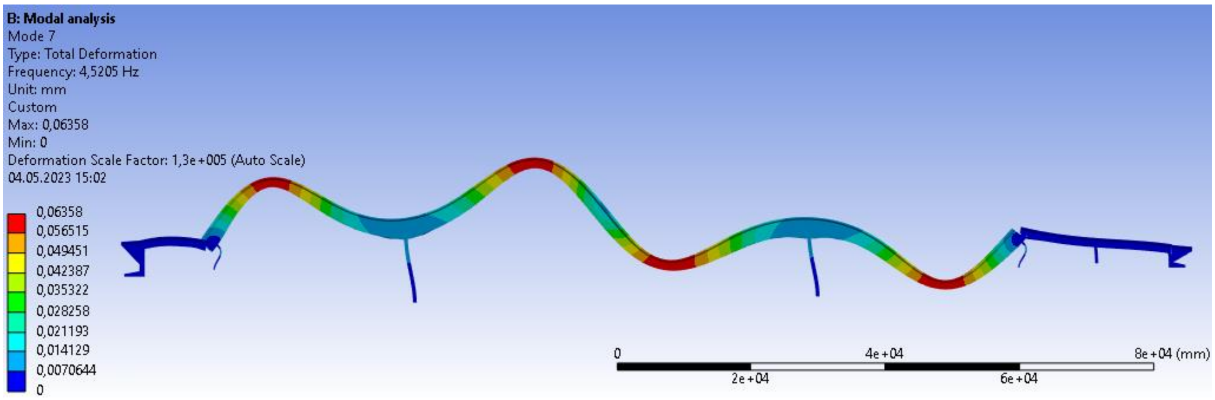

B: Modal analysis
Mode 7
Type: Total Deformation
Frequency: 4,5205 Hz
Unit: mm
Custom
Max: 0,06358
Min: 0
Deformation Scale Factor: 1,3e+005 (Auto Scale)
04.05.2023 15:02

Figure 30: Mode 7 shape for the solid model viewed from the side (Z direction).

Mode 7 on the solid model is a longitudinal mode shape, mainly with translation of movement in X direction and rotation around the Z axis. Mode 7 on the solid model corresponds well (94%) with mode 7 on the beam model. Mode 7 is recommended for comparison with operational mode analysis results.

Mode 8:

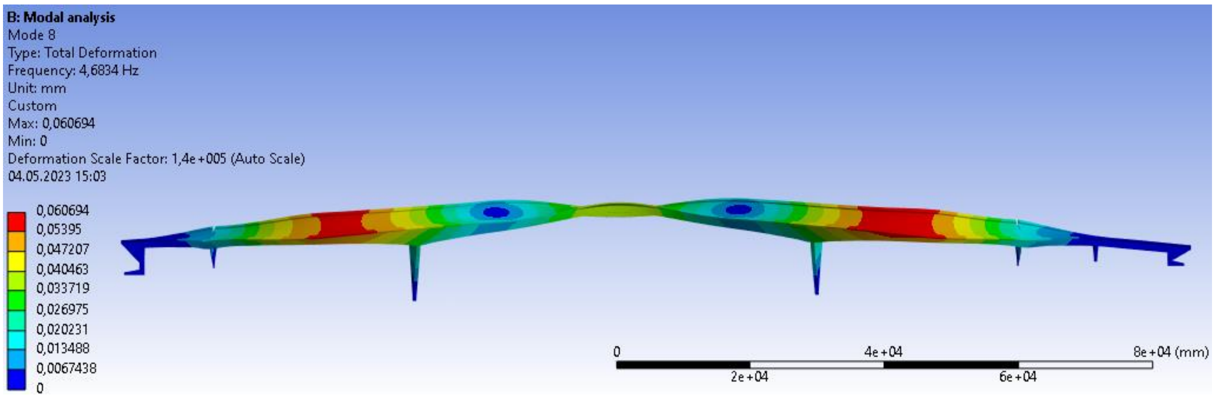

B: Modal analysis
Mode 8
Type: Total Deformation
Frequency: 4,6834 Hz
Unit: mm
Custom
Max: 0,060694
Min: 0
Deformation Scale Factor: 1,4e+005 (Auto Scale)
04.05.2023 15:03

Figure 31: Mode 8 shape for the solid model viewed from the side (Z direction).

Mode 8 on the solid model is a transverse mode shape, mainly with translation of movement in Z direction and rotation around the X and Y axes. Mode 8 on the solid model corresponds well (97,7%) with mode 11 on the beam model. Mode 8 is recommended for comparison with operational mode analysis results.

Mode 9:

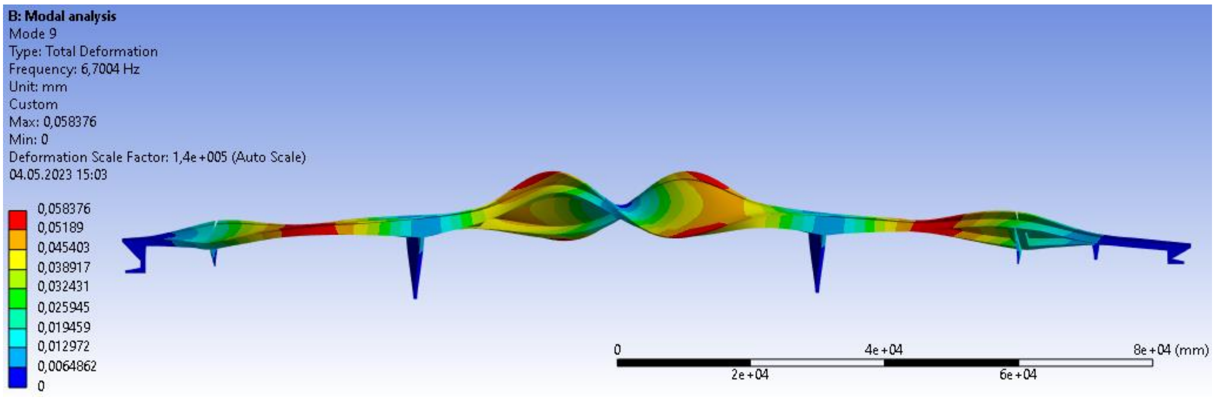

Figure 32: Mode 9 shape for the solid model viewed from the side (Z direction).

Mode 9 on the solid model is a transverse mode shape, mainly with rotation around the X and Y axes. Mode 9 on the solid model corresponds well (93,5%) with mode 14 on the beam model. Mode 9 is recommended for comparison with operational mode analysis results.

Mode 10:

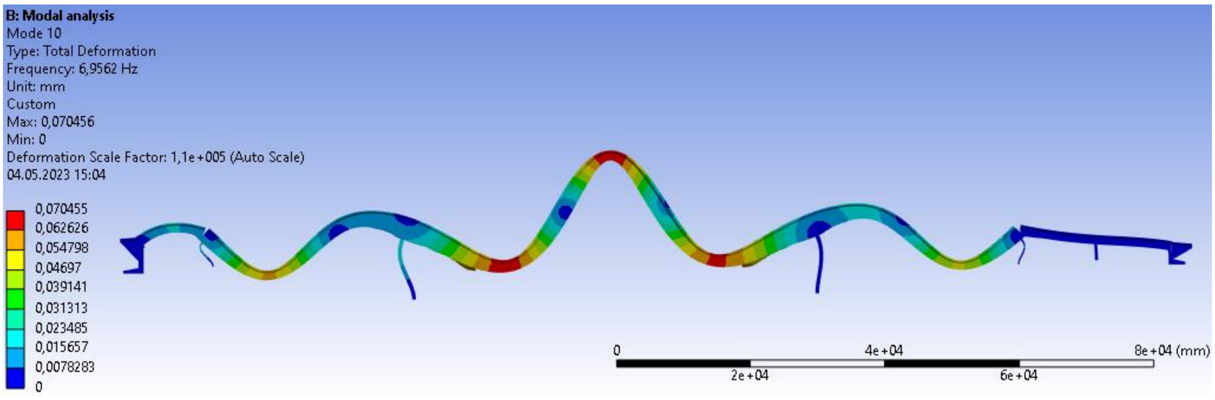

Figure 33: Mode 10 shape for the solid model viewed from the side (Z direction).

Mode 10 on the solid model is a longitudinal mode shape, mainly with translation of movement in X and Y direction and rotation around the Z axis. Mode 10 on the solid model corresponds well (94,3%) with mode 12 on the beam model. Mode 10 is recommended for comparison with operational mode analysis results.

Mode 11:

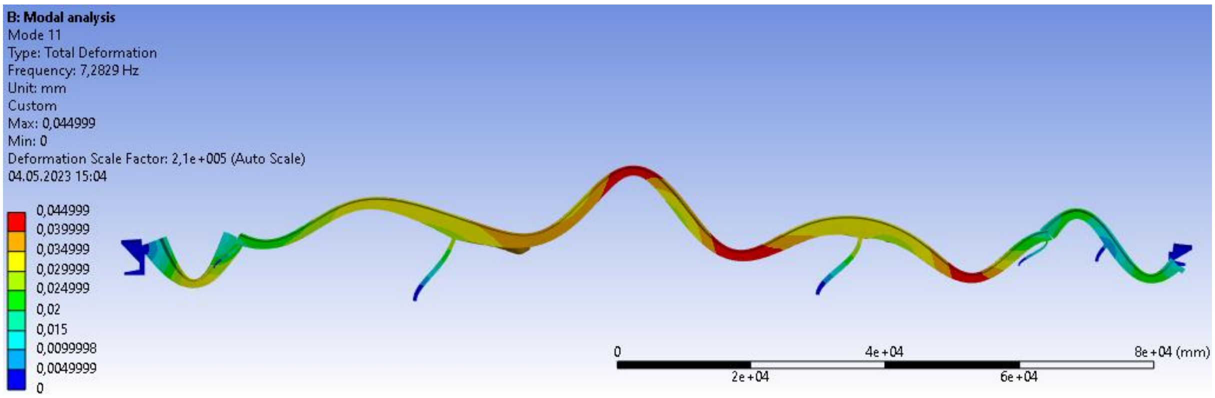

Figure 34: Mode 11 shape for the solid model viewed from the side (Z direction).

Mode 11 on the solid model is a longitudinal mode shape, mainly with translation of movement in X direction and rotation around the Z axis. Mode 11 has a relatively high participation factor. Mode 11 is recommended for comparison with operational mode analysis results.

Mode 15:

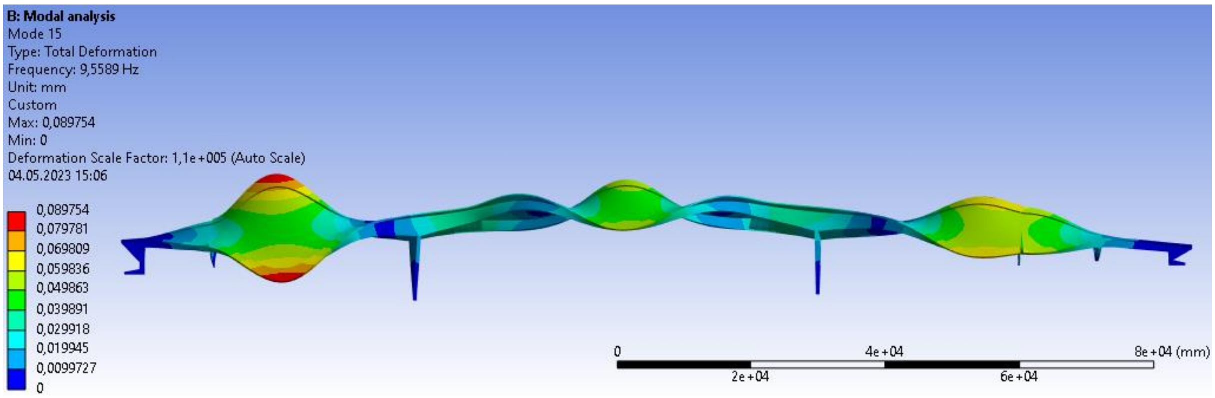

Figure 35: Mode 15 shape for the solid model viewed from the side (Z direction).

Mode 15 on the solid model is a transverse mode shape, mainly with translation of movement in Z direction and rotation around the X, Y and Z axes. Mode 15 on the solid model corresponds well (93,6%) with mode 20 on the beam model. Mode 15 is recommended for comparison with operational mode analysis results.

Mode 16:

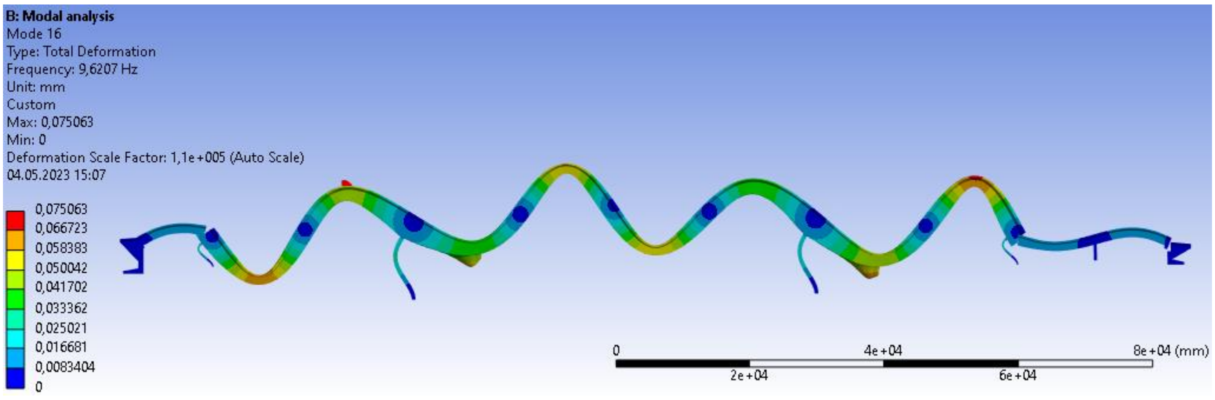

Figure 36: Mode 16 shape for the solid model viewed from the side (Z direction).

Mode 16 on the solid model is a longitudinal mode shape, mainly with rotation around the Y and Z axis. Mode 16 on the solid model corresponds well (97,8%) with mode 18 on the beam model. Mode 16 is recommended for comparison with operational mode analysis results.

Mode 17:

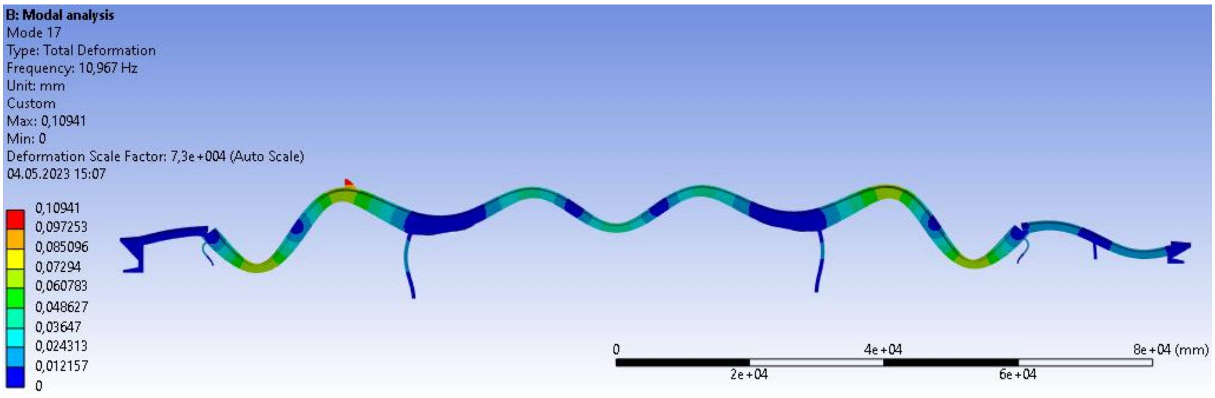

Figure 37: Mode 17 shape for the solid model viewed from the side (Z direction).

Mode 17 on the solid model is a longitudinal mode shape, mainly with translation of movement in Y direction and rotation around the Z axis. Mode 17 has an intermediate participation factor. Mode 17 is recommended for comparison with operational mode analysis results.

Mode 19:

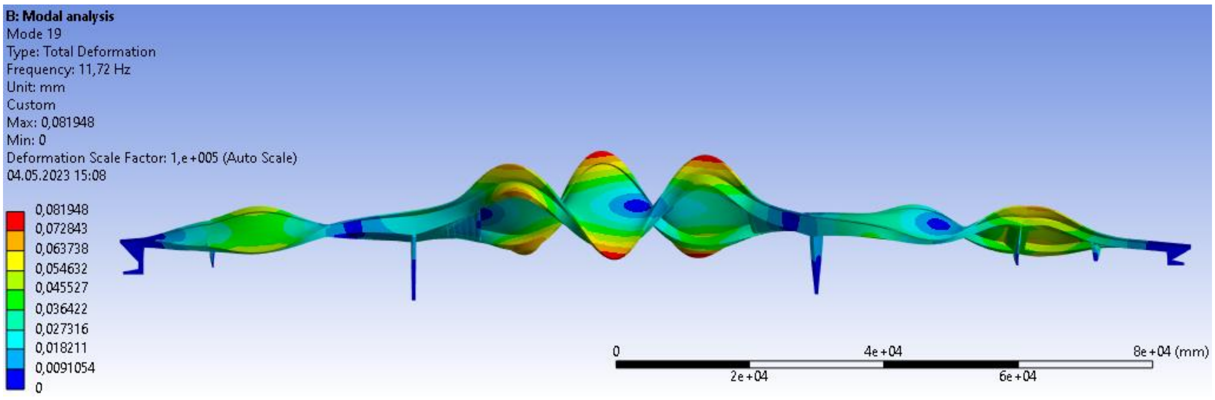

Figure 38: Mode 19 shape for the solid model viewed from the side (Z direction).

Mode 19 on the solid model is a transverse mode shape, mainly with rotation around the X and Y axes. Mode 19 has a relatively high participation factor. Mode 19 is recommended for comparison with operational mode analysis results.

Mode 20:

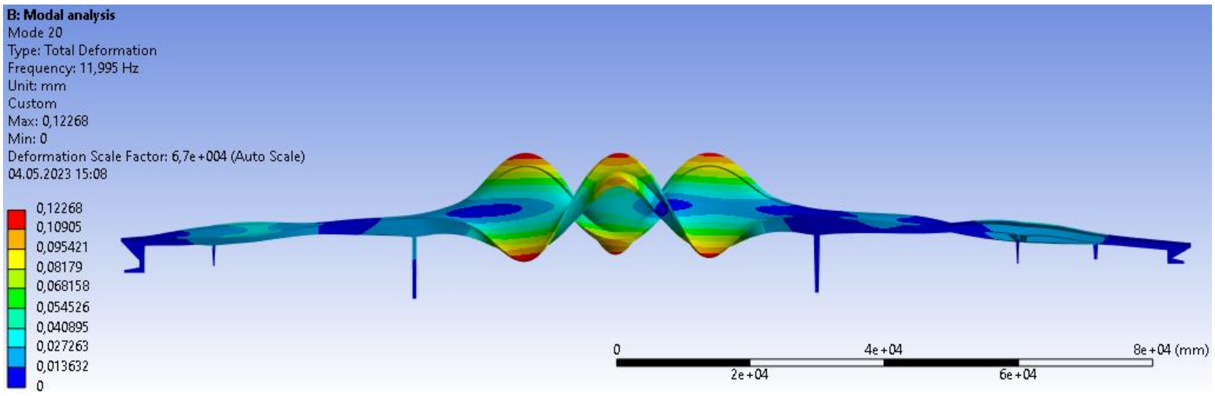

Figure 39: Mode 20 shape for the solid model viewed from the side (Z direction).

Mode 20 on the solid model is a transverse mode shape, mainly with rotation around the X and Y axes. Mode 20 has a relatively high participation factor. Mode 20 is recommended for comparison with operational mode analysis results.

4.2.2 Beam model modes

Here the 14 modes from the beam model that is recommended for OMA comparison is shown:

Mode 1:

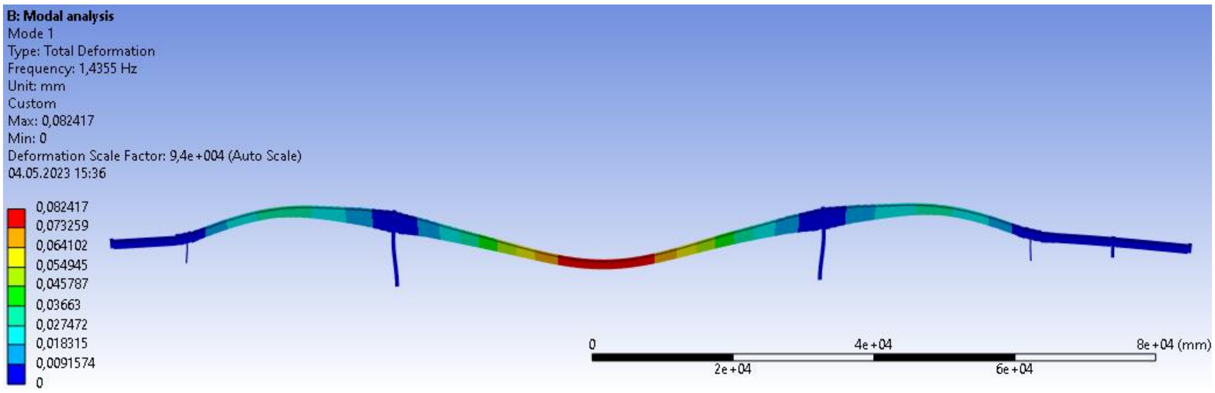

B: Modal analysis
Mode 1
Type: Total Deformation
Frequency: 1,4355 Hz
Unit: mm
Custom
Max: 0,082417
Min: 0
Deformation Scale Factor: 9,4e+004 (Auto Scale)
04.05.2023 15:36

Figure 40: Mode 1 shape for the beam model viewed from the side (Z direction).

Mode 1 on the beam model is a longitudinal mode shape, mainly with translation of movement in Y direction and rotation around the Z axis. Mode 1 on the beam model corresponds well (99,5%) with mode 1 on the solid model. Mode 1 is recommended for comparison with operational mode analysis results.

Mode 2:

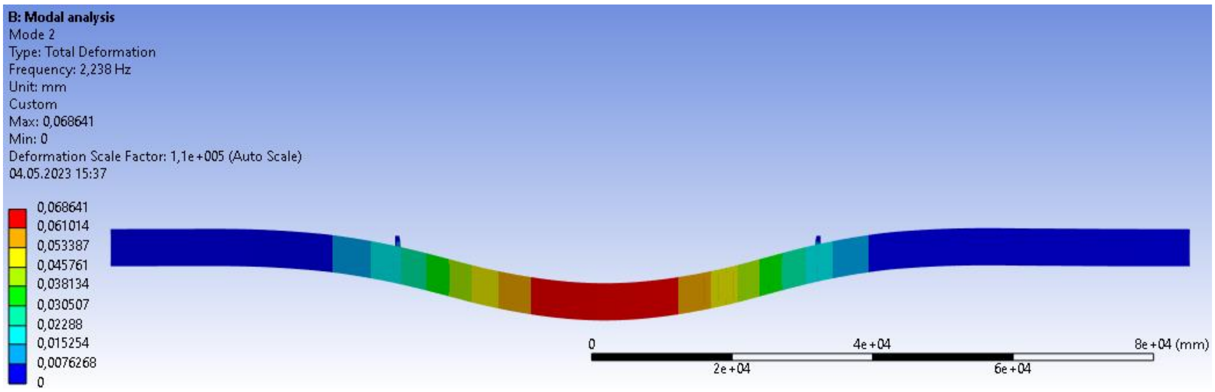

B: Modal analysis
Mode 2
Type: Total Deformation
Frequency: 2,238 Hz
Unit: mm
Custom
Max: 0,068641
Min: 0
Deformation Scale Factor: 1,1e+005 (Auto Scale)
04.05.2023 15:37

Figure 41: Mode 2 shape for the beam model viewed from the top (Y direction).

Mode 2 on the beam model is a transverse mode shape, mainly with translation of movement in Z direction and rotation around the X and Y axes. Mode 2 on the beam model corresponds well (98,8%) with mode 2 on the solid model. Mode 2 is recommended for comparison with operational mode analysis results.

Mode 3:

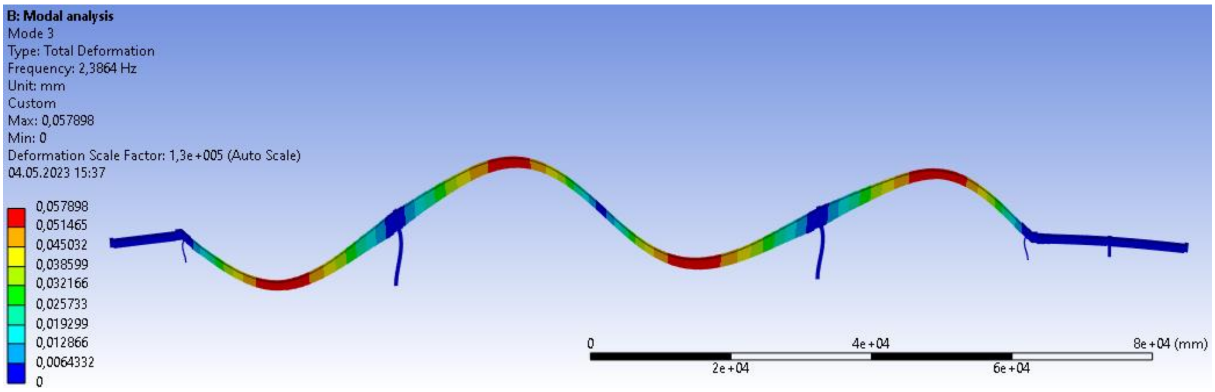
B: Modal analysis
Mode 3
Type: Total Deformation
Frequency: 2,3864 Hz
Unit: mm
Custom
Max: 0,057898
Min: 0
Deformation Scale Factor: 1,3e+005 (Auto Scale)
04.05.2023 15:37

Figure 42: Mode 3 shape for the beam model viewed from the side (Z direction).

Mode 3 on the beam model is a longitudinal mode shape, mainly with rotation around the Z axis. Mode 3 on the beam model corresponds well (99,4%) with mode 3 on the solid model. Mode 3 is recommended for comparison with operational mode analysis results.

Mode 4:

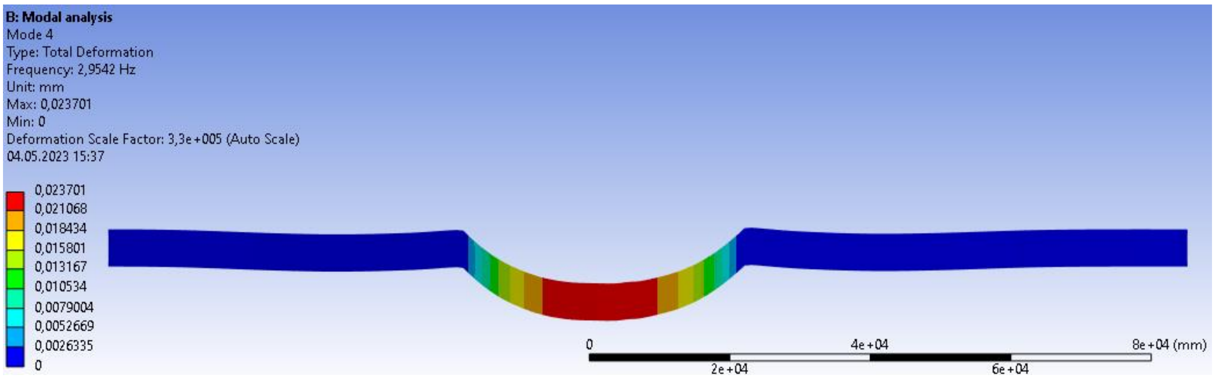
B: Modal analysis
Mode 4
Type: Total Deformation
Frequency: 2,9542 Hz
Unit: mm
Max: 0,023701
Min: 0
Deformation Scale Factor: 3,3e+005 (Auto Scale)
04.05.2023 15:37

Figure 43: Mode 4 shape for the beam model viewed from the top (Y direction).

Mode 4 on the beam model is a transverse mode shape, mainly with rotation around the X and Y axes. Mode 4 has a relatively high participation factor. Mode 4 is recommended for comparison with operational mode analysis results.

Mode 5:

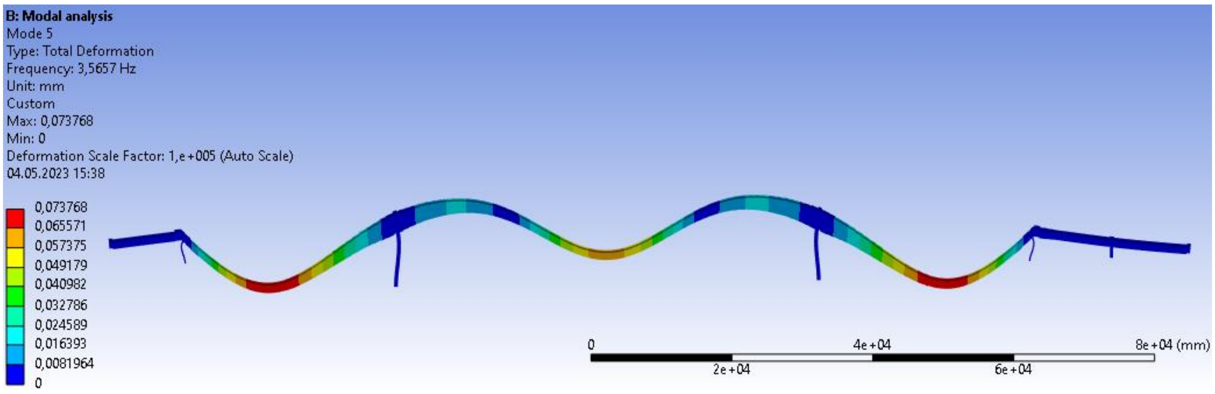
B: Modal analysis
Mode 5
Type: Total Deformation
Frequency: 3,5657 Hz
Unit: mm
Custom
Max: 0,073768
Min: 0
Deformation Scale Factor: 1,e+005 (Auto Scale)
04.05.2023 15:38

Figure 44: Mode 5 shape for the beam model viewed from the side (Z direction).

Mode 5 on the beam model is a longitudinal mode shape, mainly with translation of movement in Y direction and very low rotation around the Z axis. Mode 5 on the beam model corresponds well (99,3%) with mode 5 on the solid model. Mode 5 is recommended for comparison with operational mode analysis results.

Mode 6:

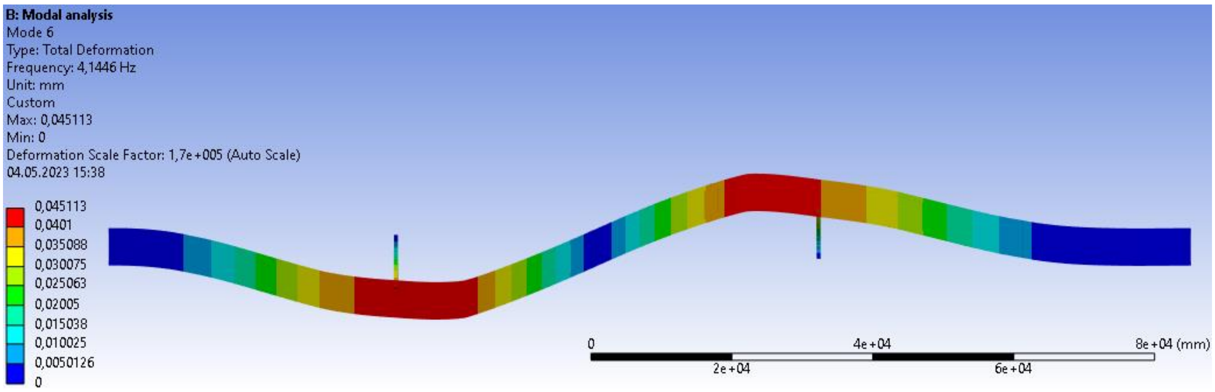
B: Modal analysis
Mode 6
Type: Total Deformation
Frequency: 4,1446 Hz
Unit: mm
Custom
Max: 0,045113
Min: 0
Deformation Scale Factor: 1,7e+005 (Auto Scale)
04.05.2023 15:38

Figure 45: Mode 6 shape for the beam model viewed from the top (Y direction).

Mode 6 on the beam model is a transverse mode shape, mainly with rotation around the X and Y axes. Mode 6 on the beam model corresponds well (99,1%) with mode 4 on the solid model. Mode 6 is recommended for comparison with operational mode analysis results.

Mode 7:

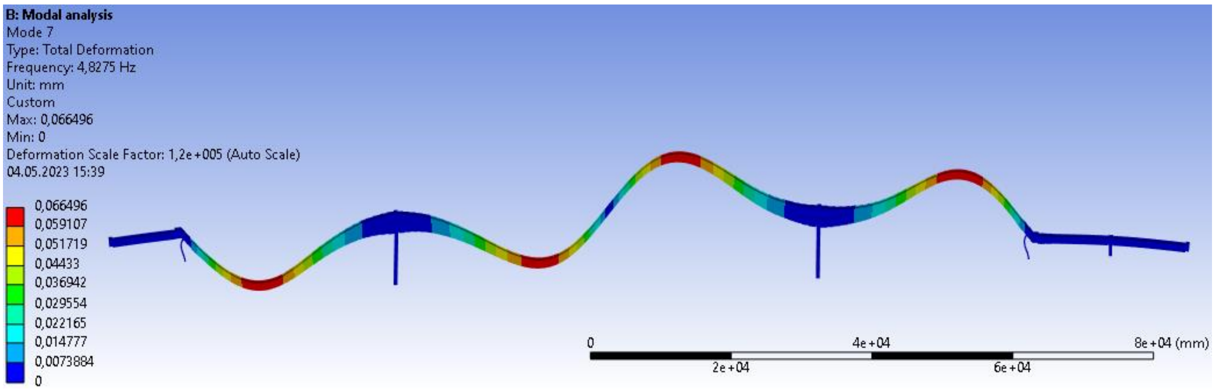

B: Modal analysis
Mode 7
Type: Total Deformation
Frequency: 4,8275 Hz
Unit: mm
Custom
Max: 0,066496
Min: 0
Deformation Scale Factor: 1,2e+005 (Auto Scale)
04.05.2023 15:39

Figure 46: Mode 7 shape for the beam model viewed from the side (Z direction).

Mode 7 on the beam model is a longitudinal mode shape, mainly with rotation around the Z axis. Mode 7 on the beam model corresponds well (94%) with mode 7 on the solid model. Mode 7 is recommended for comparison with operational mode analysis results.

Mode 8:

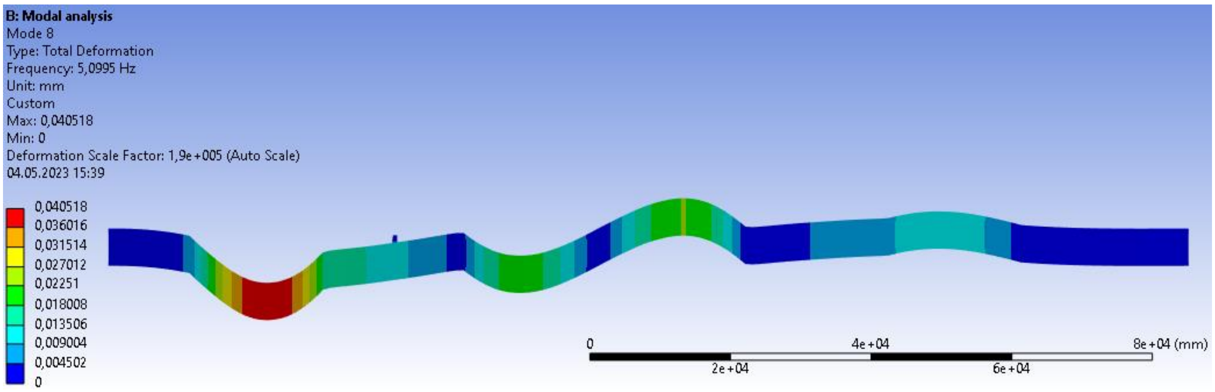

B: Modal analysis
Mode 8
Type: Total Deformation
Frequency: 5,0995 Hz
Unit: mm
Custom
Max: 0,040518
Min: 0
Deformation Scale Factor: 1,9e+005 (Auto Scale)
04.05.2023 15:39

Figure 47: Mode 8 shape for the beam model viewed from the top (Y direction).

Mode 8 on the beam model is a transverse mode shape, mainly with rotation around the X and Y axes. Mode 8 has a relatively high participation factor. Mode 8 is recommended for comparison with operational mode analysis results.

Mode 11:

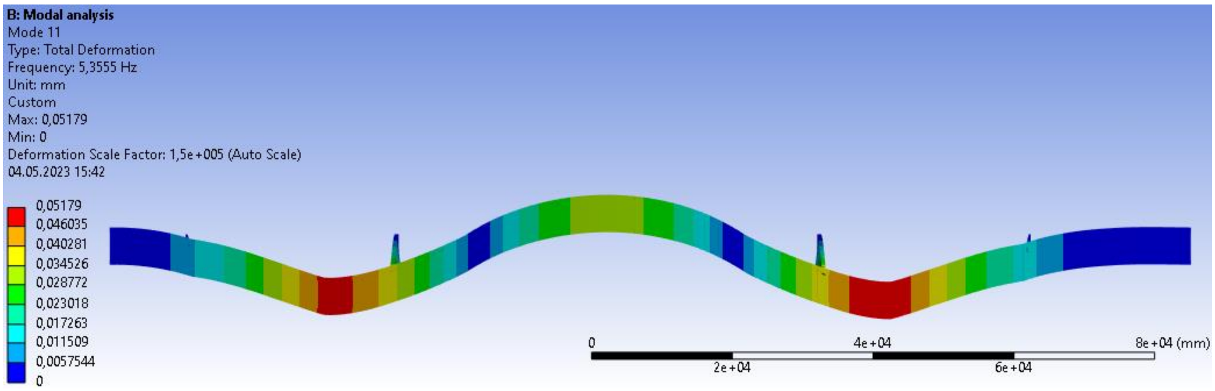

Figure 48: Mode 11 shape for the beam model viewed from the top (Y direction).

Mode 11 on the beam model is a transverse mode shape, mainly with translation of movement in Z direction and rotation around the X and Y axes. Mode 11 on the beam model corresponds well (97,7%) with mode 8 on the solid model. Mode 11 is recommended for comparison with operational mode analysis results.

Mode 12:

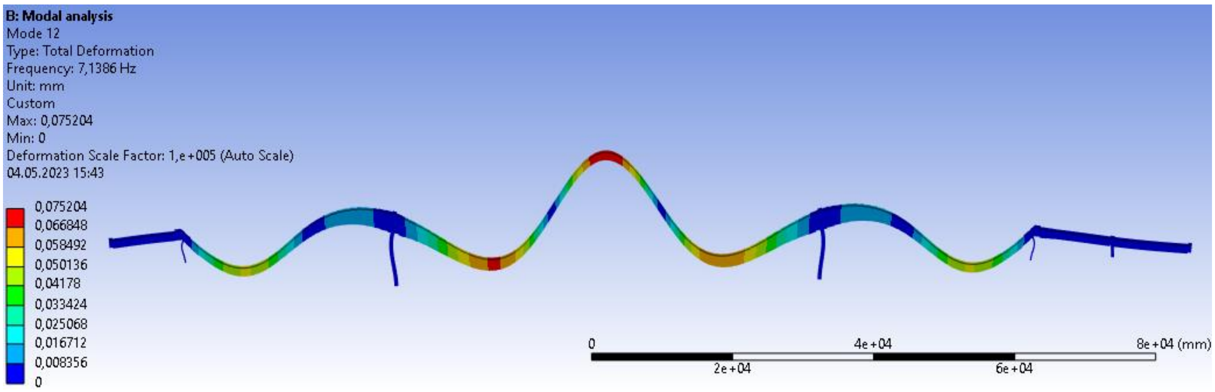

Figure 49: Mode 12 shape for the beam model viewed from the side (Z direction).

Mode 12 on the beam model is a longitudinal mode shape, mainly with translation of movement in Y direction and rotation around the Z axis. Mode 12 on the beam model corresponds well (94,3%) with mode 10 on the solid model. Mode 12 is recommended for comparison with operational mode analysis results.

Mode 14:

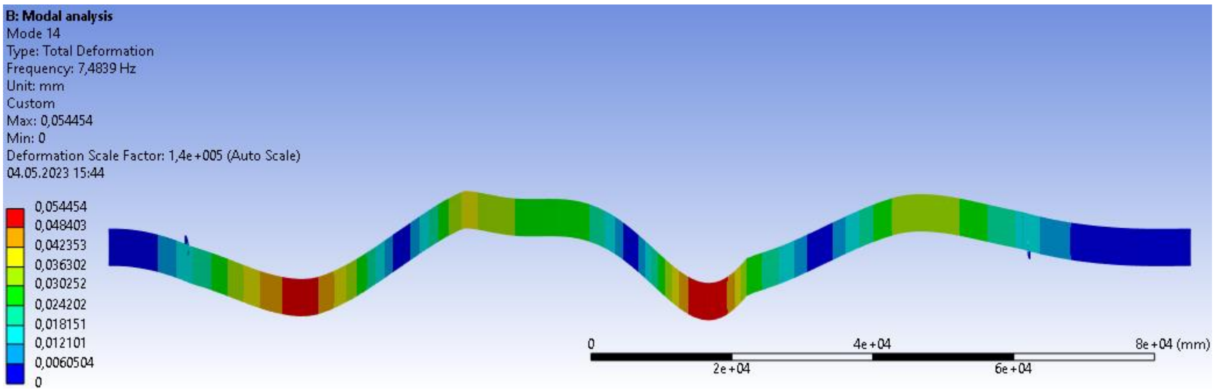

B: Modal analysis
Mode 14
Type: Total Deformation
Frequency: 7,4839 Hz
Unit: mm
Custom
Max: 0,054454
Min: 0
Deformation Scale Factor: 1,4e+005 (Auto Scale)
04.05.2023 15:44

Figure 50: Mode 14 shape for the beam model viewed from the top (Y direction).

Mode 14 on the beam model is a transverse mode shape, mainly with rotation around the X and Y axes. Mode 14 on the beam model corresponds well (93,5%) with mode 9 on the solid model. Mode 14 is recommended for comparison with operational mode analysis results.

Mode 15:

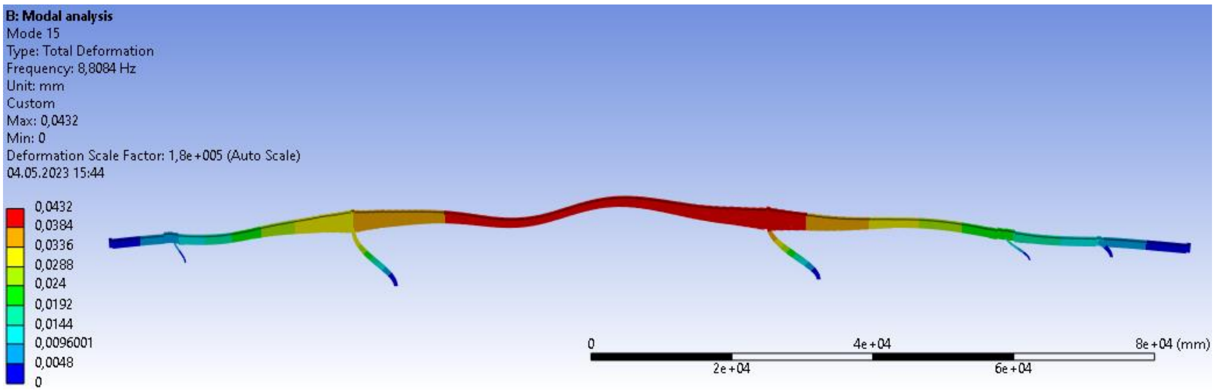

B: Modal analysis
Mode 15
Type: Total Deformation
Frequency: 8,8084 Hz
Unit: mm
Custom
Max: 0,0432
Min: 0
Deformation Scale Factor: 1,8e+005 (Auto Scale)
04.05.2023 15:44

Figure 51: Mode 15 shape for the beam model viewed from the side (Z direction).

Mode 15 on the beam model is a longitudinal mode shape, mainly with translation of movement in X direction and rotation around the Z axis. Mode 15 has a relatively high participation factor. Mode 15 is recommended for comparison with operational mode analysis results.

Mode 18:

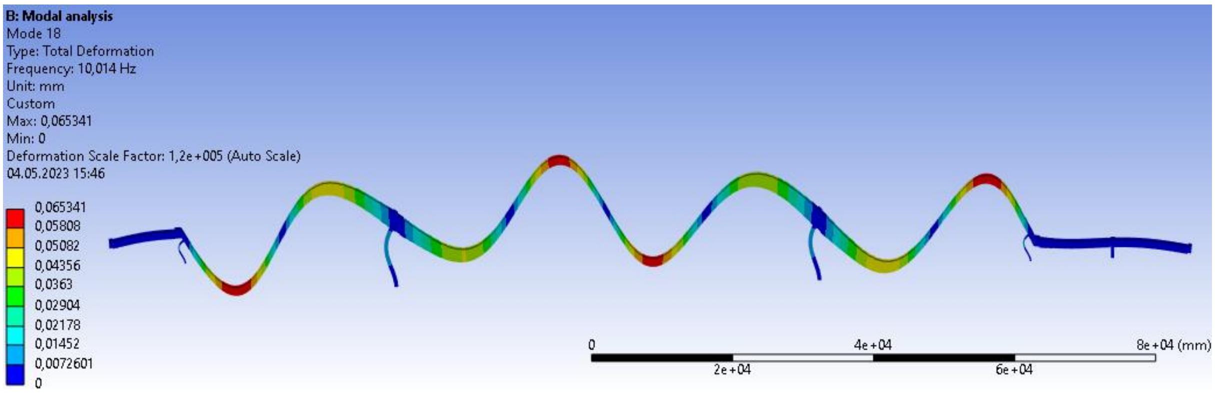

Figure 52: Mode 18 shape for the beam model viewed from the side (Z direction).

Mode 18 on the beam model is a longitudinal mode shape, mainly with rotation around the Z axis. Mode 18 on the beam model corresponds well (97,8%) with mode 16 on the solid model. Mode 18 is recommended for comparison with operational mode analysis results.

Mode 20:

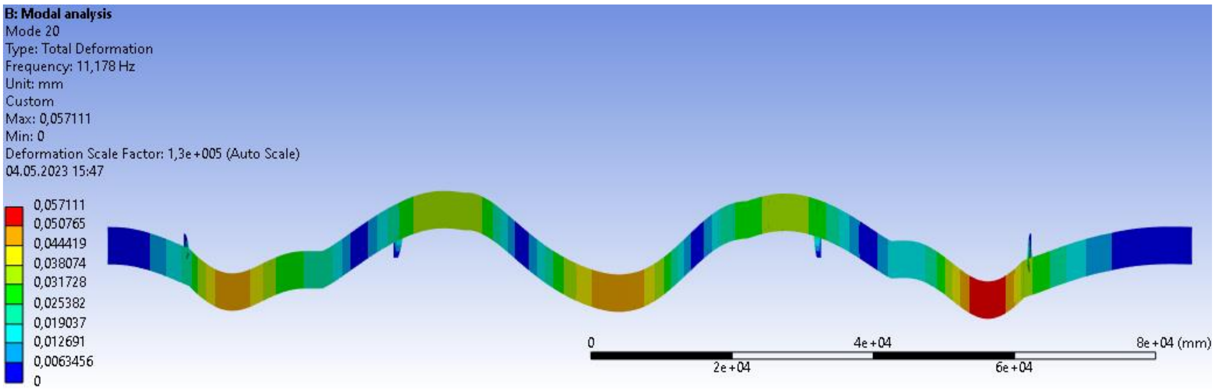

Figure 53: Mode 20 shape for the beam model viewed from the top (Y direction).

Mode 20 on the beam model is a transverse mode shape, mainly with rotation around the X and Y axes. Mode 20 on the beam model corresponds well (93,6%) with mode 15 on the solid model. Mode 20 is recommended for comparison with operational mode analysis results.

5 Discussion

The modelling process was carried out as precise as possible with the existing documentation of the bridge. Performing the modelling in SpaceClaim [5] probably had both negative and positive effects. On the negative side the candidate experienced some lag while sketching in SpaceClaim [5], maybe because of the large scale of the model. On the positive side, modelling in Ansys SpaceClaim [5] made the transfer to Ansys Workbench [6] and Ansys Mechanical [7] a lot easier than if the model was modelled outside of the Ansys software [9], as all features was retained within the Ansys software [9]. While not doing so, compatibility issues between different software packages can arise, that could further cause problems that could require time consuming repairs and loss of features. The models presented in this thesis is not perfect and do need additional complexity added like rebars (slack reinforcement), post-tensioning tendons, more accurate material properties and models that account for creep and losses, which can be interesting aspects for further work.

The deflection is corresponding well between the models when the post tensioning system is deactivated, with just 9% difference. After the post tensioning system is added, the deflection difference rises to 96%. These results may point towards a weakness in the way the post tensioning system is simulated and/or differences in the element technology.

Since the solid model gives expected results for deflection, and compressive and tensile stress, the solid model results are given the most confidence. The quite high deflection of the beam with post tensioning of 70,753 mm is considered unrealistic compared to the deflection of the solid model with post tensioning of 36,08 mm, which is more realistic for a concrete structure. The modal analyses were pre-stressed from the static structural analyses, and even though the deflections of the models were quite far apart, the results of the frequencies and mode shapes corresponded quite well. This tells us the static structural pre-stress has a low impact on the modal analysis, which makes sense because the modal analysis computations are based on the stiffness and mass of the structure. Even though the impact was small, it was interesting seeing the pre-stress having some impact on the modal analysis.

6 Conclusion

The modelling process was complicated and took a lot of time to do with adequate precision, particularly with the beam model. The documentation of the bridge construction is hand drawn and hard to interpret at some points. The documentation is spread across many different reports

[12], [13], [14], [15], [23], [25], [27], [28]. Preparations were needed to get the coordinates of the bridge into the CAD software to set the stage for solid modelling.

A solid element model and a beam element model has been produced, and their weight and volume correspond well (0,24% difference). The solid model demands a lot more computational power and gives results that makes more sense for a concrete bridge structure compared to the beam model. The solid element technology is based on a more precise theory versus the beam theory, which is a simplified technology that adds a cross section to a line. Additionally, the beam model contains more simplifications than the solid model. Hence more confidence is placed in the solid model, but the beam model can be useful for quick analyses when low on computing power or if the complexity of the analyses increases.

Out of the total of 40 modes extracted, 20 modes from each model, 30 modes are recommended for comparison with operational modes, 16 modes from the solid model and 14 modes from the beam model. There is good correspondence between the modal analysis results of the solid and beam model, with 11 out of 20 modes corresponding with over 90% similarity in mode shapes and less than 20% frequency error. Since 11 out of the 30 recommended modes are the same, there is in fact 19 modes being recommended for comparison with operational modes. The results appear to be realistic as the mode shapes materialize as one would expect in a structure with the scale and shape of Herøysund bridge.

All in all, the candidate is satisfied with the results from this analysis. All the goals of the thesis and the problem description is achieved, and several interesting aspects have been added like modal assurance criterion, structural analysis, modal analysis, participation factors etc. Through the work on this analysis, the candidate has learned a lot about the Ansys software [9], finite element modelling, element selection and usage, relevant load cases for bridges, modal analysis, modal result interpretation, document interpretation, structural health monitoring, and civil engineering structural assessment. Also, the candidate has gained a lot of general knowledge about bridge constructions.

The candidate is confident that the results of this thesis can be used further as a contribution to the Herøy FoU project to develop methods of structural health monitoring of bridges. The results from the analyses can be used to better understand why Herøysund bridge has poor structural health. The modal analysis developed in this thesis can be further used to compare with the operational modes that will be extracted from the bridge in the future.

7 Future work

In this chapter the candidate will elaborate on some points that could be of interest for future work:

- Static structural analysis of multiple different load cases applied to the bridge at various positions. “Håndbok V412 Bæreevneklassifisering av bruer, laster” [24] gives several different load cases that could be studied and added to the analysis to give a broader picture of the bridge behaviour.
- Once the operational modes have been extracted from the bridge, and the data has been processed and analysed, the operational modes data should be compared to the results of this thesis, for example by employing the modal assurance criterion. Then the models developed in this thesis should be calibrated as precisely as possible to depict the operational modes, this is also called model updating. This can be one of the topics for master thesis in the future.
- In the Ansys module NVH toolkit [31], there is a function for determining which properties should be adjusted on the finite element model to represent the data it is being compared to. For example, it can determine which property, such as stiffness, strength, density, etc, is the most efficient to modify, and it will range these properties according to their efficiency. This will make the process of producing a digital twin of the bridge a lot more efficient.
- The modelling of the post tensioning system should be investigated further. In this thesis the post tensioning forces are simulated by horizontal forces that compress the main span longitudinally. This simulated post tensioning method seems to function well on the solid model, but its precision could be improved. This method does not function as anticipated for the beam model. Perhaps modelling the entire post tensioning system with conduits and cables will result in a more accurate representation.
- The modelling and implementation of the rebars (lax reinforcement) could be investigated further, perhaps in a future master thesis.
- The known damages on the bridge (corroded tendons and rebars, cracks in the concrete, insufficient grout in tendon conduits etc.) construction can be implemented in the models to get more realistic results from the analysis.
- The work accomplished in this thesis will be submitted as a scientific paper in a journal in Norwegian list in the near future.

Works cited

[1] Autodesk Inc, “Autodesk Inventor,” 2023. https://www.autodesk.com/products/inventor/overview?term=1-YEAR&tab=subscription (accessed May 12, 2023).

[2] Autodesk Inc, “Autodesk Autocad,” 2023. https://www.autodesk.com/products/autocad/overview?term=1-YEAR&tab=subscription (accessed May 12, 2023).

[3] Microsoft corporation, “Microsoft Word,” 2018. https://www.microsoft.com/en-ww/microsoft-365/word?market=af (accessed May 12, 2023).

[4] Microsoft corporation, “Microsoft excel,” 2018. https://www.microsoft.com/en-us/microsoft-365/excel (accessed May 12, 2023).

[5] ANSYS Inc, “Ansys SpaceClaim.” ANSYS Inc, 2023. [Online]. Available: https://www.ansys.com/

[6] ANSYS Inc, “Ansys Workbench.” ANSYS Inc, 2023. [Online]. Available: https://www.ansys.com/

[7] Ansys Inc, “Ansys Mechanical,” 2023. https://www.ansys.com/products/structures/ansys-mechanical (accessed May 11, 2023).

[8] T. A. Martius-Hammer and I. Rambæk, “Milliarder å spare med smartere forvaltning av infrastruktur,” 2023. https://kommunikasjon.ntb.no/pressemelding/milliarder-a-spare-med-smartere-forvaltning-av-infrastruktur?publisherId=7235542&releaseId=17954617

[9] Ansys Inc, “Ansys Software,” 2023. https://www.ansys.com/ (accessed May 12, 2023).

[10] K. Tangrand and H. Singh, “Analysis of Civil Engineering Infrastructure in Norway with Solutions Based on Structural Health Monitoring and Artificial Intelligence,” pp. 1–21.

[11] VG, “De forsømte broene,” 2017. https://www.vg.no/spesial/2017/de-forsomte-broene/kart/#inspeksjon

[12] AAS-Jacobsen, “Herøysund bru.pdf,” 2019.

[13] L. H. Fredheim, “18-1069 HERØYSUND BRU,” 2017.

[14] M. Holmqvist, D. I. Ab, and R. Antonsen, “Herøysund bridge,” 2020.

[15] A. Sveen, “18-1069 Herøysund bru. Bæreevneberegninger,” 2020.

[16] A. Jukic and K. Ekfeldt, “Concrete Bridge Design with FEM,” 2012.

[17] ANSYS Inc, “ANSYS help SOLID187,” 2022. https://ansyshelp.ansys.com/account/secured?returnurl=/Views/Secured/corp/v231/en/ans_elem/Hlp_E_SOLID187.html?q=solid187

[18] ANSYS Inc, “ANSYS help SOLID186,” 2022. https://ansyshelp.ansys.com/account/secured?returnurl=/Views/Secured/corp/v231/en/ans_elem/Hlp_E_SOLID186.html?q=solid186

[19] ANSYS Inc, “General Element Formulations.” https://ansyshelp.ansys.com/account/secured?returnurl=/Views/Secured/corp/v231/en/ans_thry/thy_geo5.html

[20] ANSYS inc., “ANSYS help BEAM188,” 2022. https://ansyshelp.ansys.com/account/secured?returnurl=/Views/Secured/corp/v193/ans_elem/Hlp_E_BEAM188.html?q=beam188

[21] HandWiki, “Timoshenko-Ehrenfest beam theory,” 2023. https://handwiki.org/wiki/Timoshenko-Ehrenfest_beam_theory

[22] ANSYS Inc, “Governing Equations of Modal Analysis — Lesson 2.” https://courses.ansys.com/index.php/courses/modal-analysis/lessons/governing-equations-of-modal-analysis-lesson-2/

[23] Ingeniør Per Gulbrandsen AS, “Hovedpilarer m-fundamenter. Trykkplate. Formtegning.pdf,” 1965.

[24] Vegdirektoratet, “VEILEDNING Håndbok V412 Baereevneklassifisering av bruer, laster,” 2021. https://www.vegvesen.no/globalassets/fag/handboker/hb-v412-bareevneklassifisering.pdf (accessed Apr. 20, 2023).

[25] Ingeniør Per Gulbrandsen AS, “Oversikt. Utforming av brubanen,” 1965.

[26] ANSYS Inc, "SpaceClaim Online Help." https://help.spaceclaim.com/2015.0.0/en/Content/Importing_and_exporting.htm

[27] Ingeniør Per Gulbrandsen AS, "Landkar Herøyholmen. Forskaling og armering.pdf," 1965.

[28] Ingeniør Per Gulbrandsen AS, "Landkar Sildval. Forskaling og armering.pdf," 1965.

[29] ANSYS inc, "17.14. POST1 - Modal Assurance Criterion (MAC)," 2023. https://ansyshelp.ansys.com/account/secured?returnurl=/Views/Secured/corp/v231/en/ans_thry/thy_post16.html

[30] Ansys Inc, " 2.3.10. Automatic Mode Pairing Algorithm." https://ansyshelp.ansys.com/account/secured?returnurl=/Views/Secured/corp/v231/en/mech_addon/ds_results_nvh-maccalc-automodepair.html?q=paired%20modes (accessed May 10, 2023).

[31] Ansys Inc, "Chapter 2: NVH Toolkit Add-on," 2023. https://ansyshelp.ansys.com/account/secured?returnurl=/Views/Secured/corp/v231/en/mech_addon/nvh_intro_addon.html?q=nvh toolkit

Appendix A: Structural and modal analysis

Table of Contents

List of Tables

List of Figures

Foreword

This appendix is a finite element analysis report on both the solid element model and the beam element model produced in this thesis.

1 Numerical analysis solid element model

1.1 Problem description

Herøysund bridge is a 154,5-metre-long cast in place concrete post-tensioned bridge with 7 axes consisting of in total 2 land vessels, 2 land spans, a main span and 5 pillars. 4 of the pillars is cast firmly into the main span deck and longitudinal beams, while the 5th pillar (axis 2) is a tilting pillar under the Sildval land span. The bridge deck is supported structurally by two longitudinal underlying loadbearing beams. The beams are 400 mm wide transversally on the main span and 600 mm wide on the land spans, and varying in height all along the span, the beams are larger at the points where pillars connect to the deck. Points where pillars connect to the deck is also structurally reinforced by transverse beams. The main span of the bridge is approximately 60 metres long. The bridge has one lane for vehicles and is 5,3 metres wide. 10 metres out from both axis 4 and 5, in both directions longitudinally, there is cast in place pressure plates between the beams, so at axis 4 and 5 the bridge consist of box sections, while the rest of the bridge is open sections.

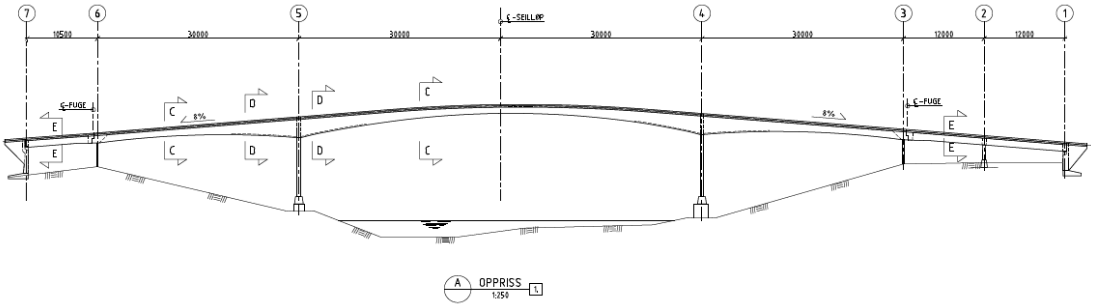

Figure 1: Vertical plane geometry of Herøysund bridge, axis 1-3 is called Sildval land span, axis 3-6 is the main span, axis 6-7 is called Herøyholmen land span. [3]

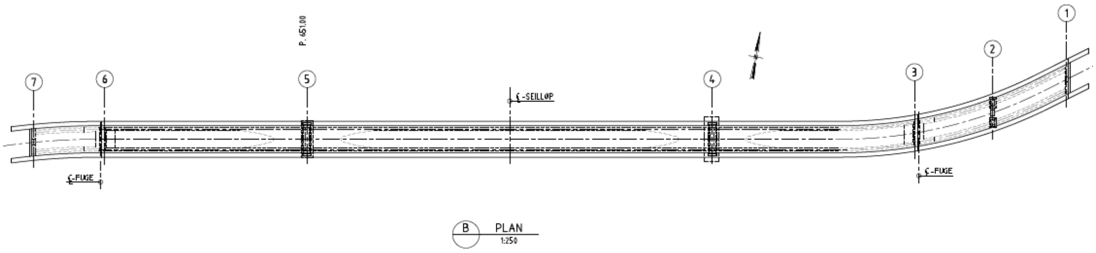

Figure 2: Horizontal plane geometry of Herøysund bridge, here the pressure plates at axis 4 and 5 is shown.[3]

In this report, the main focus of the static structural analysis is to serve as a pre-stress condition for the modal analysis. Further some results from the static structural analysis will be presented, with a focus on the middle of the main span of the bridge, as this is where the concrete load bearing beams has started cracking.

1.2 Units

Throughout the project work and in all calculations, the SI unit system is used. Deflection is presented in millimetres, stress is presented in megapascal, moment is presented in newton metres, frequencies are presented in Hz, volume is presented in cubic metres, mass is presented in kilograms or tonnes.

1.3 Geometry

Here three cross sections from the bridge will be presented: main span, box sections at main pillars and land spans cross sections. It is important to remember that there are variations in height of the beams and thicknesses of box sections, so these are just general cross sections from three important points of the bridge.

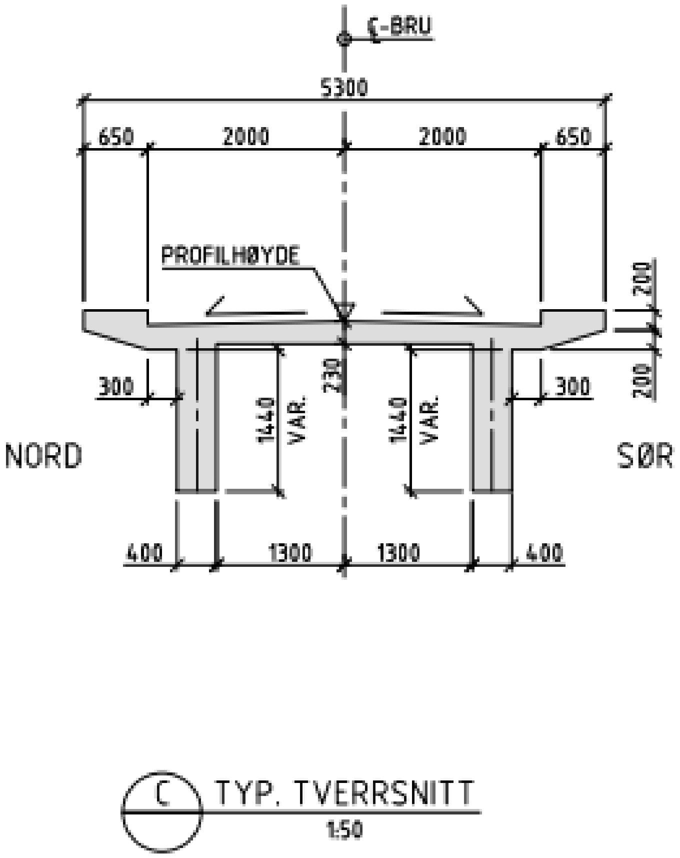

Figure 3: Typical cross section in the bridge main span, axis 3-6, see figure 1 point C for position of this particular cross section. [3]

In figure 3 a typical cross section of the bridge main span is shown, axis 3-6, except 10 metres in both directions from the two main pillars, where there are box sections as shown below. The only dimension that varies between axis 3-6 is the height of the load bearing beams and reinforcements close to the pillars.

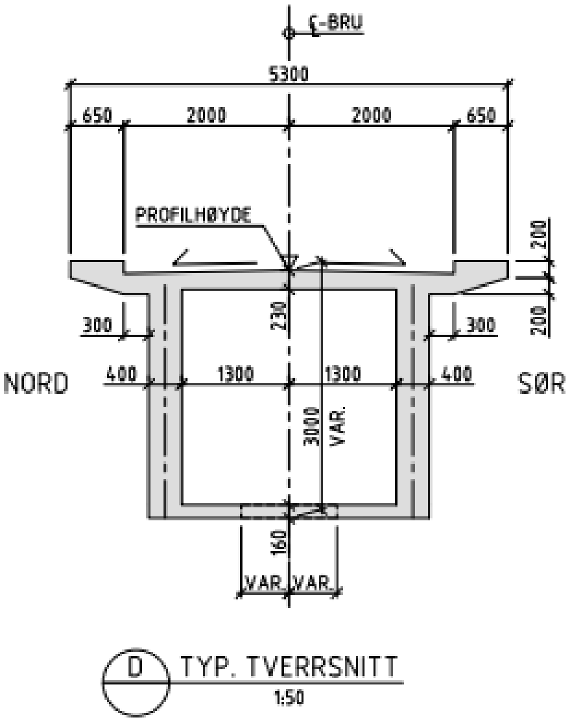

Figure 4: Typical cross section in the bridge main span, but only 10 metres in both directions from the two main pillars (axes 4 and 5). See figure 1 point D for position of this particular cross section. [3]

In figure 4 a typical cross section of the box sections positioned 10 metres in both directions from the main pillars is shown. The beam height and thickness of under girder varies. The cross sections directly at the main pillars (on axes 4 and 5) are filled with concrete, so that there is no empty space inside the box sections, as shown in figure 5 just below.

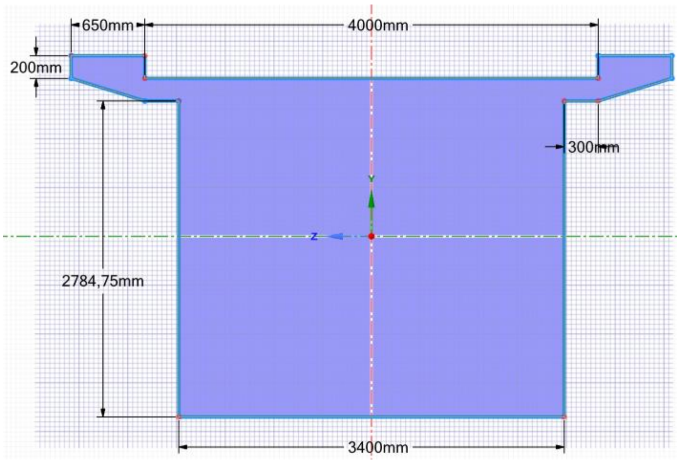

Figure 5: Typical cross section directly at the two main pillars.

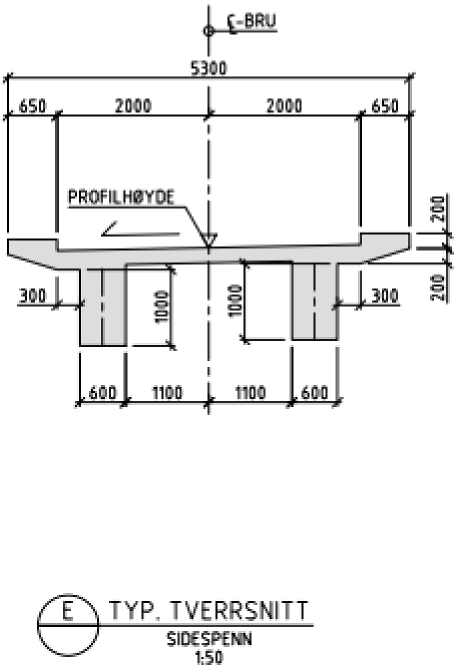

Figure 6: Typical cross section in the land spans. See figure 1 point E for positioning of this particular cross section. [3]

In figure 6, a typical cross section of the land span is shown. Beam height varies, but not much. Note the beams are 200 mm thicker in the land spans compared to the main span.

1.4 Coordinate system

The coordinate system of the model and analyses is described here.

Positive y direction = up vertically.

Negative y-direction = down vertically.

Positive x-direction = longitudinally along the bridge horizontally, from axes 7 to 1.

Negative x-direction = longitudinally along the bridge horizontally, from axes 1 to 7

Positive z direction = transversally on the bridge model horizontally, towards the viewer, looking at the bridge as in figure 1.

Negative z direction = transversally on the bridge model horizontally, away from the viewer, looking at the bridge as in figure 1.

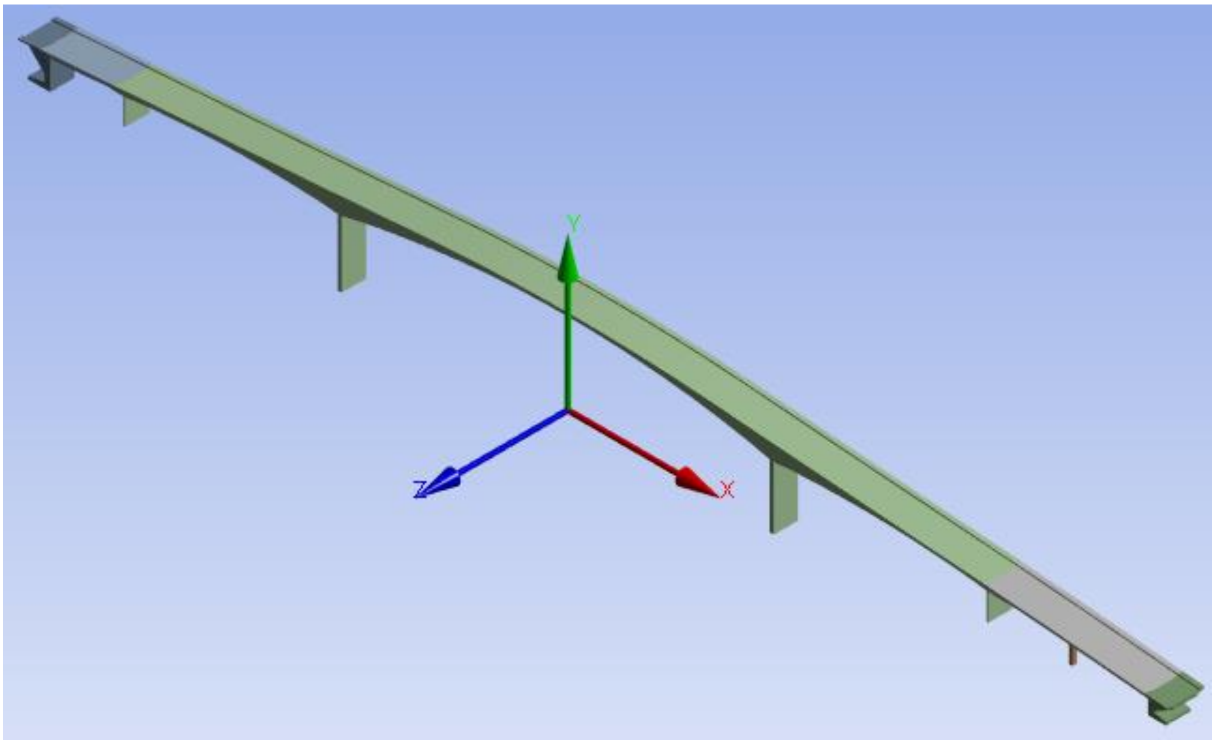

Figure 7: Coordinate system shown on model

1.5 Boundary conditions and loads for solid model

Here the loads inflicted on the bridge in this analysis is presented. This analysis mainly focuses on the natural frequencies and modal shapes of the bridge, but the loads is of importance as they can have a more or less significant influence on the mode shapes and frequencies. The static structural loads are applied to the model to represent as good as possible a realistic steady state of the bridge, then they are transferred as pre-stress from the structural analysis to the modal analysis.

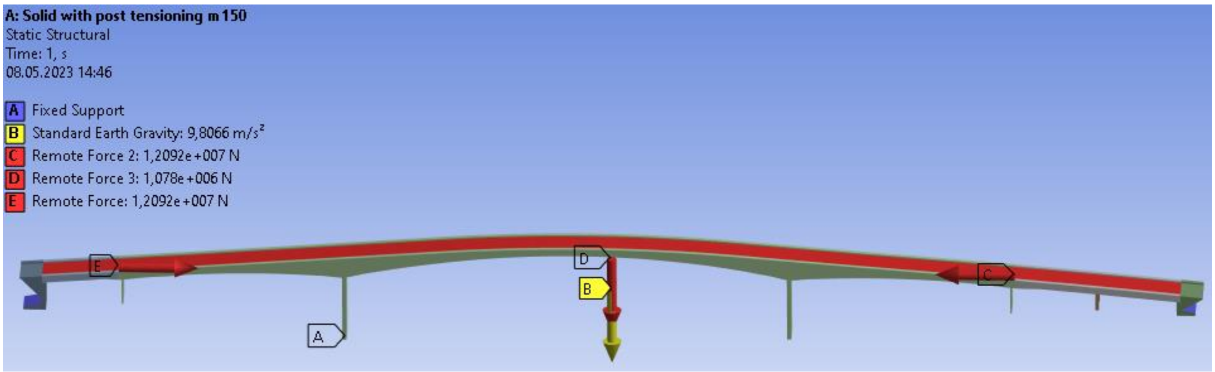

Figure 8: Loads and boundary conditions solid element model.

1.5.1 Boundary conditions

The model is fixed for translation and rotation on the bottom of each pillar and at the bottom and outside walls of the land vessels.

The land spans are connected on each end to the land vessels and main span by a joint allowing rotation in z direction, but no other rotation or translation.

The Sildval land span is connected to the tilting pillar by a joint allowing rotation in z direction, but no other rotation or translation.

1.5.2 Gravity

A gravity constant of 9,8066 m/s^2 is placed in the analysis, imparting on all masses of the system.

1.5.3 Post tensioning system

The post tensioning system of the bridge consist of 18 cables through the main span of the bridge imparting 137 tonnes horizontally in the longitudinal direction of the main span.

$$\frac{137\,000\,Kg \;\cdot\; 18\,tendons \;\cdot\; 9{,}8066\,m/s^2}{2} = 12091{,}5378\,kN \qquad 1.1$$

This is simulated by a force of 12091,5378 kN acting horizontally in the longitudinal direction of the bridge on both sides of the main span.

1.5.4 Asphalt and railing

Asphalt and railing are not modelled, but rather simulated by a pressure of 7kN/m bridge length over the span of the bridge. According to "handbok V412, Bæreevneklassifisering av bruer, laster" [4], chapter 4, page 38 from Statens Vegvesen, which is the governing body for bridge constructions in Norway, these are the relevant loads and magnitudes for Herøysund bridge:

Asphalt mass: 25 kN/m^3, railing mass: 0,5 kN/m.

$$4\,m * 0{,}06\,m \cdot 25\frac{kN}{m^3} + 2 \cdot 0{,}5\frac{kN}{m} = 7\frac{kN}{m} \qquad 1.2$$

$$7\frac{kN}{m} \cdot 154\,m = 1078\,kN \qquad 1.3$$

1.6 Materials

The pillars, bridge spans and land vessels are assigned the Ansys Granta [5] Concrete material model, with modifications to tensile strength and compressive strength.

The main span of the bridge is cast in place with concrete of quality B400. According to Statens Vegvesens "Håndbok V413 Bæreevneklassifisering av bruer, materialer"[6], these are the compressive and tensile properties for B400 concrete:

Tensile yield strength: 1,6 MPa.

Compressive yield strength: 22,4 MPa.

The minor pressure plates between the tilting pillar and Sildval land span and between the land spans and the land vessels are assigned the Ansys Granta [5] material Structural steel.

Table 1: Concrete material properties

Property	Value
Density	2392 Kg/m^3
Temperature	23° C
Coefficient of thermal expansion	0,00001015 C^{-1}
Young's modulus	19360 MPa
Poisson's ratio	0,1414
Bulk modulus	8998 MPa
Shear modulus	8480,8 MPa
Tensile yield strength	1,6 MPa

Table 2: Structural steel material properties

Property	Value
Density	7850 Kg/m^3
Temperature	22° C
Coefficient of thermal expansion	0,000012 C^{-1}
Young's modulus	200000 MPa
Poisson's ratio	0,3
Bulk modulus	166670 MPa
Shear modulus	76923 MPa
Tensile yield strength	250 MPa
Compressive yield strength	250 MPa
Tensile ultimate strength	460 MPa

1.7 Elements used on the solid model

Here the elements used in this analysis is presented.

1.7.1 SOLID186

The element SOLID186 is used for the minor pressure plates connecting the tilting pillar and land vessels to the bridge spans. Also, the tilting pillar is meshed in this element type. For results, the parts using this element type is disregarded.

SOLID 186 element is a higher order 3D 20-node solid element which exhibits quadratic displacement behaviour. The element is defined by 20 nodes each with three degrees of freedom per node: translations in the nodal x, y, and z directions. The element supports plasticity, creep, stress stiffening, hyper elasticity, large deflection, and large strain capabilities. It also has mixed formulation capability for simulating deformations of nearly incompressible elastoplastic materials, and fully incompressible hyper elastic materials.

In this analysis quadratic element shape is used for SOLID186.

[7]

1.7.2 SOLID187

The element SOLID187 is used for main span, land spans and land vessels.

SOLID187 element is a high-order 3D, 10-node element. The element has a quadratic displacement behaviour and is well suited to modelling irregular meshes (such as those produced from various CAD/CAM systems).

The element is defined by 10 nodes each with three degrees of freedom at each node: translations in the nodal x, y, and z directions. The element has plasticity, hyper elasticity, creep, stress stiffening, large deflection, and large strain capabilities. It also has mixed formulation capability for simulating deformations of nearly incompressible elastoplastic materials, and fully incompressible hyper elastic materials.

[8]

1.8 Mesh on solid model

1.8.1 Mesh for structural analysis of solid model

The solid model is meshed with an element size of 150mm for static structural analysis.

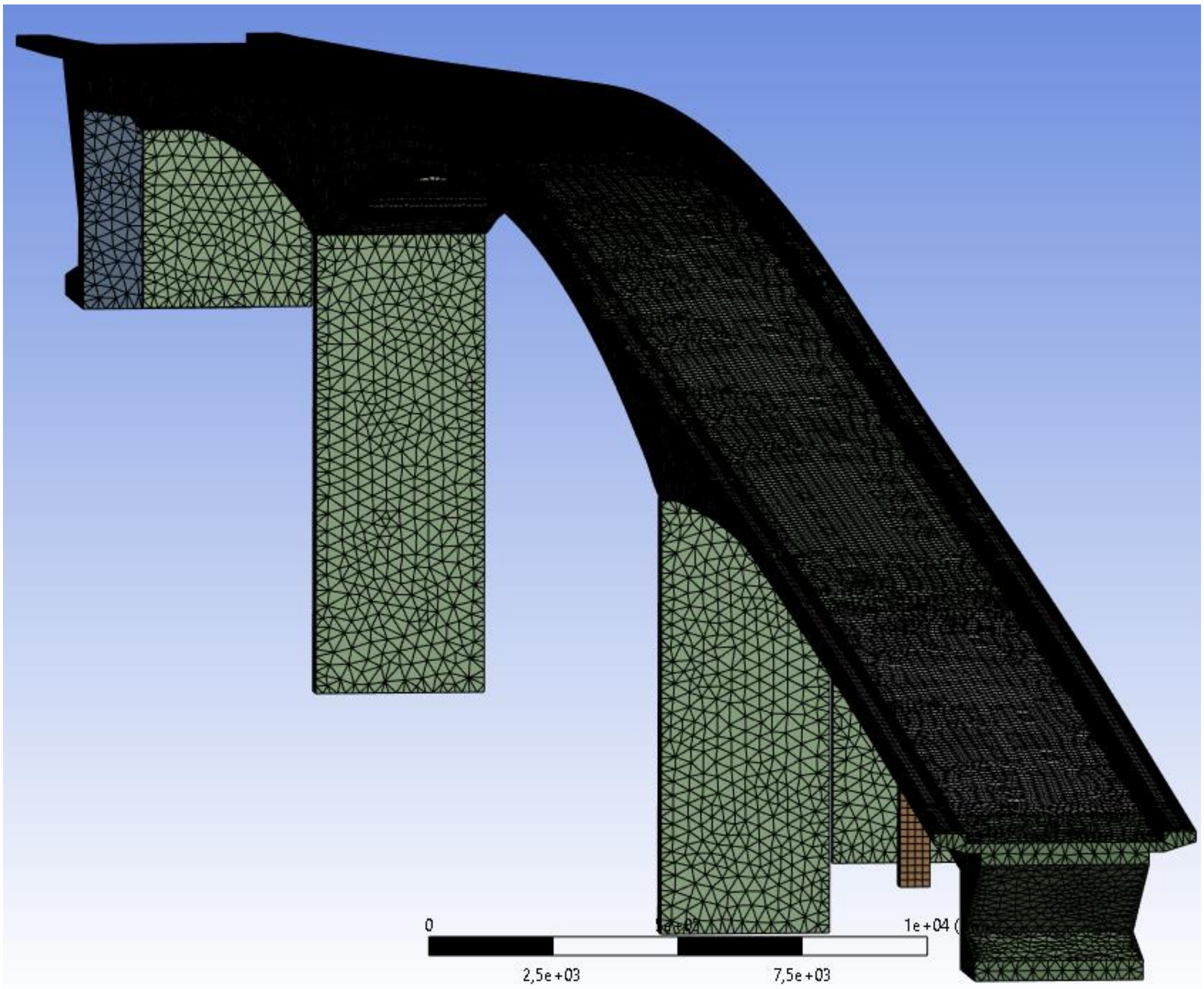

Figure 9: Solid model mesh.

For SOLID186: Quadratic elements.

For SOLID187: Tetrahedral elements.

1.9 Solid model mesh convergence control

1.9.1 Mesh convergence control for structural analysis of solid model

Mesh convergence control have been performed, the results from four different mesh refinements in equal increments are compared to each other, with respect to deflection, minimum principal stress, and maximum principal stress to check for mesh convergence. The four mesh refinements are of element size: 300 mm, 250 mm, 200 mm and 150 mm. For the deflection results, maximum values were used, materialising in the middle of the main span of the bridge. For stress, the middle of the main span was probed for the max/min values due to the occurrence of stress singularities (shown later in the report) in certain spots, like in sharp corners where the pillars meet the bridge. More accurate positions of the probes are shown in the results section. The convergence criteria are set to less than 1%. The following formulas was used to calculate mesh convergence:

$$\frac{|\mathrm{u}_{\mathrm{max,m1}}|-|\mathrm{u}_{\mathrm{max,m2}}|}{|\mathrm{u}_{\mathrm{maks,m1}}|} \cdot 100 = \% < 1\% \text{ OK} \tag{1.4}$$

$$\frac{|\sigma_{\mathrm{min,m1}}| - |\sigma_{\mathrm{min,m2}}|}{|\sigma_{\mathrm{min,m1}}|} \cdot 100 = \% < \ 1\% \text{ OK} \tag{1.5}$$

$$\frac{|\sigma_{\mathrm{max,m1}}| - |\sigma_{\mathrm{max,m2}}|}{|\sigma_{\mathrm{min,m1}}|} \cdot 100 = \ \% > \ 1\% \text{ OK} \tag{1.6}$$

Table 3 shows that the mesh element size of 150 mm is adequate for the static structural analysis of the solid model, and this is the mesh that will be used for the final analysis and results section of the static structural analysis of the solid model.

Table 3: Mesh convergence control for deflection and stress on solid model.

N#	Element size [mm]	Nodes	Elements	Max. deflection		Min. stress		Max. stress	
				[mm]	Conv. error [%]	[MPa]	Conv. error [%]	[MPa]	Conv. error [%]
1	300	124482	69672	36,225		5,8224		1,2963	
2	250	168860	93643	36,152	0,2	5,8404	0,3	1,2814	1,15
3	200	249698	141630	36,174	0,06	5,8494	0,15	1,2805	0,07
4	150	413582	238721	36,08	0,26	5,8662	0,28	1,2692	0,88

1.9.2 Mesh convergence control for modal analysis on solid model

Here, the results from four different mesh refinements in equal increments are compared to each other, with respect to the 20 first modes to check for mesh convergence. The four mesh refinements are of element size: 300 mm, 250 mm, 200 mm and 150 mm. The convergence criteria are set to less than 1%. The following formulas was used to calculate mesh convergence:

$$\frac{|\mathrm{f}_{\mathrm{mode1,m1}}| - |\mathrm{f}_{\mathrm{mode1,m2}}|}{|\mathrm{f}_{\mathrm{mode1,m1}}|} \cdot 100 = \% < 1\% \text{ OK} \qquad 1.7$$

Table 4 shows that the mesh element size of 150mm is adequate for the modal analysis of the solid model, and this is the mesh that will be used for the final analysis and results section of the modal analysis of the solid model.

Even though there is no significant increase of mesh convergence through the refinements, the results converge well over a relatively large range of mesh refinements.

Table 4: Mesh convergence control for modes on solid model.

Mode#	Element size [mm]						
	300	250		200		150	
	Nodes	Nodes		Nodes		Nodes	
	124482	168860		249698		413582	
	Elements	Elements		Elements		Elements	
	69672	93643		141630		238721	
	Frequency [Hz]	Frequency [Hz]	Conv. error [%]	Frequency [Hz]	Conv. error [%]	Frequency [Hz]	Conv. error [%]
1	1,3766	1,3755	0,08	1,3746	0,07	1,3736	0,07
2	1,8178	1,8172	0,03	1,8167	0,03	1,816	0,04
3	2,4136	2,4119	0,07	2,411	0,04	2,41	0,04
4	3,4279	3,4262	0,05	3,4255	0,02	3,4238	0,05
5	3,7656	3,7634	0,06	3,7616	0,05	3,7607	0,02
6	3,9583	3,9463	0,30	3,9335	0,32	3,9187	0,38
7	4,5253	4,524	0,03	4,5222	0,04	4,5205	0,04
8	4,6895	4,687	0,05	4,6855	0,03	4,6834	0,04
9	6,7137	6,7088	0,07	6,7044	0,07	6,7004	0,06
10	6,9653	6,961	0,06	6,9586	0,03	6,9562	0,03
11	7,2996	7,2937	0,08	7,2913	0,03	7,2829	0,12
12	7,5164	7,4938	0,30	7,465	0,38	7,4381	0,36
13	8,7579	8,7263	0,36	8,6966	0,34	8,6627	0,39
14	8,8748	8,8228	0,59	8,7938	0,33	8,781	0,15
15	9,5879	9,5771	0,11	9,567	0,11	9,5589	0,08
16	9,6336	9,6272	0,07	9,6237	0,04	9,6207	0,03
17	10,984	10,978	0,05	10,973	0,05	10,967	0,05
18	11,545	11,543	0,02	11,539	0,03	11,536	0,03
19	11,785	11,761	0,20	11,74	0,18	11,72	0,17
20	12,095	12,065	0,25	12,028	0,31	11,995	0,27

1.10 Solid model analysis results

Here the results of the static structural analysis and modal analysis of the solid model are presented.

1.10.1 Solid model total deflection

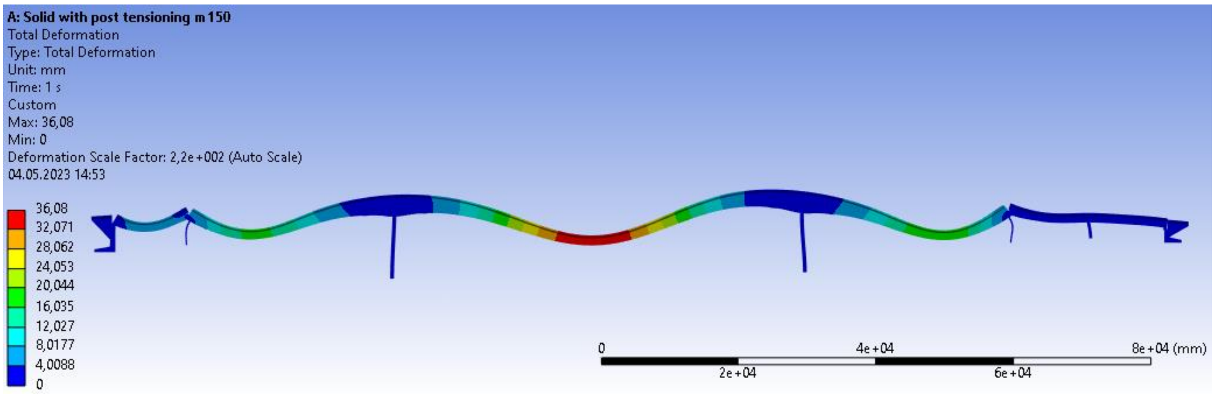

Figure 10: Total deflection of solid model; 36,08 mm, appearing in the middle of the main span of the bridge, in negative y-direction (vertically).

Shown in figure 10 is the total deflection of the solid model. It is shown in a scale factor to make it easier to see where it is taking place. Max deflection = 36,06 mm in the middle of the main span (approximately 83 metres from axis 7 in positive x direction) in negative y- direction (vertically).

1.10.2 Solid model minimum principal stress

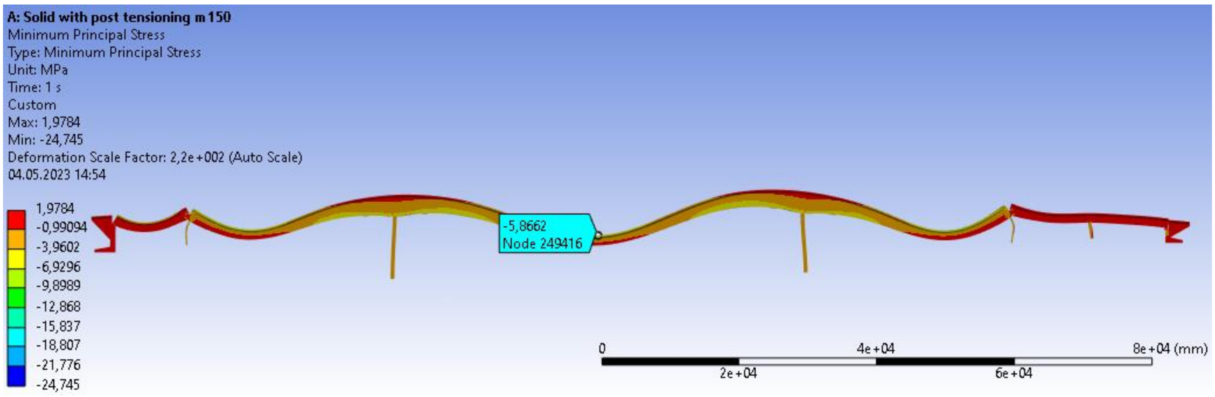

Figure 11: Minimum principal stress (compressive) of solid model main span; σ_3 = -5,8662 MPa, appearing in the middle of the main span on the top surface of the walkway.

Shown in figure 11 is the minimum principal stress (compressive) σ_3 = -5,8662 MPa in the solid model main span (approximately 83 metres from axis 7 in positive x direction). There are larger values of stress in the model, the largest of them are singularities and should be disregarded.

For this report the most interesting place to view stress is the middle of the main span, as this is where the bridge is damaged and where the main focus of structural health is.

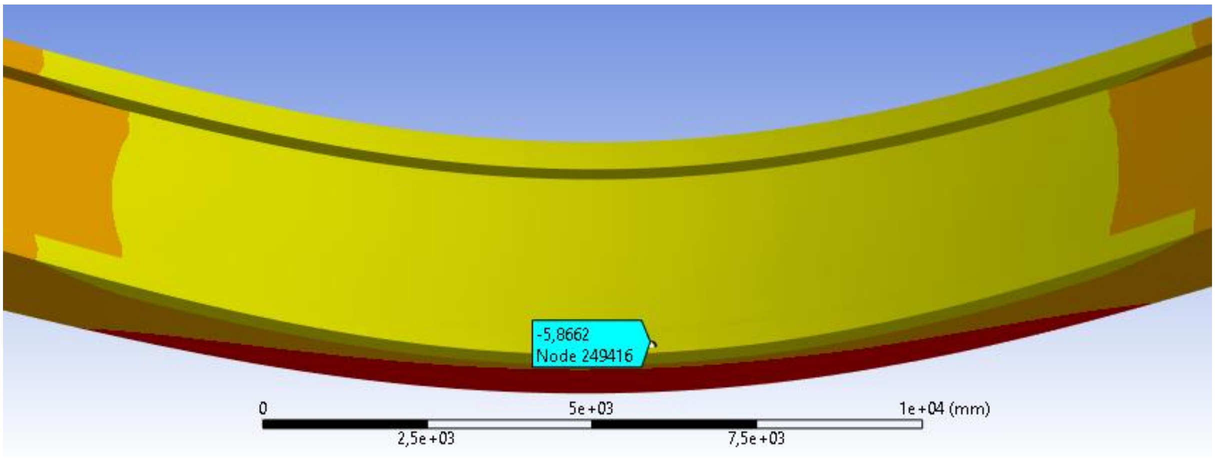

Figure 12: Minimum principal stress (compressive) = σ_3 = 5,8662 MPa, detailed view.

In figure 12 a more detailed view of the top surface of the middle of the main span is shown. The maximum compressive stress is as shown on the walkways.

f_{cn} = 22,4 N/mm^2 = 22,4 MPa. Compared to the result from the analysis σ_3 = -5,8662 MPa, there is a safety margin of approximately 3,8.

1.10.3 Solid model maximum principal stress

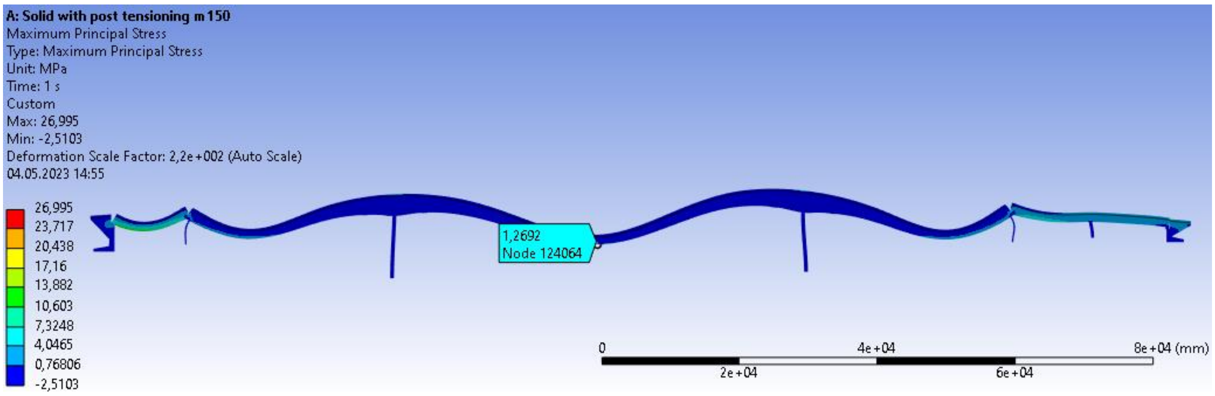

A: Solid with post tensioning m150
Maximum Principal Stress
Type: Maximum Principal Stress
Unit: MPa
Time: 1 s
Custom
Max: 26,995
Min: -2,5103
Deformation Scale Factor: 2,2e+002 (Auto Scale)
04.05.2023 14:55

Figure 13:Maximum principal stress (tensile) of solid model main span; σ_1 = 1,2696 MPa, appearing in the middle of the main on the bottom of the beams.

Shown in figure 13 is the maximum principal stress (tensile) σ_1 = 1,2696 MPa in the middle of the main span. There are larger values of stress in the model, the largest of them are singularities and should be disregarded. For this report the most interesting place to view stress is the middle of the main span (approximately 83 metres from axis 7 in positive x direction), as this is where the bridge is damaged and where the main focus of structural health is. Stress singularities is further described in chapter 1.10.4.

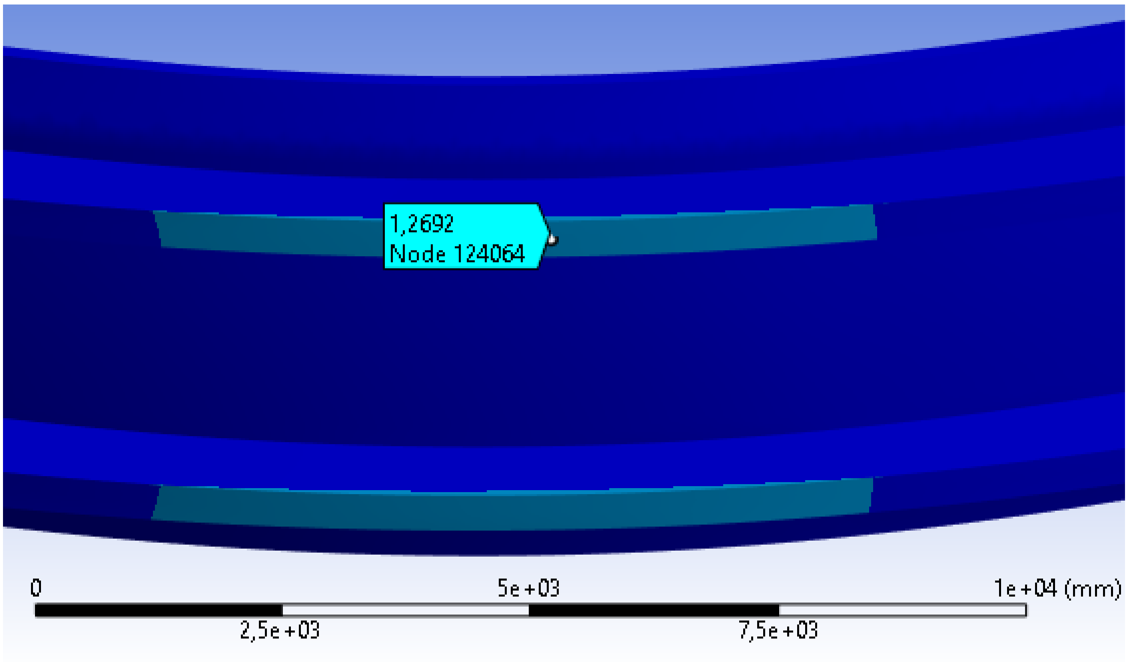

Figure 14: Maximum principal stress (tensile) = $\sigma_1 =$ 1,2692 MPa detailed view.

In figure 14 a more detailed view of the bottom of the load bearing beams in the middle of the main span (approximately 83 metres from axis 7 in positive x direction) is shown. The maximum tensile stress is as shown on the bottom of the load bearing beams.

f_{tn} = 1,6 N/mm^2 = 1,6 MPa. Compared to the result from the analysis σ_1 = 1,2692 MPa, there is a safety margin of approximately 1,26. This is not considered a very safe safety factor, so this may point towards why there has formed cracks in the bottom of the load bearing beams in the middle of the main span.

1.10.4 Solid model stress singularities

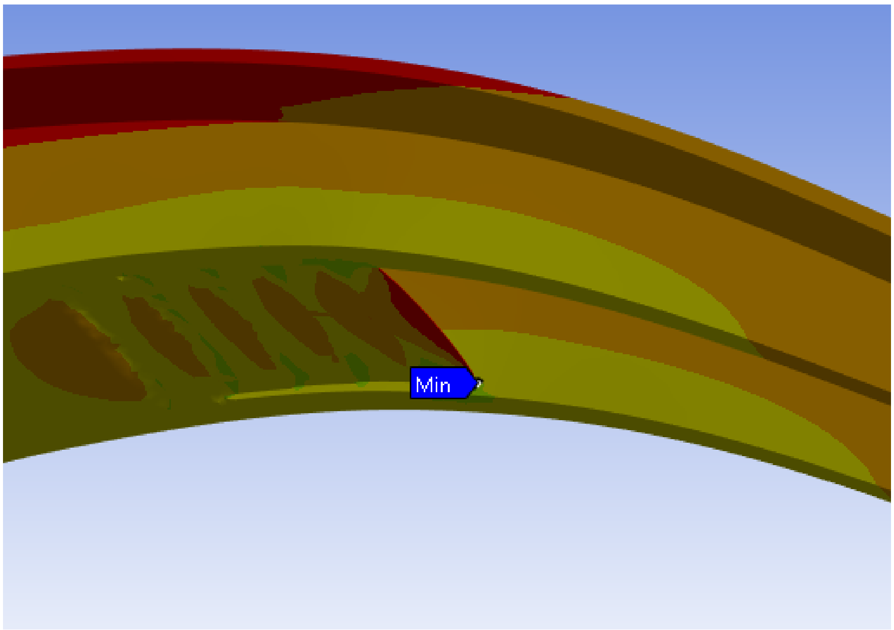

Figure 15: Stress singularities for minimum principal stress.

Stress singularities for min principal stress, occurring in the pressure plates at the main pillars.

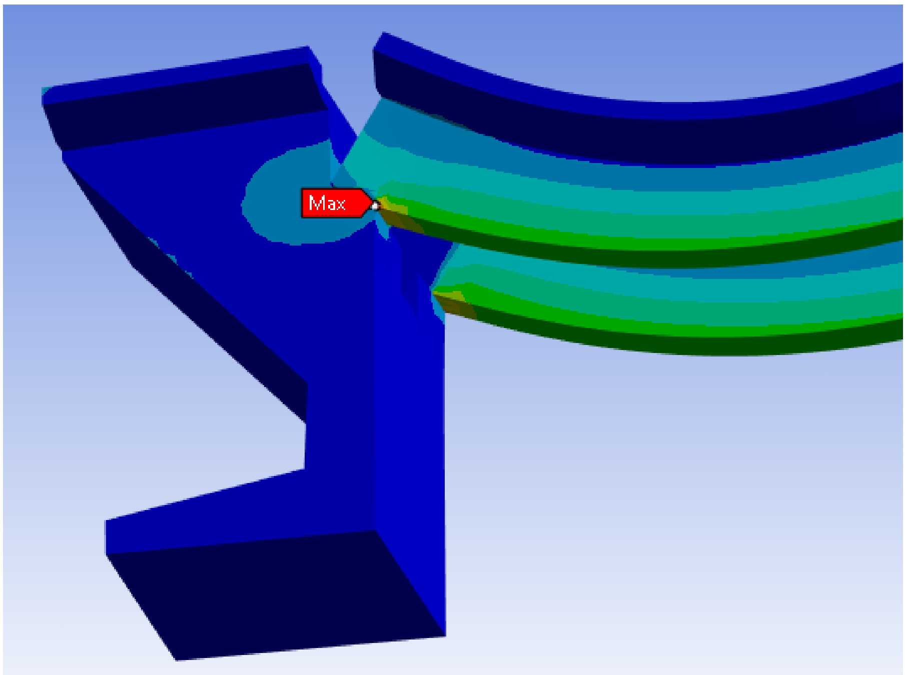

Figure 16: Stress singularities for maximum principal stress.

Stress singularities for max principal stress, occurring in the connection between the land vessel and land span at Sildval side (axis 1).

1.10.5 Vector principal elastic strain on solid model

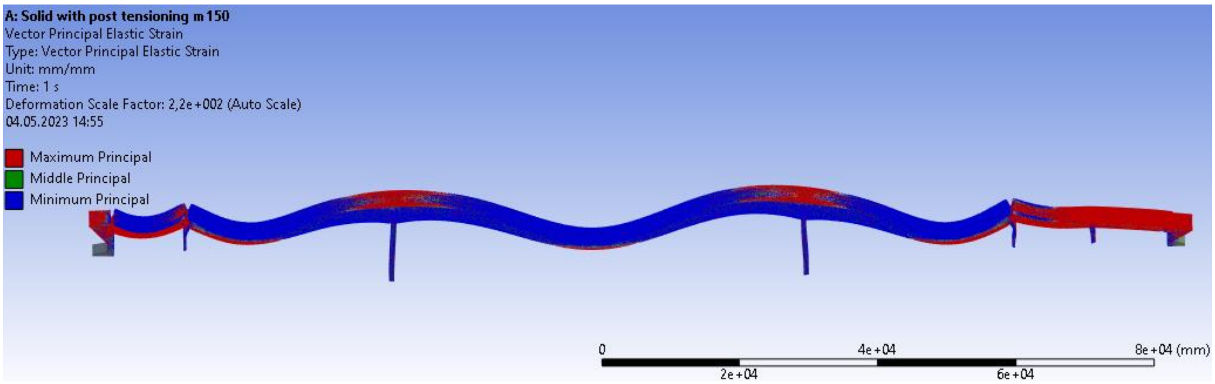

Figure 17:Vector principal elastic strain top of bridge.

Vector principal elastic strain is a good result to visualize where the tensile forces form in the construction. As shown in figure 17 and 18, the tensile forces in the main span mainly materialize in the top surface of the bridge just over the main pillars, and in the bottom of the beams in the middle of the main span. There is also a lot of tensile forces acting on the land spans and land vessels. These tensile forces are most likely due to the boundary conditions combined with the post tensioning system, where the post tensioning forces pull the land spans and land vessels towards the middle, and the land spans and land vessels are locked in translations and rotations of movement in all directions except rotation around the Z axis, thus they should be disregarded.

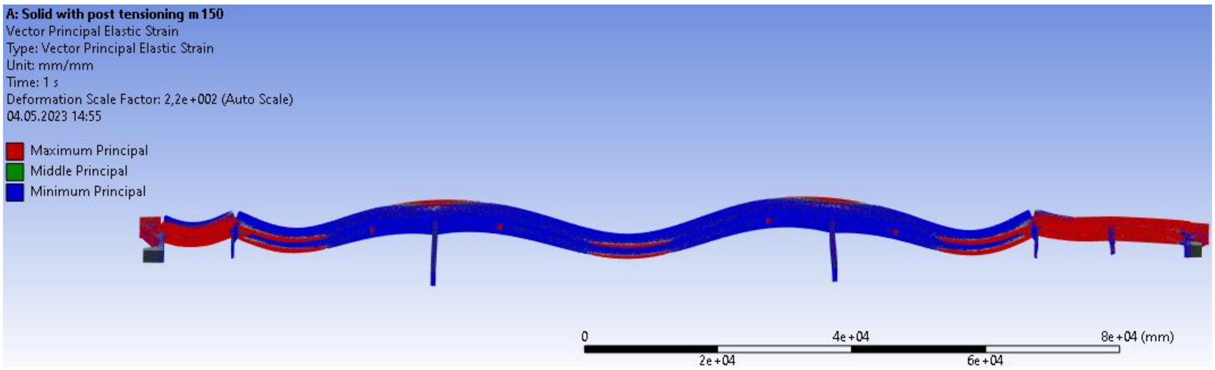

Figure 18: Vector principal elastic strain bottom of bridge.

1.10.6 Solid model without post tensioning

To confirm the technique of simulating the post tensioning system using horizontal forces clamping the main span together, the post tensioning forces was removed from the model, and results were compared.

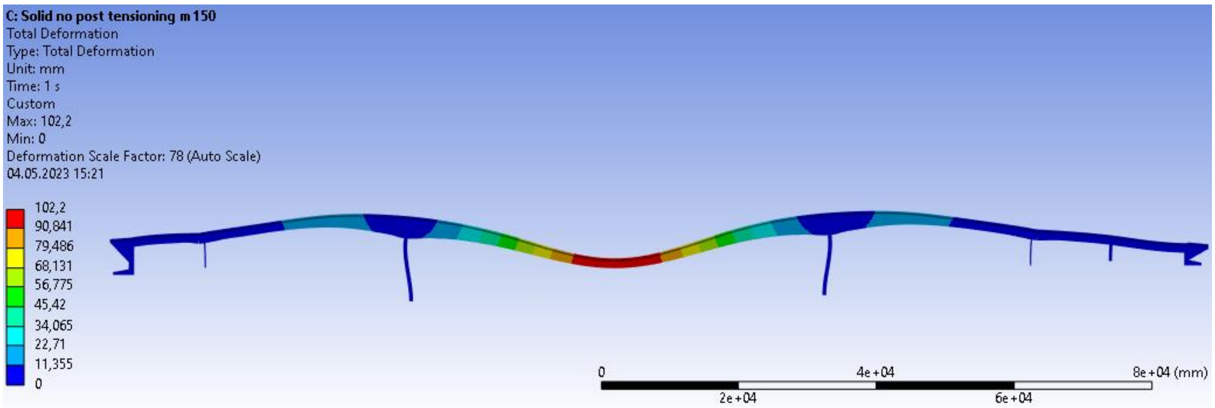

C: Solid no post tensioning m 150
Total Deformation
Type: Total Deformation
Unit: mm
Time: 1 s
Custom
Max: 102,2
Min: 0
Deformation Scale Factor: 78 (Auto Scale)
04.05.2023 15:21

Figure 19: Total deflection of the solid model without post tensioning: 102,2 mm.

Shown in figure 19 is the total deflection of the bridge after the post tensioning forces was removed from the analysis. Total deflection with the post tensioning system is 36,08 mm, and without the post tensioning system total deflection is 102,2 mm. This gives an indication that the technique of simulating the post tensioning system with horizontal forces does work as intended.

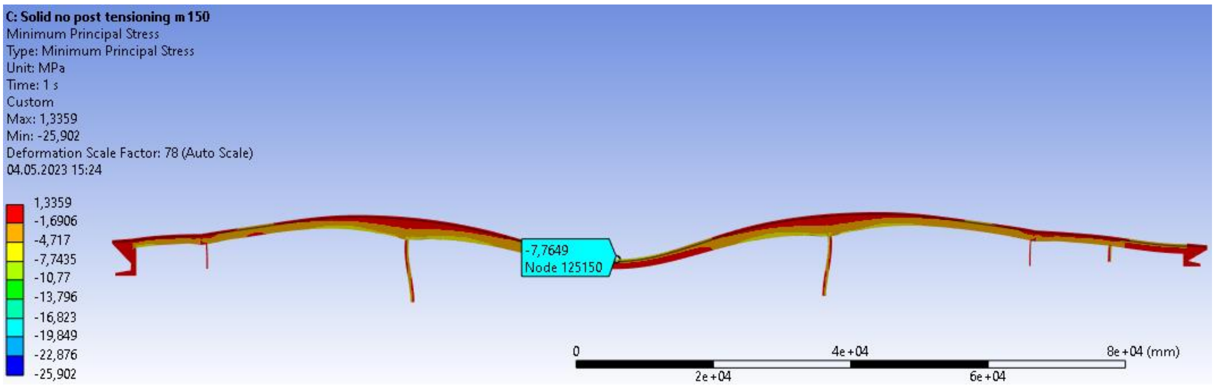

C: Solid no post tensioning m 150
Minimum Principal Stress
Type: Minimum Principal Stress
Unit: MPa
Time: 1 s
Custom
Max: 1,3359
Min: -25,902
Deformation Scale Factor: 78 (Auto Scale)
04.05.2023 15:24

Figure 20: Minimum principal stress of the solid model without post tensioning: -7,7649 MPa.

Shown in figure 20 and 21 is the minimum principal stress of the bridge main span after the post tensioning forces was removed from the analysis. Minimum principal stress with the post tensining system is -5,8662 MPa, while without the post tensioning system minimum principal stress is -7,7649 MPa. The compressive stress decreased with the post tensioning system, which is as intended.

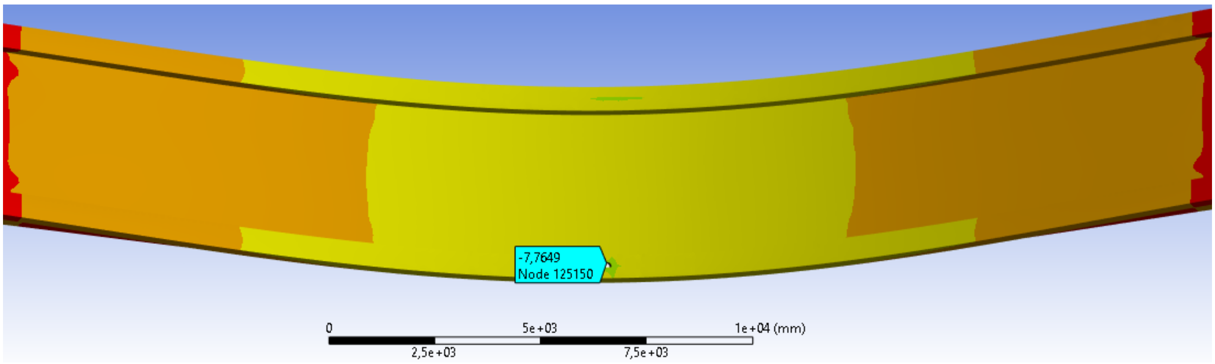

Figure 21: Details of minimum principal stress of the solid model without post tensioning: -7,7649 MPa.

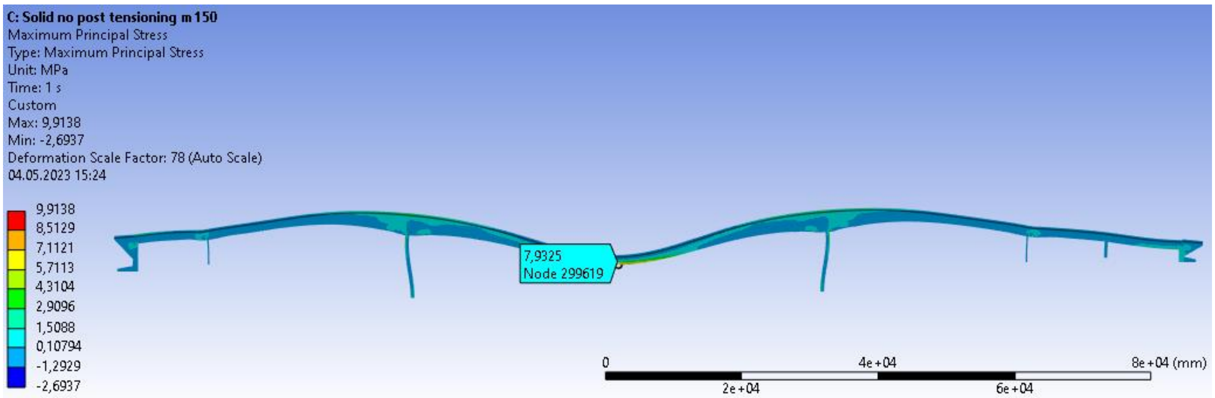

Figure 22: Maximum principal stress of the solid model without post tensioning: 7,9138 MPa.

Shown in figure 22 and 23 is the maximum principal elastic stress of the bridge solid model after the post tensining forces was removed from the analysis. Maximum principal stress with the post tensinng system is 1,2692 MPa while without the post tensining system maximum principal stress is 7,9325 MPa. This tells us that without the post tensioning system, the concrete would not withstand the stress, as the concrete f_{tn} = 1,6 MPa. When the post tensioning system is added to the model, the stress drops to 1,2692 MPa, which shows that the simulated post tensioning system is working as intended.

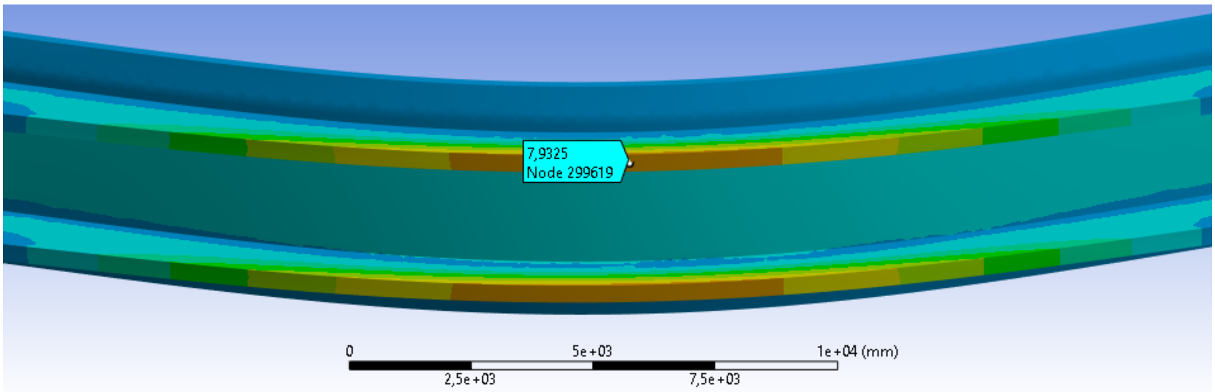

Figure 23: Maximum principal stress of the solid model without post tensioning: 7,9138 MPa.

1.10.7 Evaluation of modes from the solid model

1.10.7.1 Solid model participation factor

Participation factor is calculated using the following formula:

$$\gamma_i = \{ø\}_i^T [M]\{D\} \tag{1.8}$$

where:

γ_i = participation factor, $\{ø\}_i^T$ = mode shapes, [M] = mass matrix, {D} = excitation direction vector.

[9]

The excitation direction vector is an assumed unit displacement vector and depends on the direction of excitation in each of the global cartesian directions and rotation about each of the axes. [10]

Table 5: natural frequencies and corresponding participation factors for the solid model.

Mode	Freq. (Hz)	Trans. X	Trans. Y	Trans. Z	Rot. X	Rot. Y	Rot. Z
Mode 1	1,3736	0,20798	-7,6584	-2,01E-4	-2,8233	0,38049	-7033,7
Mode 2	1,816	-2,88E-4	-4,13E-4	21,655	2,80E+5	19401	-17,158
Mode 3	2,41	-3,0039	-0,11428	-5,49E-4	-6,784	24,086	-2,95E+5
Mode 4	3,4238	7,94E-4	-1,53E-3	-0,40611	-11677	7,89E+5	37,564
Mode 5	3,7607	-0,28029	-15,89	6,96E-5	1,9653	-36,57	-7131,4
Mode 6	3,9187	1,23E-3	-3,86E-5	4,2053	31095	-17700	87,973
Mode 7	4,5205	-9,8773	-5,78E-2	-9,56E-3	-107,72	121,02	-4,55E+5
Mode 8	4,6834	-8,39E-3	1,42E-3	16,326	1,73E+5	-49810	-244,46
Mode 9	6,7004	8,95E-3	8,17E-3	-0,6157	-7905,8	5,6E+5	-84,844
Mode 10	6,9562	-6,8593	-10,508	7,45E-4	5,3352	367,33	1,09E+5
Mode 11	7,2829	26,356	-4,9144	2,16E-3	20,961	-108,05	-4,68E+5
Mode 12	7,4381	-6,21E-3	-1,80E-3	-6,73E-2	-5,6879	-11961	101,31
Mode 13	8,6627	-1,48E-3	-5,33E-4	2,7821	11495	-23994	40,088
Mode 14	8,781	-5,44E-4	-1,92E-4	-2,8577	-19079	-29413	22,357
Mode 15	9,5589	3,02E-2	-5,46E-3	6,459	71930	-1,83E+5	-1062,9
Mode 16	9,6207	-4,0033	0,76351	4,79E-2	538,93	-1379,6	1,44E+5
Mode 17	10,967	5,12E-2	6,5382	-4,05E-3	-48,541	589,63	-47334
Mode 18	11,536	-3,1397	-1,175	1,19E-3	23,809	-390,57	-2,47E+5
Mode 19	11,72	-3,59E-3	-1,58E-2	-2,6457	-27736	5,12E+5	-79,052
Mode 20	11,995	3,12E-3	4,99E-3	-2,7146	-14371	2,51E+5	745,18

1.10.7.2 Solid model effective mass

Effective mass is calculated using the following formula:

$$M_{ei} = \frac{\gamma_i^2}{\{\text{ø}\}_i^T [M]\{D\}} \qquad 1.9$$

$$\{\text{ø}\}_i^T [M]\{D\} = 1 \qquad 1.10$$

$$M_{eff,i} = \gamma_i^2 \qquad 1.11$$

where: γ_i = participation factor, $\{ø\}_i^T$ = mode shapes, [M] = mass matrix, {D} = excitation direction vector. [11]

Table 6: Natural frequencies and corresponding effective mass for the solid model. M=mode.

Mode	Freq. (Hz)	Trans. X [tonne]	Trans. Y [tonne]	Trans. Z [tonne]	Rot. X [tonne mm mm]	Rot. Y [tonne mm mm]	Rot. Z [tonne mm mm]
M 1	1,3736	4,32e-2	58,65	4,038e-8	7,9711	0,14478	4,9473e+7
M 2	1,816	8,28e-8	1,703e-7	468,95	7,8187e+10	3,7641e+8	294,4
M 3	2,41	9,0231	1,306e-2	3,016e-7	46,023	580,11	8,681e+10
M 4	3,4238	6,30e-7	2,354e-6	0,16493	1,3635e+8	6,2193e+11	1411,1
M 5	3,7607	7,85e-2	252,48	4,838e-9	3,8623	1337,4	5,0857e+7
M 6	3,9187	1,51e-6	1,490e-9	17,684	9,6687e+8	3,1329e+8	7739,2
M 7	4,5205	97,561	3,344e-3	9,142e-5	11603	14647	2,0735e+11
M 8	4,6834	7,03e-5	2,029e-6	266,52	2,9996e+10	2,481e+9	59759
M 9	6,7004	8,01e-5	6,682e-5	0,37909	6,2502e+7	3,1329e+11	7198,6
M 10	6,9562	47,05	110,42	5,545e-7	28,465	1,3493e+5	1,1897e+10
M 11	7,2829	694,65	24,152	4,679e-6	439,35	11674	2,1898e+11
M 12	7,4381	3,85e-5	3,228e-6	4,528e-3	32,353	1,4307e+8	10264
M 13	8,6627	2,18e-6	2,839e-7	7,7403	1,3214e+8	5,7571e+8	1607
M 14	8,781	2,96e-7	3,687e-8	8,1666	3,64e+8	8,6515e+8	499,83
M 15	9,5589	9,09e-4	2,983e-5	41,718	5,174e+9	3,3394e+10	1,1297e+6
M 16	9,6207	16,026	0,58295	2,292e-3	2,9045e+5	1,9032e+6	2,0772e+10
M 17	10,967	2,62e-3	42,747	1,636e-5	2356,3	3,4766e+5	2,2405e+9
M 18	11,536	9,8578	1,3806	1,423e-6	566,88	1,5255e+5	6,1234e+10
M 19	11,72	1,29e-5	2,50e-4	6,9998	7,6927e+8	2,6189e+11	6249,3
M 20	11,995	9,72e-6	2,486e-5	7,3692	2,0651e+8	6,2986e+10	5,553e+5
Sum		874,29	490,43	825,7	1,1599e+11	1,2983e+12	6,0938e+11

1.10.8 Solid model cumulative effective mass fraction

Cumulative effective mass fraction for the ith mode is calculated using the following formula:

$$\bar{M}_{ei} = \frac{\sum_{j=1}^{i} M_{ej}}{\sum_{j=1}^{N} ej}, \qquad 1.12$$

where N is the total number of nodes. [12]

Table 7: Cumulative effective mass fraction for the solid model.

Mode	Freq. (Hz)	Trans. X	Trans. Y	Trans. Z	Rot. X	Rot. Y	Rot. Z
Mode 1	1,3736	4,947e-5	0,11959	4,891e-11	6,87e-11	1,1152e-13	8,1186e-5
Mode 2	1,816	4,947e-5	0,11959	0,56794	0,67406	2,8993e-4	8,118e-5
Mode 3	2,41	1,037e-2	0,11962	0,56794	0,67406	2,8993e-4	0,14254
Mode 4	3,4238	1,037e-2	0,11962	0,56814	0,67523	0,47934	0,14254
Mode 5	3,7607	1,046e-2	0,63442	0,56814	0,67523	0,47934	0,14262
Mode 6	3,9187	1,046e-2	0,63442	0,58956	0,68357	0,47959	0,14262
Mode 7	4,5205	0,12205	0,63443	0,58956	0,68357	0,47959	0,48288
Mode 8	4,6834	0,12205	0,63443	0,91234	0,94216	0,4815	0,48288
Mode 9	6,7004	0,12205	0,63443	0,9128	0,9427	0,72281	0,48288
Mode 10	6,9562	0,17586	0,85959	0,9128	0,9427	0,72281	0,5024
Mode 11	7,2829	0,97039	0,90883	0,9128	0,9427	0,72281	0,86175
Mode 12	7,4381	0,97039	0,90883	0,91281	0,9427	0,72292	0,86175
Mode 13	8,6627	0,97039	0,90883	0,92218	0,94384	0,72337	0,86175
Mode 14	8,781	0,97039	0,90883	0,93207	0,94698	0,72403	0,86175
Mode 15	9,5589	0,97039	0,90883	0,9826	0,99159	0,74976	0,86175
Mode 16	9,6207	0,98872	0,91002	0,9826	0,99159	0,74976	0,89584
Mode 17	10,967	0,98872	0,99718	0,9826	0,99159	0,74976	0,89951
Mode 18	11,536	1,	1,	0,9826	0,99159	0,74976	1,
Mode 19	11,72	1,	1,	0,99108	0,99822	0,95148	1,
Mode 20	11,995	1,	1,	1,	1,	1,	1,

1.10.8.1 Solid model ratio of effective mass to total mass

Ratio of effective mass to total mass is calculated by dividing effective mass by the total mass of the system. This parameter is used to ensure all significant modes has been extracted from the modal analysis. Hence the most interesting result from this parameter is the sum, seen in the bottom of table 8. It is common practice to shoot for achieving at least 0,8 or 0,9 in all of the DOF's. This would mean one would have 80% or 90 % of the total mass is represented in the extracted modes. Experiments have been done by extracting 100 modes from the solid model, and all modes above 20 was deemed to be outside of the scope of this thesis.

Table 8: Ratio of effective mass to total mass for the solid model. M=mode.

Mode	Freq. (Hz)	Trans. X	Trans. Y	Trans. Z	Rot. X	Rot. Y	Rot. Z
M 1	1,3736	3,5888e-5	4,866e-2	3,35e-11	5,813e-11	4,98e-14	1,6304e-5
M 2	1,816	6,873e-11	1,412e-10	0,38907	0,57019	1,297e-4	9,702e-11
M 3	2,41	7,4862e-3	1,0836e-5	2,5e-10	3,356e-10	1,99e-10	2,8609e-2
M 4	3,4238	5,232e-10	1,953e-9	1,368e-4	9,9431e-4	0,2143	4,650e-10
M 5	3,7607	6,5183e-5	0,20947	4,01e-12	2,816e-11	4,60e-10	1,676e-5
M 6	3,9187	1,2565e-9	1,236e-12	1,467e-2	7,051e-3	1,079e-4	2,5505e-9
M 7	4,5205	8,0943e-2	2,7751e-6	7,585e-8	8,4618e-8	5,046e-9	6,8332e-2
M 8	4,6834	5,8359e-8	1,6841e-9	0,22113	0,21875	8,548e-4	1,9694e-8
M 9	6,7004	6,6487e-8	5,5438e-8	3,145e-4	4,558e-4	0,10795	2,3723e-9
M 10	6,9562	3,9036e-2	9,1614e-2	4,60e-10	2,075e-10	4,649e-8	3,9208e-3
M 11	7,2829	0,57633	2,0038e-2	3,882e-9	3,204e-9	4,022e-9	7,2165e-2
M 12	7,4381	3,1961e-8	2,6785e-9	3,757e-6	2,35e-10	4,929e-5	3,3827e-9
M 13	8,6627	1,809e-9	2,35e-10	6,42e-3	9,636e-4	1,983e-4	5,2961e-10
M 14	8,781	2,45e-10	3,05e-11	6,775e-3	2,654e-3	2,981e-4	1,647e-10
M 15	9,5589	7,541e-7	2,475e-8	3,461e-2	3,773e-2	1,150e-2	3,7231e-7
M 16	9,6207	1,329e-2	4,836e-4	1,902e-6	2,118e-6	6,558e-7	6,8454e-3
M 17	10,967	2,175e-6	3,546e-2	1,358e-8	1,718e-8	1,198e-7	7,3836e-4
M 18	11,536	8,178e-3	1,145e-3	1,18e-9	4,134e-9	5,256e-8	2,018e-2
M 19	11,72	1,07e-8	2,075e-7	5,807e-3	5,61e-3	9,024e-2	2,0595e-9
M 20	11,995	8,066e-9	2,062e-8	6,114e-3	1,506e-3	2,170e-2	1,83e-7
Sum		0,72537	0,40689	0,68506	0,8459	0,44734	0,20082

The participation factor and effective mass gives a perspective into how much mass is moving in each direction for each mode. A high value indicates that the mode will be excited by excitations in that direction. These values can be used to gain an understanding of the significance of each mode.

Higher frequency modes are usually negligible as the lower frequency modes usually dominate due to the fact that it takes less energy to vibrate at lower frequencies. From this it could be said it is as easy as just selecting the first six modes, as they are the lower frequency ones. But it can also be interesting to see if there are any other significant modes using the participation factor and effective mass.

In table 5 and 6 the 20 first natural frequencies and their corresponding participation factors and effective masses is shown. For translations, all absolute values over 5 is shown in green, while for rotations, all absolute values over 1000 is shown in green. This gives a good perspective on how much movement each mode has and in which direction they move.

In table 7 the 20 first natural frequencies and their corresponding cumulative effective mass fraction is shown. The points of interest in this table are when we have large jumps in values between two modes. This shows that a big fraction of effective mass is pertained to the second of the two modes.

From the participation factor, effective mass and cumulative effective mass results, we can see there are several active modes after the first six, and most notably, mode 7, 8, 9, 10, 11, 15, 16, 17, 19 and 20 is quite significant.

1.10.8.2 Solid model mode shapes

Mode 1:

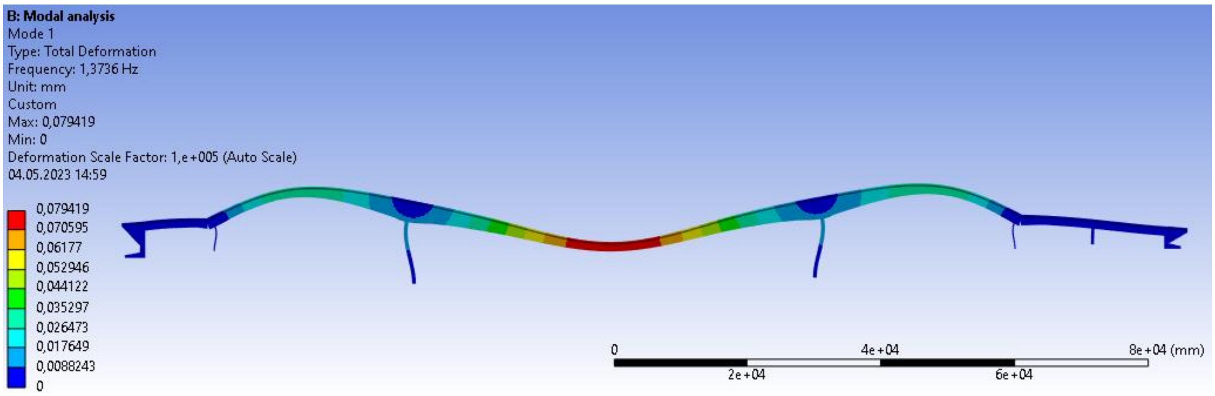

Figure 24: Mode 1 shape for the solid model viewed from the side (Z direction).

Mode 1 on the solid model is a longitudinal mode shape, mainly with translation of movement in Y direction and rotation around the Z axis. Mode 1 on the solid model corresponds well (99,5%) with mode 1 on the beam model. Mode 1 is recommended for comparison with operational mode analysis results.

Mode 2:

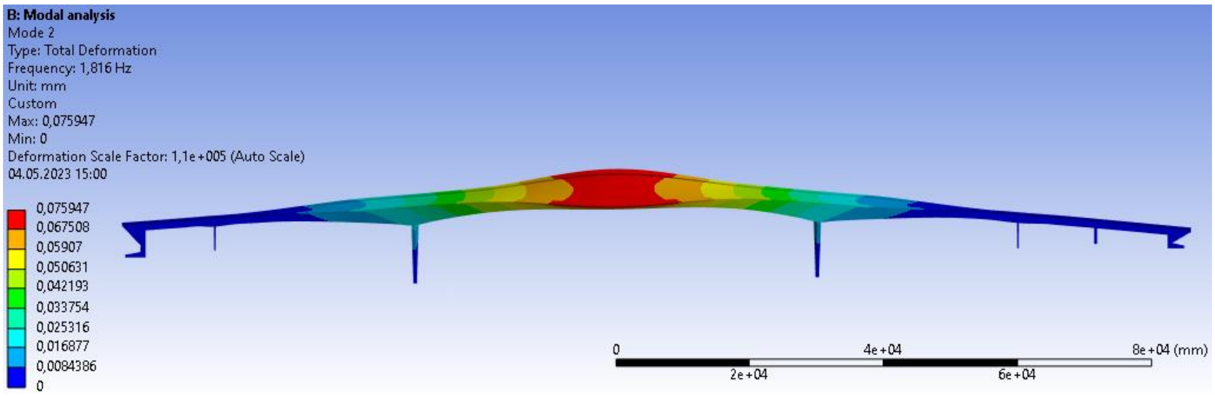

Figure 25: Mode 2 shape for the solid model viewed from the side (Z direction).

Mode 2 on the solid model is a transverse mode shape, mainly with translation of movement in Z direction and rotation around the X and Y axes. Mode 2 on the solid model corresponds well (98,8%) with mode 2 on the beam model. Mode 2 is recommended for comparison with operational mode analysis results.

Mode 3:

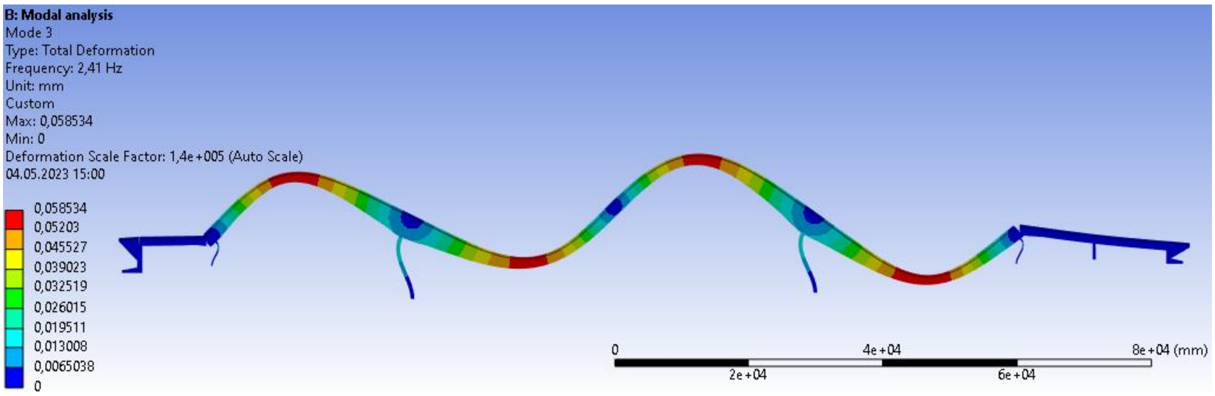

Figure 26: Mode 3 shape for the solid model viewed from the side (Z direction).

Mode 3 on the solid model is a longitudinal mode shape, mainly with rotation around the Z axis. Mode 3 on the solid model corresponds well (99,4%) with mode 3 on the beam model. Mode 3 is recommended for comparison with operational mode analysis results.

Mode 4:

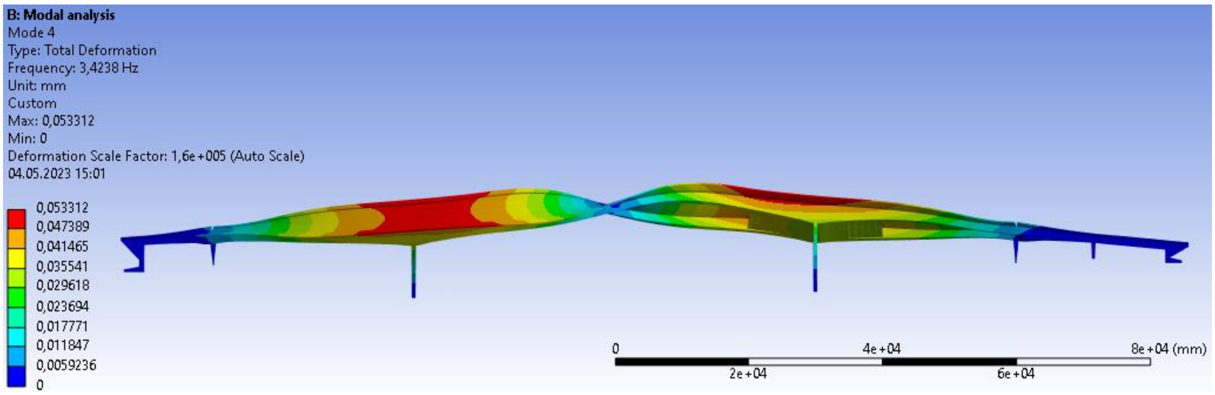

Figure 27: Mode 4 shape for the solid model viewed from the side (Z direction).

Mode 4 on the solid model is a transverse mode shape, mainly with rotation around the X and Y axes. Mode 4 on the solid model corresponds well (99,1%) with mode 6 on the beam model. Mode 4 is recommended for comparison with operational mode analysis results.

Mode 5:

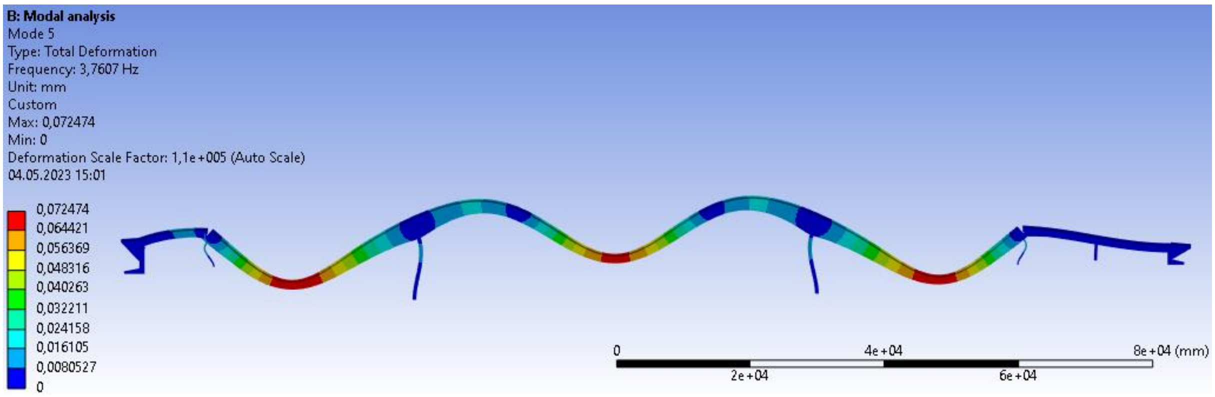

Figure 28: Mode 5 shape for the solid model viewed from the side (Z direction).

Mode 5 on the solid model is a longitudinal mode shape, mainly with translation of movement in Y direction and rotation around the Z axis. Mode 5 on the solid model corresponds well (99,3%) with mode 5 on the beam model. Mode 5 is recommended for comparison with operational mode analysis results.

Mode 6:

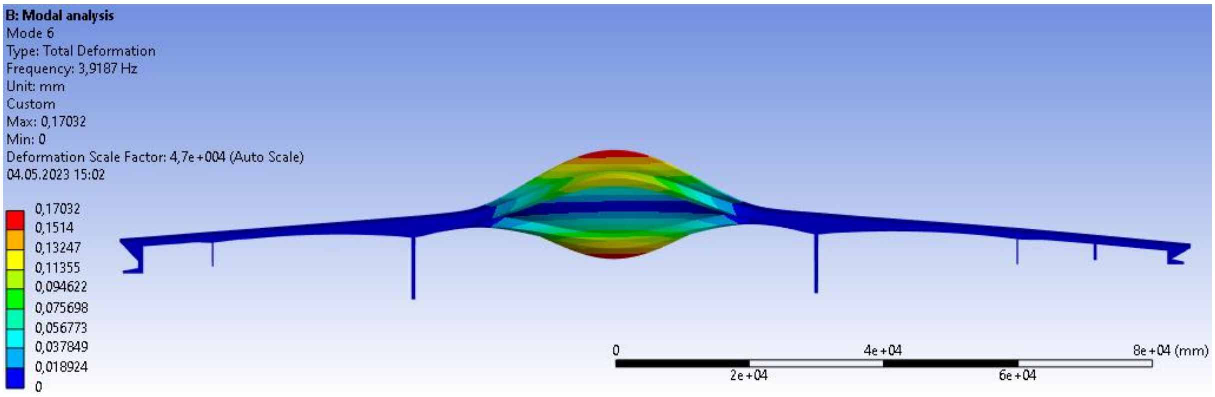

Figure 29: Mode 6 shape for the solid model viewed from the side (Z direction).

Mode 6 on the solid model is a transverse mode shape, mainly with rotation around the X and Y axes. Mode 6 has a relatively high participation factor and low frequency. Mode 6 is recommended for comparison with operational mode analysis results.

Mode 7:

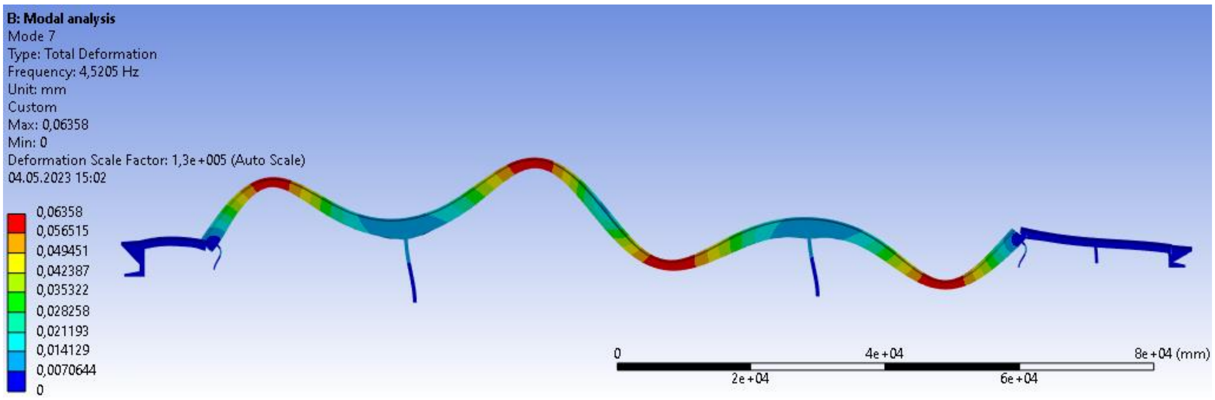

Figure 30: Mode 7 shape for the solid model viewed from the side (Z direction).

Mode 7 on the solid model is a longitudinal mode shape, mainly with translation of movement in X direction and rotation around the Z axis. Mode 7 on the solid model corresponds well (94%) with mode 7 on the beam model. Mode 7 is recommended for comparison with operational mode analysis results.

Mode 8:

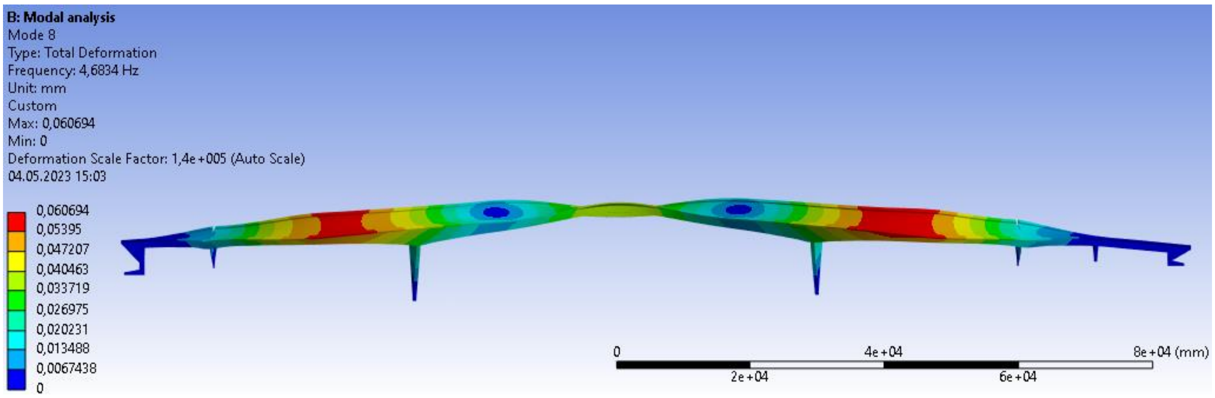

Figure 31: Mode 8 shape for the solid model viewed from the side (Z direction).

Mode 8 on the solid model is a transverse mode shape, mainly with translation of movement in Z direction and rotation around the X and Y axes. Mode 8 on the solid model corresponds well (97,7%) with mode 11 on the beam model. Mode 8 is recommended for comparison with operational mode analysis results.

Mode 9:

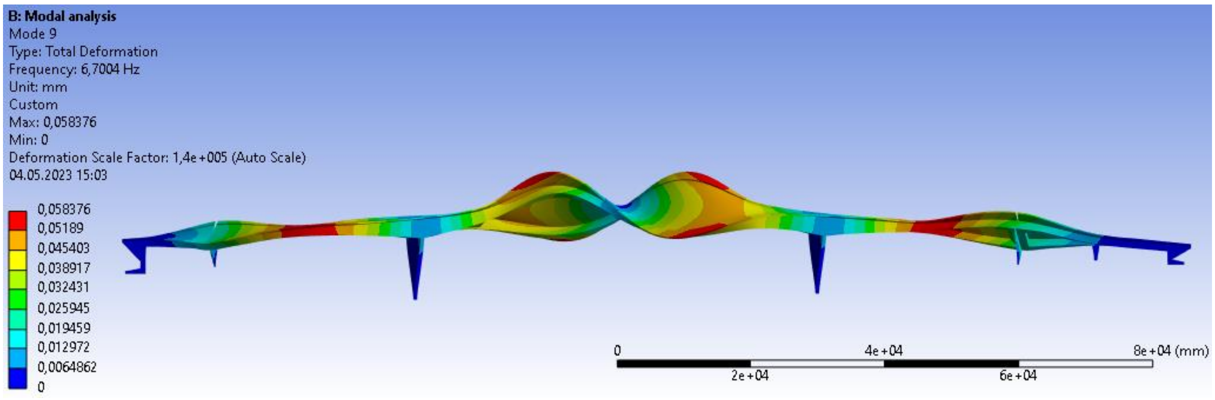

B: Modal analysis
Mode 9
Type: Total Deformation
Frequency: 6,7004 Hz
Unit: mm
Custom
Max: 0,058376
Min: 0
Deformation Scale Factor: 1,4e+005 (Auto Scale)
04.05.2023 15:03

Figure 32: Mode 9 shape for the solid model viewed from the side (Z direction).

Mode 9 on the solid model is a transverse mode shape, mainly with rotation around the X and Y axes. Mode 9 on the solid model corresponds well (93,5%) with mode 14 on the beam model. Mode 9 is recommended for comparison with operational mode analysis results.

Mode 10:

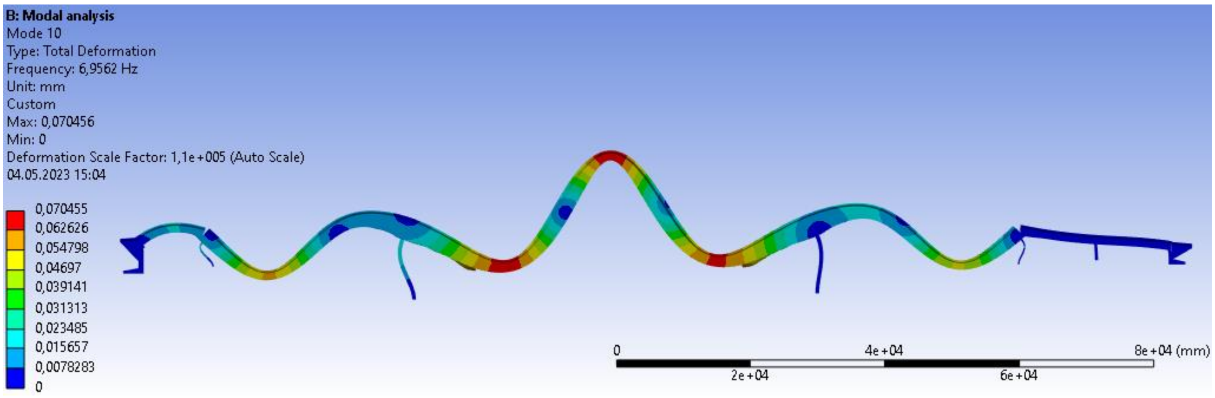

B: Modal analysis
Mode 10
Type: Total Deformation
Frequency: 6,9562 Hz
Unit: mm
Custom
Max: 0,070456
Min: 0
Deformation Scale Factor: 1,1e+005 (Auto Scale)
04.05.2023 15:04

Figure 33: Mode 10 shape for the solid model viewed from the side (Z direction).

Mode 10 on the solid model is a longitudinal mode shape, mainly with translation of movement in X and Y direction and rotation around the Z axis. Mode 10 on the solid model corresponds well (94,3%) with mode 12 on the beam model. Mode 10 is recommended for comparison with operational mode analysis results.

Mode 11:

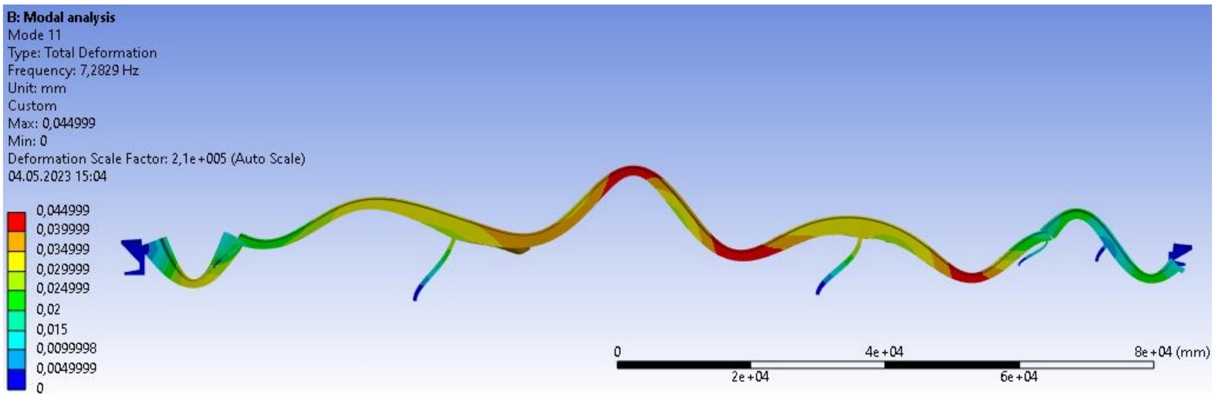

Figure 34: Mode 11 shape for the solid model viewed from the side (Z direction).

Mode 11 on the solid model is a longitudinal mode shape, mainly with translation of movement in X direction and rotation around the Z axis. Mode 11 has a relatively high participation factor. Mode 11 is recommended for comparison with operational mode analysis results.

Mode 12:

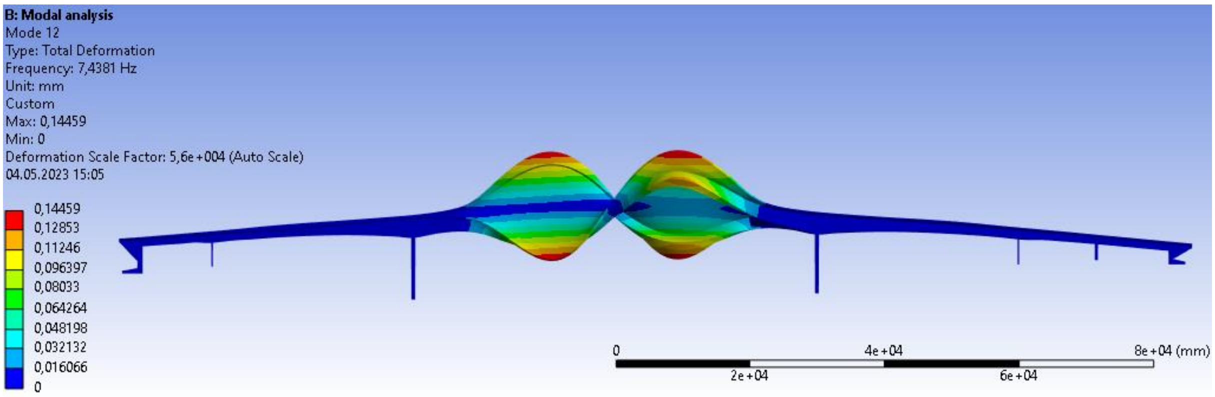

Figure 35: Mode 12 shape for the solid model viewed from the side (Z direction).

Mode 12 on the solid model is a transverse mode shape, mainly with rotation around the Y axis. Mode 12 has a relatively low participation factor and is quite local to the middle of the main span and is not prioritized for comparison with operational mode analysis results.

Mode 13:

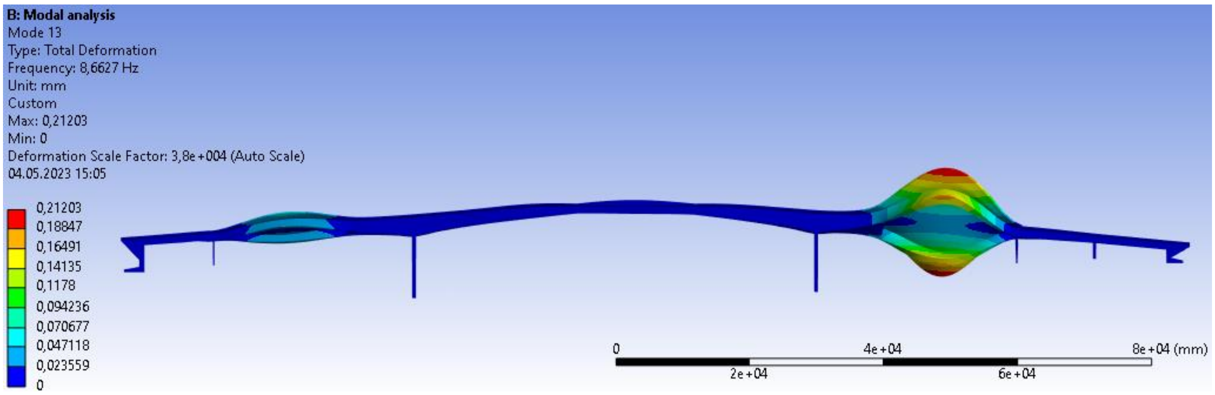

Figure 36: Mode 13 shape for the solid model viewed from the side (Z direction).

Mode 13 on the solid model is a transverse mode shape, mainly with rotation around the X and Y axes. Mode 13 has a relatively low participation factor and is quite local to the Sildval side of the main span and is not prioritized for comparison with operational mode analysis results.

Mode 14:

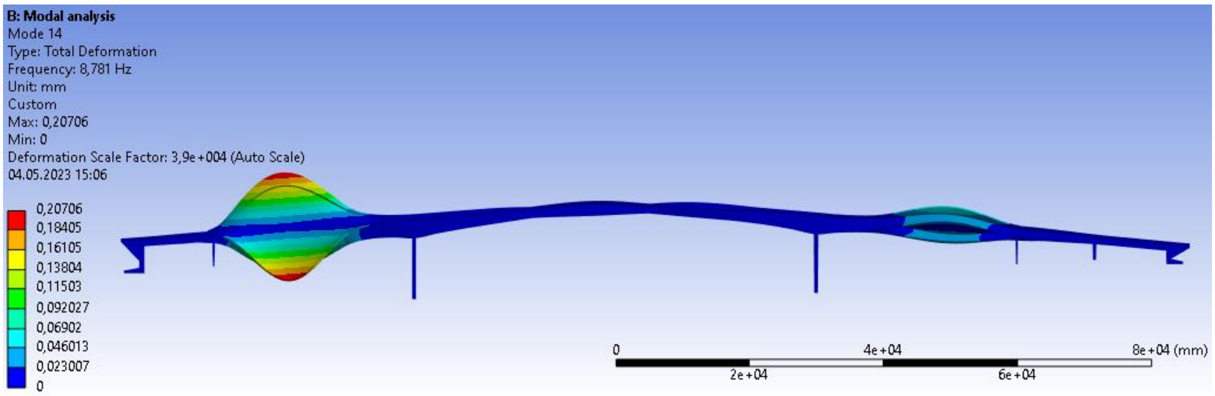

Figure 37: Mode 14 shape for the solid model viewed from the side (Z direction).

Mode 14 on the solid model is a transverse mode shape, mainly with rotation around the X and Y axes. Mode 14 has a relatively low participation factor and is quite local to the Herøyholmen side of the main span and is not prioritized for comparison with operational mode analysis results.

Mode 15:

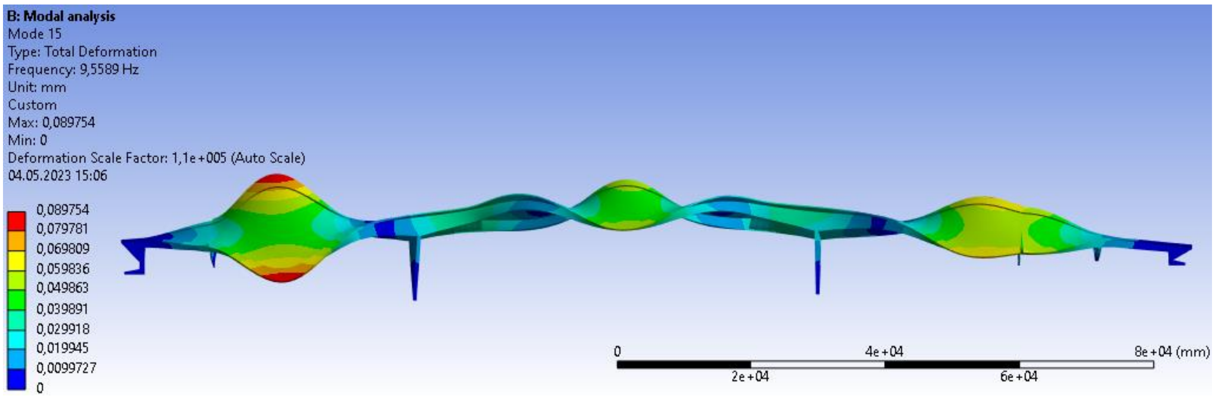

Figure 38: Mode 15 shape for the solid model viewed from the side (Z direction).

Mode 15 on the solid model is a transverse mode shape, mainly with translation of movement in Z direction and rotation around the X, Y and Z axes. Mode 15 on the solid model corresponds well (93,6%) with mode 20 on the beam model. Mode 15 is recommended for comparison with operational mode analysis results.

Mode 16:

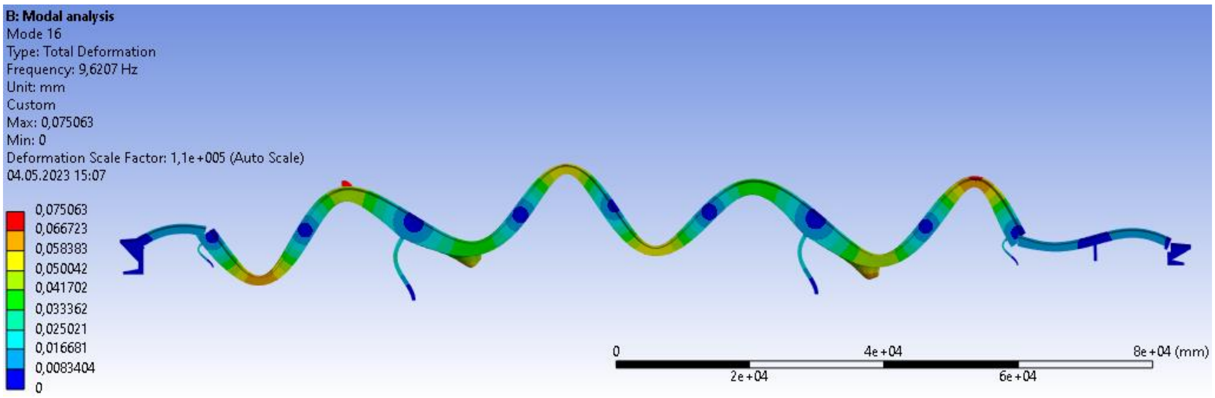

Figure 39: Mode 16 shape for the solid model viewed from the side (Z direction).

Mode 16 on the solid model is a longitudinal mode shape, mainly with rotation around the Y and Z axis. Mode 16 on the solid model corresponds well (97,8%) with mode 18 on the beam model. Mode 16 is recommended for comparison with operational mode analysis results.

Mode 17:

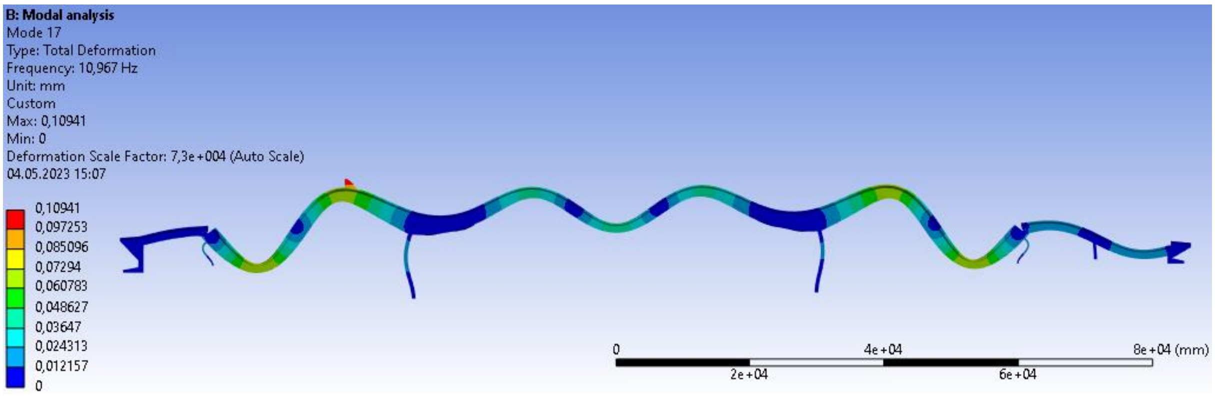

Figure 40: Mode 17 shape for the solid model viewed from the side (Z direction).

Mode 17 on the solid model is a longitudinal mode shape, mainly with translation of movement in Y direction and rotation around the Z axis. Mode 17 has an intermediate participation factor. Mode 17 is recommended for comparison with operational mode analysis results.

Mode 18:

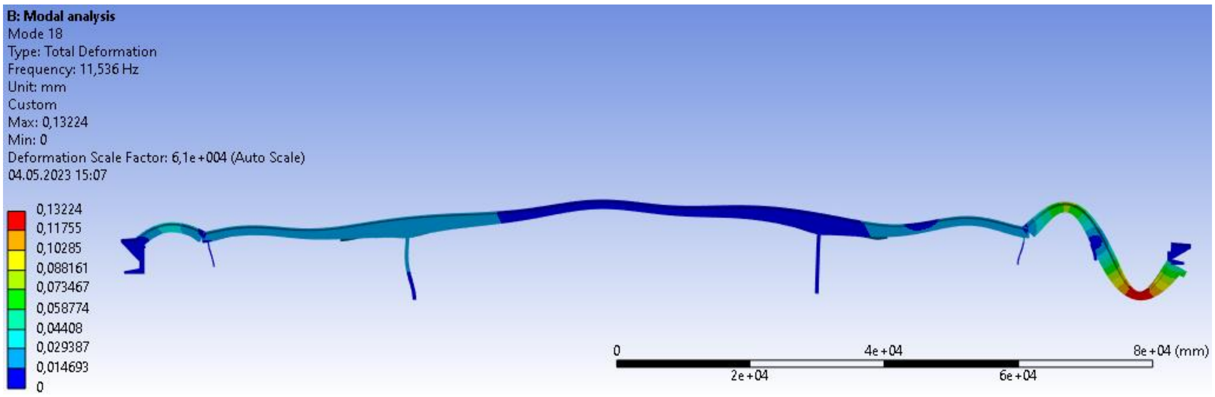

Figure 41: Mode 18 shape for the solid model viewed from the side (Z direction).

Mode 18 on the solid model is a longitudinal mode shape, mainly with rotation around the Z axis. Mode 18 has a relatively low participation factor and is quite local to the Sildval land span and is not prioritized for comparison with operational mode analysis results.

Mode 19:

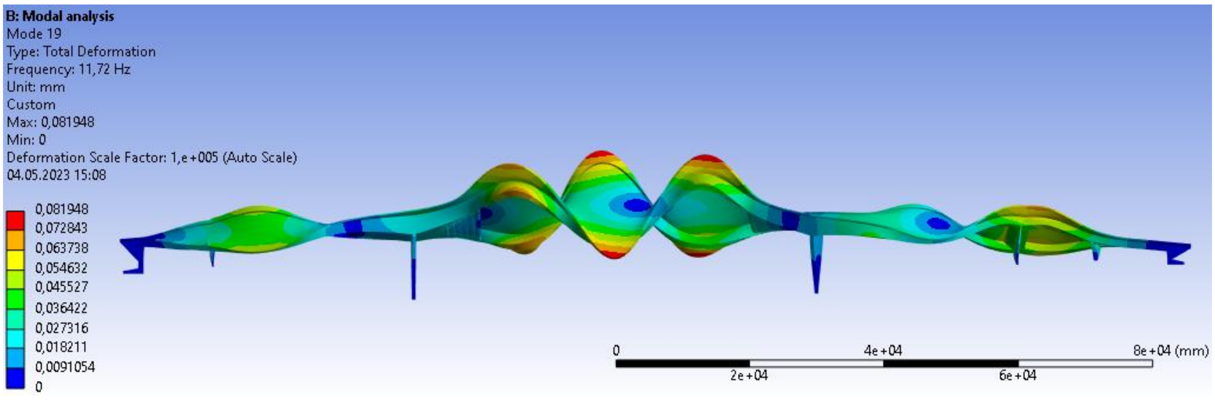

Figure 42: Mode 19 shape for the solid model viewed from the side (Z direction).

Mode 19 on the solid model is a transverse mode shape, mainly with rotation around the X and Y axes. Mode 19 has a relatively high participation factor. Mode 19 is recommended for comparison with operational mode analysis results.

Mode 20:

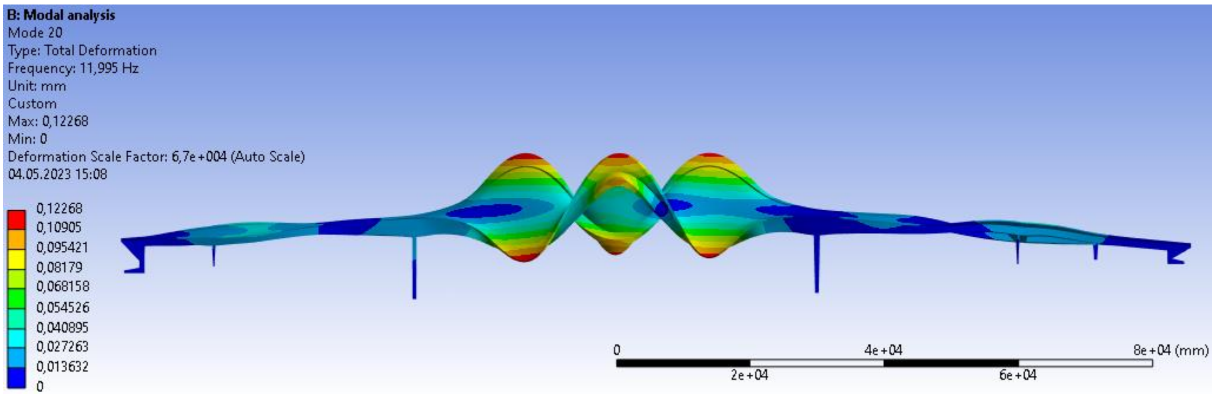

Figure 43: Mode 20 shape for the solid model viewed from the side (Z direction).

Mode 20 on the solid model is a transverse mode shape, mainly with rotation around the X and Y axes. Mode 20 has a relatively high participation factor. Mode 20 is recommended for comparison with operational mode analysis results.

1.10.9 Solid model volume and mass

Volume of solid model: 445,15 m^3. Mass of solid model: 1064800 Kg = 1064,8 tons. These values are derived excluding the volume of the minor pressure plates and land vessels, to make them comparable to the beam model, that is modelled without minor pressure plates and land vessels.

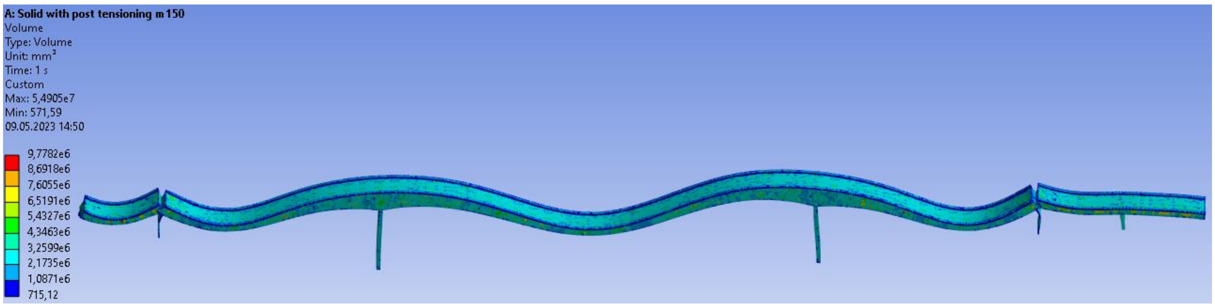

Figure 44: Volume distribution of the solid model.

2 Numerical analysis beam element model

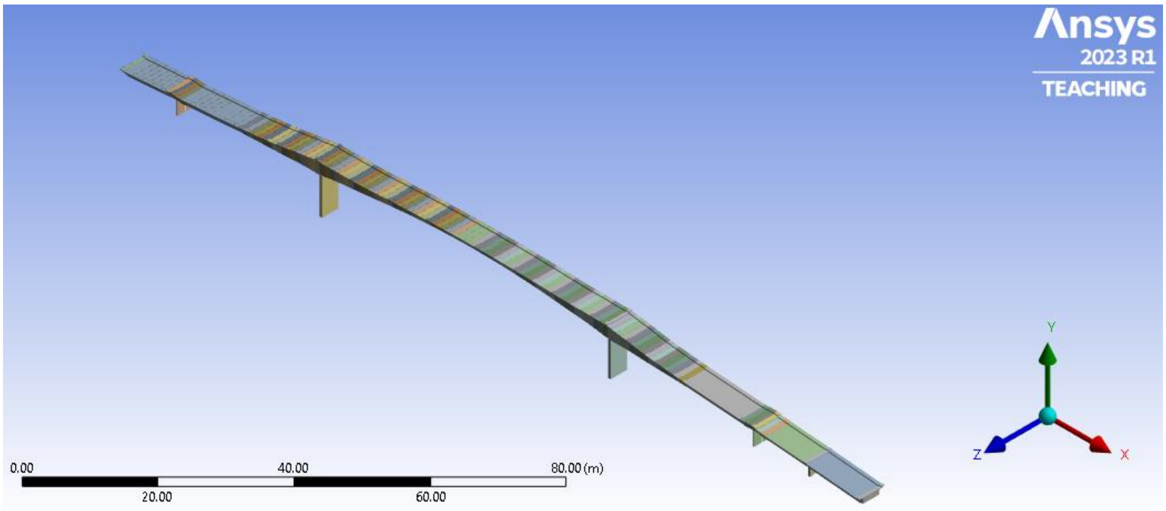

2.1 Problem description

The same problem description as for the solid model: Herøysund bridge is a 154,5-metre-long cast in place concrete post-tensioned bridge with 7 axes consisting of in total 2 land vessels, 2 land spans, a main span and 5 pillars. 4 of the pillars is cast firmly into the main span deck and longitudinal beams, while the 5th pillar is a tilting pillar under the Sildval land span. The bridge deck is supported structurally by two longitudinal underlying loadbearing beams. The beams are 400 mm wide transversally on the main span and 600 mm wide on the land spans, and varying in height all along the span, the beams are larger at the points where pillars connect to the deck. Points where pillars connect to the deck is also structurally reinforced by transverse beams. The main span of the bridge is approximately 60 metres long. The bridge has one lane for vehicles and is 5,3 metres wide. 10 metres out from both axis 4 and 5, in both directions longitudinally, there is cast in pressure plates between the beams, so there the bridge consist of box sections, while the rest of the bridge is open sections.

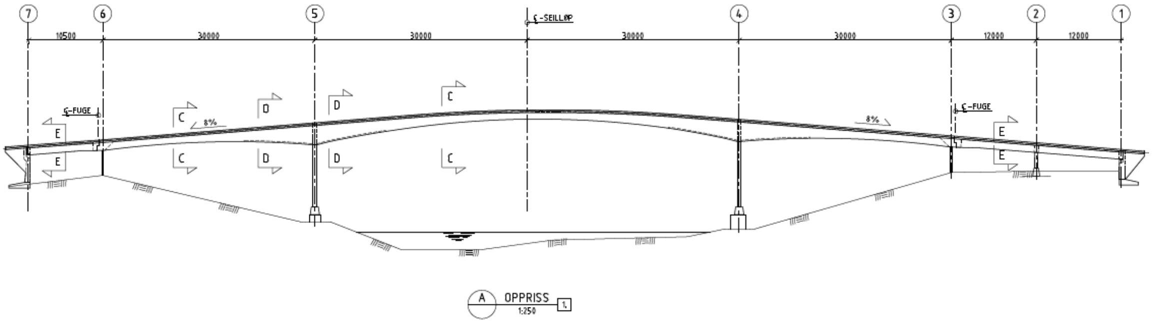

Figure 45: Vertical plane geometry of Herøysund bridge, axis 1-3 is called Sildval landspan, axis 3-6 is the main span, axis 6-7 is called Herøyholmen landspan. [3]

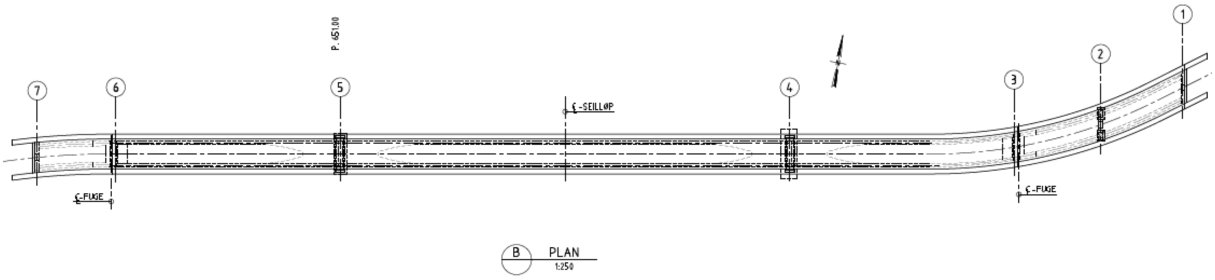

Figure 46: Horizontal plane geometry of Herøysund bridge, here the pressure plates at axis 4 and 5 is shown. [3]

2.2 Units

Throughout the project work and in all calculations, the SI unit system is used. Deflection is presented in millimetres, stress is presented in megapascal, moment is presented in newton metres, frequencies are presented in Hz, volume is presented in cubic metres, mass is presented in kilograms.

2.3 Geometry

The geometry of the bridge is described in the solid model analysis earlier in this analysis report.

2.4 Boundary conditions and loads for beam model

Here the loads and boundary conditions put on the bridge in this analysis is presented. This analysis mainly focuses on the natural frequencies and modal shapes of the bridge, but the loads is of importance as they are transferred as pre-stress from the structural analysis to the modal analysis.

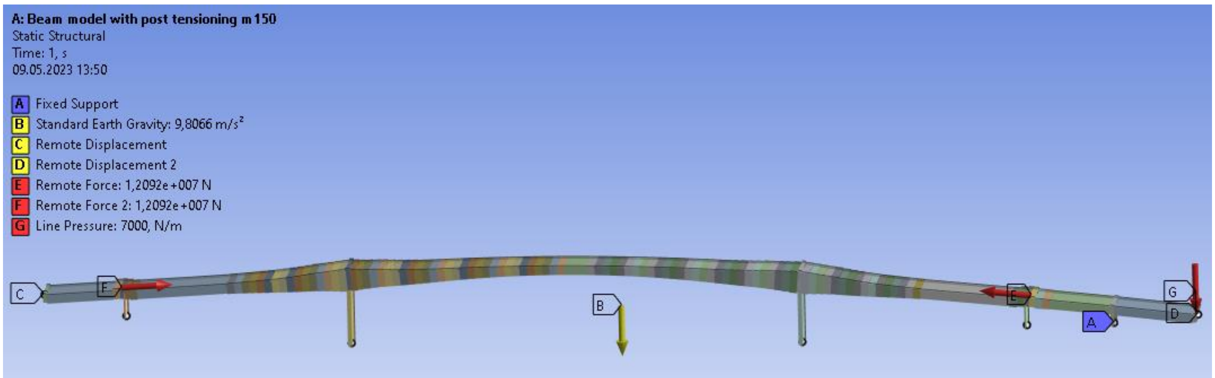

A: Beam model with post tensioning m150
Static Structural
Time: 1, s
09.05.2023 13:50

A Fixed Support
B Standard Earth Gravity: 9,8066 m/s²
C Remote Displacement
D Remote Displacement 2
E Remote Force: 1,2092e+007 N
F Remote Force 2: 1,2092e+007 N
G Line Pressure: 7000, N/m

Figure 47: Boundary conditions and loads for the beam model.

2.4.1 Boundary conditions

The model is fixed for translation and rotation on the bottom of each pillar and at the bottom and outside walls of the land vessels.

The land spans are connected by a joint on each end to the land vessel and main span by a joint allowing rotation in z direction, but no other rotation or translation.

The Sildval land span is connected to the tilting pillar by a joint allowing rotation in z direction, but no other rotation or translation.

Fixed supports:

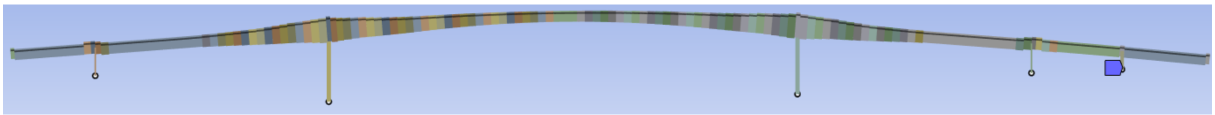

Figure 48: Placement of the fixed supports on the bottom of the pillars

Revolute z supports:

Figure 49: Remote supports on each end of the bridge, allowing no translation in x, y, z and no rotation about x, y. Allowing only rotation about z axis.

2.4.2 Gravity

A gravity constant of 9,81 m/s^2 is placed in the analysis, imparting on all masses of the system.

2.4.3 Post tensioning system

The post tensioning system of the bridge consist of 18 cables through the main span of the bridge imparting 137 tonnes horizontally in the longitudinal direction of the main span.

$$\frac{137\,000\,Kg \cdot 18 \cdot 9{,}8066\,m/s^2}{2} = 12091{,}5378\,kN \qquad 2.1$$

This is simulated by a force of 12091,5378 kN on both sides of the main span, placed on the vertexes of the beam lines. To make the beam model as similar as possible to the solid model, the post tensioning forces point of application was moved 325 mm up from the vertices, so that they apply a moment to the bridge main span.

Figure 50: The post tensioning system simulated by two opposing remote forces on each end of the main span

2.4.4 Asphalt and railing

Asphalt and railing are not modelled, but rather simulated by a pressure of 7kN/m bridge length over the span of the bridge. According to "handbok V412, Bæreevneklassifisering av bruer, laster" [4], chapter 4, page 38 from Statens Vegvesen, which is the governing body for bridge constructions in Norway, these are the relevant loads and magnitudes for Herøysund bridge:

Asphalt mass: 25k N/m^3, railing mass: 0,5 kN/m.

$$4\,m \cdot 0{,}06\,m \cdot 25\frac{kN}{m^3} + 2 \cdot 0{,}5\frac{kN}{m} = 7\frac{kN}{m} \qquad 2.2$$

Line pressure:

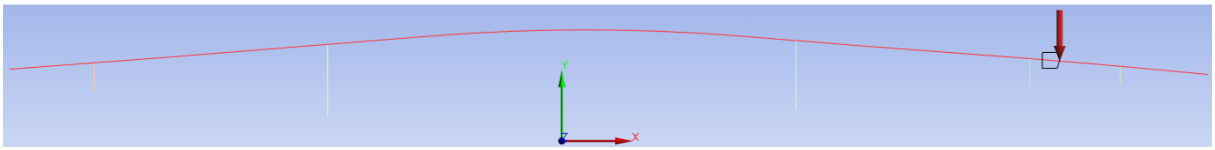

Figure 51: Asphalt and railing mass simulated by a line pressure of 7 kN/m applied on the elastic line of the beams

2.5 Materials

The same concrete material as in the solid element analysis is used for the beam element analysis.

2.6 Elements used on beam model

Here the elements used in this analysis is presented.

2.6.1 BEAM188

BEAM188 is used for all elements in the beam model. BEAM188 is suitable for analysing slender to moderately thick beam structures. The element is based on Timoshenko beam theory including shear-deformation effects. The element provides options for unrestrained warping and restrained warping of cross-sections.

The element is a linear, quadratic, or cubic two-node beam element in 3D. BEAM188 has six or seven degrees of freedom at each node; these include translations in the x, y, and z directions and rotations about the x, y, and z directions. A seventh degree of freedom (warping magnitude) is optional. This element is well-suited for linear, large rotation, and/or large strain nonlinear applications.

The element includes stress stiffness terms, by default, in any analysis with large deflection. The provided stress-stiffness terms enable the elements to analyse flexural, lateral, and torsional stability problems (using eigenvalue buckling, or collapse studies with arc length methods or nonlinear stabilization).

Elasticity, plasticity, creep and other nonlinear material models are supported. A cross-section associated with this element type can be a built-up section referencing more than one material. Added mass, hydrodynamic added mass and loading, and buoyant loading are available.

BEAM188 is based on Timoshenko beam theory, which is a first-order shear-deformation theory: transverse-shear strain is constant through the cross-section (that means, cross-sections remain plane and undistorted after deformation).

The element can be used for slender or stout beams. Due to the limitations of first-order shear-deformation theory, slender to moderately thick beams are possible to analyse.

[13]

2.7 Mesh on beam model

The beam model is meshed with element size of 150 mm both for static structural analysis and for modal analysis.

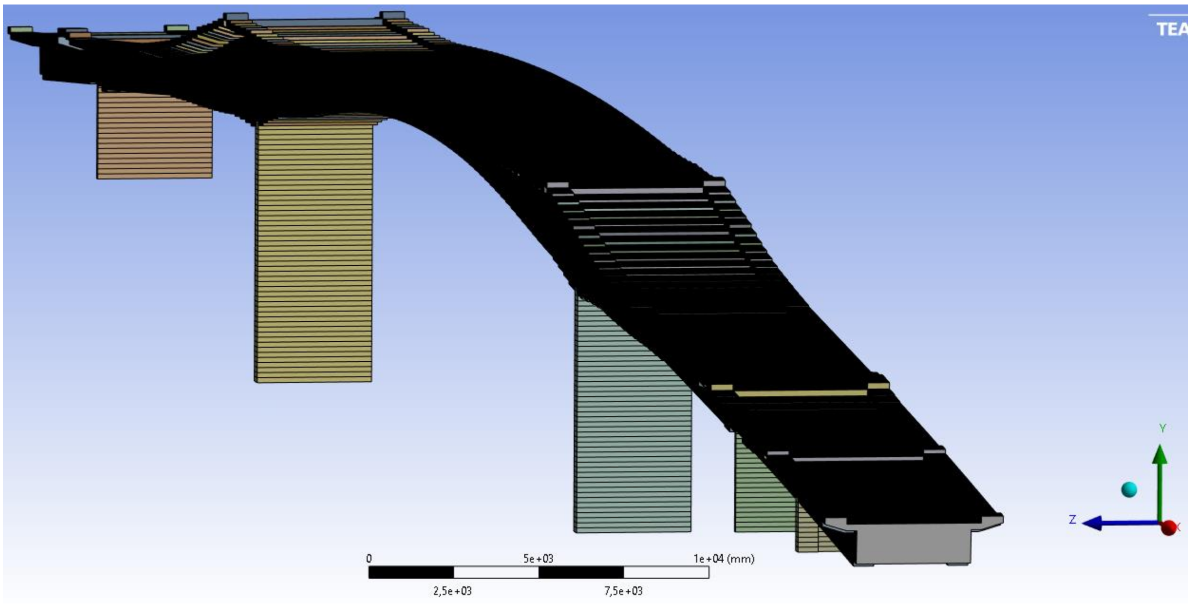

Figure 52: Beam model mesh details

2.8 Beam model mesh convergence control

2.8.1 Mesh convergence control for structural analysis of beam model

Mesh convergence control have been performed, the results from four different mesh refinements in equal increments are compared to each other, with respect to deflection, minimum moment, and maximum moment. The four mesh refinements are of element size: 300 mm, 250 mm, 200 mm and 150 mm. For the deflection and moment results, maximum and minimum values were used. The convergence criteria are set to less than 1%. The following formulas was used to calculate mesh convergence:

$$\frac{|\mathrm{u}_{\mathrm{max,m1}}| - |\mathrm{u}_{\mathrm{max,m2}}|}{|\mathrm{u}_{\mathrm{maks,m1}}|} \cdot 100 = \% < 1\%\ \mathrm{OK} \tag{2.3}$$

$$\frac{|\mathrm{M}_{\mathrm{min,m1}}| - |\mathrm{M}_{\mathrm{min,m2}}|}{|\mathrm{M}_{\mathrm{min,m1}}|} \cdot 100 = \% < 1\%\ \mathrm{OK} \tag{2.4}$$

$$\frac{|\mathrm{M}_{\mathrm{maks,m1}}| - |\mathrm{M}_{\mathrm{maks,m2}}|}{|\mathrm{M}_{\mathrm{maks,m1}}|} \cdot 100 = \% < 1\%\ \mathrm{OK} \tag{2.5}$$

Table 9 shows that the mesh element size of 150 mm is adequate for the static structural analysis of the beam model, and this is the mesh that will be used for the final analysis and results section of the static structural analysis of the beam model.

Table 9: Mesh convergence control for deflection and moments on beam model.

N#	Element size [mm]	Nodes	Elements	Max. deflection		Min. moment		Max. moment	
				[mm]	Conv. error [%]	[kNm]	Conv. error [%]	[kNm]	Conv. error [%]
1	300	1434	1349	70,753		16514		3992,5	
2	250	1514	1409	70,753	0	16515	0,006	3992,5	0
3	200	1864	1733	70,753	0	16515	0	3992,7	0,005
4	150	2552	2374	70,753	0	16515	0	3992,7	0

2.8.2 Mesh convergence control for modal analysis on beam model

Here, the 20 first modes are compared using several different refinements in similar increments to check for mesh convergence. The convergence criteria are set to less than 1%. The following formulas was used to calculate mesh convergence:

$$\frac{|\mathrm{f}_{\mathrm{mode1,m1}}| - |\mathrm{f}_{\mathrm{mode1,m2}}|}{|\mathrm{f}_{\mathrm{mode1,m1}}|} \cdot 100 = \% < 1\% \ \mathrm{OK} \tag{2.6}$$

Table 10 shows that a mesh element size of 150 mm is adequate for the modal analysis.

Table 10: Mesh convergence control for modes on beam model.

Mode#	Element size [mm]						
	300	250		200		150	
	Nodes	Nodes		Nodes		Nodes	
	1434	1514		1864		2552	
	Elements	Elements		Elements		Elements	
	1349	1409		1733		2374	
	Frequency [Hz]	Frequency [Hz]	Conv. error [%]	Frequency [Hz]	Conv. error [%]	Frequency [Hz]	Conv. error [%]
1	1,4355	1,4355	0	1,4355	0	1,4355	0
2	2,238	2,238	0	2,238	0	2,238	0
3	2,3864	2,3864	0	2,3864	0	2,3864	0
4	2,9542	2,9542	0	2,9542	0	2,9542	0
5	3,5657	3,5657	0	3,5657	0	3,5657	0
6	4,1446	4,1446	0	4,1446	0	4,1446	0
7	4,8275	4,8275	0	4,8275	0	4,8275	0
8	5,0995	5,0995	0	5,0995	0	5,0995	0
9	5,1315	5,1315	0	5,1315	0	5,1315	0
10	5,1732	5,1732	0	5,1732	0	5,1732	0
11	5,3555	5,3555	0	5,3555	0	5,3555	0
12	7,1386	7,1386	0	7,1386	0	7,1386	0
13	7,3325	7,3325	0	7,3325	0	7,3325	0
14	7,4839	7,4839	0	7,4839	0	7,4839	0
15	8,8084	8,8084	0	8,8084	0	8,8084	0
16	9,5965	9,5965	0	9,5965	0	9,5965	0
17	9,9185	9,9185	0	9,9185	0	9,9185	0
18	10,014	10,014	0	10,014	0	10,014	0
19	10,163	10,163	0	10,163	0	10,163	0
20	11,178	11,178	0	11,178	0	11,178	0

2.9 Beam model analysis results

Here the results of the static structural analysis and modal analysis of the beam model analysis are presented.

2.9.1 Beam model total deflection

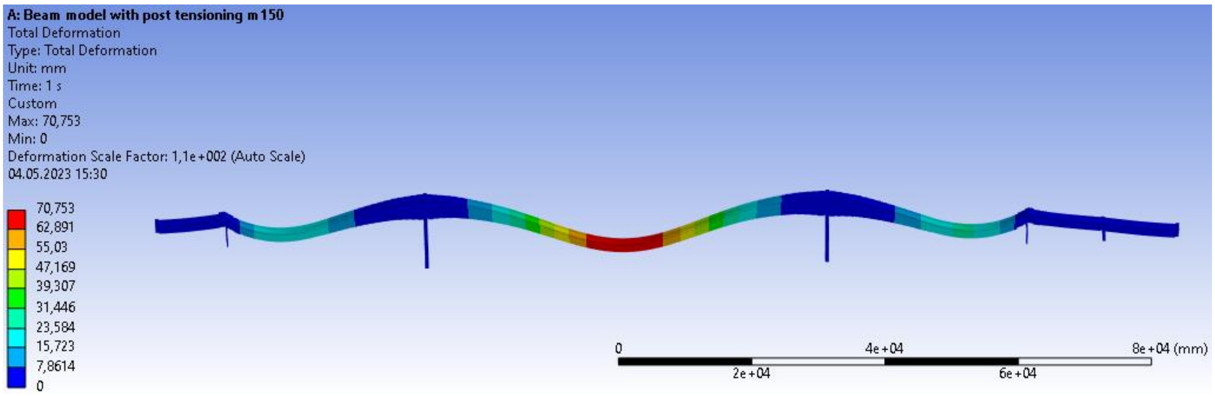

A: Beam model with post tensioning m150
Total Deformation
Type: Total Deformation
Unit: mm
Time: 1 s
Custom
Max: 70,753
Min: 0
Deformation Scale Factor: 1,1e+002 (Auto Scale)
04.05.2023 15:30

Figure 53: Total deflection of the bridge is 70,753 mm.

Total deflection = 70,753 mm, in negative y-direction, as shown in figure 53. Maximum deflection occurs in the middle of the bridge main span (approximately 83 metres from axis 7 in positive x direction).

2.9.2 Beam model directional deflection (y)

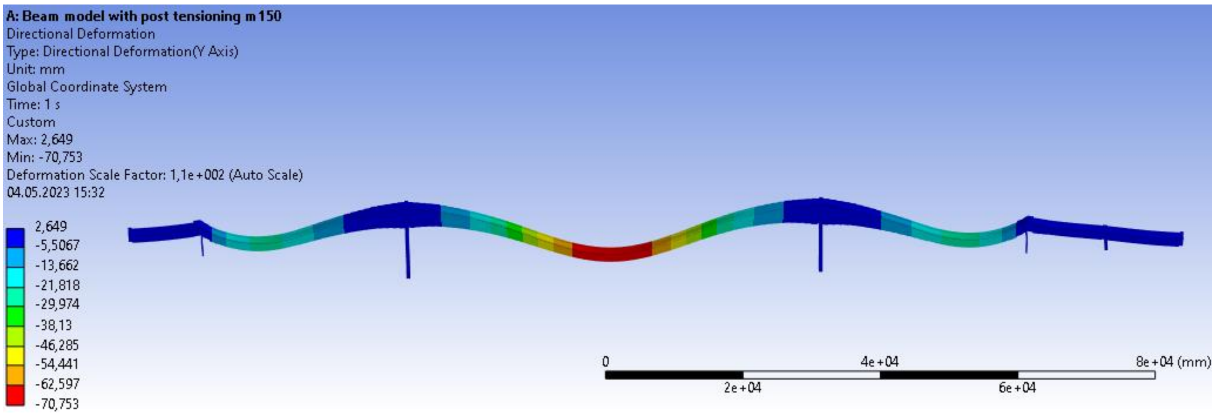

A: Beam model with post tensioning m150
Directional Deformation
Type: Directional Deformation(Y Axis)
Unit: mm
Global Coordinate System
Time: 1 s
Custom
Max: 2,649
Min: -70,753
Deformation Scale Factor: 1,1e+002 (Auto Scale)
04.05.2023 15:32

Figure 54: Directional deflection in y direction (vertical) is -70,753 mm.

Directional deflection in y-direction = -70,753 mm approximately 83 metres from axis 7 in positive x direction.

2.9.3 Beam model moment (z)

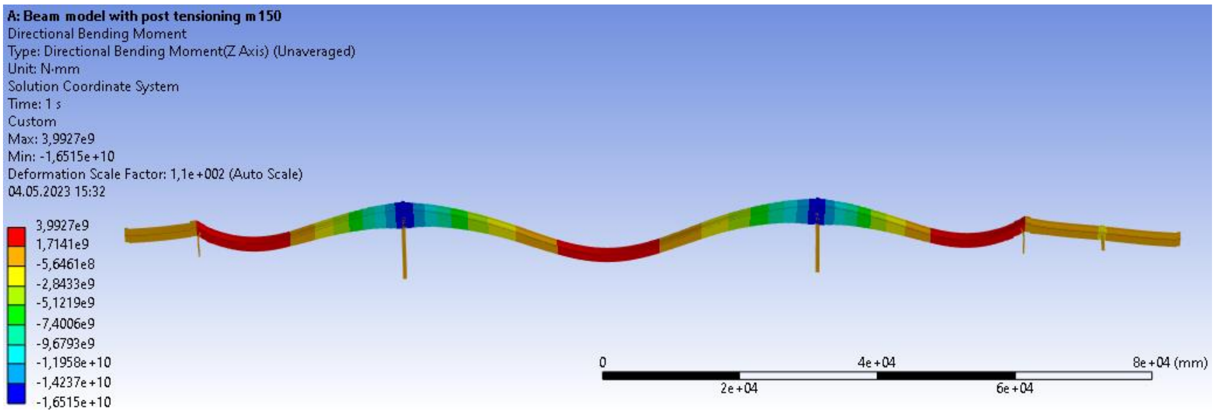

A: Beam model with post tensioning m150
Directional Bending Moment
Type: Directional Bending Moment(Z Axis) (Unaveraged)
Unit: N·mm
Solution Coordinate System
Time: 1 s
Custom
Max: 3,9927e9
Min: -1,6515e+10
Deformation Scale Factor: 1,1e+002 (Auto Scale)
04.05.2023 15:32

Figure 55: Moment in the bridge construction, Mmax= 3992,7 kNm, Mmin= -16515 kNm.

Shown in figure 55, minimum moment occurs just over the main pillars (axes 4 and 5), while maximum moment occurs at each end of the main span (axes 3 and 6) and in the middle of the bridge main span (approximately 83 metres from axis 7 in positive x direction).

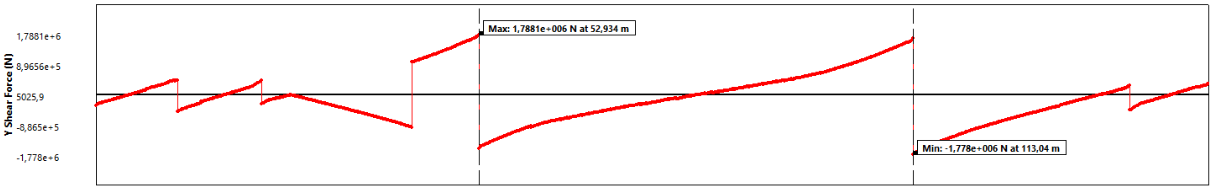

Figure 56: Shear force diagram in the Y axis of the beam model. T_{min} = -1778 kN, T_{max} = 1788,1 kN.

From figure 56, minimum shear force = -1778 kN at 113,04 metres from axis 7, maximum shear force = 1788,1 kN at 52,934 metres from axis 7.

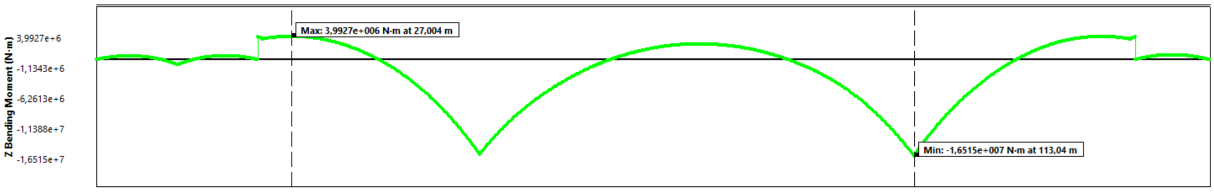

Figure 57: Bending moment diagram around Z axis (transverse axis) of the beam model, Mmin= -16515 kNm. Mmax= 3992,7 kNm.

In figure 57 the bending moment diagram around the Z axis is shown. In each side of the main span there is a step up in moment due to the post tensioning forces being displaced 325 mm up from the vertices at each side of the main span. Minimum moment = -16515 kNm at 27,004 metres from axis 7. Maximum moment = 3992,7 kNm at 113,04 metres from axis 7.

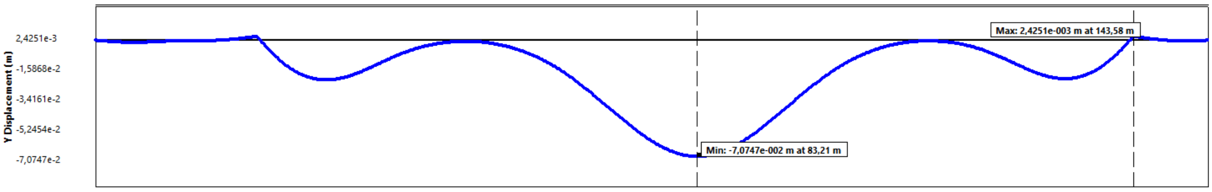

Figure 58: Deflection diagram in the y axis of the beam model.

In figure 58, a deflection diagram of the beam model is presented. Maximum deflection is in negative y-direction (down) at 83,21 metres from axis 7.

2.9.4 Beam model without post tensioning

To confirm the technique of simulating the post tensioning system using horizontal forces clamping the main span together, the post tensioning forces was removed from the model, and results were compared.

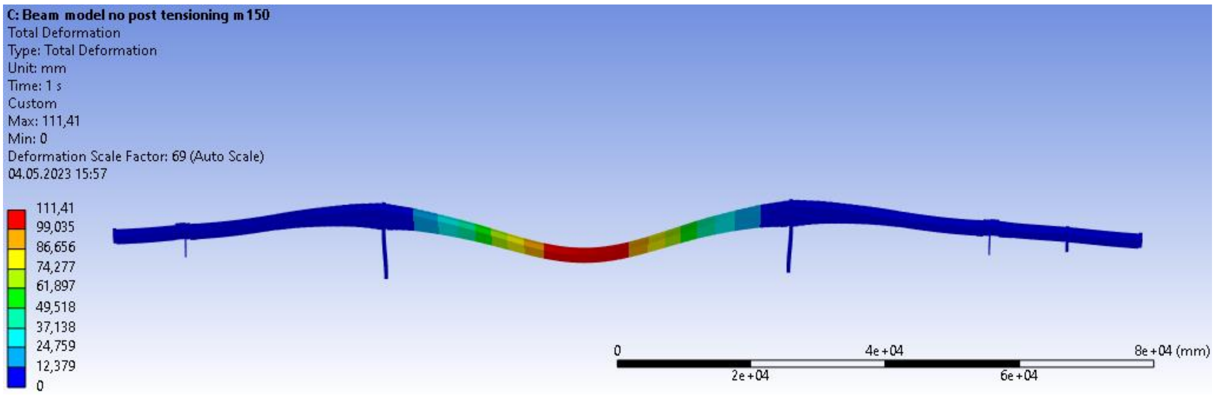

C: Beam model no post tensioning m150
Total Deformation
Type: Total Deformation
Unit: mm
Time: 1 s
Custom
Max: 111,41
Min: 0
Deformation Scale Factor: 69 (Auto Scale)
04.05.2023 15:57

Figure 59: Total deflection of the solid model without post tensioning: 111,41 mm.

Shown in figure 59 is the total deflection of the bridge after the post tensioning forces was removed from the analysis. Total deflection with the post tensioning system is 70,753 mm, and without the post tensioning system total deflection is 111,41 mm. This gives an indication that the technique of simulating the post tensioning system with horizontal forces does work as intended. Although later in this report the comparison of the effects of the post tensioning on the solid and beam model will reveal that the post tensioning forces has less effect on the beam model than on the solid model.

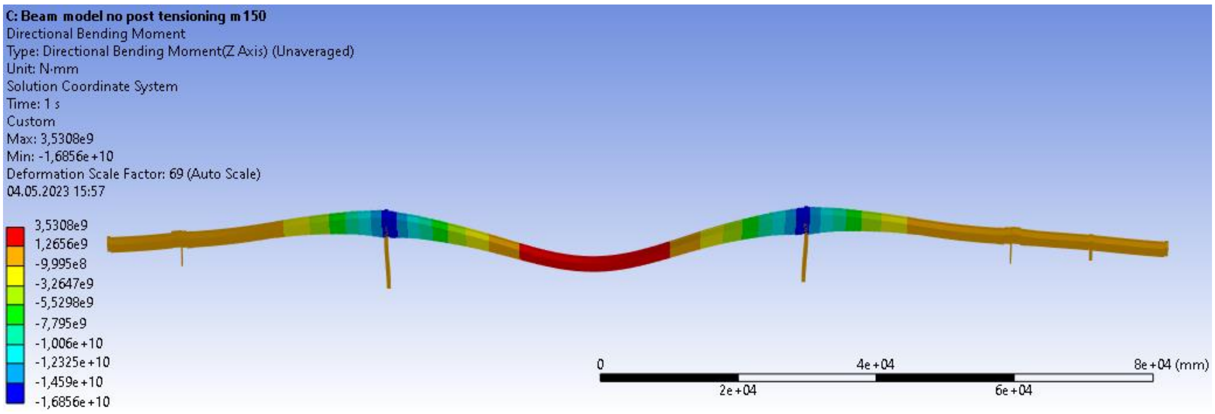

C: Beam model no post tensioning m150
Directional Bending Moment
Type: Directional Bending Moment(Z Axis) (Unaveraged)
Unit: N·mm
Solution Coordinate System
Time: 1 s
Custom
Max: 3,5308e9
Min: -1,6856e+10
Deformation Scale Factor: 69 (Auto Scale)
04.05.2023 15:57

Figure 60: Bending moment of the solid model without post tensioning: Min: 3530,5 kNm Max: 16850 kNm.

2.9.5 Evaluation of modes from the beam model

2.9.5.1 Beam model participation factor

Participation factor is calculated using the following formula:

$$\gamma_i = \{ø\}_i^T [M]\{D\} \quad 2.7$$

where:

γ_i = participation factor, $\{ø\}_i^T$ = mode shapes, [M] = mass matrix, {D} = excitation direction vector, [9]

The excitation direction vector is an assumed unit displacement vector and depends on the direction of excitation in each of the global cartesian directions and rotation about each of the axes. [10]

Table 11: Natural frequencies and corresponding participation factors for the beam model. M = mode.

Mode	Freq. (Hz)	Trans. X	Trans. Y	Trans. Z	Rot. X	Rot. Y	Rot. Z
M 1	1,4355	0,47261	-8,7006	-6,509e-5	-1,2154	0,1913	-9336,6
M 2	2,238	4,491e-8	1,187e-4	19,994	2,7595e+5	24756	0,46103
M 3	2,3864	-0,18692	-0,2025	-3,645e-6	-0,31511	3,2878	3,3511e+5
M 4	2,9542	2,782e-5	-1,848e-3	4,1995	36402	4369,9	1,8998
M 5	3,5657	0,20094	-15,991	-5,275e-5	1,3876	8,2436	-33,54
M 6	4,1446	-1,292e-4	-7,054e-5	9,712e-2	-5652,9	7,1114e+5	-43,22
M 7	4,8275	2,2188	0,26359	2,603e-3	19,824	238,84	5,8504e+5
M 8	5,0995	-1,728e-3	1,203e-5	2,8163	23700	3,2065e+5	-419,29
M 9	5,1315	-1,142e-4	3,001e-4	7,0666	67414	-48437	-25,294
M 10	5,1732	-5,847e-4	-2,118e-4	5,0142	47985	-1,487e+5	-151
M 11	5,3555	1,536e-4	5,922e-4	15,466	1,8983e+5	-52544	32,714
M 12	7,1386	-0,7653	-11,064	5,11e-3	49,547	-215,41	7829,7
M 13	7,3325	1,27e-3	1,397e-2	3,1823	30594	-2,721e+5	-3,9773
M 14	7,4839	4,482e-4	4,395e-3	1,7424	14920	3,8014e+5	-15,805
M 15	8,8084	-29,089	9,217e-2	3,649e-5	0,37058	-4,8159	3,8466e+5
M 16	9,5965	-9,248e-4	-2,313e-4	-0,61762	-7195,8	1,3105e+5	94,164
M 17	9,9185	4,140e-4	-8,817e-4	2,0446	21970	-13925	-189,58
M 18	10,014	-0,36628	9,237e-2	4,349e-3	47,907	-36,83	1,0791e+5
M 19	10,163	4,163e-4	9,558e-4	0,34348	3620,1	60331	-96,835
M 20	11,178	9,358e-5	1,281e-3	4,5142	49597	-62648	-17,22

2.9.5.2 Beam model effective mass

Effective mass is calculated using the following formula:

$$M_{ei} = \frac{\gamma_i^2}{\{ø\}_i^T [M]\{D\}} \qquad 2.8$$

$$\{ø\}_i^T [M]\{D\} = 1 \qquad 2.9$$

$$M_{eff,i} = \gamma_i^2 \qquad 2.10$$

where:

γ_i = participation factor, $\{ø\}_i^T$ = mode shapes, [M] = mass matrix, {D} = excitation direction vector.

[11]

Table 12: Natural frequencies and corresponding effective mass for the beam model. M=mode.

Mode	Freq. (Hz)	Trans. X [tonne]	Trans. Y [tonne]	Trans. Z [tonne]	Rot. X [tonne mm mm]	Rot. Y [tonne mm mm]	Rot. Z [tonne mm mm]
M 1	1,4355	0,22336	75,7	4,236e-9	1,4771	3,6595e-2	8,7171e+7
M 2	2,238	2,01e-15	1,409e-8	399,76	7,615e+10	6,1287e+8	0,21255
M 3	2,3864	3,493e-2	4,1e-2	1,32e-11	9,9294e-2	10,809	1,123e+11
M 4	2,9542	7,74e-10	3,416e-6	17,636	1,3251e+9	1,9096e+7	3,6092
M 5	3,5657	4,037e-2	255,7	2,782e-9	1,9255	67,956	1124,9
M 6	4,1446	1,67e-8	4,977e-9	9,433e-3	3,1956e+7	5,0573e+11	1868
M 7	4,8275	4,923	6,947e-2	6,775e-6	392,97	57046	3,4227e+11
M 8	5,0995	2,987e-6	1,44e-10	7,9313	5,6167e+8	1,0282e+11	1,7581e+5
M 9	5,1315	1,305e-8	9,011e-8	49,937	4,5447e+9	2,3461e+9	639,79
M 10	5,1732	3,419e-7	4,489e-8	25,142	2,3026e+9	2,2133e+10	22801
M 11	5,3555	2,361e-8	3,507e-7	239,2	3,6034e+10	2,7608e+9	1070,2
M 12	7,1386	0,58569	122,4	2,612e-5	2454,9	46403	6,1304e+7
M 13	7,3325	1,613e-6	1,953e-4	10,127	9,3602e+8	7,4076e+10	15,819
M 14	7,4839	2,008e-7	1,932e-5	3,0359	2,2262e+8	1,4451e+11	249,79
M 15	8,8084	846,16	8,497e-3	1,331e-9	0,13733	23,193	1,4796e+11
M 16	9,5965	8,553e-7	5,35e-8	0,38146	5,1779e+7	1,7175e+10	8866,9
M 17	9,9185	1,714e-7	7,775e-7	4,1802	4,8269e+8	1,9391e+8	35941
M 18	10,014	0,13416	8,533e-3	1,891e-5	2295	1356,4	1,1645e+10
M 19	10,163	1,733e-7	9,136e-7	0,11798	1,3105e+7	3,6398e+9	9377
M 20	11,178	8,757e-9	1,643e-6	20,378	2,4599e+9	3,9248e+9	296,54
Sum		852,1	453,93	777,84	1,2512e+11	8,7993e+11	6,1433e+11

2.9.6 Beam model cumulative effective mass fraction

Cumulative effective mass fraction for the i^{th} mode is calculated using the following formula:

$$\bar{M}_{ei} = \frac{\sum_{j=1}^{i} M_{ej}}{\sum_{j=1}^{N} ej}, \qquad 2.11$$

where: N is the total number of nodes.

[12]

Table 13: Cumulative effective mass fraction for the beam model.

Mode	Freq. (Hz)	Trans. X	Trans. Y	Trans. Z	Rot. X	Rot. Y	Rot. Z
Mode 1	1,4355	2,6213e-4	0,16676	5,446e-12	1,18e-11	4,158e-14	1,41e-4
Mode 2	2,238	2,6213e-4	0,16676	0,51394	0,60863	6,9649e-4	1,41e-4
Mode 3	2,3864	3,0313e-4	0,16686	0,51394	0,60863	6,9649e-4	0,18294
Mode 4	2,9542	3,0313e-4	0,16686	0,53661	0,61923	7,1819e-4	0,18294
Mode 5	3,5657	3,5052e-4	0,73016	0,53661	0,61923	7,1819e-4	0,18294
Mode 6	4,1446	3,5052e-4	0,73016	0,53662	0,61948	0,57545	0,18294
Mode 7	4,8275	6,128e-3	0,73031	0,53662	0,61948	0,57545	0,74009
Mode 8	5,0995	6,128e-3	0,73031	0,54682	0,62397	0,6923	0,74009
Mode 9	5,1315	6,128e-3	0,73031	0,61102	0,66029	0,69496	0,74009
Mode 10	5,1732	6,128e-3	0,73031	0,64334	0,6787	0,72012	0,74009
Mode 11	5,3555	6,128e-3	0,73031	0,95086	0,9667	0,72325	0,74009
Mode 12	7,1386	6,8153e-3	0,99996	0,95086	0,9667	0,72325	0,74019
Mode 13	7,3325	6,8153e-3	0,99996	0,96388	0,97418	0,80744	0,74019
Mode 14	7,4839	6,8153e-3	0,99996	0,96779	0,97596	0,97166	0,74019
Mode 15	8,8084	0,99984	0,99998	0,96779	0,97596	0,97166	0,98104
Mode 16	9,5965	0,99984	0,99998	0,96828	0,97638	0,99118	0,98104
Mode 17	9,9185	0,99984	0,99998	0,97365	0,98023	0,9914	0,98104
Mode 18	10,014	1,	1,	0,97365	0,98023	0,9914	1,
Mode 19	10,163	1,	1,	0,9738	0,98034	0,99554	1,
Mode 20	11,178	1,	1,	1,	1,	1,	1,

2.9.6.1 Beam model ratio of effective mass to total mass

Ratio of effective mass to total mass is calculated by dividing effective mass by the total mass of the system. This parameter is used to ensure all significant modes has been extracted from the modal analysis. Hence the most interesting result from this parameter is the sum, seen in the bottom of table 14. It is common practice to shoot for achieving at least 0,8 or 0,9 in all of the DOF’s. This would mean one would have 80% or 90 % of the total mass is represented in the extracted modes. Experiments have been done by extracting 100 modes from the solid model, and all modes above 20 was deemed to be outside of the scope of this thesis.

Table 14: Ratio of effective mass to total mass for the beam model. M=mode.

Mode	F (Hz)	Trans. X	Trans. Y	Trans. Z	Rot. X	Rot. Y	Rot. Z
M 1	1,4355	2,1027e-4	7,1262e-2	3,988e-12	1,008e-11	1,768e-14	3,9423e-5
M 2	2,238	1,898e-18	1,326e-11	0,37632	0,51986	2,9618e-4	9,612e-14
M 3	2,3864	3,289e-5	3,8602e-5	1,251e-14	6,778e-13	5,223e-12	5,0787e-2
M 4	2,9542	7,288e-13	3,2162e-9	1,6602e-2	9,0462e-3	9,2285e-6	1,632e-12
M 5	3,5657	3,8e-5	0,24071	2,619e-12	1,314e-11	3,284e-11	5,087e-10
M 6	4,1446	1,572e-11	4,685e-12	8,8804e-6	2,1816e-4	0,2444	8,447e-10
M 7	4,8275	4,6343e-3	6,5404e-5	6,3785e-9	2,6828e-9	2,7568e-8	0,15479
M 8	5,0995	2,8126e-9	1,363e-13	7,4663e-3	3,8345e-3	4,9687e-2	7,9507e-8
M 9	5,1315	1,228e-11	8,483e-11	4,7009e-2	3,1026e-2	1,1338e-3	2,893e-10
M 10	5,1732	3,219e-10	4,226e-11	2,3668e-2	1,572e-2	1,0696e-2	1,0312e-8
M 11	5,3555	2,223e-11	3,302e-10	0,22518	0,246	1,3342e-3	4,839e-10
M 12	7,1386	5,5135e-4	0,11523	2,4588e-8	1,6759e-8	2,2425e-8	2,7724e-5
M 13	7,3325	1,5189e-9	1,8391e-7	9,5331e-3	6,3901e-3	3,5798e-2	7,154e-12
M 14	7,4839	1,891e-10	1,8191e-8	2,8579e-3	1,5198e-3	6,9837e-2	1,129e-10
M 15	8,8084	0,79655	7,9988e-6	1,253e-12	9,375e-13	1,12e-11	6,6915e-2
M 16	9,5965	8,051e-10	5,036e-11	3,5909e-4	3,5349e-4	8,2999e-3	4,01e-9
M 17	9,9185	1,614e-10	7,319e-10	3,9351e-3	3,2953e-3	9,3712e-5	1,6254e-8
M 18	10,014	1,263e-4	8,0335e-6	1,7808e-8	1,5668e-8	6,555e-10	5,2663e-3
M 19	10,163	1,631e-10	8,601e-10	1,1106e-4	8,9469e-5	1,759e-3	4,2407e-9
M 20	11,178	8,244e-12	1,5469e-9	1,9183e-2	1,6793e-2	1,8967e-3	1,341e-10
Sum		0,80214	0,42732	0,73223	0,85415	0,42524	0,27783

The participation factor and effective mass gives a perspective into how much mass is moving in each direction for each mode. A high value indicates that the mode will be excited by excitations in that direction. These values can be used to gain an understanding of the significance of each mode.

Higher frequency modes are usually negligible as the lower frequency modes usually dominate due to the fact that it takes less energy to vibrate at lower frequencies. From this it could be said it is as easy as just selecting the first six modes, as they are the lower frequency ones. But it can also be interesting to see if there are any other significant modes using the participation factor and effective mass.

In table 11 and 12 the 20 first natural frequencies and their corresponding participation factors and effective masses is shown. For translations, all absolute values over 5 is shown in green, while for rotations, all absolute values over 1000 is shown in green. This gives a good perspective on how much movement each mode has and in which direction they move.

In table 13 the 20 first natural frequencies and their corresponding cumulative effective mass fraction is shown. The points of interest in this table are when we have large jumps in values between two modes. This shows that a big fraction of effective mass is pertained to the second of the two.

From the participation factor, effective mass and cumulative effective mass results, we can see there are several active modes after the first six, and most notably, mode 7, 8, 11, 12, 14, 15, 18 and 20 is quite significant.

2.9.7 Beam model mode shapes

Mode 1:

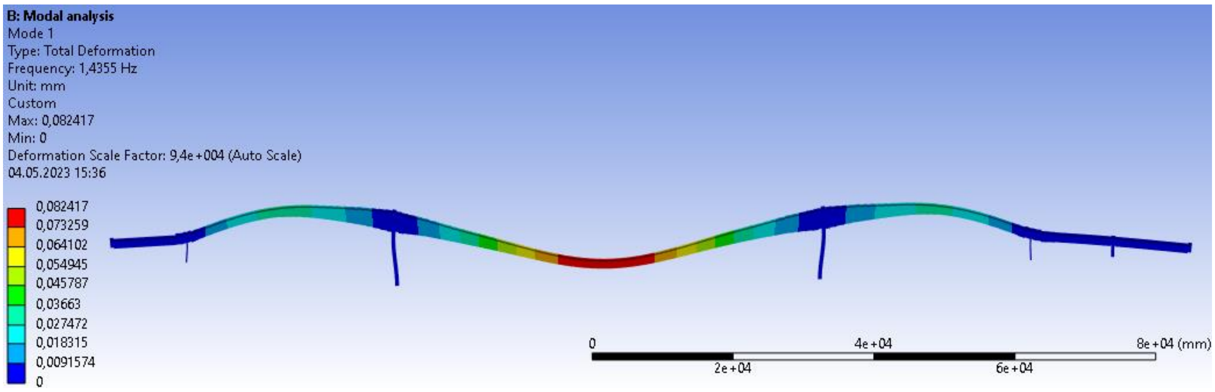

B: Modal analysis
Mode 1
Type: Total Deformation
Frequency: 1,4355 Hz
Unit: mm
Custom
Max: 0,082417
Min: 0
Deformation Scale Factor: 9,4e+004 (Auto Scale)
04.05.2023 15:36

Figure 61: Mode 1 shape for the beam model viewed from the side (Z direction).

Mode 1 on the beam model is a longitudinal mode shape, mainly with translation of movement in Y direction and rotation around the Z axis. Mode 1 on the beam model corresponds well (99,5%) with mode 1 on the solid model. Mode 1 is recommended for comparison with operational mode analysis results.

Mode 2:

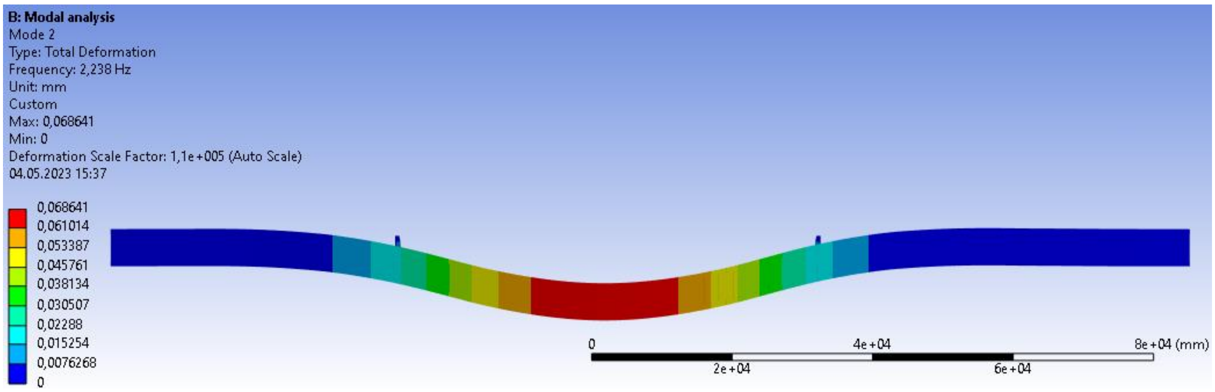

B: Modal analysis
Mode 2
Type: Total Deformation
Frequency: 2,238 Hz
Unit: mm
Custom
Max: 0,068641
Min: 0
Deformation Scale Factor: 1,1e+005 (Auto Scale)
04.05.2023 15:37

Figure 62: Mode 2 shape for the beam model viewed from the top (Y direction).

Mode 2 on the beam model is a transverse mode shape, mainly with translation of movement in Z direction and rotation around the X and Y axes. Mode 2 on the beam model corresponds well (98,8%) with mode 2 on the solid model. Mode 2 is recommended for comparison with operational mode analysis results.

Mode 3:

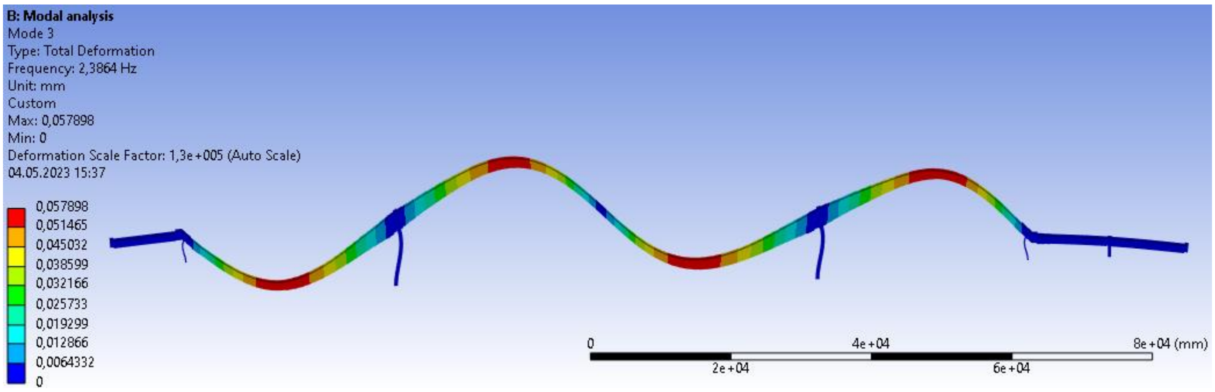

Figure 63: Mode 3 shape for the beam model viewed from the side (Z direction).

Mode 3 on the beam model is a longitudinal mode shape, mainly with rotation around the Z axis. Mode 3 on the beam model corresponds well (99,4%) with mode 3 on the solid model. Mode 3 is recommended for comparison with operational mode analysis results.

Mode 4:

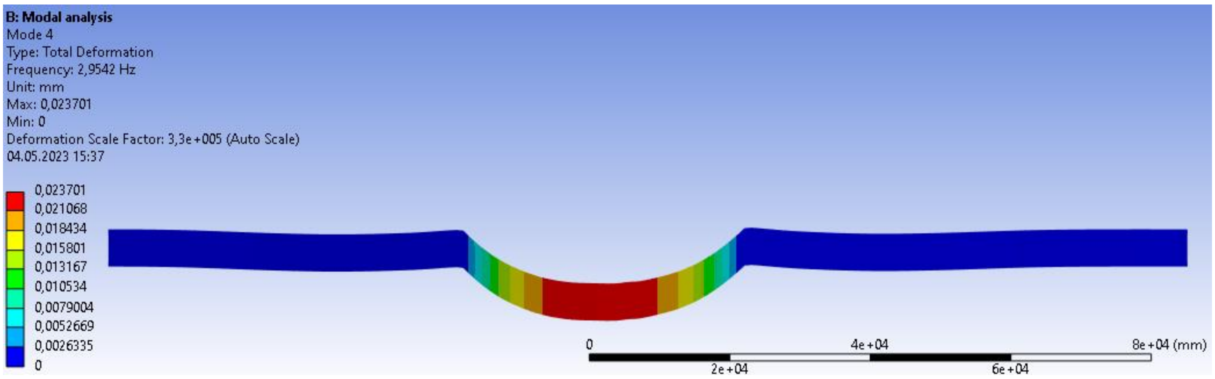

Figure 64: Mode 4 shape for the beam model viewed from the top (Y direction).

Mode 4 on the beam model is a transverse mode shape, mainly with rotation around the X and Y axes. Mode 4 has a relatively high participation factor. Mode 4 is recommended for comparison with operational mode analysis results.

Mode 5:

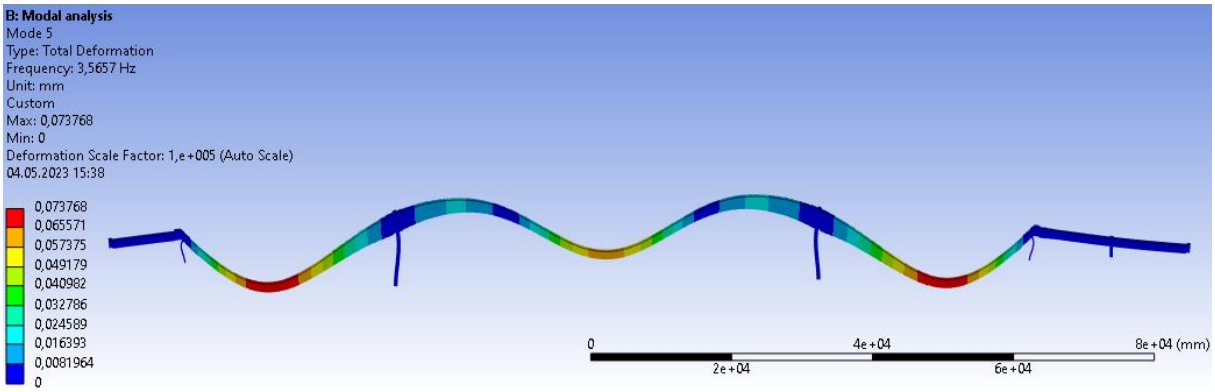

Figure 65: Mode 5 shape for the beam model viewed from the side (Z direction).

Mode 5 on the beam model is a longitudinal mode shape, mainly with translation of movement in Y direction and very low rotation around the Z axis. Mode 5 on the beam model corresponds well (99,3%) with mode 5 on the solid model. Mode 5 is recommended for comparison with operational mode analysis results.

Mode 6:

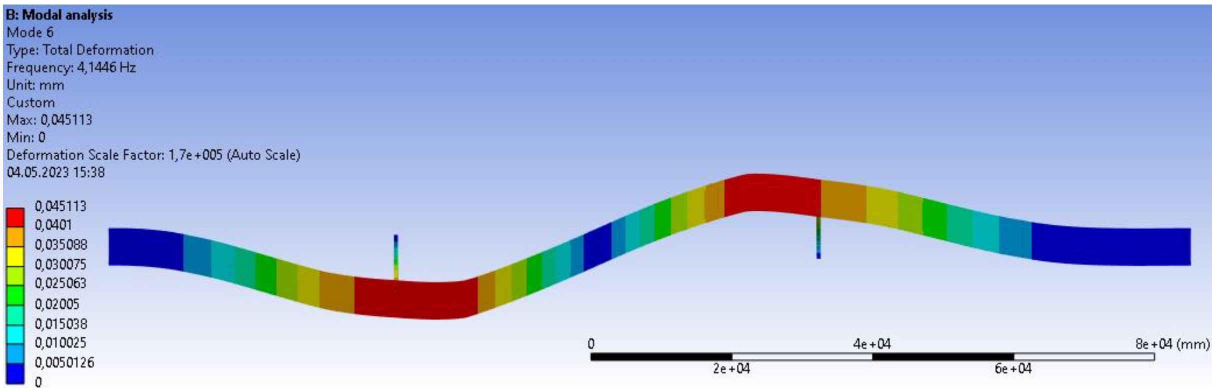

Figure 66: Mode 6 shape for the beam model viewed from the top (Y direction).

Mode 6 on the beam model is a transverse mode shape, mainly with rotation around the X and Y axes. Mode 6 on the beam model corresponds well (99,1%) with mode 4 on the solid model. Mode 6 is recommended for comparison with operational mode analysis results.

Mode 7:

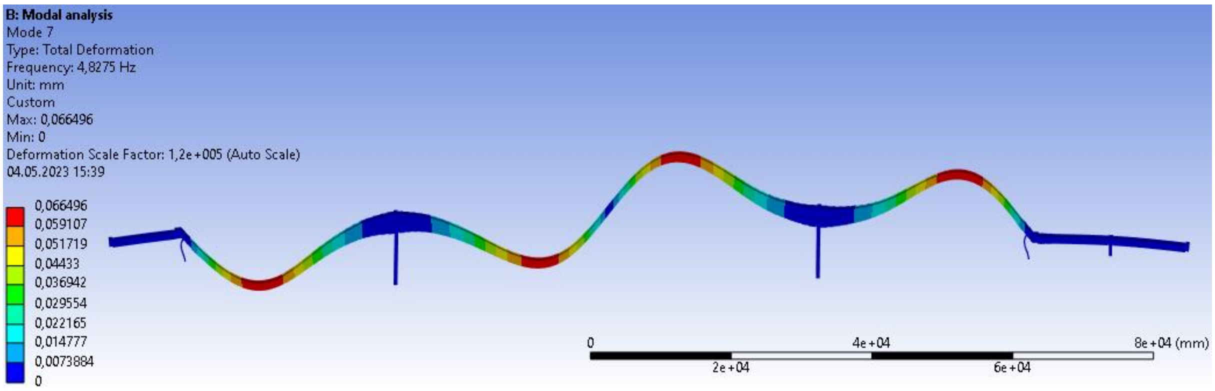

Figure 67: Mode 7 shape for the beam model viewed from the side (Z direction).

Mode 7 on the beam model is a longitudinal mode shape, mainly with rotation around the Z axis. Mode 7 on the beam model corresponds well (94%) with mode 7 on the solid model. Mode 7 is recommended for comparison with operational mode analysis results.

Mode 8:

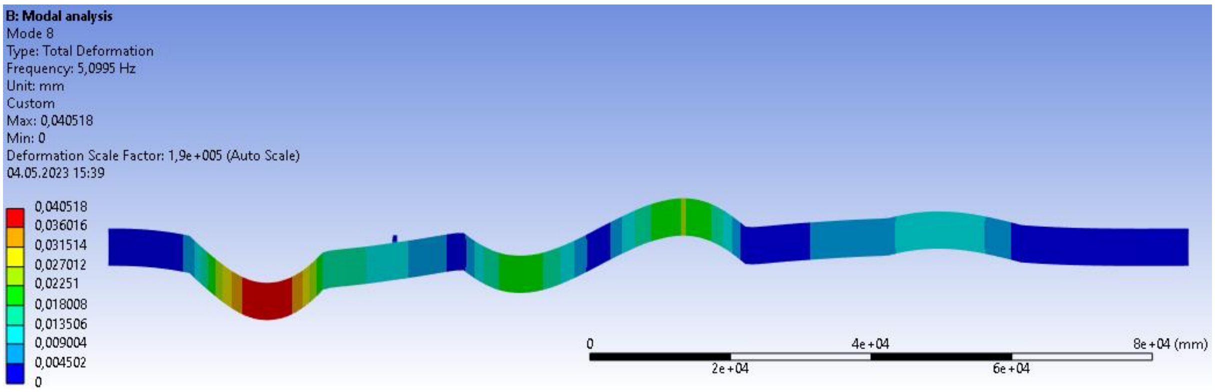

Figure 68: Mode 8 shape for the beam model viewed from the top (Y direction).

Mode 8 on the beam model is a transverse mode shape, mainly with rotation around the X and Y axes. Mode 8 has a relatively high participation factor. Mode 8 is recommended for comparison with operational mode analysis results.

Mode 9:

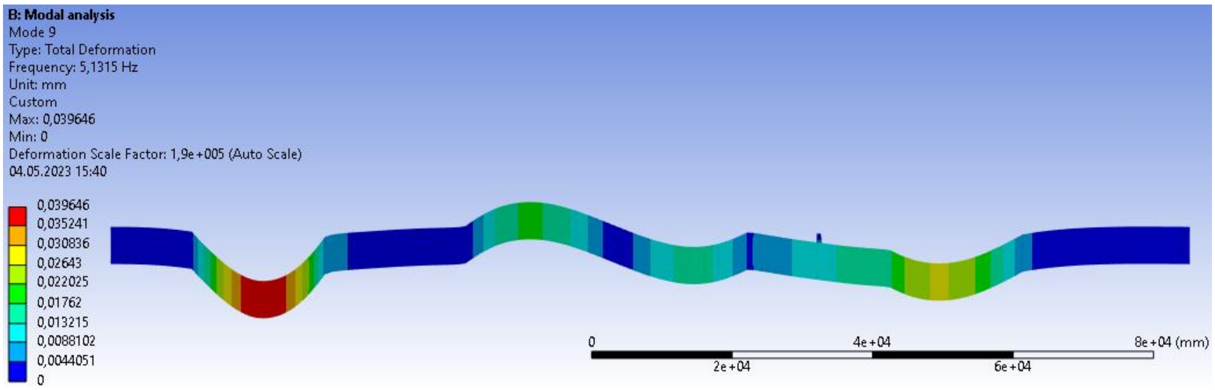

Figure 69: Mode 9 shape for the beam model viewed from the top (Y direction).

Mode 9 on the beam model is a transverse mode shape, mainly with translation of movement in Z direction and rotation around the X and Y axes. Mode 9 is locally active on the Herøyholmen side of the main span, and not particularly active in the rest of the bridge. Mode 9 is not prioritized for comparison with operational mode analysis results.

Mode 10:

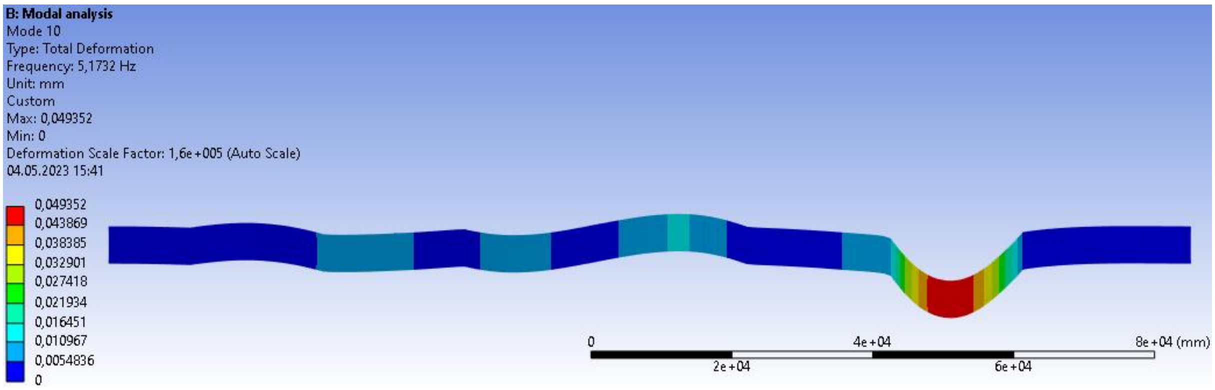

Figure 70: Mode 10 shape for the beam model viewed from the top (Y direction).

Mode 10 on the beam model is a transverse mode shape, mainly with translation of movement in Z direction and rotation around the X and Y axes. Mode 10 is locally active in the Sildval side of the main span, and not particularly active in the rest of the bridge. Mode 10 is not prioritized for comparison with operational mode analysis results.

Mode 11:

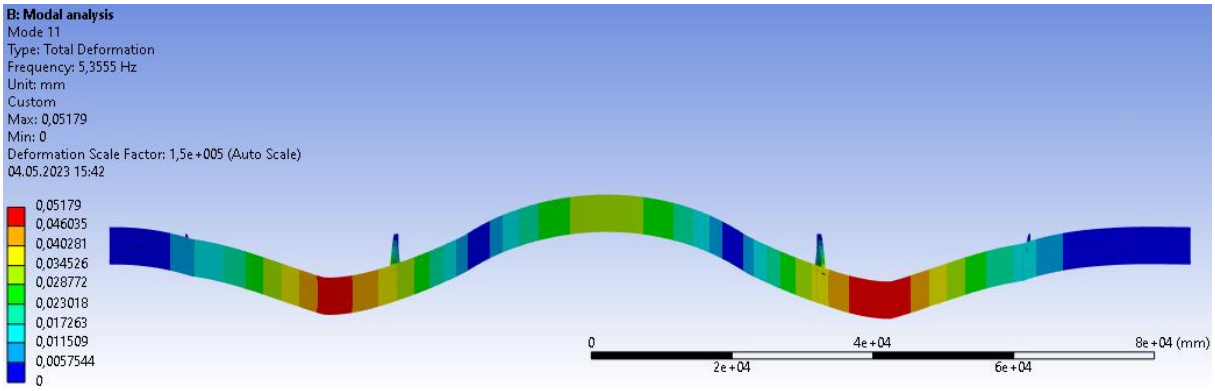

B: Modal analysis
Mode 11
Type: Total Deformation
Frequency: 5,3555 Hz
Unit: mm
Custom
Max: 0,05179
Min: 0
Deformation Scale Factor: 1,5e+005 (Auto Scale)
04.05.2023 15:42

Figure 71: Mode 11 shape for the beam model viewed from the top (Y direction).

Mode 11 on the beam model is a transverse mode shape, mainly with translation of movement in Z direction and rotation around the X and Y axes. Mode 11 on the beam model corresponds well (97,7%) with mode 8 on the solid model. Mode 11 is recommended for comparison with operational mode analysis results.

Mode 12:

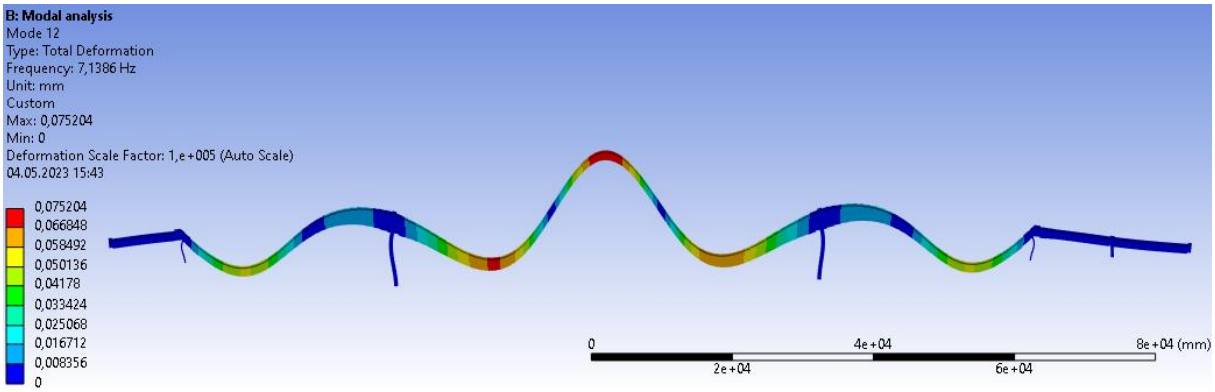

B: Modal analysis
Mode 12
Type: Total Deformation
Frequency: 7,1386 Hz
Unit: mm
Custom
Max: 0,075204
Min: 0
Deformation Scale Factor: 1,e+005 (Auto Scale)
04.05.2023 15:43

Figure 72: Mode 12 shape for the beam model viewed from the side (Z direction).

Mode 12 on the beam model is a longitudinal mode shape, mainly with translation of movement in Y direction and rotation around the Z axis. Mode 12 on the beam model corresponds well (94,3%) with mode 10 on the solid model. Mode 12 is recommended for comparison with operational mode analysis results.

Mode 13:

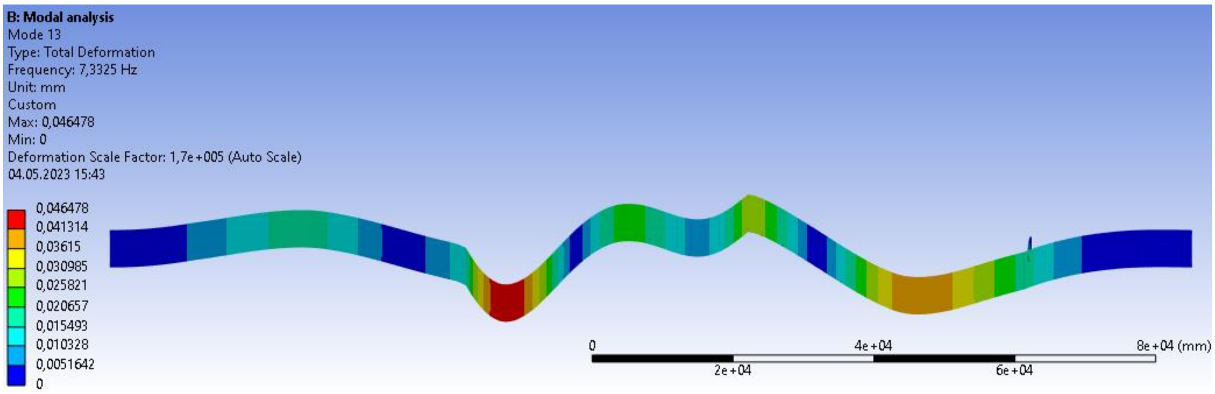

B: Modal analysis
Mode 13
Type: Total Deformation
Frequency: 7,3325 Hz
Unit: mm
Custom
Max: 0,046478
Min: 0
Deformation Scale Factor: 1,7e+005 (Auto Scale)
04.05.2023 15:43

Figure 73: Mode 13 shape for the beam model viewed from the top (Y direction).

Mode 13 on the beam model is a transverse mode shape, mainly with rotation around the X and Y axes. Mode 13 has a relatively low participation factor and is locally focused on the Herøyholmen side of the main span and is not prioritized for comparison with operational mode analysis results.

Mode 14:

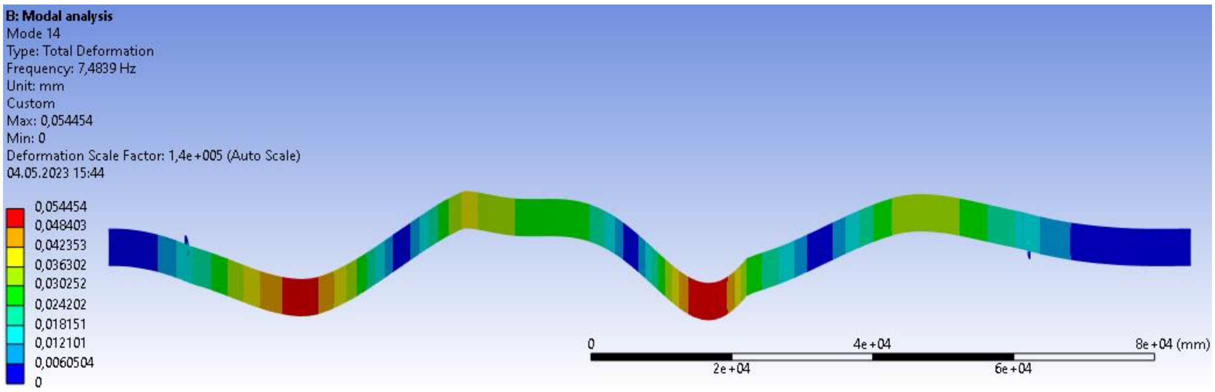

B: Modal analysis
Mode 14
Type: Total Deformation
Frequency: 7,4839 Hz
Unit: mm
Custom
Max: 0,054454
Min: 0
Deformation Scale Factor: 1,4e+005 (Auto Scale)
04.05.2023 15:44

Figure 74: Mode 14 shape for the beam model viewed from the top (Y direction).

Mode 14 on the beam model is a transverse mode shape, mainly with rotation around the X and Y axes. Mode 14 on the beam model corresponds well (93,5%) with mode 9 on the solid model. Mode 14 is recommended for comparison with operational mode analysis results.

Mode 15:

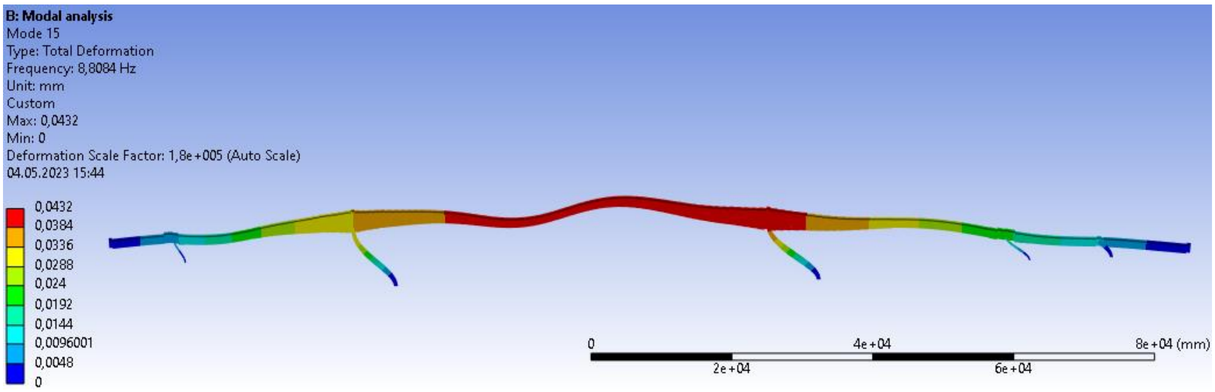

Figure 75: Mode 15 shape for the beam model viewed from the side (Z direction).

Mode 15 on the beam model is a longitudinal mode shape, mainly with translation of movement in X direction and rotation around the Z axis. Mode 15 has a relatively high participation factor. Mode 15 is recommended for comparison with operational mode analysis results.

Mode 16:

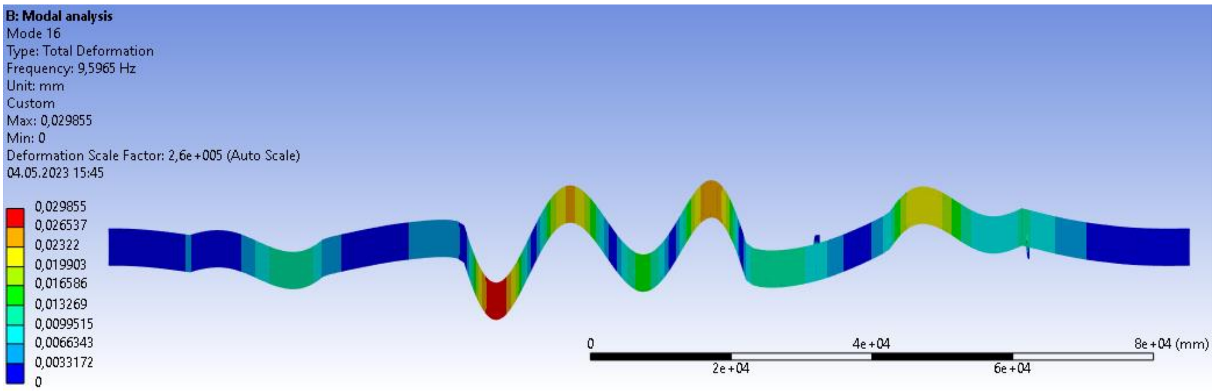

Figure 76: Mode 16 shape for the beam model viewed from the top (Y direction).

Mode 16 on the beam model is a transverse mode shape, mainly with rotation around the X and Y axis. Mode 16 has a relatively low participation factor and is not prioritized for comparison with operational mode analysis results.

Mode 17:

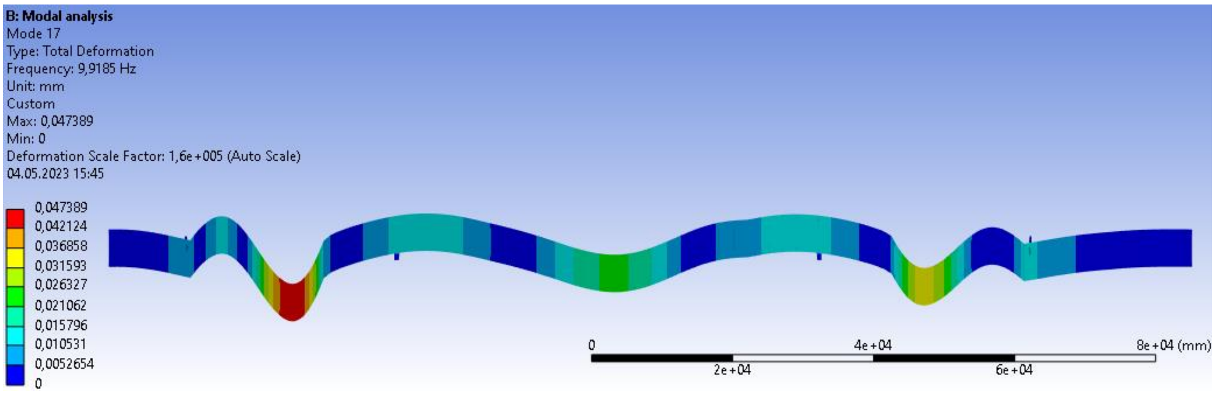

B: Modal analysis
Mode 17
Type: Total Deformation
Frequency: 9,9185 Hz
Unit: mm
Custom
Max: 0,047389
Min: 0
Deformation Scale Factor: 1,6e+005 (Auto Scale)
04.05.2023 15:45

Figure 77: Mode 17 shape for the beam model viewed from the top (Y direction).

Mode 17 on the beam model is a transverse mode shape, mainly with rotation around the X and Y axes. Mode 17 has a relatively low participation factor and is mostly locally active in the Herøyholmen side of the main span. Mode 17 is not prioritized for comparison with operational mode analysis results.

Mode 18:

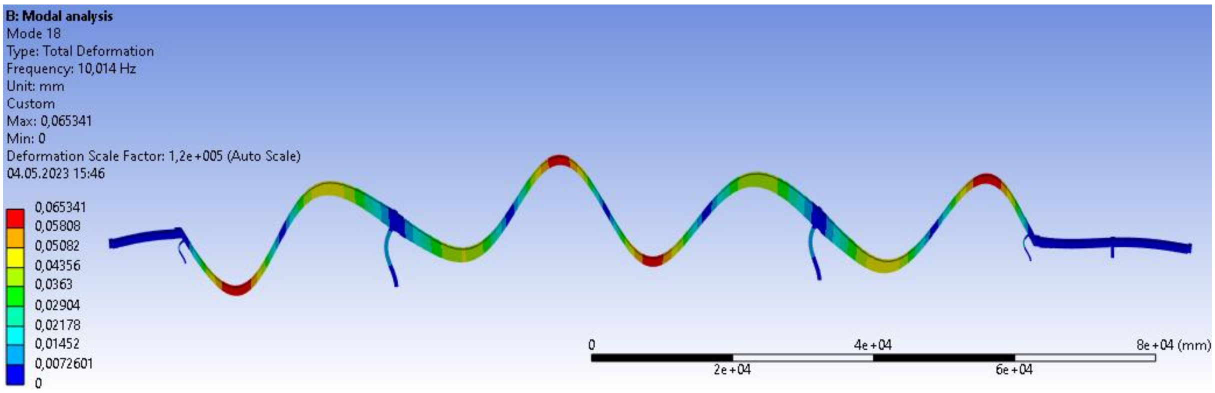

B: Modal analysis
Mode 18
Type: Total Deformation
Frequency: 10,014 Hz
Unit: mm
Custom
Max: 0,065341
Min: 0
Deformation Scale Factor: 1,2e+005 (Auto Scale)
04.05.2023 15:46

Figure 78: Mode 18 shape for the beam model viewed from the side (Z direction).

Mode 18 on the beam model is a longitudinal mode shape, mainly with rotation around the Z axis. Mode 18 on the beam model corresponds well (97,8%) with mode 16 on the solid model. Mode 18 is recommended for comparison with operational mode analysis results.

Mode 19:

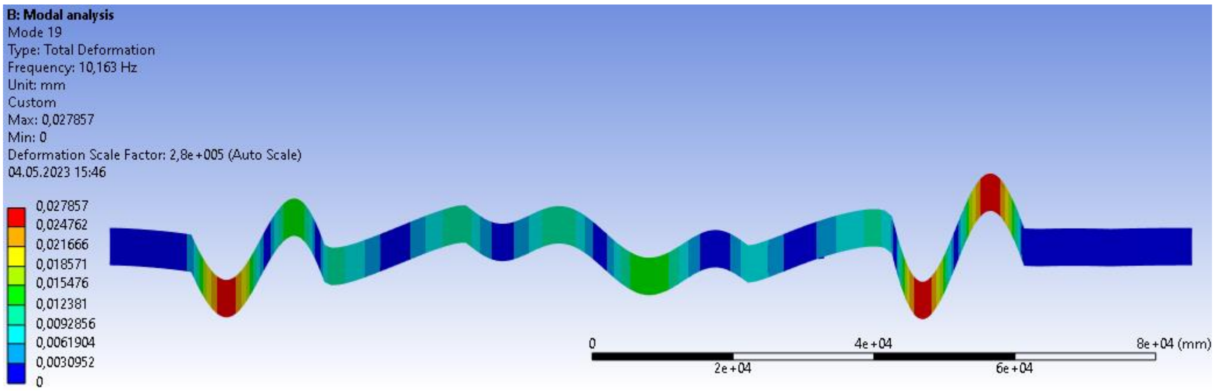

B: Modal analysis
Mode 19
Type: Total Deformation
Frequency: 10,163 Hz
Unit: mm
Custom
Max: 0,027857
Min: 0
Deformation Scale Factor: 2,8e+005 (Auto Scale)
04.05.2023 15:46

Figure 79: Mode 19 shape for the beam model viewed from the top (Y direction).

Mode 19 on the beam model is a transverse mode shape, mainly with rotation around the X and Y axes. Mode 19 has a relatively low participation factor and is mostly active locally in both ends of the main span. Mode 19 is not prioritized for comparison with operational mode analysis results.

Mode 20:

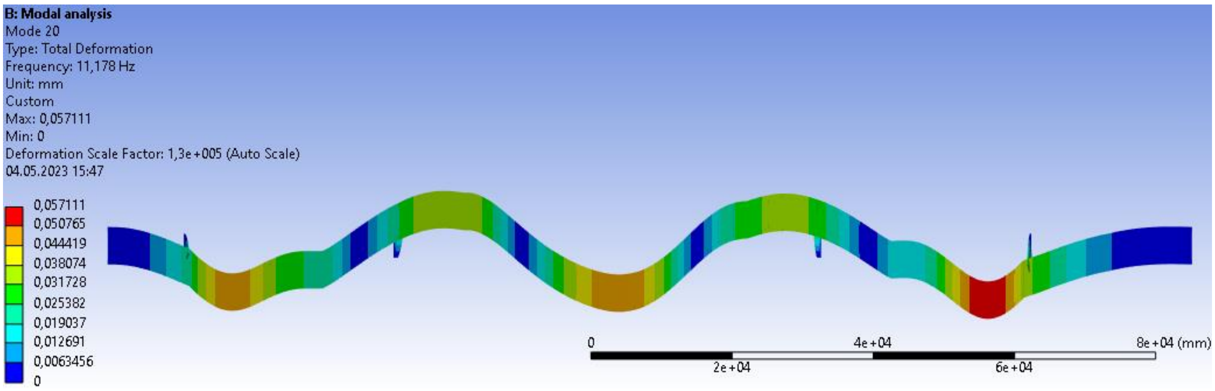

B: Modal analysis
Mode 20
Type: Total Deformation
Frequency: 11,178 Hz
Unit: mm
Custom
Max: 0,057111
Min: 0
Deformation Scale Factor: 1,3e+005 (Auto Scale)
04.05.2023 15:47

Figure 80: Mode 20 shape for the beam model viewed from the top (Y direction).

Mode 20 on the beam model is a transverse mode shape, mainly with rotation around the X and Y axes. Mode 20 on the beam model corresponds well (93,6%) with mode 15 on the solid model. Mode 20 is recommended for comparison with operational mode analysis results.

2.9.8 Beam model volume and mass

Volume of beam model: 444,1 m^3.

Mass of beam model: 1062300 Kg = 1062,3 tons.

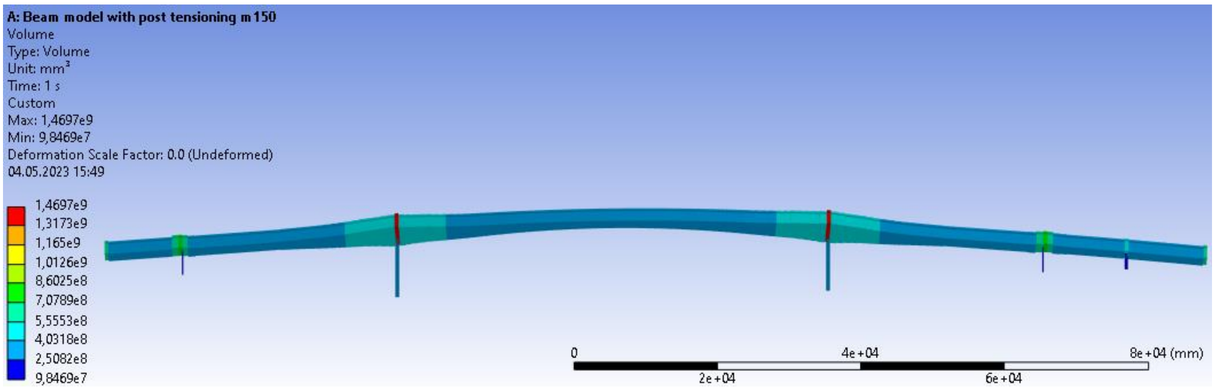

Figure 81: Volume distribution of beam sections.

3 Comparing solid and beam element model analyses

3.1 Deflection

Table 15: Comparison of deflections between non post tensioned and post tensioned solid and beam model.

	Without post tensioning [mm]	With post tensioning [mm]	Difference [%]
Solid	102,2	36,08	64
Beam	111,41	70,753	36,5
Difference [%]	9	96	

Table 15 shows a comparison of the effects on deflection the post tensioning is inducing on the solid and beam model. The table also compares deflections on the solid and beam model. From these results we can see the post tensioning system has more effect on the solid model than on the beam model. It is also apparent that there is a smaller difference between the deflections of the models when the post tensioning system is removed. To get a clue on which model to put confidence in, these results can be compared to other structural analyses and real-world tests conducted in the report from AAS-Jacobsen titled “18-1069 Herøysund bru. Bæreevneberegninger” [14].

In the AAS-Jacobsen report there have been conducted a structural analysis and real-world test placing 50 tonnes evenly distributed over the middle of the main span.

The AAS-Jacobsen analysis gave a deflection of the middle of the main span of 45 mm, and in the real-world test they measured 31 mm to 33 mm deflection in the middle of the main span. Since they in the AAS-Jacobsen report compare these results, it is unclear if the deflection results from their analysis is presented excluding the deflection from mass of the bridge and gravity as the measured deflection cannot include deflection from mass of the bridge and gravity.

The same case of 50 tonnes evenly distributed on 16 metres in the middle of the main span was added to both the beam and solid model in this analysis, which gave these results:

Deflection solid = 41,338 mm, deflection beam = 40,037 mm.

Holding this together with the high deflection of the beam model (70,753 mm) and relatively low deflection of the solid model (36,08 mm) found in this thesis, the results from the solid model is considered to be the most reliable.

3.2 Volume and mass

The table below shows a difference in volume and mass between the solid and beam model of 0,24%, which is an acceptable difference and well within the accuracy one would expect from a conversion between solid and beam element models.

Table 16: comparison of volume and mass of the solid and beam model.

	Volume [m^3]	Mass [Kg]
Solid	445,15	1062300
Beam	444,1	1064800
Difference [%]	0,24	0,24

3.3 CPU time

Table 17: Specifications of the computer used for the analyses.

Processor	Intel® Core™ i9-10980XE CPU @ 3.00 GHz
RAM	128 GB

Table 18: CPU time comparison for static structural analysis.

Parameter	Solid element model	Beam element model
Total CPU time for all threads	50,9 seconds	1,9 seconds
Sum of memory used on all processes	10115 MB	546 MB
Total amount of I/O written to disk	3.3 GB	0,0 GB
Total amount of I/O read from disk	1,7 GB	0,0 GB

Table 19: CPU time comparison for modal analysis.

Parameter	Solid element model	Beam element model
Total CPU time for all threads	166,6 seconds	3,8 seconds
Sum of memory used on all processes	20406 MB	205 MB
Total amount of I/O written to disk	6.6 GB	0,1 GB
Total amount of I/O read from disk	84 GB	0,4 GB

Table 18 and 19 shows CPU time for Structural and odal analyses respectively. Comparing the CPU time of solid and beam analyses, it is apparent that the beam model requires a lot less resources to compute than the solid model, which can be useful for quick analyses when low on computing power or if the analyses is made more complex in the future. Although the engineering hours required to convert the solid model to a beam model (approximately 75 hours) is most likely not worth it compared to buying more computing power.

3.4 Frequencies and modal shapes

For the modal analysis both models have been analysed using the same static structural precondition as pre-stress. The results from both models were then compared to each other using the modal assurance criterion index.

3.4.1 Modal assurance criterion theory

The modal assurance criterion between two real solutions is computed using the equation:

$$mac\left(ø_i^{(1)}, ø_j^{(2)}\right) = \frac{(ø_i^{(1)^t} \cdot m^{(k)} \cdot ø_j^{(2)})^2}{(ø_i^{(1)^t} \cdot m^{(k)} \cdot ø_i^{(1)})(ø_j^{(2)^t} \cdot m^{(k)} \cdot ø_j^{(2)})} \qquad 3.1$$

Where:

$ø_i^{(1)}$ is the i'th solution vector of solution 1. (From file 1)

$ø_j^{(2)}$ is the j'th solution vector of solution 2. (From the .rst file)

[15]

3.4.2 Modal assurance criterion

The modal assurance criterion is used to compare the modes extracted from the solid model to the modes extracted from the beam model. It gives answers to how similar each mode in the two models is in a table and presents them as values ranging from 0 to 1 in each cell, where 0 means the modes are totally different, and 1 means the modes are exactly the same. These numbers can of course be multiplied by 100 to give a percentage of match.

First a general comparison between all the modes was extracted. Nodes in both models was automatically matched to the nearest nodes, and their eigenvectors was compared. A node matching tolerance of 10 mm was used.

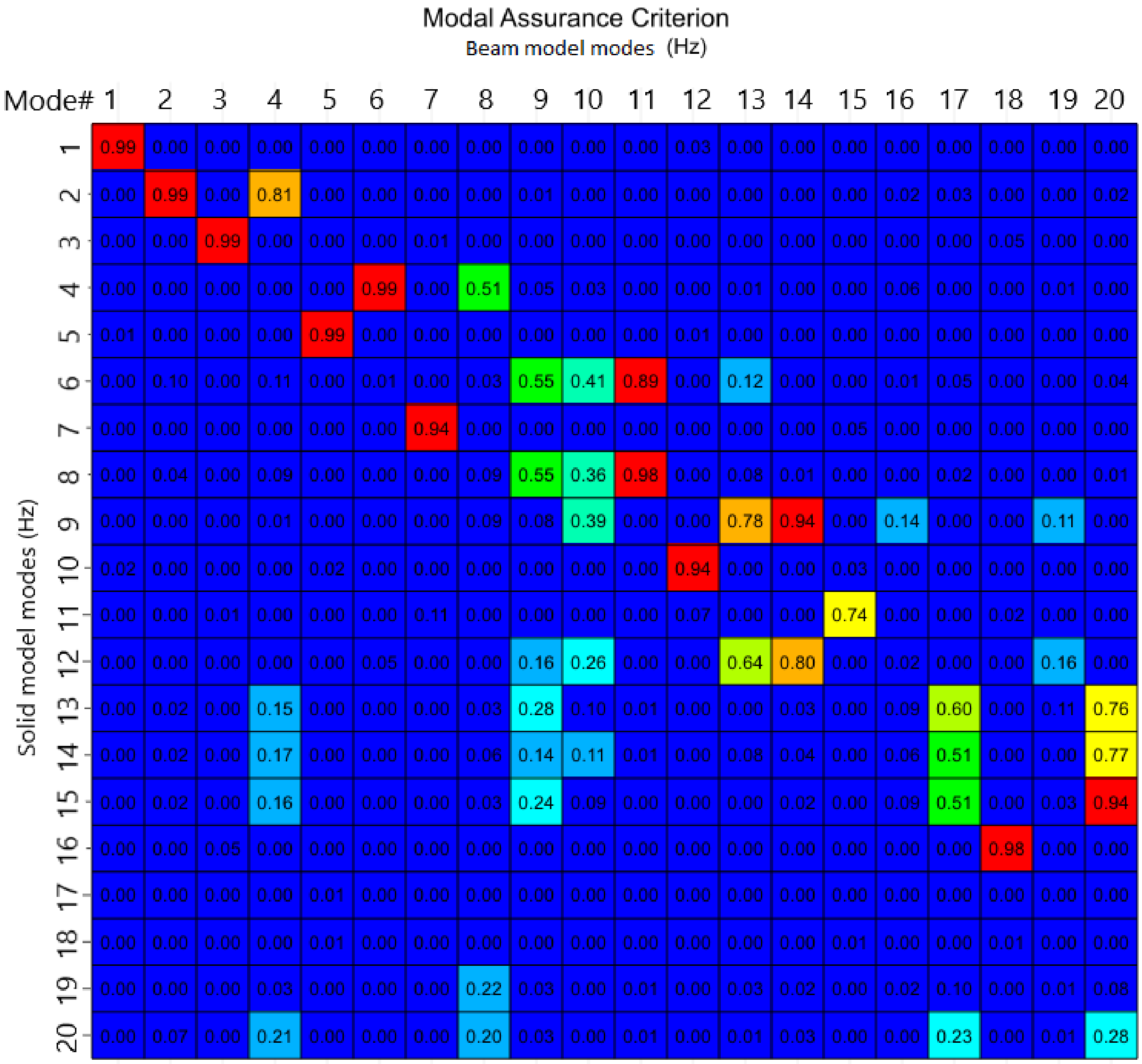

Modal Assurance Criterion

Beam model modes (Hz)

Solid model modes (Hz)

Mode#	1	2	3	4	5	6	7	8	9	10	11	12	13	14	15	16	17	18	19	20
1	0.99	0.00	0.00	0.00	0.00	0.00	0.00	0.00	0.00	0.00	0.00	0.03	0.00	0.00	0.00	0.00	0.00	0.00	0.00	0.00
2	0.00	0.99	0.00	0.81	0.00	0.00	0.00	0.00	0.01	0.00	0.00	0.00	0.00	0.00	0.00	0.02	0.03	0.00	0.00	0.02
3	0.00	0.00	0.99	0.00	0.00	0.00	0.01	0.00	0.00	0.00	0.00	0.00	0.00	0.00	0.00	0.00	0.00	0.05	0.00	0.00
4	0.00	0.00	0.00	0.00	0.00	0.99	0.00	0.51	0.05	0.03	0.00	0.00	0.01	0.00	0.00	0.06	0.00	0.00	0.01	0.00
5	0.01	0.00	0.00	0.00	0.99	0.00	0.00	0.00	0.00	0.00	0.00	0.01	0.00	0.00	0.00	0.00	0.00	0.00	0.00	0.00
6	0.00	0.10	0.00	0.11	0.00	0.01	0.00	0.03	0.55	0.41	0.89	0.00	0.12	0.00	0.00	0.01	0.05	0.00	0.00	0.04
7	0.00	0.00	0.00	0.00	0.00	0.00	0.94	0.00	0.00	0.00	0.00	0.00	0.00	0.00	0.05	0.00	0.00	0.00	0.00	0.00
8	0.00	0.04	0.00	0.09	0.00	0.00	0.00	0.09	0.55	0.36	0.98	0.00	0.08	0.01	0.00	0.00	0.02	0.00	0.00	0.01
9	0.00	0.00	0.00	0.01	0.00	0.00	0.00	0.09	0.08	0.39	0.00	0.00	0.78	0.94	0.00	0.14	0.00	0.00	0.11	0.00
10	0.02	0.00	0.00	0.00	0.02	0.00	0.00	0.00	0.00	0.00	0.00	0.94	0.00	0.00	0.03	0.00	0.00	0.00	0.00	0.00
11	0.00	0.00	0.01	0.00	0.00	0.00	0.11	0.00	0.00	0.00	0.00	0.07	0.00	0.00	0.74	0.00	0.00	0.02	0.00	0.00
12	0.00	0.00	0.00	0.00	0.00	0.05	0.00	0.00	0.16	0.26	0.00	0.00	0.64	0.80	0.00	0.02	0.00	0.00	0.16	0.00
13	0.00	0.02	0.00	0.15	0.00	0.00	0.00	0.03	0.28	0.10	0.01	0.00	0.00	0.03	0.00	0.09	0.60	0.00	0.11	0.76
14	0.00	0.02	0.00	0.17	0.00	0.00	0.00	0.06	0.14	0.11	0.01	0.00	0.08	0.04	0.00	0.06	0.51	0.00	0.00	0.77
15	0.00	0.02	0.00	0.16	0.00	0.00	0.00	0.03	0.24	0.09	0.00	0.00	0.00	0.02	0.00	0.09	0.51	0.00	0.03	0.94
16	0.00	0.00	0.05	0.00	0.00	0.00	0.00	0.00	0.00	0.00	0.00	0.00	0.00	0.00	0.00	0.00	0.00	0.98	0.00	0.00
17	0.00	0.00	0.00	0.00	0.01	0.00	0.00	0.00	0.00	0.00	0.00	0.00	0.00	0.00	0.00	0.00	0.00	0.00	0.00	0.00
18	0.00	0.00	0.00	0.00	0.01	0.00	0.00	0.00	0.00	0.00	0.00	0.00	0.00	0.00	0.01	0.00	0.00	0.01	0.00	0.00
19	0.00	0.00	0.00	0.03	0.00	0.00	0.00	0.22	0.03	0.00	0.01	0.00	0.03	0.02	0.00	0.02	0.10	0.00	0.01	0.08
20	0.00	0.07	0.00	0.21	0.00	0.00	0.00	0.20	0.03	0.00	0.01	0.00	0.01	0.03	0.00	0.00	0.23	0.00	0.01	0.28

Figure 82: Modal assurance criterion using unpaired modes, comparing modes 1-20 in both models.

In figure 82 it is shown what modes match and how good the match is, comparing all 20 first modes of the solid model to all the 20 first modes of the beam model. But there is a way to show this in a compressed table, containing only the important information using "mode pairing".

Modes were paired using the "pair modes" function in the MAC calculator, this function sets several criteria for the mac table, and with the correct settings it only shows the modes with a good match between the two models in the MAC table. These criteria take into account how good match there is between the frequencies of each mode in addition to the regular MAC criterions. More information about mode pairing can be found in the Ansys help web page [16].

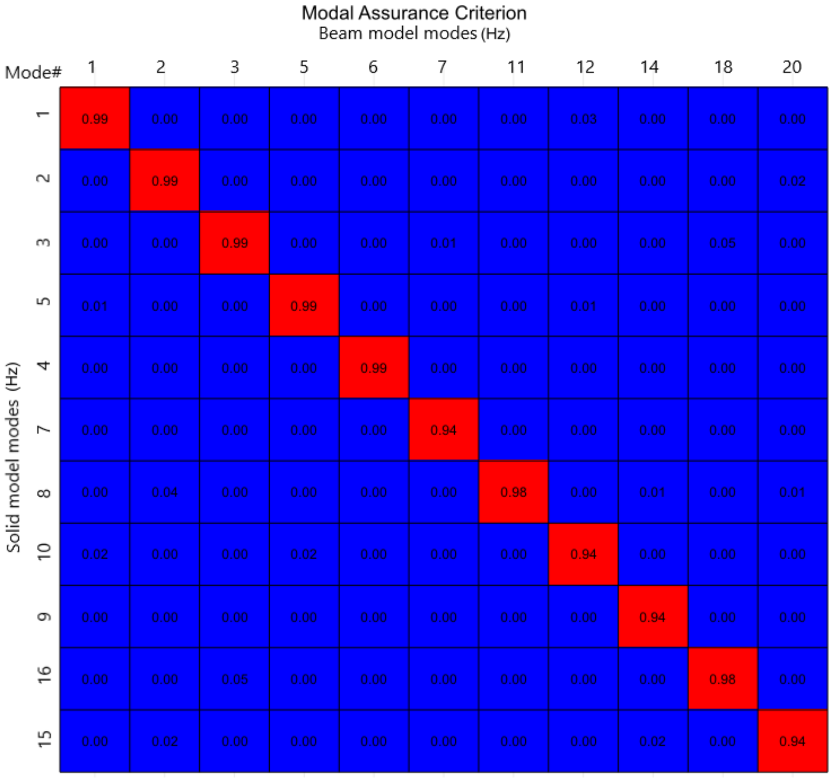

Mode#	1	2	3	5	6	7	11	12	14	18	20
1	0.99	0.00	0.00	0.00	0.00	0.00	0.00	0.03	0.00	0.00	0.00
2	0.00	0.99	0.00	0.00	0.00	0.00	0.00	0.00	0.00	0.00	0.02
3	0.00	0.00	0.99	0.00	0.00	0.01	0.00	0.00	0.00	0.05	0.00
5	0.01	0.00	0.00	0.99	0.00	0.00	0.00	0.01	0.00	0.00	0.00
4	0.00	0.00	0.00	0.00	0.99	0.00	0.00	0.00	0.00	0.00	0.00
7	0.00	0.00	0.00	0.00	0.00	0.94	0.00	0.00	0.00	0.00	0.00
8	0.00	0.04	0.00	0.00	0.00	0.00	0.98	0.00	0.01	0.00	0.01
10	0.02	0.00	0.00	0.02	0.00	0.00	0.00	0.94	0.00	0.00	0.00
9	0.00	0.00	0.00	0.00	0.00	0.00	0.00	0.00	0.94	0.00	0.00
16	0.00	0.00	0.05	0.00	0.00	0.00	0.00	0.00	0.00	0.98	0.00
15	0.00	0.02	0.00	0.00	0.00	0.00	0.00	0.00	0.02	0.00	0.94

Figure 83: Modal assurance criterion using paired modes.

In figure 83 it is shown what modes correspond well (over 90%). The factor of correlation is shown in each cell, where 0 is completely different and 1 is completely similar.

Table 20: Frequency comparison between paired modes on solid and beam model including their respective MAC values.

Solid mode#	Beam mode#	Frequency error	MAC
Mode 1	Mode 1	-0,1 Hz (-4,3%)	0,995
Mode 2	Mode 2	-0,4% (-18,9%)	0,988
Mode 3	Mode 3	0,0 Hz (0%)	0,994
Mode 5	Mode 5	0,2 Hz (5,5%)	0,993
Mode 4	Mode 6	-0,7 Hz (-17,4%)	0,991
Mode 7	Mode 7	-0,3 Hz (-6,4%)	0,940
Mode 8	Mode 11	-0,7 Hz (-12,5%)	0,977
Mode 10	Mode 12	-0,2 Hz (-2,6%)	0,943
Mode 9	Mode 14	-0,8 Hz (-10,5%)	0,935
Mode 16	Mode 18	-0,4 Hz (3,9%)	0,978
Mode 15	Mode20	-1,6 Hz (14,5%)	0,936

In table 20 the modes with a good match is shown including a frequency comparison between paired modes on the solid and beam model and their MAC values. Frequency errors range from 0% to 18,9%, while MAC values range from 93,5% to 99,5%.

3.4.3 Matched modes

Here the 11 modes that gave a correspondence above 90% is shown side by side for a visual comparison of the mode shapes.

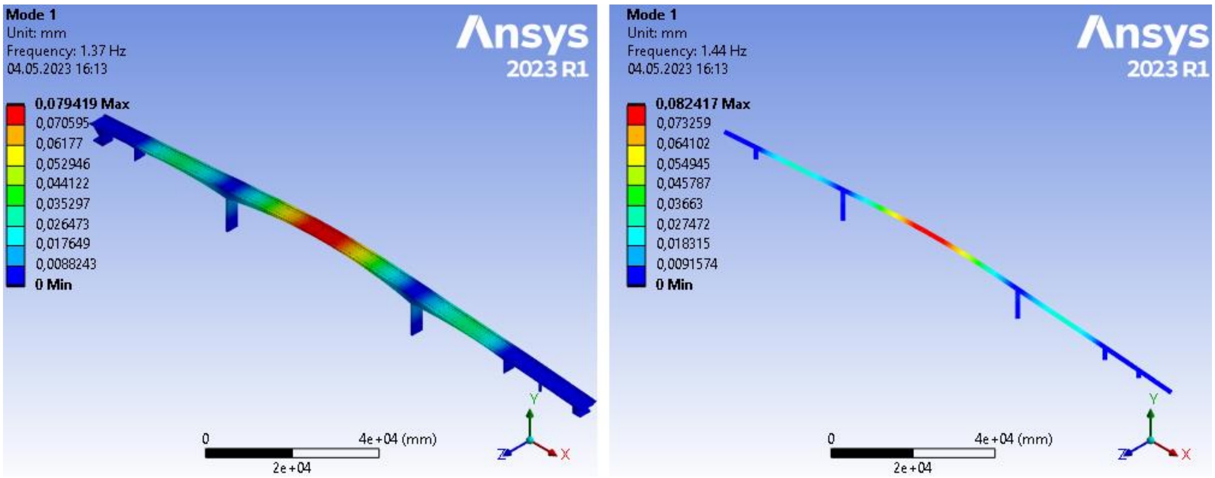

Figure 84: Mode 1 on the solid model matched by 99,5% with mode 1 on the beam model. Frequency error: -4,3%.

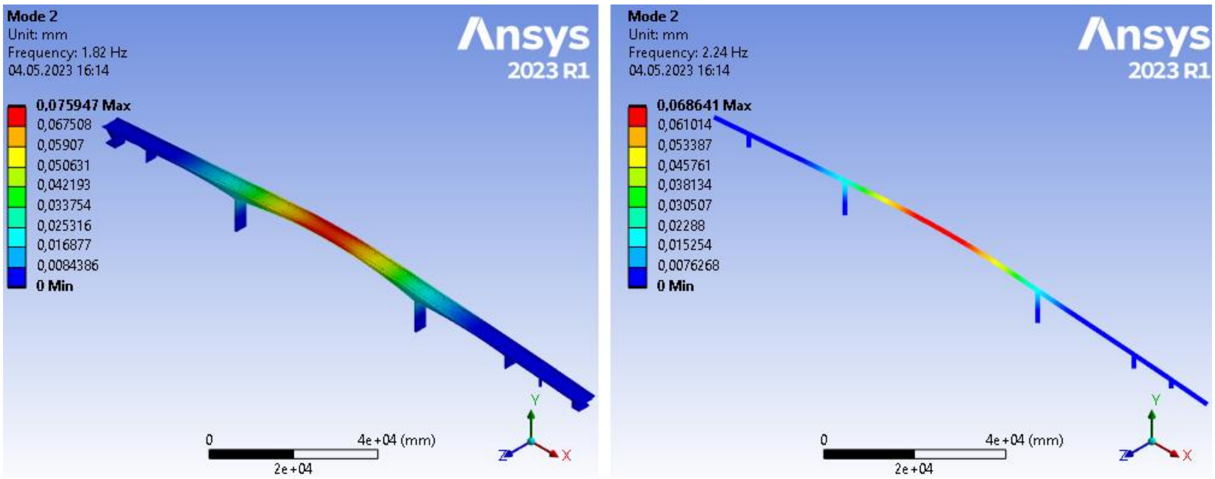

Figure 85: Mode 2 on the solid model matched by 98,8% with mode 2 on the beam model. Frequency error: -18,9%.

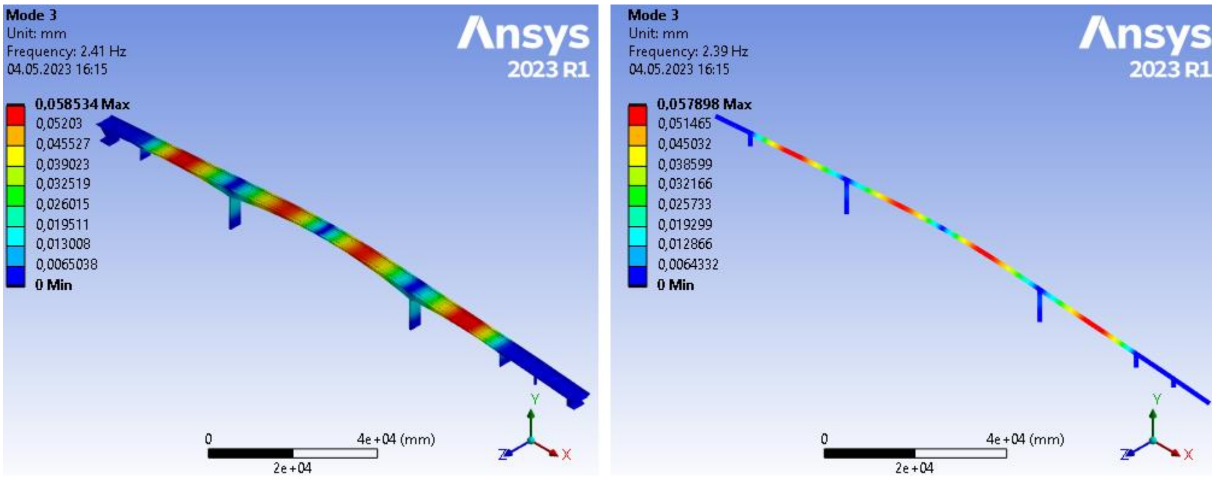

Figure 86: Mode 3 on the solid model matched by 99,4% with mode 3 on the beam model. Frequency error: 1%.

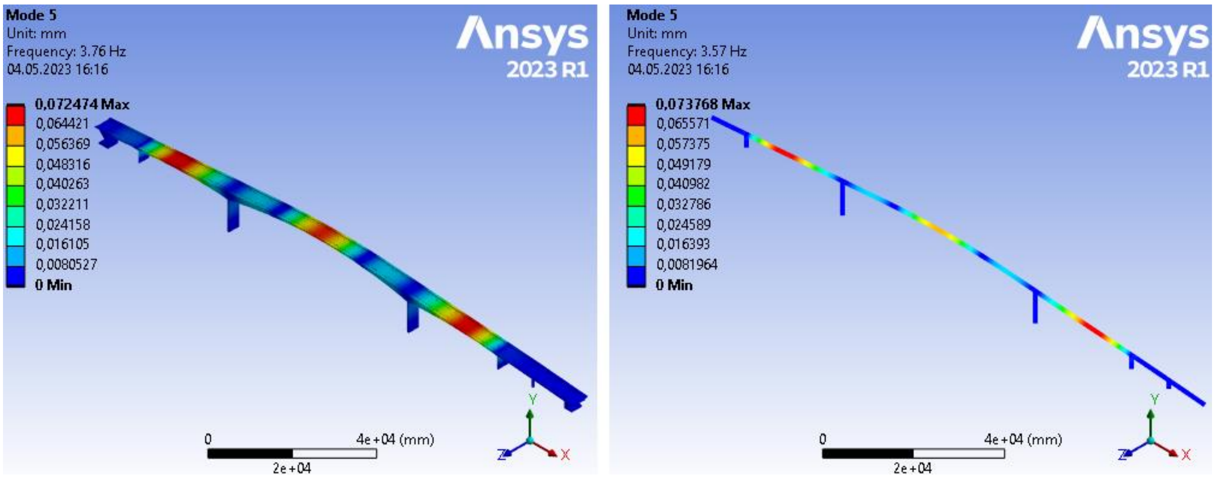

Figure 87: Mode 5 on the solid model matched by 99,3% with mode 5 on the beam model. Frequency error: 5,5%.

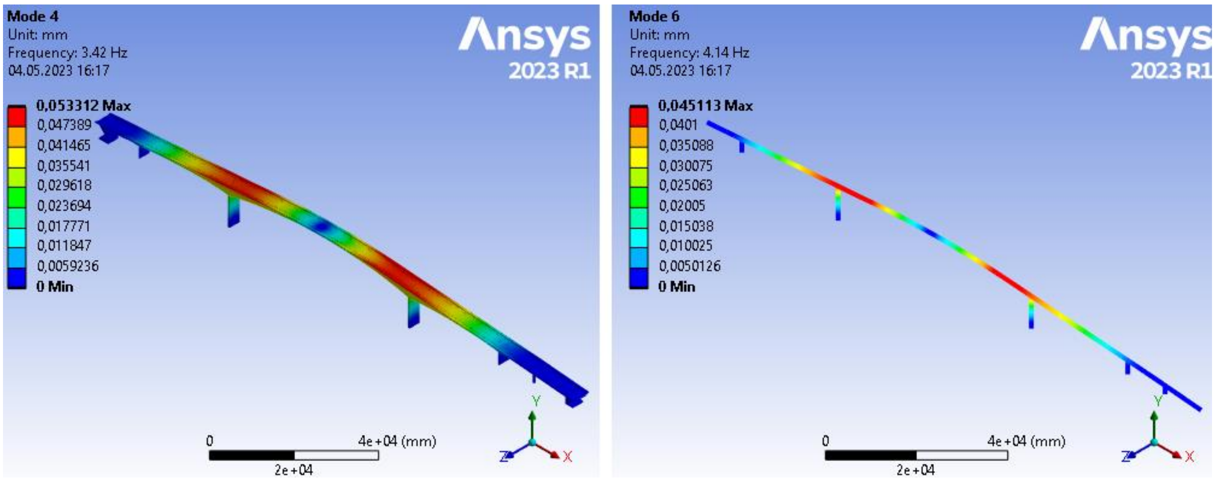

Figure 88: Mode 4 on the solid model matched by 99,1% with mode 6 on the beam model. Frequency error: -17,4%.

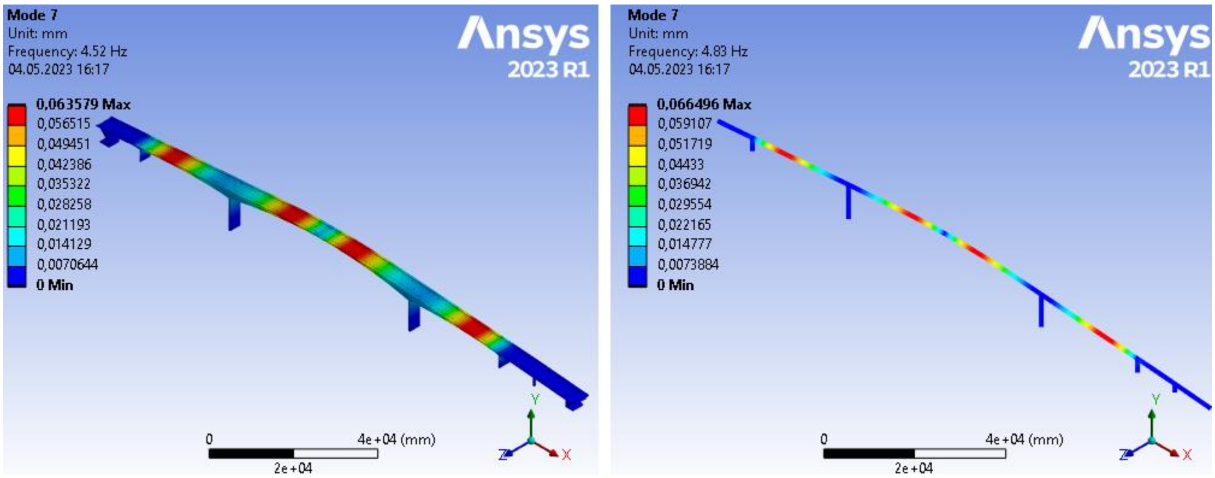

Figure 89: Mode 7 on the solid model matched by 94% with mode 7 on the beam model. Frequency error: -6,4%.

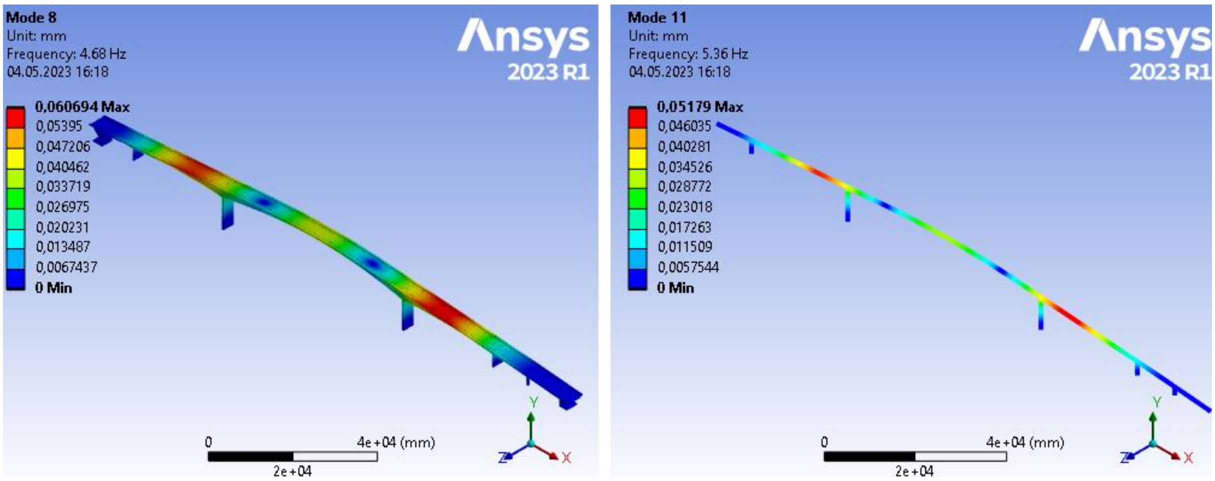

Figure 90: Mode 1 on the solid model matched by 97,7% with mode 1 on the beam model. Frequency error: -12,5%.

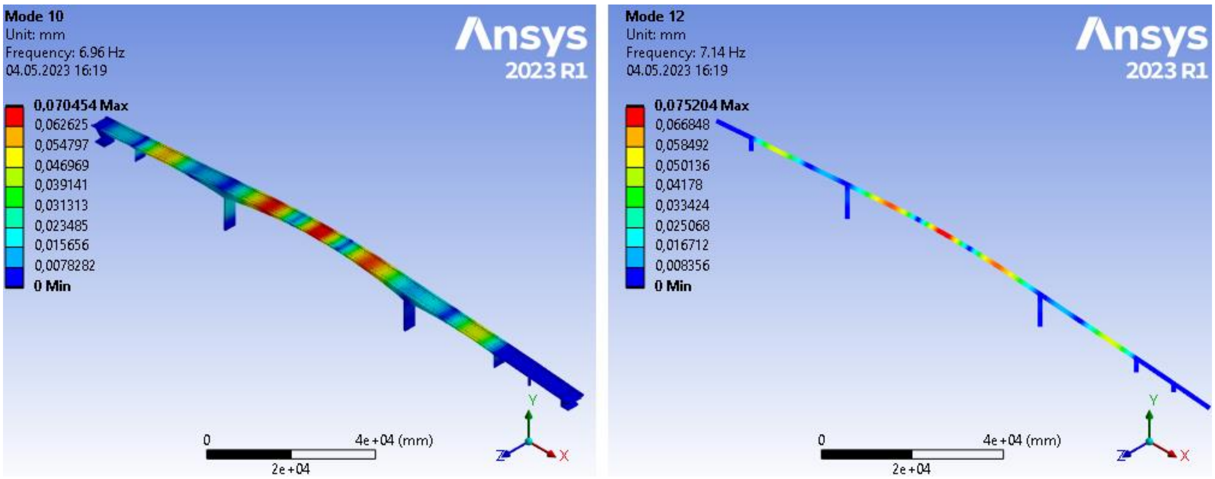

Figure 91: Mode 10 on the solid model matched by 94,3% with mode 12 on the beam model. Frequency error: -2,6%.

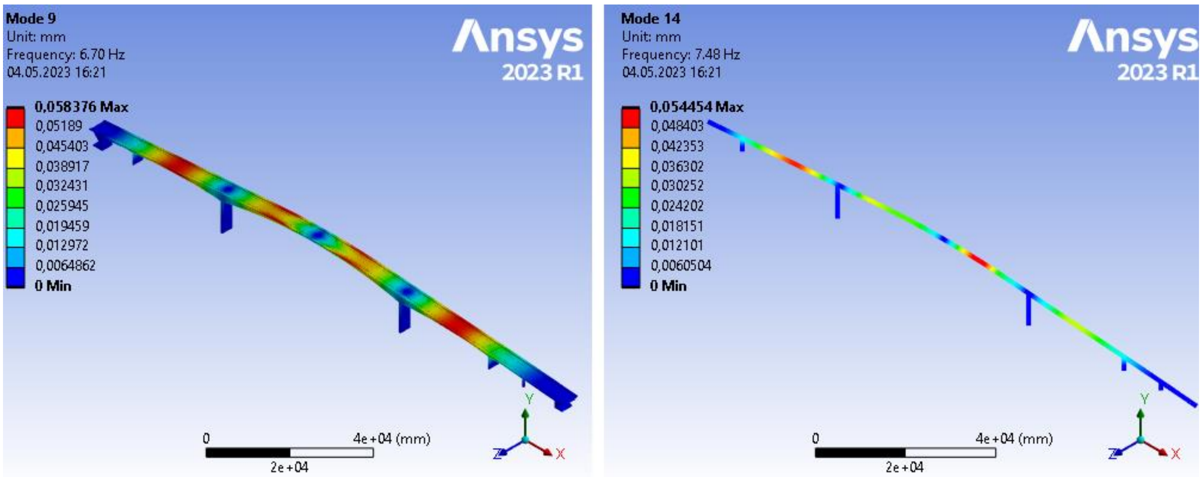

Figure 92: Mode 9 on the solid model matched by 93,5% with mode 14 on the beam model. Frequency error: -10,5%.

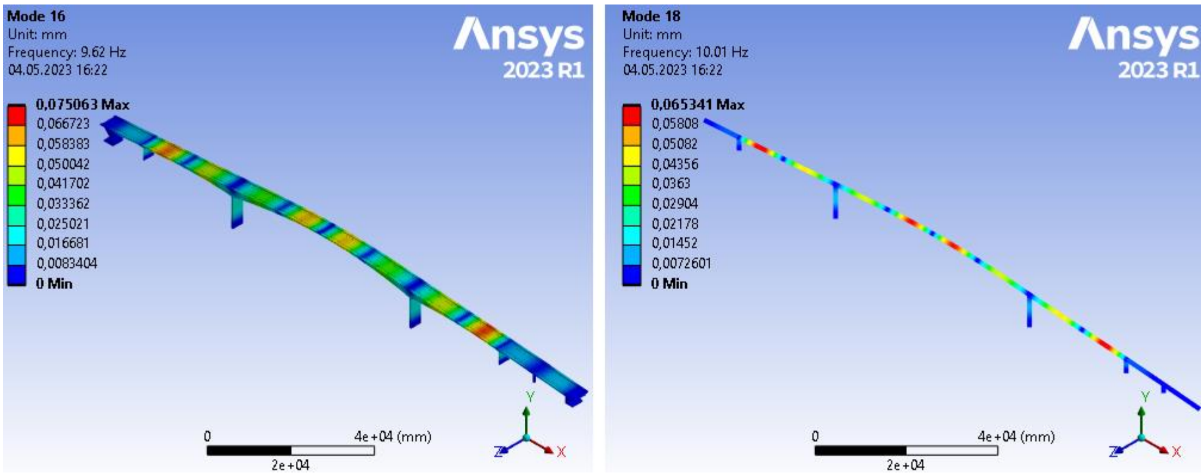

Figure 93: Mode 16 on the solid model matched by 97,8% with mode 18 on the beam model. Frequency error: 3,9%.

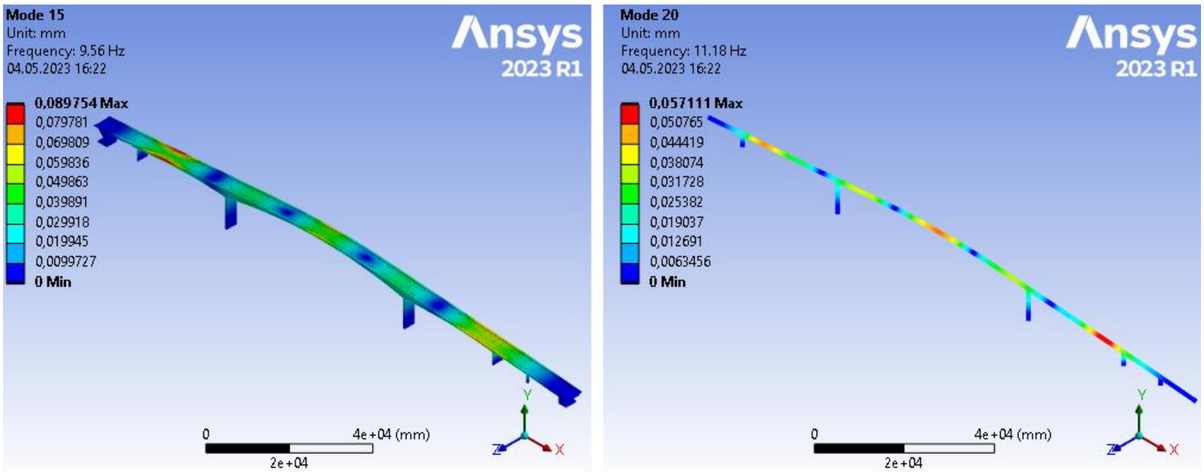

Figure 94: Mode 15 on the solid model matched by 93,6% with mode 20 on the beam model. Frequency error: -14,5%.

Table 21: Matched nodes table including COMAC.

Nodes solid model	Nodes beam model	COMAC (UX)	COMAC (UY)	COMAC (UZ)	COMAC (ROTX)	COMAC (ROTY)	COMAC (ROTZ)
19973	65	0	0	0	0	0	0
34311	2576	0	0.1494	0.0948	0	0	0
34386	28	0	0.1538	0	0	0	0
34402	2585	0	0.1534	0	0	0	0
34488	23	0	0.1500	0.0936	0	0	0
37580	2549	0	0	0	0	0	0
40890	69	0	0	0	0	0	0
48624	2588	0	0.1419	0	0	0	0
48703	2597	0	0.1330	0	0	0	0
49022	8	0	0	0	0	0	0
49119	49	0	0.1402	0	0	0	0
50052	3	0	0	0	0	0	0
58733	170	0	0.5263	0.0826	0	0	0
58735	198	0	0.5244	0	0	0	0
58759	191	0	0.5135	0.0787	0	0	0
58764	177	0	0	0.0753	0	0	0
58765	163	0	0.5096	0.0617	0	0	0
59095	276	0	0.4448	0.0568	0	0	0
88587	253	1.5639E-3	9.0179E-3	0.0308	0	0	0
88624	211	3.0965E-3	0.3546	0.0116	0	0	0
88769	226	2.0833E-4	0.2225	0.0105	0	0	0
88780	192	0	0.0894	0.0172	0	0	0
88817	164	4.7686E-4	0.0515	6.2773E-3	0	0	0
88826	273	1.9566E-3	0.1762	0.0165	0	0	0
88827	2745	6.6217E-4	0.0101	0.0186	0	0	0
88832	2734	1.7556E-4	0.1177	0.0163	0	0	0
89812	2676	0	0.0254	9.6420E-3	0	0	0
89888	2716	1.6578E-3	0.1437	0.0156	0	0	0
89929	2648	7.6845E-4	0.3034	0.0220	0	0	0
89934	2655	0	0.3693	0.0178	0	0	0
129430	713	4.6998E-3	0.2371	0.0347	0	0	0
129435	3649	0.0109	0.0356	0.0601	0	0	0
129439	3214	1.6692E-3	0.0708	8.5635E-3	0	0	0
129444	1072	5.1251E-4	0.0584	0.0190	0	0	0
129447	1154	9.2472E-5	0.0528	0.0531	0	0	0
129449	3507	4.3856E-4	0.0587	0.1122	0	0	0
129452	3813	1.2579E-3	0.0855	0.2122	0	0	0
129457	1175	1.8823E-3	0.1587	0.2305	0	0	0
129460	1075	3.6127E-3	0.1169	0.1343	0	0	0
129462	3323	1.0140E-3	0.0531	0.0792	0	0	0
129465	3237	3.2635E-4	0.0413	0.0340	0	0	0
129467	1432	1.1866E-4	0.0109	0.0197	0	0	0

Nodes solid model	Nodes beam model	COMAC (UX)	COMAC (UY)	COMAC (UZ)	COMAC (ROTX)	COMAC (ROTY)	COMAC (ROTZ)
129475	2854	6.9765E-4	0.1085	0.0165	0	0	0
129595	640	3.6634E-3	0.0523	0.0152	0	0	0
129646	3757	7.5326E-3	0.1035	0.1374	0	0	0
129648	1361	3.3369E-3	0.0443	0.0183	0	0	0
129650	3196	1.4591E-3	0.0323	0.0837	0	0	0
129652	3280	1.4722E-3	0.0471	0.1276	0	0	0
129655	1132	8.7564E-3	0.0633	0.0352	0	0	0
129657	1218	3.1974E-3	0.1656	0.2465	0	0	0
129664	1113	3.5585E-3	0.0955	0.2186	0	0	0
129667	1031	1.3613E-3	0.0703	0.0909	0	0	0
129669	3275	8.9063E-4	0.0469	0.0616	0	0	0
129671	3203	3.0461E-3	0.0516	0.0103	0	0	0
129672	3690	5.0158E-3	0.0409	0.0188	0	0	0
129675	3608	5.5424E-3	0.0612	0.0184	0	0	0
129680	680	0.0185	0.1329	0.1132	0	0	0
129694	2891	0.0113	0.1250	0.0811	0	0	0
129703	3569	3.3854E-3	0.1269	0.0286	0	0	0
129706	3574	4.7195E-4	0.0790	0.0204	0	0	0
130362	2942	5.1901E-4	0.0315	8.1637E-3	0	0	0
130581	1170	7.0855E-4	0.0597	0.1018	0	0	0
130583	1252	9.1171E-4	0.0563	0.1467	0	0	0
130587	1077	2.0585E-3	0.0795	0.1086	0	0	0
130589	1034	2.6855E-3	0.0787	0.0994	0	0	0
130598	2859	3.6861E-3	0.1250	0.0305	0	0	0
130600	583	2.5532E-3	0.0532	7.0419E-3	0	0	0
130601	2896	2.2714E-3	0.0727	0.0253	0	0	0
130623	2982	2.0078E-3	0.0941	0.0314	0	0	0
130627	708	5.0850E-4	0.0737	0.0110	0	0	0
130630	1474	1.9522E-4	0.0649	0.0140	0	0	0
130635	1355	1.4441E-4	0.0504	0.0137	0	0	0
130639	3706	8.3496E-4	0.0467	9.8645E-3	0	0	0
130645	3270	3.5567E-3	0.0740	0.0116	0	0	0
130647	3311	0.0157	0.0423	0.0303	0	0	0
130649	3373	1.9185E-3	0.0639	0.1717	0	0	0
130651	3400	2.4025E-3	0.0654	0.2005	0	0	0
130657	1211	4.4883E-3	0.1369	0.0197	0	0	0
130660	1293	1.3390E-3	0.1108	8.3951E-3	0	0	0
130667	3476	7.0889E-5	0.0705	0.0390	0	0	0
130668	3433	1.5553E-3	0.1227	0.1379	0	0	0
130675	941	6.4154E-5	0.0205	0.0182	0	0	0
130676	3189	6.3494E-4	3.7198E-3	0.0299	0	0	0
130677	1427	1.5716E-4	0.0256	0.0201	0	0	0
130680	1349	2.6402E-4	0.0498	0.0207	0	0	0

Nodes solid model	Nodes beam model	COMAC (UX)	COMAC (UY)	COMAC (UZ)	COMAC (ROTX)	COMAC (ROTY)	COMAC (ROTZ)
130684	553	1.4867E-3	0.1256	0.0187	0	0	0
130761	2962	6.4446E-3	0.0992	0.0482	0	0	0
130763	3562	5.8817E-3	0.1233	0.0319	0	0	0
131271	1510	8.4010E-3	0.0906	0.0449	0	0	0
131286	2849	1.2219E-3	0.0846	8.4734E-3	0	0	0
131288	1468	1.9842E-3	0.0778	0.0416	0	0	0
131290	3727	1.7885E-3	0.0292	0.0766	0	0	0
131335	3378	7.1541E-3	0.0656	0.0278	0	0	0
131400	887	2.8005E-3	0.0269	7.3928E-3	0	0	0
131412	1015	1.9600E-4	0.0431	0.0390	0	0	0
131417	933	9.9509E-4	0.0469	0.1042	0	0	0
131420	1412	1.0374E-3	0.0401	0.0712	0	0	0
131423	1350	4.9950E-3	0.0380	0.0159	0	0	0
131429	3789	1.3094E-3	0.0607	6.6449E-3	0	0	0
131432	3011	1.3930E-3	0.1190	0.0291	0	0	0
131435	2991	0	0.0979	0.0292	0	0	0
131438	3335	0.0108	0.0430	0.0422	0	0	0
131548	3512	0.0133	0.0744	0.0546	0	0	0
131557	3471	0.0170	0.0922	0.0666	0	0	0
131606	595	9.2767E-3	0.1191	0.0671	0	0	0
131609	558	7.1478E-3	0.2368	0.0787	0	0	0
131616	936	9.3280E-4	0.0622	0.0118	0	0	0
134820	1249	2.4386E-4	0.0705	0.0281	0	0	0
134821	1279	2.4216E-4	0.0467	0.1010	0	0	0
134823	2908	1.0913E-3	0.0257	6.1807E-3	0	0	0
134826	985	3.1659E-3	0.0697	0.1394	0	0	0
134828	3404	4.5422E-3	0.1420	0.2153	0	0	0
260805	502	2.0187E-3	0.0374	0.0205	0	0	0
328972	648	1.7298E-3	0.0347	0.0191	0	0	0
328973	2945	1.7362E-3	0.0363	0.0192	0	0	0
328984	2974	2.0491E-3	0.0801	0.0267	0	0	0
329002	3807	1.2052E-3	0.1257	0.0378	0	0	0
329003	1504	1.1068E-3	0.1122	0.0326	0	0	0
329021	1324	5.3786E-4	0.0382	0.0101	0	0	0
329032	1381	2.5160E-4	0.0448	0.0128	0	0	0
329057	943	1.1346E-3	0.0600	7.7990E-3	0	0	0
329058	3260	1.2009E-3	0.0614	7.9271E-3	0	0	0
329105	3481	3.8072E-3	0.1352	0.0209	0	0	0
329106	1180	6.8171E-3	0.1189	0.0242	0	0	0
329123	3563	4.7807E-3	0.0993	0.0169	0	0	0
329135	1291	2.8014E-3	0.0540	0.0155	0	0	0
329136	3587	3.4537E-3	0.0581	0.0139	0	0	0
329154	3501	5.7524E-3	0.1118	0.0111	0	0	0

Nodes solid model	Nodes beam model	COMAC (UX)	COMAC (UY)	COMAC (UZ)	COMAC (ROTX)	COMAC (ROTY)	COMAC (ROTZ)
329165	3446	7.1363E-3	0.1038	0.0192	0	0	0
329171	1119	8.4702E-5	0.0509	0.0475	0	0	0
329202	966	1.7972E-4	0.0431	0.0360	0	0	0
329227	1403	4.1215E-4	0.0323	0.0224	0	0	0
329255	1319	6.9823E-4	0.0495	0.0392	0	0	0
329256	3613	9.4311E-4	0.0512	0.0301	0	0	0
329287	3799	2.4285E-3	0.1074	0.0297	0	0	0
329306	562	3.7343E-3	0.1043	0.0216	0	0	0
329307	2870	4.0954E-3	0.1103	0.0356	0	0	0
329338	616	3.6920E-3	0.0545	0.0216	0	0	0
330185	2907	2.9672E-3	0.0329	0.0101	0	0	0
330495	2875	2.0476E-3	0.0507	4.8667E-3	0	0	0
330496	579	2.9089E-3	0.0944	0.0174	0	0	0
330561	3197	1.9392E-3	0.0575	0.0222	0	0	0
330562	954	8.0219E-3	0.0657	0.0392	0	0	0
330574	3310	0.0128	0.0509	0.0508	0	0	0
330604	3544	1.9868E-3	0.1271	6.9508E-3	0	0	0
330621	1278	2.1017E-3	0.1222	9.7582E-3	0	0	0
330622	3522	1.7548E-4	0.0656	0.0292	0	0	0
330623	1242	1.9252E-4	0.0664	0.0269	0	0	0
330634	3440	1.2555E-3	0.0900	0.1368	0	0	0
330635	1139	2.3996E-3	0.1724	0.2102	0	0	0
330657	3358	1.9665E-4	0.0529	0.0267	0	0	0
330664	3301	1.4846E-4	0.0499	0.0234	0	0	0
330700	1340	3.3491E-3	0.0391	0.0117	0	0	0
330712	3764	0.0139	0.0751	0.0793	0	0	0
330730	2994	4.5552E-4	0.0976	0.0121	0	0	0
330742	2979	2.0772E-3	0.0786	0.0294	0	0	0
330874	1486	4.4355E-4	0.0914	0.0194	0	0	0
330875	3794	5.8947E-4	0.0978	0.0205	0	0	0
330895	1391	7.6436E-4	0.0582	8.2064E-3	0	0	0
330896	3685	1.5186E-3	0.0729	0.0130	0	0	0
330916	1033	0.0141	0.0583	0.0584	0	0	0
330924	3458	0.0120	0.1193	0.0496	0	0	0
330941	1422	3.2357E-3	0.0645	0.0526	0	0	0
330942	3737	1.6619E-3	0.0444	0.0213	0	0	0
331156	620	1.2966E-3	0.0360	0.0125	0	0	0
336044	657	4.1009E-4	0.0218	0.0131	0	0	0
337374	3721	4.2192E-4	0.0281	0.0272	0	0	0
337411	1150	3.8573E-3	0.1682	0.1865	0	0	0
337445	3697	1.3707E-3	0.0382	0.0623	0	0	0
337454	1386	7.3431E-4	0.0406	0.0509	0	0	0
337463	1301	7.8481E-4	0.0549	0.0492	0	0	0

Nodes solid model	Nodes beam model	COMAC (UX)	COMAC (UY)	COMAC (UZ)	COMAC (ROTX)	COMAC (ROTY)	COMAC (ROTZ)
337492	1497	4.6893E-4	0.0665	8.9281E-3	0	0	0
337697	677	2.4023E-3	0.0772	0.0218	0	0	0
337712	697	7.7669E-3	0.1766	0.0370	0	0	0
337727	536	3.7446E-3	0.1121	0.0204	0	0	0
337759	3639	0	0	0	0	0	0
337774	3680	0	0	0	0	0	0
337794	3218	0	0	0	0	0	0
337804	3244	0	0	0	0	0	0
337863	1144	0	0.7745	0	0	0	0
337888	3538	0	0.0574	0	0	0	0
337903	3816	0	0.9132	0	0	0	0
337923	1193	0	0.1373	0	0	0	0
337967	3262	0	0	0	0	0	0
338026	3618	0	3.6876	0	0	0	0
338064	574	0	0.6284	0	0	0	0
338975	2930	0	3.0704	0	0	0	0

In table 21 the matched nodes from each of the two models are shown. Also, coordinate modal assurance criterion (COMAC) is shown for each DOF of each node pair. COMAC is an extension to the MAC calculator that identifies the degrees of freedom that are the source of low correlation between the models. This can be used in further work to refine the models to get a better correlation between the two models.

COMAC is calculated as follows:

$$COMAC_x = \frac{\sum_i^M\left[\left(ø_{i,x}^1 \cdot ø_{i,x}^{2*}\right) \cdot \left(ø_{i,x}^2 \cdot ø_{i,x}^{1*}\right)\right]}{\sum_i^M\left(ø_{i,x}^1 \cdot ø_{i,x}^{1*}\right) \cdot \sum_i^M\left(ø_{i,x}^2 \cdot ø_{i,x}^{2*}\right)}, \qquad 3.2$$

where:

COMAC$_x$ is the COMAC value for degree of freedom (DOF) x,
M is the number of paired modes in both models,
$(ø_{i,x}^1)_i^M$ is the set of file 1 (solid model in this case) mode shapes at DOF x for all paired modes,
$(ø_{i,x}^2)_i^M$ is the set of file 2 (beam model in this case) mode shapes at DOF x for all paired

modes,

$ø_{i,x}^{f*}$ is the complex conjugate of $ø_{i,x}^{f}$, f=(1,2).

More details about the COMAC can be found in the Ansys help page [17]

4 Discussion of structural and modal analyses

The correspondence between the solid and beam models with respect to volume and mass is quite good, with just 0,24% difference. Also, the deflection is corresponding well between the models when the post tensioning system is deactivated, with just 9% difference. After the post tensioning system is added, the deflection difference rises to 96%. Since the solid model gives expected results for deflection, and compressive and tensile stress, the solid model results are given the most confidence. The quite high deflection of the beam with post tensioning of 70,753 mm is considered unrealistic compared to the deflection of the solid model with post tensioning of 36,08 mm, which is more realistic for a concrete structure and gives better correspondence with the results found in the AAS-Jacobsen structural analysis report “18-1069 Herøysund bru. Bæreevneberegninger» [14].

Although there are several weaknesses to the models and analyses presented in this thesis. This is due to the fact that the candidate made some assumptions as recommended by the supervisors at the start of the thesis, such as:

- The rebars (slack reinforcement) is not modelled, and if implemented in the future should give more reliable results. The rebars can either be modelled or the material properties can be modified to simulate the rebars in the concrete, although this is a task for future work.
- The post tensioning system is not modelled, but rather simulated by horizontal forces clamping the main span together, it is not known how accurate this technique is, and implementing the post tensioning system in a more intricate way in the future may give more reliable results.
- The concrete material used in these analyses is standard concrete from Ansys Granta [5], and in the future there can be conducted tests on the material to derive more accurate material properties for the analysis.

- The analyses conducted in this thesis is completely linear. A more realistic behaviour of the bridge can be achieved using nonlinear joints and activating nonlinearity in the analysis, although this will increase CPU time and may give convergence issues.
- Another assumption made in this analysis is that creep and losses are not considered. The concrete surely has attained some creep over the lifespan of 57 years and there are surely losses in the post tensioning system as well.
- The bridge is in this thesis modelled as if completely undamaged, and in the future, it would be interesting to see if the known damages on the bridge can be implemented in the models.

The modal analyses were pre-stressed from the static structural analyses, and even though the deflections of the models were quite far apart, the results of the frequencies and mode shapes corresponded quite well. This tells us the static structural pre-stress has a low impact on the modal analysis, which makes sense because the modal analysis computations are based on the stiffness and mass of the structure. Even though the impact was small, it was interesting seeing the pre-stress having some impact on the modal analysis. Comparing the CPU time of solid and beam analyses, it is apparent that the beam model requires a lot less resources to compute than the solid model, which can be useful for quick analyses when low on computing power or if the analyses is made more complex in the future. Although the engineering hours required to convert the solid model to a beam model (approximately 75 hours) is most likely not worth it compared to buying more computing power.

5 Conclusion of structural and modal analyses

The structural analysis results of the solid and beam models were corresponding well without the post tensioning forces, but after the post tensioning forces were added, the static structural results vary quite a lot in deflection. The main objective in this thesis (model a solid and a beam model of Herøysund bridge and to extract modal analysis results), is achieved. There is good correspondence between the modal analysis results of the solid and beam model, with 11 out of 20 modes corresponding with over 90% similarity in mode shapes and less than 20% frequency error. The results appear to be realistic as the mode shapes materialize as one would expect in a structure with the scale and shape of Herøysund bridge. Although the results should be read with some scepticism as there is several details missing in these models, as rebars (slack reinforcement), post tensioned cables, creep and loss factors and nonlinear joints. These details should be added in future work to make the results from the models more reliable.

The solid model demands a lot more computational power and gives results that makes more sense for a concrete bridge structure compared to the beam model. The solid element technology is based on a more precise theory (elasticity theory) versus the beam theory (Timoshenko), which is a simplified technology that adds a cross section to a line. Also, the beam model contains more simplifications than the solid model. Hence more confidence is placed in the solid model, but the beam model can be useful for quick analyses with a low amount of computing power, for example in-situ on a laptop.

All in all, the candidate is satisfied with the results from this analysis. All the goals of the thesis and problem description is satisfied, and several interesting aspects has been added like modal assurance criterion, structural analysis etc. Through the work on this analysis, the candidate has learned a lot about the Ansys software [18], modal analysis, modal result interpretation, document interpretation, structural health monitoring and civil engineering structural assessment.

Works cited

[1] Microsoft corporation, ‘Microsoft Word’, 2018. https://www.microsoft.com/en-ww/microsoft-365/word?market=af (accessed May 12, 2023).

[2] Microsoft corporation, ‘Microsoft excel’, 2018. https://www.microsoft.com/en-us/microsoft-365/excel (accessed May 12, 2023).

[3] AAS-Jacobsen, ‘Herøysund bru.pdf’, 2019.

[4] Vegdirektoratet, ‘VEILEDNING Håndbok V412 Baereevneklassifisering av bruer, laster’, 2021. https://www.vegvesen.no/globalassets/fag/handboker/hb-v412-bareevneklassifisering.pdf (accessed Apr. 20, 2023).

[5] Ansys Inc, ‘Granta Edupack’. Ansys Inc, 2023.

[6] Vegdirektoratet, ‘Bæreevneklassifisering av bruer , materialer’, 2021. chrome-extension://efaidnbmnnnibpcajpcglclefindmkaj/https://www.vegvesen.no/globalassets/fag/handboker/hb-v413-bareevneklassifisering.pdf

[7] ANSYS Inc, ‘ANSYS help SOLID186’, 2022. https://ansyshelp.ansys.com/account/secured?returnurl=/Views/Secured/corp/v231/en/ans_elem/Hlp_E_SOLID186.html?q=solid186

[8] ANSYS Inc, ‘ANSYS help SOLID187’, 2022. https://ansyshelp.ansys.com/account/secured?returnurl=/Views/Secured/corp/v231/en/ans_elem/Hlp_E_SOLID187.html?q=solid187

[9] Ansys Inc, ‘15.3.3. Participation Factors’. https://ansyshelp.ansys.com/account/secured?returnurl=/Views/Secured/corp/v231/en/ans_thry/thy_anproc3.html%23anproc_modal_pfact (accessed May 07, 2023).

[10] Ansys Inc, ‘Mode Participation Factor and Effective Mass — Lesson 4’, 2021. https://www.youtube.com/watch?v=TO0gD-GpTfU (accessed May 07, 2023).

[11] Ansys Inc, ‘15.7.7 Effective Mass and Cumulative Mass Fraction’. https://ansyshelp.ansys.com/account/secured?returnurl=/Views/Secured/corp/v231/en/ans_thry/thy_anproc7.html%23anpeffectmass (accessed May 07, 2023).

[12] Ansys Inc, ‘15.7.7. Effective Mass and Cumulative Mass Fraction’. https://ansyshelp.ansys.com/account/secured?returnurl=/Views/Secured/corp/v231/en/ans_thry/thy_anproc7.html%23anpeffectmass

[13] ANSYS inc., ‘ANSYS help BEAM188’, 2022. https://ansyshelp.ansys.com/account/secured?returnurl=/Views/Secured/corp/v193/ans_elem/Hlp_E_BEAM188.html?q=beam188

[14] A. Sveen, ‘18-1069 Herøysund bru. Bæreevneberegninger’, 2020.

[15] ANSYS inc, ‘17.14. POST1 - Modal Assurance Criterion (MAC)’, 2023. https://ansyshelp.ansys.com/account/secured?returnurl=/Views/Secured/corp/v231/en/ans_thry/thy_post16.html

[16] Ansys Inc, ‘ 2.3.10. Automatic Mode Pairing Algorithm’. https://ansyshelp.ansys.com/account/secured?returnurl=/Views/Secured/corp/v231/en/mech_addon/ds_results_nvh-maccalc-automodepair.html?q=paired%20modes (accessed May 10, 2023).

[17] Ansys Inc, ‘2.3.9. Coordinate Modal Assurance Criterion Calculation’. https://ansyshelp.ansys.com/account/secured?returnurl=/Views/Secured/corp/v231/en/mech_addon/ds_results_nvh-maccalc-comac.html?q=comac (accessed May 10, 2023).

[18] Ansys Inc, ‘Ansys Software’, 2023. https://www.ansys.com/ (accessed May 12, 2023).

Appendix B Discretizations

Table of Contents

List of Tables

List of Figures

Foreword

This appendix will give a brief overview of the discretizations performed during the modelling part of this thesis.

1 Discretization of pressure plates

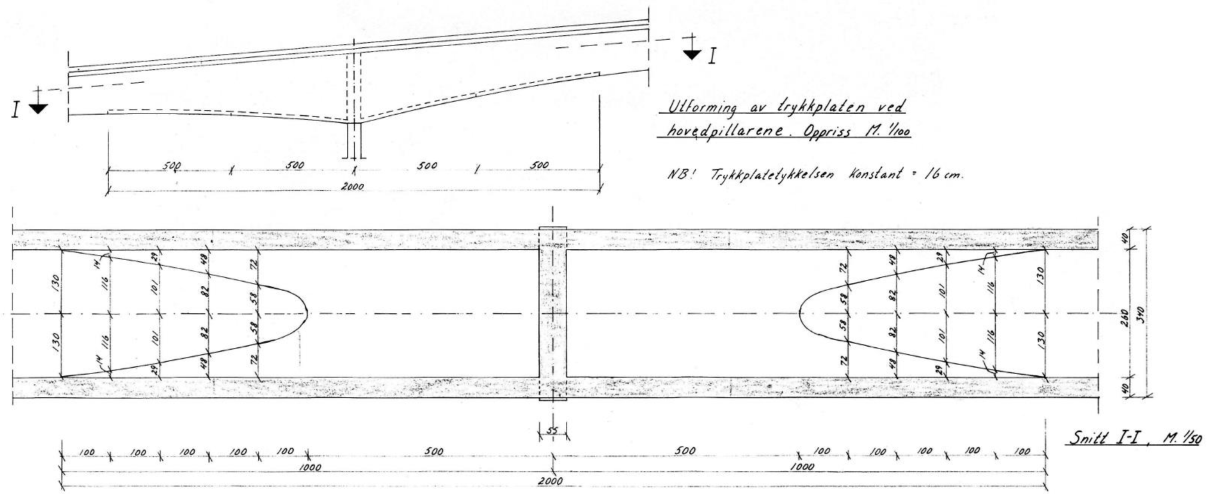

Figure 1: Geometry of the pressure plates [5].

To discretize the pressure plates on the main pillars, the section with the oval cut-out was divided into 1-metre-long sections, the volume of half of the section was calculated and multiplied by 2. The arched side geometry is not described in the documentation for the bridge, so it was mocked up in CAD to get a better estimate of the volume of this section.

1.1 Section1:

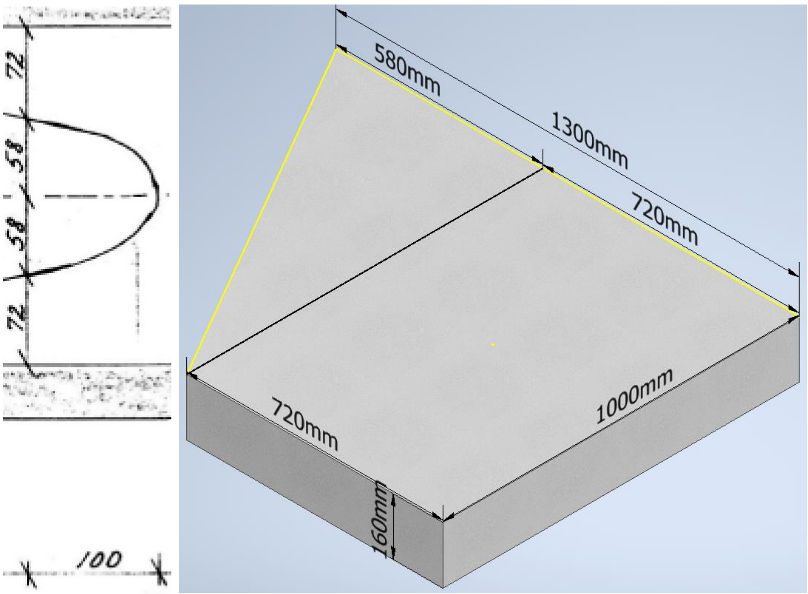

Figure 2: Section 1 geometry [5].

Table 1: Original dimensions section 1

w_r	width rectangle	720 mm
w_t	width triangle	580 mm
w_{r+t}	width rectangle + width triangle	1300 mm
l	length	1000 mm
h_o	original height	160 mm

Volume rectangle:

$$V_r = w_r l h_o = 720\,mm \cdot 1000\,mm \cdot 160\,mm = 115200000\,mm^3 \tag{1.1}$$

Volume triangle:

$$V_t = \frac{w_t l h_o}{2} = \frac{580\,mm \cdot 1000\,mm \cdot 160\,mm}{2} = 46400000\,mm^3 \tag{1.2}$$

Total volume of rectangle and triangle multiplied by 2 for both sides:

$$\begin{aligned} V_{tot} = (V_r + V_t) \cdot 2 = (115200000\,mm^3 + 46400000\,mm^3) \cdot 2 \\ = 323200000\,mm^3 \end{aligned} \tag{1.3}$$

Depth of discretized section:

$$h_n = new \text{ height} = \frac{V_{tot}}{l w_n} = \frac{323200000\,mm^3}{1000\,mm \cdot 2600\,mm} = 124{,}3\,mm \tag{1.4}$$

Correction for arced side:

Since the documentation of the bridge does not describe the arched sides geometry, the geometry was mocked up in the CAD software to get an approximation of the area of the surface of the geometry:

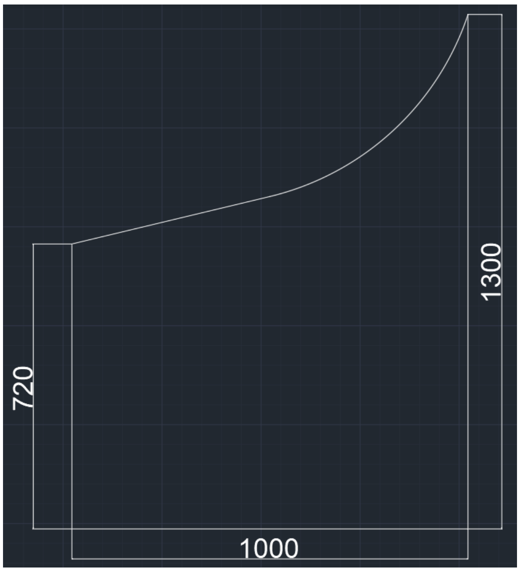

Figure 3: Autocad sketch of section 1 [2].

The CAD software gives A = area = 884632,8006 mm^2.

Total volume multiplied by 2 for both sides:

$$V_{tot} = A \cdot h_o \cdot 2 = 884632{,}8006\ mm^2 \cdot 160\ mm \cdot 2 = 283082496{,}192\ mm^3 \qquad 1.5$$

Both sides:

$$h_n = \frac{V_{tot}}{lw_n} = \frac{283082496{,}192 mm^3}{1000\ mm \cdot 2600\ mm} = 108{,}88\ mm \approx 110\ mm \qquad 1.6$$

Table 2: New dimensions section 1.

w_n	new width	2600 mm
h_n	new width	110 mm

1.2 Section 2

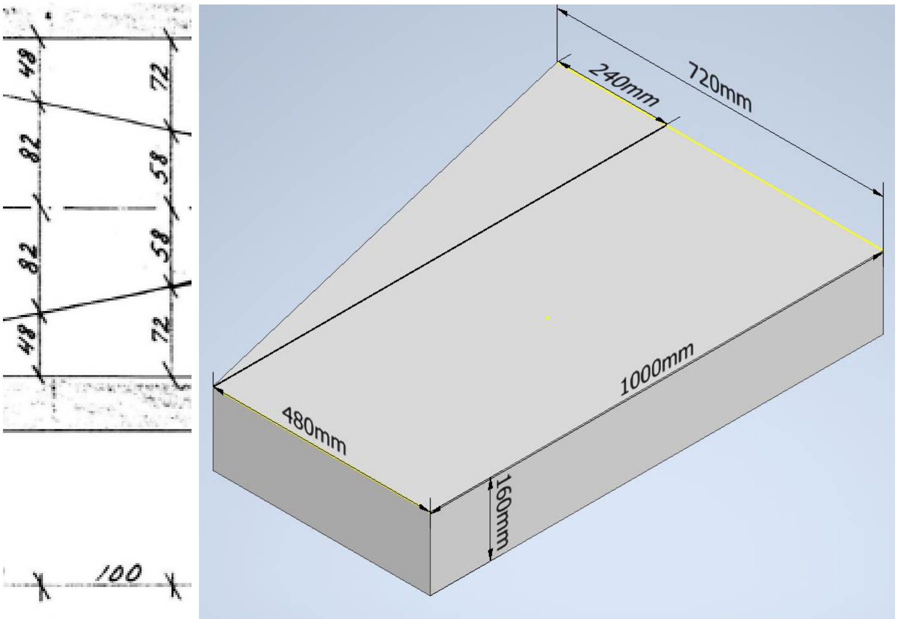

Figure 4: Section 2 geometry [5].

Table 3: Original dimensions section 2.

w_r	width rectangle	480 mm
w_t	width triangle	240 mm
w_{r+t}	width rectangle + width triangle	720 mm
l	length	1000 mm
h_o	original height	160 mm

Volume rectangle:

$$V_r = w_r l h_o = 480\ mm \cdot 1000\ mm \cdot 160\ mm = 76800000\ mm^3 \qquad 1.7$$

Volume triangle:

$$V_t = \frac{w_t l h_o}{2} = \frac{240\ mm \cdot 1000\ mm \cdot 160\ mm}{2} = 19200000\ mm^3 \qquad 1.8$$

Total volume of rectangle and triangle multiplied by 2 for both sides:

$$V_{tot} = (V_r + V_t) \cdot 2 = (76800000\,mm^3 + 19200000\,mm^3) \cdot 2 = 192000000\,mm^3 \qquad 1.9$$

Depth of discretized section:

$$h_n = new \text{ height} = \frac{V_{tot}}{lw_n} = \frac{192000000\,mm^3}{1000\,mm \cdot 2600\,mm} = 73{,}84\,mm \qquad 1.10$$

Table 4: New dimensions section 2.

w_n	new width	2600 mm
h_n	new height	73,84 mm

1.3 Section 3

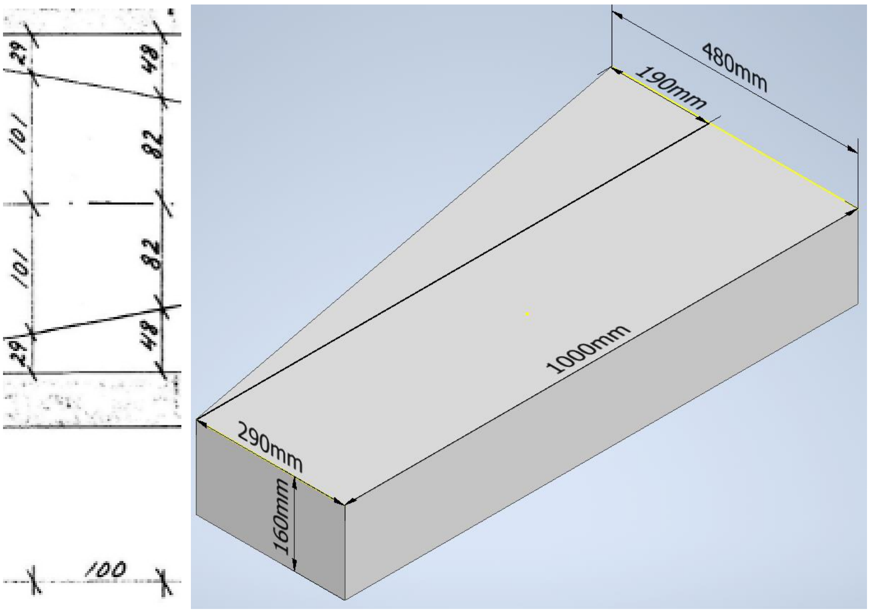

Figure 5: Section 3 geometry [5].

Table 5: Original dimensions section 3.

w_r	width rectangle	290 mm
w_t	width triangle	190 mm
w_{r+t}	width rectangle + width triangle	480 mm
l	length	1000 mm
h_o	original height	160 mm

Volume rectangle:

$$V_r = w_r l h_o = 290\ mm \cdot 1000\ mm \cdot 160\ mm = 46400000\ mm^3 \tag{1.11}$$

Volume triangle:

$$V_t = \frac{w_t l h_o}{2} = \frac{190\ mm \cdot 1000\ mm \cdot 160\ mm}{2} = 15200000\ mm^3 \tag{1.12}$$

Total volume of rectangle and triangle multiplied by 2 for both sides:

$$\begin{aligned} V_{tot} &= (V_r + V_t) \cdot 2 = (46400000\ mm^3 + 15200000\ mm^3) \cdot 2 \\ &= 123200000\ mm^3 \end{aligned} \tag{1.13}$$

Depth of discretized section:

$$h_n = new \text{ height} = \frac{V_{tot}}{l w_n} = \frac{123200000\ mm^3}{1000\ mm \cdot 2600\ mm} = 47{,}38\ mm \tag{1.14}$$

Table 6: New dimensions section 3.

w_n	new width	2600 mm
h_n	new height	47,38 mm

1.4 Section 4

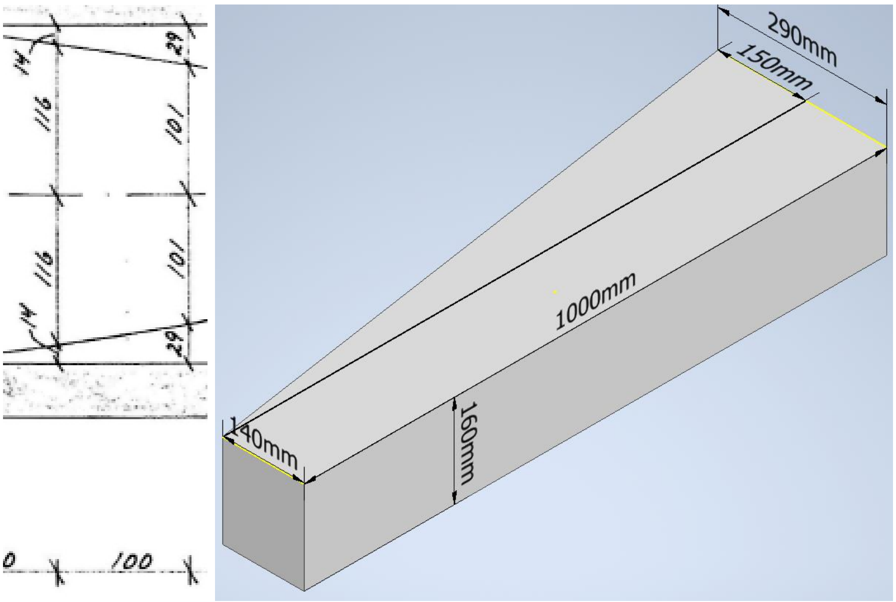

Figure 6: Section 4 geometry [5].

Table 7: Original dimensions section 4.

w_r	width rectangle	140 mm
w_t	width triangle	150 mm
w_{r+t}	width rectangle + width triangle	290 mm
l	length	1000 mm
h_o	original height	160 mm

Volume rectangle:

$$V_r = w_r l h_o = 140\,mm \cdot 1000\,mm \cdot 160\,mm = 22400000\,mm^3 \tag{1.15}$$

Volume triangle:

$$V_t = \frac{w_t l h_o}{2} = \frac{150\,mm \cdot 1000\,mm \cdot 160\,mm}{2} = 12000000\,mm^3 \tag{1.16}$$

Total volume of rectangle and triangle multiplied by 2 for both sides:

$$V_{tot} = (V_r + V_t) \cdot 2 = (22400000\,mm^3 + 12000000\,mm^3) \cdot 2 \\ = 68800000\,mm^3 \qquad 1.17$$

Depth of discretized section:

$$h_n = new\ \text{height} = \frac{V_{tot}}{lw_n} = \frac{68800000\,mm^3}{1000\,mm \cdot 2600\,mm} = 26{,}46\,mm \qquad 1.18$$

Table 8: New dimensions section 4.

w_n	new width	2600 mm
h_n	new height	26,46 mm

1.5 Section 5

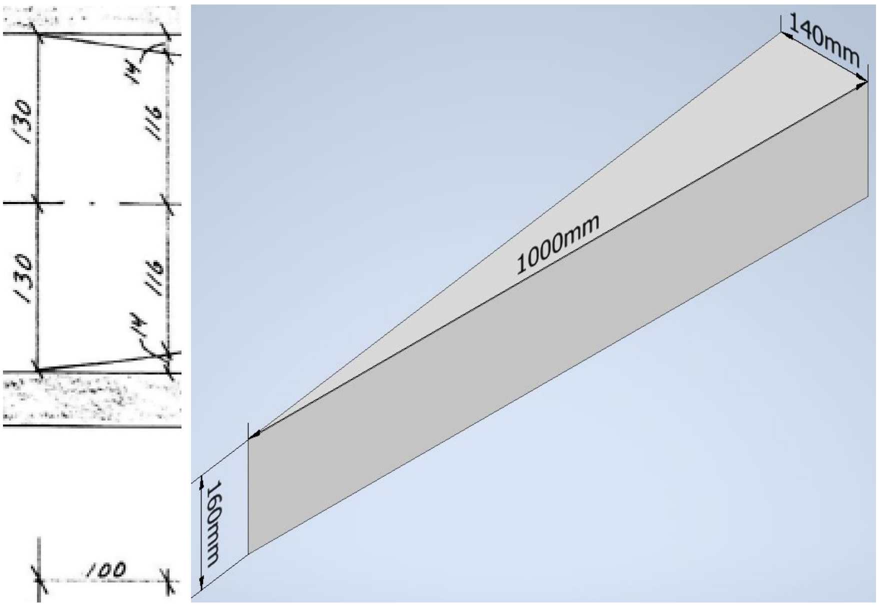

Figure 7: Section 5 geometry [5].

Table 9: Original dimensions section 5.

w_t	width triangle	140 mm
l	length	1000 mm
h_o	original height	160 mm

Volume triangle:

$$V_t = \frac{w_t l h_o}{2} = \frac{140\,mm \cdot 1000\,mm \cdot 160\,mm}{2} = 11200000\,mm^3 \qquad 1.19$$

Multiplied by 2 for both sides:

$$V_{tot} = V_t \cdot 2 = 11200000\,mm^3 \cdot 2 = 22400000\,mm^3 \qquad 1.20$$

Depth of discretized section:

$$h_n = new \text{ height} = \frac{V_{tot}}{l w_n} = \frac{22400000\,mm^3}{1000\,mm \cdot 2600\,mm} = 8{,}62\,mm \qquad 1.21$$

Table 10: New dimensions section 5.

w_n	new width	2600 mm
h_n	new height	73,84 mm

2 Discretization of tilting pillar

For the beam model the tilting pillar was discretized to a constant cross section by spreading the volume of the transverse beam at the top onto the space between the pillar legs. This discretization is only applied to the beam model.

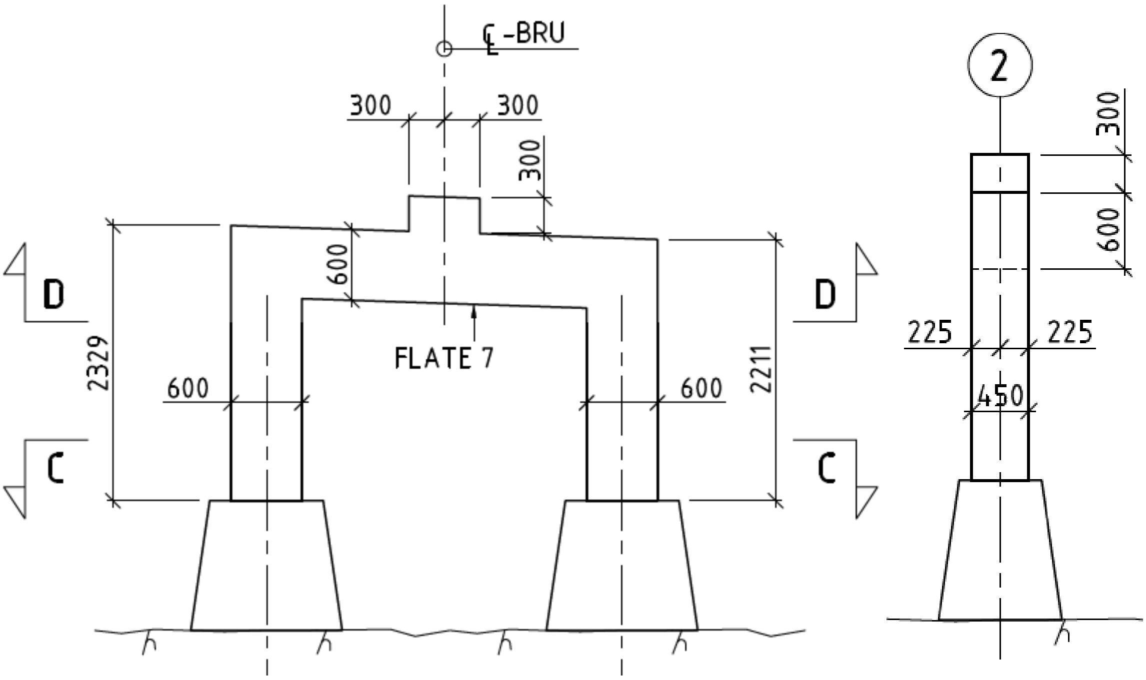

Figure 8: Tilting pillar geometry [6].

The height of the pillar was set to 2329 mm at both legs to make it planar in the horizontal plane.

Table 11: Dimensions of the transverse beam.

h	height of transverse beam	600 mm
w	width of transverse beam	450 mm

The length of the transverse beam is found by subtracting the width of the legs of the pillar from the distance between the outer faces of the longitudinal beams of the bridge.

Table 12: Dimensions of pillar

w_{fp}	width of legs of pillars	$2 \cdot 600$ mm = 1200 mm
d_{fb}	distance between the outer faces of the longitudinal beams	3400 mm

$$l = d_{fb} - w_{fp} = 3400\ mm - 1200\ mm = 2200\ mm \tag{2.1}$$

l = length of transverse beam = 2200 mm

Volume transverse beam:

$$V = hlw = 600\ mm \cdot 450\ mm \cdot 2200\ mm = 594000000\ mm^3 \tag{2.2}$$

Table 13: Dimensions of the space between the pillar legs

l_{bp}	length between pillars	2200 mm
h_{bp}	height between pillars	2329 mm-600 mm=1729 mm
w_{ns}	width of new section	

$$w_{ns} = \frac{V}{l_{bp} h_{bp}} = \frac{594000000\ mm^3}{2200\ mm \cdot 1729\ mm} = 156{,}16\ mm \approx 156\ mm \tag{2.3}$$

New width of discretized transverse beam: 156 mm.

Works cited

[1] Autodesk Inc, “Autodesk Inventor,” 2023. https://www.autodesk.com/products/inventor/overview?term=1-YEAR&tab=subscription (accessed May 12, 2023).

[2] Autodesk Inc, “Autodesk Autocad,” 2023. https://www.autodesk.com/products/autocad/overview?term=1-YEAR&tab=subscription (accessed May 12, 2023).

[3] Microsoft corporation, “Microsoft Word,” 2018. https://www.microsoft.com/en-ww/microsoft-365/word?market=af (accessed May 12, 2023).

[4] Microsoft corporation, “Microsoft excel,” 2018. https://www.microsoft.com/en-us/microsoft-365/excel (accessed May 12, 2023).

[5] Ingeniør Per Gulbrandsen AS, “Hovedpilarer m-fundamenter. Trykkplate. Formtegning.pdf,” 1965.

[6] AAS-Jacobsen, “Herøysund bru.pdf,” 2019.

Appendix C Presentation

During the master thesis work, the candidate was invited by the supervisor Harpal Singh to present the work accomplished at the time. This was on March 22. 2023. The candidate presented together with the fellow candidate Zeeshan Azad about the models developed and some preliminary analysis results.

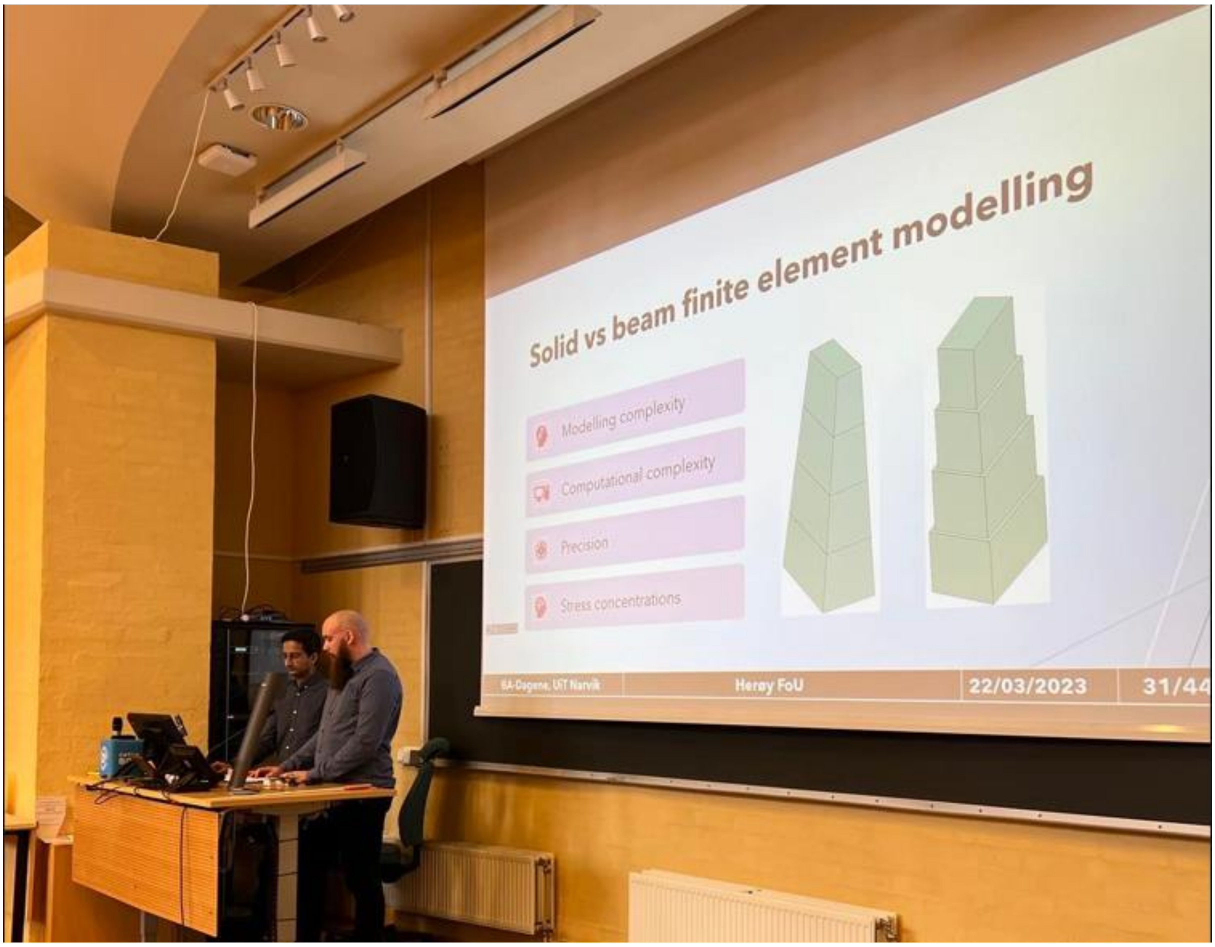

Solid vs beam finite element modelling

Modelling complexity

Computational complexity

Precision

Stress concentrations

BA-Dagene, UiT Narvik | Herøy FoU | 22/03/2023 | 31/44

Figure 1: Presentation at the "bygg og anleggsdagen".

Appendix D: Files

Files submitted with the thesis, compressed together in a .rar file:

- Solid element model.
- Beam element model.
- Solid model analysis.
- Beam model analysis.
- RST input file from beam model for MAC calculator.
- Three files for importing curves of bridge geometry.